



Provided by the author(s) and University of Galway in accordance with publisher policies. Please cite the published version when available.

|                  |   |
|------------------|---|
| Title            | Design and synthesis of novel constrained glycomimetics as inhibitors of galectins and galactosidases |
| Author(s)        | Hever, Eoin   |
| Publication Date | 2023-10-10  |
| Publisher        | NUI Galway  |
| Item record      | <a href="http://hdl.handle.net/10379/17952">http://hdl.handle.net/10379/17952</a>                     |

Downloaded 2024-04-28T03:42:02Z

Some rights reserved. For more information, please see the item record link above.



**Design and Synthesis of Novel Constrained Glycomimetics  
as Inhibitors of Galectins and Galactosidases**

**By**

**Eoin Hever**



OLLSCOIL NA  
GAILLIMH  
UNIVERSITY  
OF GALWAY

A Thesis presented to  
The University of Galway  
For the degree of  
Doctor of Philosophy

Based on the research carried out in the  
School of Biological and Chemical Sciences,  
The University of Galway

Under the supervision and direction of  
Prof. Paul V. Murphy  
The University of Galway

## **Declaration**

This thesis has not been submitted before, in whole or in part, to this or any other university for any degree, and is, except where otherwise stated, the original work of the author.

---

Eoin Hever

## Abstract

Chapter 1 gives a brief introduction to carbohydrate structure, discussing factors influencing reactivity and conformation, such as the anomeric and exo-anomeric effect. Chapter 1 mentions methods of structural analysis of carbohydrates. A description of the structure and biological function of galectins, in diseases such as inflammation and cancer is next given. Natural ligands for galectins are discussed, giving examples of published data obtained from affinity measurements. A review of glycomimetic research is included and focuses particularly on work from the Nilsson laboratory in Lund, Sweden with collaborators such as H. Leffler, H. Blanchard and R. Pieters and industry partners Galecto Inc. The chapter concludes by introducing *C*-glycosides and the concept of the conformational constraint, the hypothesis investigated in this thesis work.

Chapter 2 describes the synthesis of five galactosidase inhibitors analogous to isopropylthiogalactoside (IPTG), a galactosidase inhibitor, and also a molecular biology tool used to induce protein expression in *E.coli* cell lines. The synthesised ligands had distinct properties, including providing spatially different arrangements of the isopropyl group relative to the galactopyranoside residue by using cyclic constraints or through influencing them via the gauche effect. The synthetic *C*-glycosides were subjected to a galactosidase inhibition study to explore the influence of the constraints or structural features on the inhibitory properties of the ligands. Results of the assay showed that although the conformational constraint improved inhibition relative to IPTG, an unconstrained *C*-galactose derivative, isopropylmethylgalactoside (also known as isobutyl-*C*-galactoside, IBCG) was the best inhibitor in the series of  $\beta$ -galactosidase from *E. Coli*. The assay indicated the enzyme may have the ability to accommodate several ligands with different presentations of the iPr group. Other *C*-galactoside derivatives synthesised by Ashis Dhara and Dr. Saidulu Konda were also tested. Molecular docking was performed to provide some rationalisation of the assay results.

Chapter 3 builds upon the galactosidase inhibitor synthesis described in chapter 2, altering the structure of the compounds to generate galectin inhibitors. Synthesis is described, followed by biological evaluation against galectins -1, -3, 8*C*, -8*N*, -9*C*, -9*N*, -4*C* and -4*N* using a fluorescence polarization competitive inhibition assay. Derivatives synthesised by Ashis Dhara were also evaluated. Inhibitors with the best results in the assay were in the high micromolar range, with some ligands showing strong selectivity for certain galectins. Molecular docking

of selected ligands was again performed, discussing conformational features of ligands and key interactions with neighbouring amino acid residues in the galectin CRD which potentially explain the measured galectin affinities.

## Acknowledgements

Firstly, I would like to sincerely thank my supervisor Prof. Paul Murphy for giving me the opportunity to undertake a PhD in his lab. His knowledge and dedication to his research is truly inspiring and was invaluable to me during my PhD. I would like to say thank you to Prof. Mikael Bols and his lab members for their guidance during my research visit to Copenhagen and to Prof. Ulf Nilsson, Prof. Hakon Leffler, Barbro Kahl Knutson and all members of the Nilsson laboratory for helping me during my visit to Lund. I would like to thank all the technical staff in the School of Biological and Chemical Sciences at the University of Galway, particularly to Dr. Roisin Doohan for her help with the NMR. I would also like to extend a thank you to the members of my viva committee: Dr. Eoin Scanlan and Dr. Pau Farras for their insightful comments and discussion. Thank you to Science Foundation Ireland and the European Molecular Biology Organisation for funding my research at home and abroad.

I would like to thank all the postgraduates in Chemistry, particularly the members of the Murphy lab, past and present. A special word of thanks goes to Ashis Dhara and Kishan Mandal for the help, discussion and most importantly, friendship over the past few years. I wish you all the best in your future career's lads.

I would like to acknowledge all my housemates in Galway over the years, especially Liam, Neville and Elliot.

Finally, I would like to thank my family, particularly my parents, Niall and Rosemarie, for their love and support during my postgraduate journey. I couldn't have done it without you, and I hope I have made you proud.

## Table of Contents

|   |     |
|---|-----|
| <b>Table of Contents</b> .....  | v   |
| <b>Symbols and Abbreviations</b> .....  | vii |
| <b>Chapter 1: Introduction</b> .....  | 1   |
| <b>Introduction to Carbohydrates</b> .....  | 2   |
| <b>Structure of Carbohydrates</b> .....   | 3   |
| <b>Galectins</b> .....  | 6   |
| <b>Galectins in Disease – Cancer</b> .....  | 6   |
| <b>Galectins in Inflammation</b> .....  | 10  |
| <b>Structure of Galectins</b> .....   | 13  |
| <b>Binding Data of Natural Ligands with Galectins</b> .....                           | 14  |
| <b>Conformational Analysis of Ligands and the Exo-Anomeric Effect</b> .....           | 17  |
| <b>Synthetic Modifications to Ligands- Development of Glycomimetics</b> .....         | 22  |
| <b>Incorporation of Conformational Constraint into Glycomimetics</b> .....            | 35  |
| <b>Aims of the Thesis</b> .....   | 38  |
| <b>References</b> .....   | 39  |
| <b>Chapter 2: Synthesis and Biological Activity of Galactosidase Inhibitors</b> ..... | 47  |
| <b>Glycosidases</b> .....   | 48  |
| <b><math>\beta</math>-Galactosidase</b> .....   | 50  |
| <b>Isopropyl-<math>\beta</math>-D-1-thiogalactopyranoside (IPTG)</b> .....            | 51  |
| <b>Synthesis</b> .....  | 53  |
| <b><math>\beta</math>-Galactosidase Inhibition Assay- Procedure and Results</b> ..... | 60  |
| <b>Discussion</b> .....   | 70  |
| <b>Molecular Docking of Selected Ligands</b> .....                                    | 75  |
| <b>Conclusions</b> .....  | 80  |
| <b>References</b> .....   | 81  |
| <b>Chapter 3: Galectin Inhibitors</b> .....   | 84  |
| <b>Synthesis</b> .....  | 85  |
| <b>Fluorescence Polarisation</b> .....  | 94  |
| <b>FP Experiment Design</b> .....   | 95  |
| <b>Method</b> .....   | 96  |
| <b>Results</b> .....  | 98  |
| <b>Discussion</b> .....   | 104 |

|  |     |
|--|-----|
| <b>Conclusions and Future Work</b> .....     | 117 |
| <b>References</b> .....                      | 118 |
| <b>Chapter 4: Experimental Section</b> ..... | 121 |
| <b>General Experimental Methods</b> .....    | 122 |
| <b>Materials and Reagents</b> .....          | 122 |
| <b>Instrumentation</b> .....                 | 122 |
| <b>Molecular Docking</b> .....               | 123 |
| <b>Relaxed coordinate scans</b> .....        | 123 |
| <b>Chapter 2-Experimental</b> .....          | 125 |
| <b>Chapter 3-Experimental</b> .....          | 141 |
| <b>References</b> .....                      | 189 |



## Symbols and Abbreviations

|                     |   |
|---------------------|---|
| Å                   | Angstrom  |
| Ac                  | Acetate   |
| Ar                  | Aromatic  |
| Bcl-2               | B-cell lymphoma 2                                   |
| BH1                 | BCL-2 (B-Cell Lymphoma-2) Homology 1                |
| Bn                  | Benzyl  |
| Bu <sub>2</sub> SnO | Dibutyl Tin Oxide                                   |
| CD95                | Cluster of differentiation 95                       |
| CD <sub>3</sub> OD  | Methanol- <i>d</i> <sub>4</sub>                     |
| COSY                | Correlation Spectroscopy                            |
| CRD                 | Carbohydrate Recognition Domain                     |
| δ, Δ                | Chemical shift in ppm downfield from TMS, Change    |
| ΔG                  | Gibbs free energy                                   |
| ΔH                  | Enthalpy of binding                                 |
| ΔS                  | Entropy of binding                                  |
| °                   | Degree  |
| d                   | Doublet (spectral)                                  |
| dd                  | Doublet of doublets (spectral)                      |
| DDQ                 | 2,3-Dichloro-5,6-dicyano-1,4-benzoquinone           |
| ddd                 | Doublet of doublets of doublets (spectral)          |
| DEPT                | Distortionless Enhancement by Polarization Transfer |
| DMDO                | Dimethyldioxirane                                   |
| DNA                 | Deoxyribonucleic acid                               |

|                       |  |
|-----------------------|--|
| dt                    | Doublet of triplets (spectral)           |
| ECM                   | Extracellular matrix                     |
| Et                    | Ethyl                                    |
| FP                    | Fluorescence Polarization                |
| Gal                   | Galactose, Galectin                      |
| Glc                   | Glucose                                  |
| GlcNAc                | N-Acetyl glucosamine                     |
| HMBC                  | Heteronuclear multiple bond correlation  |
| HPLC                  | High performance liquid chromatography   |
| HRMS                  | High-Resolution Mass Spectrometry        |
| HSQC                  | Heteronuclear single quantum correlation |
| Hz                    | Hertz                                    |
| IBCG                  | Isobutyl <i>C</i> -galactoside           |
| IC <sub>50</sub>      | Half maximal inhibitory concentration    |
| IPTG                  | Isopropyl-β-D-1-thiogalactopyranose      |
| ITC                   | Isothermal Calorimetry                   |
| <i>J</i>              | Coupling constant (nmr), in Hz           |
| <i>K</i> <sub>a</sub> | Association constant                     |
| kcal                  | kilocalorie                              |
| <i>K</i> <sub>D</sub> | Disassociation constant                  |
| <i>K</i> <sub>i</sub> | Inhibitory constant                      |
| LacNAc                | N-Acetyl lactosamine                     |
| LUMO                  | Lowest unoccupied molecular orbital      |
| m                     | Multiplet                                |

|                                   |  |
|-----------------------------------|--|
| <i>m</i>                          | <i>meta</i>  |
| M                                 | Molar  |
| M+                                | Mass of the molecular ion (mass spectrometry)                |
| <i>m</i> CPBA                     | <i>meta</i> -Chloroperoxybenzoic acid                        |
| Me                                | Methyl   |
| Me <sub>3</sub> N•SO <sub>3</sub> | Sulfur trioxide-trimethylamine complex                       |
| MHz                               | Megahertz  |
| mL, μL                            | Millilitre, microlitre                                       |
| mol, mmol                         | Mole, millimole  |
| mM, μM                            | Millimolar, micromolar                                       |
| MTT                               | 3-(4,5-dimethylthiazol-2-yl)-2,5-diphenyltetrazolium bromide |
| N <sub>3</sub>                    | Azide  |
| NMR                               | Nuclear Magnetic Resonance                                   |
| nM                                | Nanomolar  |
| NOE                               | Nuclear Overhauser Effect                                    |
| <i>o</i>                          | <i>ortho</i>   |
| PANC-1                            | Human Pancreatic Cancer Cell Line                            |
| PDB                               | Protein Data Bank  |
| PDC                               | Pyridinium dichromate  |
| PMB                               | <i>para</i> -Methoxybenzyl                                   |
| <i>p</i> NP                       | <i>para</i> -Nitrophenol                                     |
| ppm                               | Parts per million (NMR)                                      |
| q                                 | Quartet (spectral)   |
| Q-TOF                             | Quadrupole Time of Flight (mass spectrometry)                |

|                  |  |
|------------------|--|
| RCM              | Ring closing metathesis                |
| R <sub>f</sub>   | Retention factor                       |
| r.t.             | Room temperature                       |
| s                | Singlet (spectral)                     |
| Sia              | Sialic Acid                            |
| siRNA            | Small interfering RNA                  |
| S <sub>N</sub> 1 | Unimolecular nucleophilic substitution |
| S <sub>N</sub> 2 | Bimolecular nucleophilic substitution  |
| t                | Triplet (spectral)                     |
| TCR              | T-cell receptor                        |
| td               | Triplet of doublets (spectral)         |
| TDG              | Thiodigalactose                        |
| Tf               | Trifluoromethanesulfonate              |
| TF Antigen       | Thomsen–Friedenreich antigen           |
| TFA              | Trifluoroacetic acid                   |
| THF              | Tetrahydrofuran                        |
| TLC              | Thin Layer Chromatography              |
| TMS              | Trimethylsilyl                         |
| Tol              | Toluene                                |
| VEGF             | Vascular endothelial growth factor     |
| W                | Water                                  |
| Wnt              | Wingless-related integration site      |
| 10-CSA           | Camphorsulfonic acid                   |
| [ ]              | Concentration in moles/litre           |

**Chapter 1: Introduction**

|   |    |
|---|----|
| <b>Introduction to Carbohydrates</b> .....                                    | 2  |
| <b>Structure of Carbohydrates</b> .....                                       | 3  |
| <b>Galectins</b> .....  | 6  |
| <b>Galectins in Disease – Cancer</b> .....                                    | 6  |
| <b>Galectins in Inflammation</b> .....  | 10 |
| <b>Structure of Galectins</b> .....   | 13 |
| <b>Binding Data of Natural Ligands with Galectins</b> .....                   | 14 |
| <b>Conformational Analysis of Ligands and the Exo-Anomeric Effect</b> .....   | 17 |
| <b>Synthetic Modifications to Ligands- Development of Glycomimetics</b> ..... | 22 |
| <b>Incorporation of Conformational Constraint into Glycomimetics</b> .....    | 35 |
| <b>Aims of the Thesis</b> .....   | 38 |
| <b>References</b> .....   | 39 |

## Introduction to Carbohydrates

Carbohydrates are among the most abundant biomolecules found in nature. Most carbohydrates are present in the form of monosaccharides, oligosaccharides, polysaccharides, glycoconjugates or natural products containing glycosides, in which sugar units are attached to each other or to aglycons via *O*-glycosidic bonds.<sup>1</sup> The term carbohydrate is widely used, though most commonly in biochemistry, where it is a synonym of ‘saccharide’, a group that includes sugars, starch and cellulose. The word saccharide comes from the Greek word ‘sákkharon’ meaning ‘sugar’<sup>2</sup> Some examples of simple sugars found in nature include the monosaccharide glucose, found in grape sugar, as well as the disaccharides sucrose and lactose found in cane sugar and milk respectively.

Carbohydrates play a diverse role in cellular biology. Polysaccharides allow for the uptake, storage and transport of energy (eg. starch and glycogen) and as structural components in plant cell walls. Glycans can be a mixture of carbohydrate structures such as glycoproteins, glycolipids and proteoglycans, all of which are present in the eukaryotic cell membrane. These and other components play an important role in many important processes such as cell growth, pathogenesis prevention, control of blood coagulation and molecular recognition processes. In humans, post translational modifications of proteins often involve formation of *-N* or *-O* linked glycosides, increasing the complexity of proteins in humans when compared to other species. Lectins are an example of proteins in humans which recognise and interact with carbohydrates.

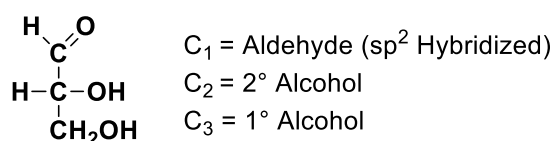
A wide variety of glycans in nature originate from their ability to form monosaccharide building blocks, which can be linked to other saccharide building blocks in pyranose or furanose ring form. An example of a monosaccharide building block is the 5-carbon ribose structure which is an important component of coenzymes, such as ATP, FAD and NAD, as well as the backbone of RNA. The related deoxyribose is a component of DNA.

Each sugar unit can lead to branching through the formation of glycosidic linkages, with the possibility of formation of an  $\alpha$ - or  $\beta$ -isomer at the anomeric centre. The position and stereochemistry of these glycosidic linkages often define the properties of sugars. Carbohydrates are no longer viewed simply as a component of a balanced diet and synthetic routes to compounds which contain sugars as part of their structure has undergone great developments in recent years due to more information becoming available about their biological relevance and potential use as components of biopharmaceutical drug treatments. The efficient stereoselective synthesis of these compounds, similar to, or better than those

found in nature has proven difficult, particularly in controlling the stereoselectivity of glycosidic link formation in high yields and in reasonable reaction times.

### Structure of Carbohydrates

Single carbohydrate units, termed ‘monosaccharides’ can exist in equilibrium as open chain structures or as a ring structure. Carbohydrates have the general formula  $C_n(H_2O)_n$ , where  $n \geq 3$ . Sugars can be three (triose), four (tetrose), five (pentose) or six (hexose) carbons in length. <sup>3</sup> Glyceraldehyde is the simplest sugar and is an example of a triose. The Fischer projection (representing the open chain form) is drawn as follows.



**D - Glyceraldehyde**

#### **Figure 1: Structure of the simplest sugar, D–Glyceraldehyde in Fischer Projection**

$C_2$  is a chiral carbon and the highest no. asymmetric centre. As the alcohol substituent is on the right, this indicates a D-sugar (*R* configuration). In contrast with D-sugars, L-sugars have an *S* configuration at the lowest chirality centre, with the bottom –OH group pointing to the left in the Fischer projection. <sup>4</sup>

Glucose is a common sugar and an example of a hexose. With 4 chiral centres there are  $2^4 = 16$  possible hexose stereoisomers. The presence of the aldehyde and alcohol on the same molecule allows for an intramolecular nucleophilic attack to take place, leading to the formation of a cyclic hemiacetal. Five and six membered cyclic hemiacetals are relatively strain free and stable and are preferred to four or seven membered rings. The cyclic structures can be represented by a Haworth projection, to indicate stereochemistry, but are more commonly displayed in their chair conformation, which represents both the stereochemistry and the conformation of the sugar. Like cyclohexane, the chair conformation is preferred over the boat due to the absence of torsional strain. When the chair conformation is viewed from the side, there is a staggered arrangement of hydrogens, which is favoured over the torsionally strained eclipsed hydrogens of the boat confirmation.

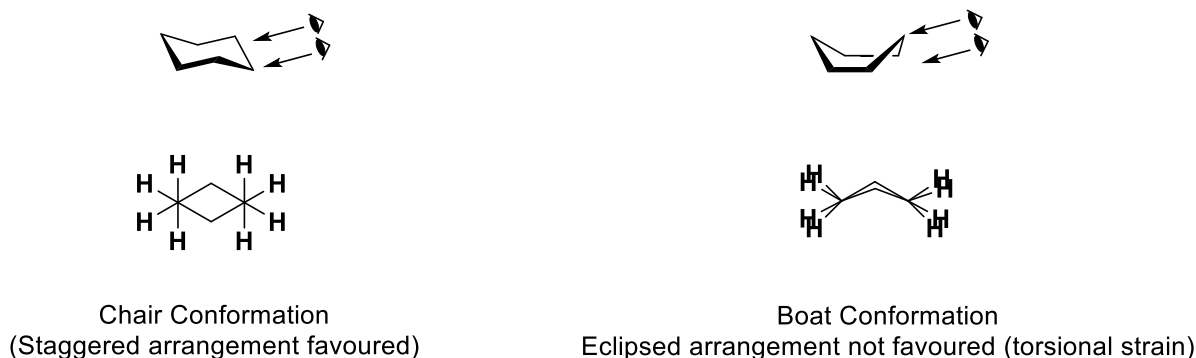
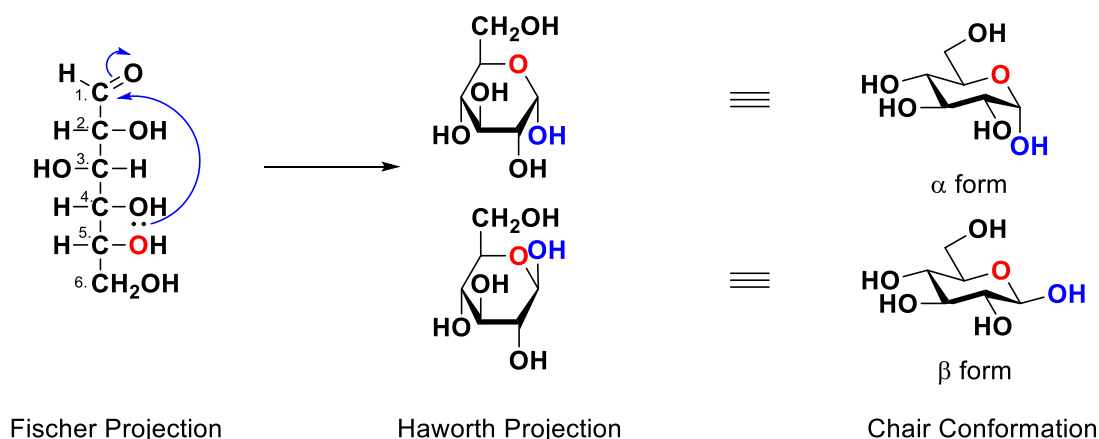


**Figure 2: Chair and boat conformation of cyclohexane displaying relative stability.**

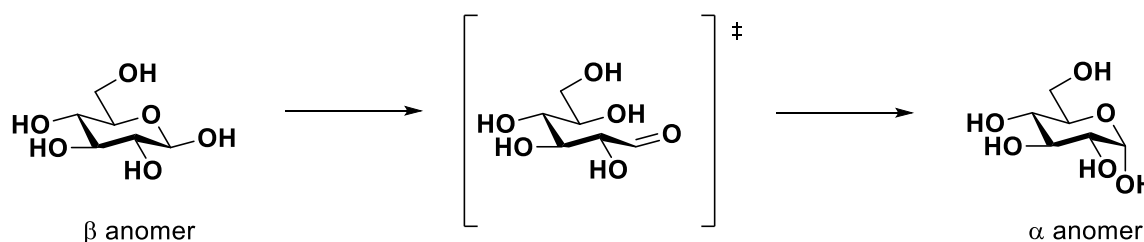
In the case of D-glucose, hydrogen atoms occupy all of the axial positions, while the sterically larger  $\text{-OH}$  and  $\text{-CH}_2\text{OH}$  groups emerge at the less hindered equatorial positions, minimizing steric repulsion. <sup>4</sup>



**Scheme 1: Different projections of Carbohydrates, showing cyclisation and stereoisomers**

A new chiral centre is generated at the former carbonyl carbon, resulting in the formation of two diastereomers, called anomers. The hemiacetal carbon is referred to as the anomeric centre. The formation of the product where the newly generated  $\text{-OH}$  group is *cis* to the  $\text{-OH}$  at the lowest chirality centre in the Fischer projection is known as the  $\alpha$ -anomer, which has axial orientation. The product with the *trans*  $\text{-OH}$  group at the anomeric centre is known as the  $\beta$ -anomer, which has equatorial orientation. The terms  $\alpha$  and  $\beta$  are used interchangeably with axial and equatorial. The presence of a wavy line at the anomeric position in a diagram indicates that the sugar can be axial or equatorial. When glucose is dissolved in water it can interconvert between the two, a process known as mutarotation.<sup>4</sup> Mutarotation occurs via a reversible ring opening of each anomer to the open chain aldehyde, followed by reclosure. Although equilibration is slow at neutral pH, it is catalysed by both acid and base.





### Scheme 2: Mutarotation of D-Glucose from $\beta$ - to $\alpha$ -anomer

The molecule will exist in equilibrium as a mixture of both anomers. The percentage of each anomer can be calculated via quantitative NMR (qNMR) spectroscopic measurements.

Glycosidic bonds can join one monosaccharide to another, as in lactose, a ligand for many carbohydrate binding proteins such as galectins. A disaccharide consists of two sugar units joined by an *O*-glycosidic bond. In the disaccharide lactose, for example, D-galactose, which differs from D-glucose in configuration at C4, is joined to D-glucose via a glycosidic linkage between the  $\beta$ -anomeric form of C1 on galactose and the hydroxyl oxygen atom on C4 of glucose. Such a linkage is called a  $\beta$ 1,4-glycosidic bond (see Figure 3). The glycosidic bond, or acetal, results from the reaction of a hemiacetal with an alcohol. In lactose, the glucose molecule on the right is known as the reducing end as it has a free anomeric carbon capable of assuming the open chain form, which can act as a reducing agent.<sup>3</sup> The galactose atom on the left cannot assume the open chain form, because the C1 atom is bound to another molecule. The binding pocket of carbohydrate recognition proteins are specific to the configuration of glycosidic linkages. An example of such proteins are the galectins.

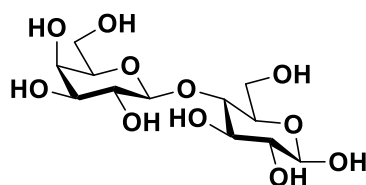


**Figure 3: Structure of  $\beta$ 1,4-lactose**

## Galectins

Galectins are a family of carbohydrate recognition proteins that bind  $\beta$ -galactosides with high specificity. Galectins found in many mammals including humans and mice<sup>5</sup> and many in other species, including birds, such as chicken,<sup>6</sup> amphibians, such as toad<sup>7</sup> fish, worms, sponges, and a fungus.<sup>8</sup> It has been discovered and named that galectins (Gals) in mammals have 15 subtypes. According to their molecular structure, they are divided into three types: (1) prototype galectins: prototype galectins are proteins containing a single carbohydrate recognition domain (CRD), which often form monomers or homodimers and includes galectin-1, galectin-2, galectin-5, galectin-7, galectin-10, galectin-11, galectin-13, galectin-14, galectin -15; (2) chimeric galectins: chimeric galectins contain two domains, a noncarbohydrate-binding *N*-terminal domain self-associating into oligomers followed by 8–129 amino acid long collagen like repeats connected to *C*-terminal carbohydrate recognition domains (CRD's) and only include galectin-3; (3) tandem-repeat galectins: tandem-repeat galectins are dimers consisting of two CRD's in a single polypeptide chain connected by a linker peptide and include galectin-4, galectin-6, galectin-8, galectin-9, galectin-12.<sup>8</sup> While galectin binding to a single saccharide ligand is typically a weak interaction, the multivalent nature of galectin–saccharide interactions results in high overall affinity. Multivalency also allows the formation of lectin-carbohydrate lattices. Both in solution and on the cell surface, multivalent galectins selectively crosslink a single species of glycoprotein to form homogeneous lectin-carbohydrate lattices. This crosslinking ability is relevant in cell biology as it can bring about cell-cell interactions. An example of galectin-mediated control over receptor endocytosis is the galectin-9-glucose transporter 2 (GLUT-2) system, where galectin-9 retains glucose receptors on the cell surface.<sup>9</sup> Galectin-1 can also promote human immunodeficiency virus infection by stabilizing viral attachments to host cells and crosslinking viral glycoproteins with target cells.<sup>10</sup> Galectin-3 interactions with *N*-acetylglucosaminyltransferase-V-modified *N*-glycans stimulate  $\alpha_5\beta_1$  integrin activation, focal adhesion remodelling, and phosphatidylinositol 3-kinase activation, thus promoting tumour cell motility.<sup>11</sup>

### Galectins in Disease – Cancer

In mammals, galectins are synthesized in the cytoplasm and then secreted to the outside of the cell by the endoplasmic reticulum and Golgi apparatus directly.<sup>12</sup> They are involved in a number of physiological processes,<sup>13</sup> particularly the origin and development of cancer<sup>14</sup> (see Figure 4) and the regulation of immunity and inflammation.<sup>15</sup> Galectins have multiple roles

in different parts of the cells, such as the cell membrane, cytoplasm, extracellular matrix, and the intracellular receptors.<sup>14</sup>

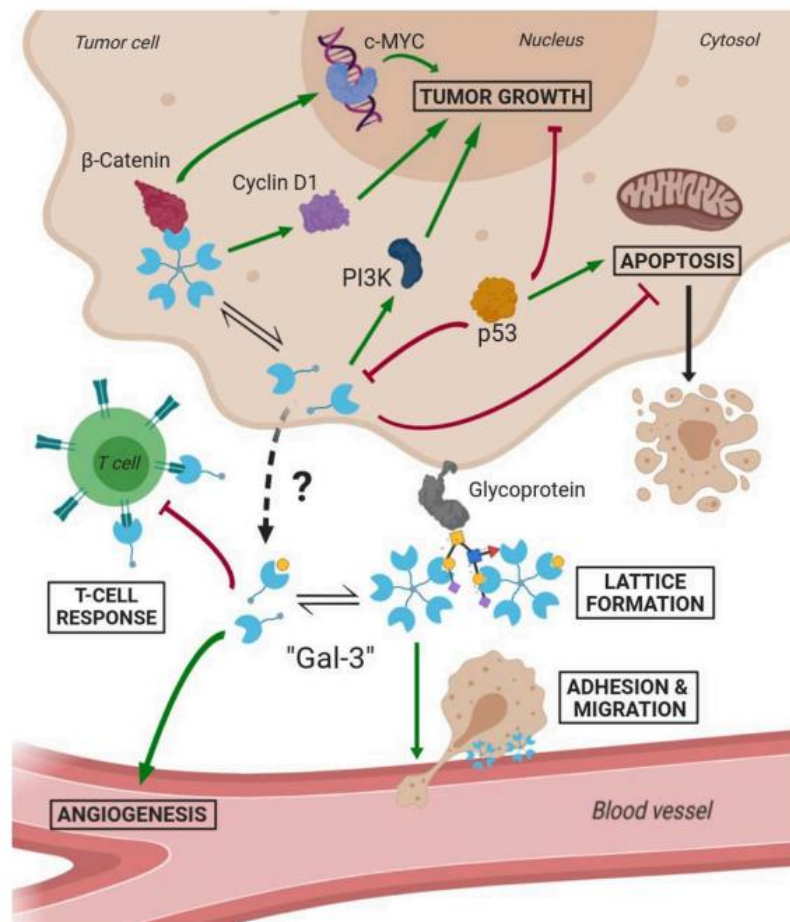


**Figure 4: Most important cellular functions of Galectin-3 in tumoral environments (Green arrows mean activation and bordeaux lines mean inhibition) Reproduced with permission from ref 13, Copyright © 2019 Frontiers Media SA Academic Publishers**

Development of various cancers is mediated by galectins through interactions with oncogenes<sup>16,17</sup> leading to tumour cell transformation. In tumour cell experiments, overexpression of Gal-1 will stimulate cell proliferation in human glioma cells<sup>18</sup> and thyroid cancer.<sup>19</sup>

Gal-3 is reported to play a tumour promotion role in the proliferation of Wnt signalling breast, colon and gastric cancer cells by interacting with  $\beta$ -catenin. Western blot experiments carried out by Raz et al<sup>20</sup> showed that gal-3 silencing drastically reduced  $\beta$ -catenin expression in three transfected pancreatic cancer cell lines. Silencing of  $\beta$ -catenin in PANC-1 cells by siRNA transfection was done to determine the effect of  $\beta$ -catenin expression on cell proliferation. An MTT assay showed a significant decrease in the proliferation rate of cells transfected with  $\beta$ -catenin-siRNA compared with the rate of control cells, thus indicating that a decrease in  $\beta$ -

catenin expression in pancreatic cancer cells is associated with decreases in cell proliferation and invasion.<sup>20</sup>

Gal-3 can increase cell growth of hepatocellular carcinoma,<sup>21</sup> glioma cells<sup>22</sup> and can induce pancreatic cancer cell proliferation. The effects of galectin-3 on the cell proliferation and cycle came about due to the translocation ability of galectin-3 into the nucleus by binding with Impotin, Sufu, and Nup98, wherein it controls the cell cycle through the interaction with cyclin A, cyclin D, cyclin E, p21 (WAF1), and p27 (KIP1), accelerating cancer cell proliferation.<sup>23</sup> MUC1 is a transmembrane glycoprotein which is typically expressed at the apical membrane of normal epithelial cells. In cancer cells, the over-expression of MUC1 and its aberrant localization around the cell membrane and in the cytoplasm favours its interaction with different protein partners such as epidermal growth factor receptor (EGFR) and can promote tumour proliferation through the activation of oncogenic signalling pathways. Galectin-3 is co expressed with MUC1 in human pancreatic ductal adenocarcinoma and favours the endocytosis of MUC1 and EGFR. Galectin-3 interacts directly with EGFR or MUC1, when MUC1 has an unsialylated TF antigen, leading to a redistribution of MUC1 on the cell surface, exposure of adhesion molecules such as E-cadherin and increase of the survival of tumour cells.<sup>24</sup>

Galectins are involved in the development of tumours through tumour immune escape, induction of apoptosis, tumour metastasis, and tumour angiogenesis.<sup>25</sup> Studies show that galectin-1 binding induces apoptosis through triggering apoptotic pathways (induction of the activation protein-1 (AP-1) transcription factor and then the activation of apoptotic pathway promoter's caspase-8 and caspase-3 and subsequent downregulation of mitochondrial Bcl-2)<sup>26</sup> and promoting T-cell receptor chain phosphorylation.<sup>27</sup> On the contrary, galectin-3 can suppress cells apoptosis and the antiapoptotic activity is given by a functional antideath (NWGR) motif, a conserved amino acid sequence located in the BH1 domain of the Bcl-2 gene family.<sup>28</sup> Galectin-3 combines with CD95/ Fas and subsequently suppresses the activation of CD95/ Fas-mediated caspase-8.<sup>29</sup> The inhibitory effect of galectin-3 on cell apoptosis is regulated by the phosphorylation/dephosphorylation of ser-6 residues, this signal transduction acts as a "switch" in binding galectin-3 to ligands.<sup>30</sup>

The role of galectins in immune responses is mainly through regulating levels of activated effector Natural Killer cells and T cells. Perillo et al.<sup>31</sup> found that galectin-1 induced the apoptosis of activated T cells and their further study<sup>32</sup> revealed that cell surface glycoconjugates, which displayed both *N*- and *O*-glycans on activated T cells, such as CD2,

TCR, and CD95 were the receptors for extracellular galectin-1. Binding of galectin-1 with cell surface receptors CD44 and CD326 promotes tumour cell metastasis to cell matrix and adhesion to vascular endothelial cells. Knockdown of galectin-1 significantly reduces lung metastatic potential in colon and breast cancer.<sup>33,34</sup> galectin-1 also promotes cancer progression through its effect on the immunosuppressive activity of CD4<sup>+</sup>CD25<sup>+</sup> T regulatory cells. O'Driscoll et al. confirmed that overexpression of galectin-3 can increase the adhesion between lung cancer cells to extracellular matrix, leading to cell motility and invasiveness, and inhibiting galectin-3 by lactose will significantly weaken this effect.<sup>35</sup> galectin-3 was also regarded as one of targeting molecules involved in the immune escape in the progression of cancers<sup>36,14</sup>

Studies showed that galectin-1 can induce angiogenesis and thiodigalactose (TDG) (structure can be seen in Figure 14) can block effects of galectin-1 through suppressing angiogenesis and protection against oxidative stress. As a chemoattractant inducing epithelial cells transfer to vascular endothelial cells in vitro and in vivo, galectin-3 is critical for tumour angiogenesis.<sup>37</sup> It contributes to the plasma membrane retention of the glycosylated cell surface protein VEGF-Receptor 2, aiding its proangiogenic function and altering its signal transduction.<sup>38</sup> Western blot experiments performed by Panjwani et al<sup>38</sup> indicated that VEGF-R2 and galectin-3 interacted in a carbohydrate-dependent manner. Knockdown of *N*-acetylglucosaminyltransferase-V, the enzyme responsible for synthesis of the high-affinity glycan ligands for galectin-3, and galectin-3 itself by transfection with lentiviral particles expressing short hairpin RNA, reduced VEGF-A mediated angiogenesis in vitro (see Figure 5).

38

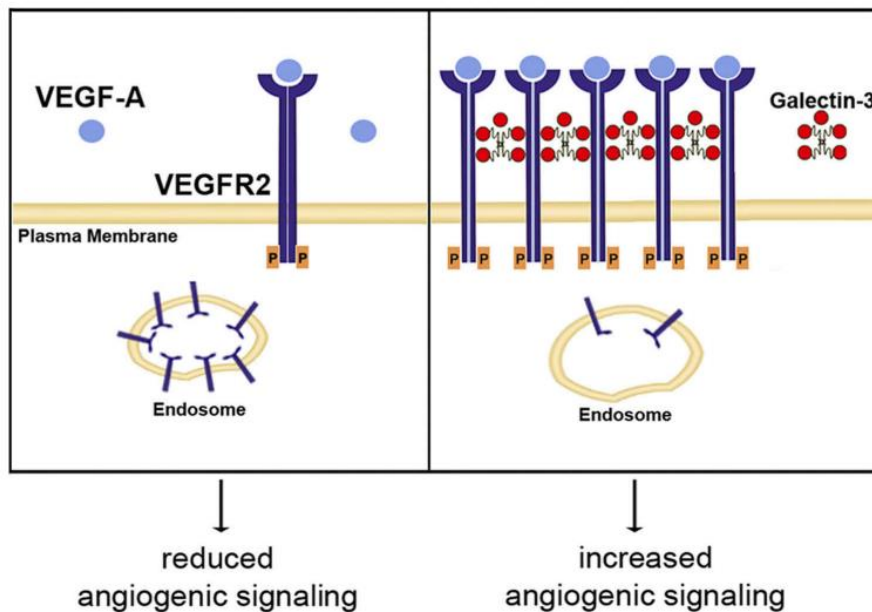


**Figure 5: Galectin-3 promotes clustering of VEGF-R2. In the absence of galectin-3, VEGF receptors accumulate in endosomal vesicles (left panel). In the presence of galectin-3, VEGF-R2 is retained on the plasma membrane and angiogenic signaling is enhanced (right panel). Reproduced with permission from ref 38, Copyright © 2011 American Society for Biochemistry and Molecular Biology, Inc. Academic Publishers**

It has been shown that the galectin-7 gene is a transcriptional target of the tumour suppressor protein p53 and may play a role in the proapoptotic function of p53.<sup>39</sup> Expression of galectin-7 is elevated in chemically induced rat mammary carcinomas<sup>40</sup> and its mRNA is detected frequently in human breast and colon cancer cell lines.<sup>41</sup> Thus, galectin-7 appears to be another member of the galectin family with regulatory activity for cell survival.

### Galectins in Inflammation

Inflammation occurs because of a number of physiological processes modulated by galectins. The proteins are responsible for a range of signalling events that lead to chemotaxis, trafficking, cytokine secretion,<sup>13</sup> cell adhesion, invasion, migration and signal transduction.<sup>14</sup>

A combination of in vitro and in vivo experiments carried out by Rabinovich et al<sup>42</sup> suggest that differential glycosylation of cell surface glycoproteins can selectively regulate the survival of T helper type 1, T helper type 2 and TH-17 effector cells. By this mechanism, galectin-1 can negatively regulate T helper type 1- and interleukin 17-producing T helper-mediated

inflammatory responses *in vivo*, providing a molecular link among differential glycosylation of T helper cells, susceptibility to cell death and termination of the inflammatory response. Other members of the galectin family may also contribute to this process, including galectin-9, which specifically binds the T helper type 1 cell surface receptor Tim-3 and can regulate autoimmune inflammation.<sup>43</sup>

Human serum transferrin is a glycoprotein synthesized mainly by hepatocytes and is involved in iron transport between sites of absorption and delivery. Transferrin has two potential *N*-glycosylation sites, usually with two bi- and/or triantennary *N*-glycans as part of their glycan moiety. Transferrin glycoforms have been analysed extensively as surrogate markers for rare genetic disorders of glycosylation and also for alcohol induced liver injury.<sup>44</sup> Galectin-3 is known to regulate the intracellular traffic of certain cellular glycoproteins by binding their glycans and has been found to bind to particular glycoforms of transferrin, playing a functional role in their intracellular trafficking after uptake.<sup>45</sup>

At the site of infection with *Streptococcus pneumoniae*,<sup>46,47</sup> the primary function of neutrophils is to eliminate the invading micro-organisms by phagocytosis and subsequent intracellular killing. Galectin-3 is shown to possess chemotactic activity for inflammatory cells, such as monocytes and macrophages. At the onset of such an infection, resident alveolar macrophages produce and secrete galectin-3, and the amount of galectin-3 released correlates to the number of transmigrated neutrophils.<sup>48</sup> This suggests that galectin-3 has a direct function in mediating the adhesion of neutrophils to the endothelium and induce extravasation into the lung. The movement of the neutrophil across the ECM requires not only the presence of a chemoattractant but also adhesion to the underlying protein/carbohydrate matrix. The involvement of galectins in adhesion to the ECM is well established.

Leukocyte recruitment was studied in galectin-3 null mutant mice. These animals showed no morphological abnormalities and had no apparent phenotypes under standard laboratory conditions.<sup>49</sup> The initial influx of phagocytic cells in response to a non-infectious inflammatory agent<sup>50,51</sup> was not affected, with the reduction in the number of granulocytes in the peritoneal cavity evident only in the late stage (after 4 days) of inflammation, suggesting that galectin-3 is of crucial importance for the maintenance of neutrophils in the tissue. Galectin-3 can promote the adhesion of neutrophils<sup>52</sup> as well as other cell types<sup>53,54</sup> to laminin in an integrin independent manner. This bridging by galectin-3 of neutrophils to laminin appears to involve activation of the cells via  $\text{Ca}^{2+}$  and  $\text{Mg}^{2+}$  dependent processes.<sup>55</sup>

Galectin-3 has been shown to induce production of Interleukin-1 in macrophages<sup>56</sup>. IL-1 is involved in a variety of immunological processes and is known to induce leukocyte adhesion molecules on vascular endothelium. Hence, in this more indirect way, galectin-3 could act as an adhesion promotor, these findings show that the prerequisites for galectin-promoted adhesion of the neutrophils to the endothelium are present.

Following adhesion, leukocytes migrate across the endothelial lining of the micro-vessels. They then start to move towards the inflammatory focus through the extracellular matrix (ECM) by chemotaxis along a gradient of chemoattractants, derived from either endogenous cells or invading microbes (see Figure 6).<sup>55</sup>

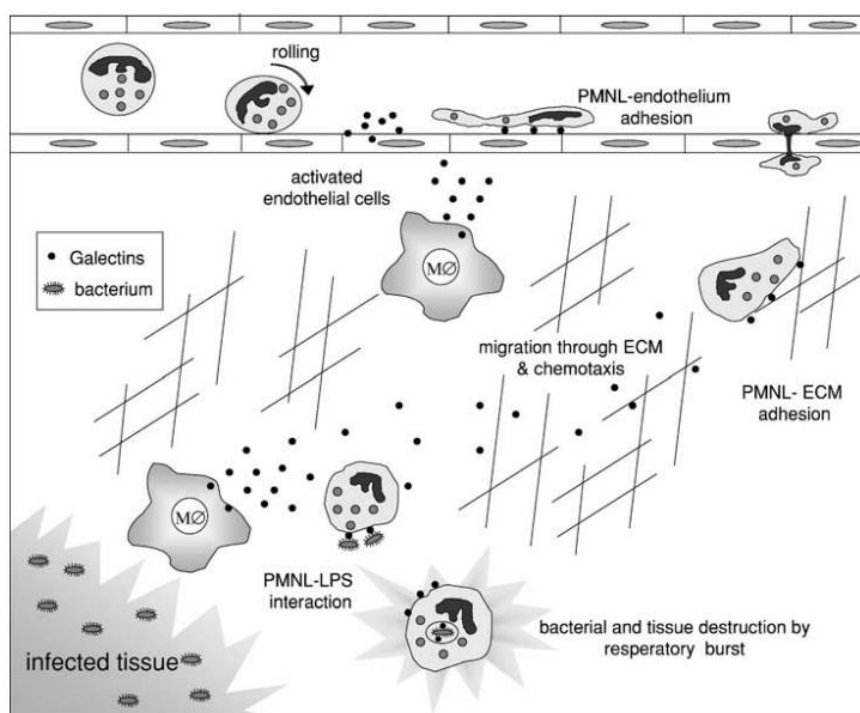


**Figure 6: Schematic overview of the involvement of galectins in the inflammatory process. Galectins (black dots), produced by e.g., macrophages (Mφ) and endothelial cells may be involved in the recruitment of polymorphonuclear leukocytes (PMNL) from the blood stream. The galectins may cross-link the PMNL with the endothelium, as well as facilitating the migration through the extracellular matrix (ECM) by being chemotactic and cross-linking the cell to the underlying protein matrix. Further, in the interaction with invading bacteria, galectins may function as opsonins, facilitating the attachment between the PMNL and bacteria. By activating the respiratory burst in the PMNL, galectins may participate in both the antibacterial defence as well as in the inflammation-associated tissue destruction. Reproduced with permission from ref 55, Copyright © 2004 Kluwer Academic Publishers.**



## Structure of Galectins

Galectins typically have a highly conserved  $\beta$ -sandwich core sequence containing  $\sim 130$  amino acids in the CRD. Figure 8 shows the two  $\beta$ -sheets (labelled F, consisting of 5 strands and S, consisting of 6 strands) as a convex and concave side respectively. The concave side forms a groove in which carbohydrate is bound, and which is long enough to hold about a linear tetrasaccharide.<sup>15</sup> Thus, the galectin-carbohydrate binding site can schematically be described as having four subsites (A-D), with a fifth site E that is less defined on the structure. Subsite C is the defining  $\beta$ -galactoside binding site of the galectins. The binding of a galactose residue in site C is the most conserved feature of galectin binding activities. Six of the seven “motif amino acids” interact with the galactose. A  ${}^4C_1$  pyranose ring and axial 4-OH is essential for these interactions to take place (see Figure 7). The mono CRD galectins can occur as monomers, dimers or higher order oligomers depending on concentration and presence of ligands. Two different dimer interfaces have been defined, one as found in galectin-1, and another as found in galectin-7 and suggested in galectin-3<sup>15</sup> (see Figure 8). Galectin-3 has a C-terminal CRD associated with an N-terminal part consisting of 18 conserved amino acids followed by 7-14 repeats, each having 8-11 amino acids that include one aromatic and multiple proline and glycine residues. The bi-CRD galectins are bivalent as monomers and might also associate into higher oligomers.<sup>15</sup>

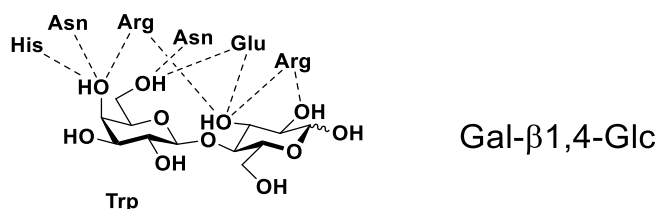
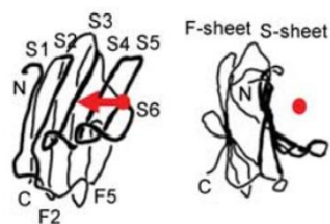


**Figure 7: Interactions between Lactose and motif amino acids in conserved binding site C of Galectin CRD**

## The galectin CRD



## Two types of dimer

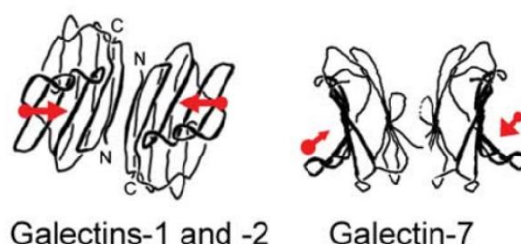


**Figure 8:** Artist's representation of  $\beta$ -sandwich CRD of Galectins -1, -2 and -7, with bound disaccharides represented as red arrows. Reproduced with permission from ref <sup>15</sup>, Copyright © 2004 Kluwer Academic Publishers

## Binding Data of Natural Ligands with Galectins

Some of the key protein-ligand interactions observed in Figure 7 include non-covalent electrostatic interactions, between arginine and axial 4-OH, hydrogen bonding between asparagine and axial 4-OH and hydrophobic interactions such as CH- $\pi$  bonds between the tryptophan residue and the  $\alpha$ -face of the sugar. The carbohydrate binding specificities of the galectin family has been the source of intense recent investigations. Isothermal titration calorimetry (ITC) provides direct determination of the thermodynamics of binding of carbohydrates to lectins and has provided important insights into the fine carbohydrate binding specificities of a wide number of lectins. Several natural ligands are observed to bind to galectins with varying degrees of specificity. Data from the study are summarised in Table 1.<sup>57</sup>

**Table 1:** Thermodynamic binding parameters of bovine heart galectin-1, murine recombinant galectin-3 and human recombinant galectin-7 with carbohydrates<sup>57</sup>

| Ligand                                 | $K_a^a$<br>( $M^{-1} \times 10^{-4}$ ) | $-\Delta H^b$<br>(kcal mol <sup>-1</sup> ) | $-\Delta G^c$<br>(kcal mol <sup>-1</sup> ) | $-T\Delta S$<br>(kcal mol <sup>-1</sup> ) | $n^e$<br>(sites/monomer) |
|--|--|--|--|---|--------------------------|
| Bovine Heart Galectin-1 (Temp. 300 K)  |  |  |  |   |                          |
| Gal- $\beta$ 1,3-GlcNAc<br>(LacNAc-I)  | 0.9                                    | 7.9  | 5.4  | 2.5                                       | 0.97                     |
| Gal- $\beta$ 1,4-GlcNAc<br>(LacNAc-II) | 1.1                                    | 9.2  | 5.5  | 3.7                                       | 1.01                     |
| Gal- $\beta$ 1,1-Gal<br>(TDG)          | 1.8                                    | 9.8  | 5.8  | 4.0                                       | 1.04                     |

|  |      |      |     |     |      |
|--|------|------|-----|-----|------|
| Gal- $\beta$ 1,4-GlcNAc-<br>$\beta$ 1,3-Gal- $\beta$ 1,4-<br>GlcNAc<br>(DiLacNAc)  | 0.74 | 11.4 | 5.3 | 6.1 | 0.94 |
| Gal- $\beta$ 1,4-GlcNAc-<br>$\beta$ 1,3-Gal- $\beta$ 1,4-<br>GlcNAc- $\beta$ 1,3-Gal-<br>$\beta$ 1,4-GlcNAc<br>(TriLacNAc)   | 2.2  | 10.1 | 5.9 | 4.2 | 0.94 |
| Gal- $\beta$ 1,3-GlcNAc-<br>$\beta$ 1,3-Gal- $\beta$ 1,4-Glc<br>(Lacto-N-tetraose)   | 1.0  | 9.7  | 5.5 | 4.2 | 0.94 |
| Temp. 287 K  |      |      |     |     |      |
| Lactose  | 0.61 | 9.7  | 5.0 | 4.7 | 0.94 |
| LacNAc-II  | 2.4  | 8.7  | 5.7 | 3.0 | 0.99 |
| Sia- $\alpha$ 2,3-Gal- $\beta$ 1,4-<br>GlcNAc<br>(2,3-Sialyl<br>LacNAc)  | 2.3  | 8.5  | 5.7 | 2.8 | 1.08 |
| Murine Recombinant Galectin-3 (Temp. 300 K)  |      |      |     |     |      |
| LacNAc-I   | 0.82 | 6.4  | 5.3 | 1.1 | 0.92 |
| LacNAc-II  | 1.9  | 7.5  | 5.9 | 1.6 | 1.01 |
| TDG  | 0.98 | 7.8  | 5.5 | 2.3 | 1.08 |
| DiLacNAc   | 3.5  | 8.8  | 6.2 | 2.6 | 1.07 |
| TriLacNAc  | 6.3  | 9.8  | 6.6 | 3.2 | 0.92 |
| Sia- $\alpha$ 2,6-Gal- $\beta$ 1,4-<br>GlcNAc (2,6-Sialyl<br>LacNAc)   | 3.2  | 9.7  | 6.2 | 3.5 | 0.98 |
| Lacto-N-tetraose   | 2.6  | 5.0  | 6.1 | 1.1 | 0.95 |
| Temp. 287 K  |      |      |     |     |      |
| LacNAc-II  | 3.7  | 9.7  | 6.0 | 3.7 | 0.95 |
| 2,3-Sialyl LacNAc  | 3.3  | 8.3  | 5.9 | 2.4 | 0.96 |
| Sia- $\alpha$ 2,6-Gal- $\beta$ 1,4-<br>GlcNAc- $\beta$ 1,3-Gal-<br>$\beta$ 1,4-Glc (2,6-<br>Sialyl Lacto-N-<br>neo-tetraose) | 2.1  | 6.4  | 5.6 | 0.8 | 1.05 |
| Sia- $\alpha$ 2,6-Gal- $\beta$ 1,4-<br>GlcNAc- $\beta$ 1,3-Gal-<br>$\beta$ 1,4-GlcNAc (2,6-<br>Sialyl DiLacNAc)              | 4.8  | 10.1 | 6.1 | 4.0 | 0.94 |
| GlcNAc- $\beta$ 1,3-Gal-<br>$\beta$ 1,4-Glc  | 0.88 | 7.7  | 5.2 | 2.5 | 0.96 |
| Human Recombinant Galectin-7 (Temp. 300 K)   |      |      |     |     |      |
| Lactose  | 0.22 | 10.6 | 4.6 | 6.0 | 1.03 |
| LacNAc-II  | 0.17 | 11.8 | 4.4 | 7.4 | 0.99 |
| Temp. 287 K  |      |      |     |     |      |
| TDG  | 0.4  | 10.0 | 4.7 | 5.3 | 1.08 |
| Lactose  | 0.49 | 10.5 | 4.8 | 5.7 | 1.02 |

|           |      |      |     |     |      |
|-----------|------|------|-----|-----|------|
| LacNAc-II | 0.63 | 11.3 | 5.0 | 6.3 | 1.07 |
| DiLacNAc  | 0.74 | 12.3 | 5.1 | 7.2 | 1.08 |
| TriLacNAc | 0.65 | 11.4 | 5.0 | 6.4 | 1.07 |

<sup>a</sup> Errors in  $K_a$  ( $1/K_D$ ) range from 1–7%; <sup>b</sup> errors in  $\Delta H$  are 1 to 4%; <sup>c</sup> errors in  $\Delta G$  are less than 2%; <sup>d</sup> errors in  $T\Delta S$  are 1-7%; <sup>e</sup> errors in  $n$  are less than 4%

The data in the table indicates that, in general, galectin-7 possesses weaker affinity for LacNAc as the primary epitope, relative to the other two galectins. For example, the  $K_a$  value for galectin-7 binding LacNAc-II is nearly 6-fold lower than the corresponding value for galectin-1 and nearly 11-fold weaker than that of galectin-3. There is little difference in the  $K_a$  values of galectin-1 for LacNAc-I ( $0.9 \times 10^4 \text{ M}^{-1}$ ) versus LacNAc-II ( $1.1 \times 10^4 \text{ M}^{-1}$ ). Galectin-3 also shows little difference in its  $K_a$  values for the two isomers. Galectin-1 and galectin-3 bind to TDG with nearly the same  $K_a$  values as LacNAc-II. The enthalpies of binding of galectin-1 to the two disaccharides are similar, as are the  $\Delta H$  values for galectin-3 binding the two sugars. the  $K_a$  values for DiLacNAc and TriLacNAc binding to galectin-1 are like that of LacNAc-II. The  $n$  values for all three carbohydrates, the number of binding sites per monomer of protein, are all close to one, indicating that all three oligosaccharides have 1:1 binding to subsite C in the protein. Galectin-7 possesses 6- to 11-fold weaker affinities for carbohydrates with LacNAc epitopes as compared to galectin-1 and galectin-3. Thus, galectin-7 differs in its carbohydrate binding specificity, in this regard, from galectin-1 and -3.<sup>57</sup>

Table 2 shows a summary of binding data for some of the ligands mentioned in Table 1 as determined by fluorescence polarisation assay. The Van der Waals interaction and the strength of the hydrogen bond involving the 2-position of the glucose/*N*-acetylglucosamine moiety represent the only significant differences between the Lactose and LacNAc complexes and presumably account for the approximately 3-fold higher binding affinity, shown by human galectin-3, for LacNAc over lactose. Galectin-1 participates in a water-mediated hydrogen bond involving the N-H of the GlcNAc moiety, meaning there is a difference in the way in which the water molecule is hydrogen bonded to the protein. Van der Waals interactions with the *N*-acetyl group are also important in galectin-1 binding, like galectin-3, it shows higher affinity for LacNAc over lactose.<sup>58</sup>

**Table 2: Dissociation constants ( $\mu\text{M}$ ) of natural ligands for galectins -1, -3 and -7 <sup>a</sup>.**

| Ligand                               | $K_D$ ( $\mu\text{M}$ ) |                         |                  |
|--------------------------------------|-------------------------|-------------------------|------------------|
|                                      | Galectin-1              | Galectin-3 <sup>b</sup> | Galectin-7       |
| Methyl $\beta$ -Galactose            | ~10000                  | 4400                    | 4800             |
| LacNAc-II                            | 70                      | 67                      | 490              |
| Methyl $\beta$ -Lactose <sup>c</sup> | 190                     | 220                     | 91 <sup>59</sup> |

|                           |             |                          |                            |
|---------------------------|-------------|--------------------------|----------------------------|
| Methyl $\beta$ -LacNAc-II | 65          | 59                       | 550                        |
| TDG <sup>d</sup>          | $24 \pm 11$ | $49 \pm 11$ <sup>e</sup> | $160 \pm 18$ <sup>60</sup> |

<sup>a</sup> Determined by a fluorescence polarization assay. <sup>b</sup> All ligands for Gal-3 evaluated at room temperature. <sup>c</sup> Methyl  $\beta$ -Galactose, LacNAc-II and Methyl  $\beta$ -Lactose for Gal-1 & Gal-7 evaluated at 4 °C. <sup>d</sup> Methyl  $\beta$ -LacNAc-II and TDG for Gal-1 & Gal-7 evaluated at 0 °C. <sup>e</sup> Average of 14 experiments provided basically the same  $K_D$  values but with improved data statistics as compared with previously reported data. <sup>61</sup>

## Conformational Analysis of Ligands and the Exo-Anomeric Effect

Detailed conformational analysis of ligands is one key aspect in determining the efficacy of a potent inhibitor. NMR is a powerful technique used to determine dihedral angles of adjacent protons in sugar molecules via the Karplus relationship (see Figure 9) and can give information on conformational preferences:

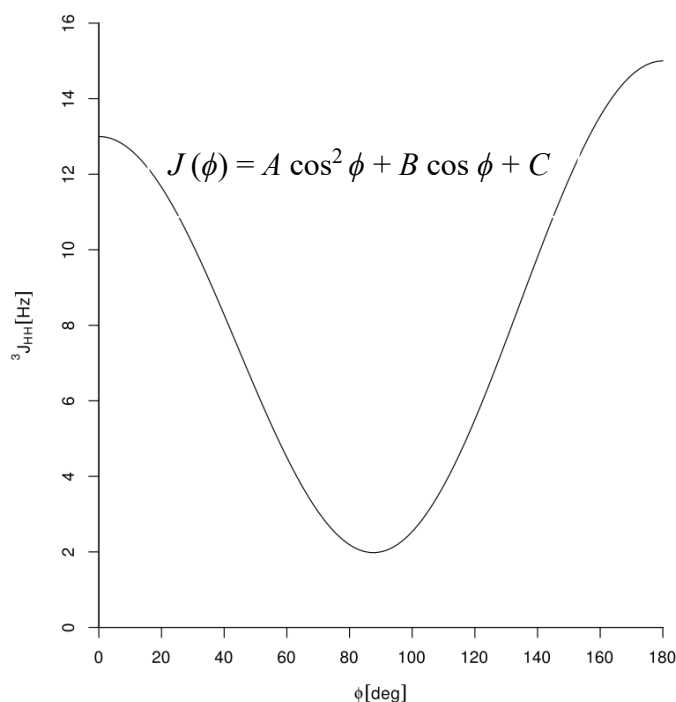


**Figure 9: Graph of the Karplus equation, where  $J$  is the  $^3J_{HH}$  coupling constant in Hz,  $\phi$  is the dihedral angle ( $^\circ$ ) and A, B, and C are empirically derived parameters whose values depend on the atoms and substituents involved.**<sup>62, 63</sup>

X-ray crystallography can complement NMR and ITC analysis, providing valuable information about 3-D structures of ligands and spatial parameters within the CRD of galectins, while giving a better understanding of (potential) protein-ligand interactions. Analysis of X-ray crystal structures of carbohydrate ligands in complex with galectins suggest that most *O*-disaccharides adopt an exo-syn conformation in the CRD. Analysis of  $\Phi$  (defined by H1'-C1'-O-C4 in lactose and  $\Psi$  (defined by C1'-O-C4-H4 in lactose) glycosidic torsion angles suggest

that a  $\Phi$  dihedral angle of  $\sim 60^\circ$  is observed in nearly every case. This is the most stable conformation of oligosaccharides in terms of their intramolecular steric and electronic repulsive interactions. Conformational flexibility/stability in *O*-disaccharides is believed to be influenced by the exo-anomeric effect, where stability results due to a lone pair of electrons anti-periplanar to the endocyclic O atom in the Newman projection (see Figure 10). In the exo-syn conformation there are less gauche and electronic repulsive interactions than the exo-anti and both are more stable than the non-exo.

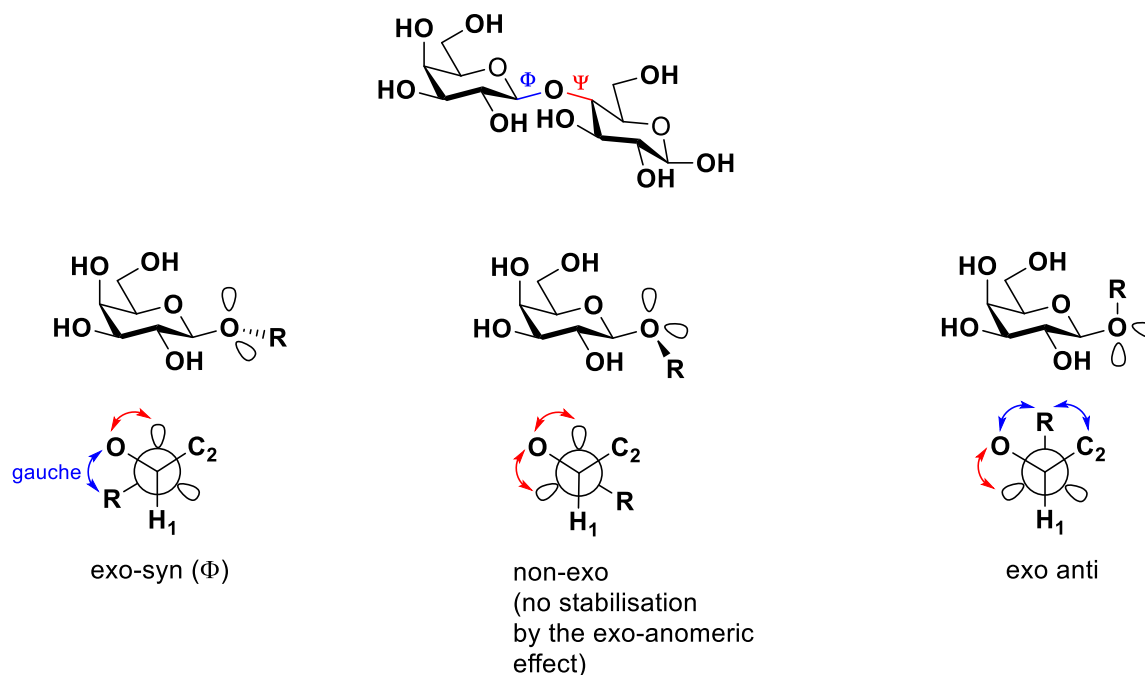


**Figure 10: Glycosidic torsion angles for conformations based on the  $\Phi$  angle in lactose**

For the  $\Psi$  angle an eclipsed conformation is preferred for lactose ( $\Psi \sim 0^\circ$ ) (see fig. 8)

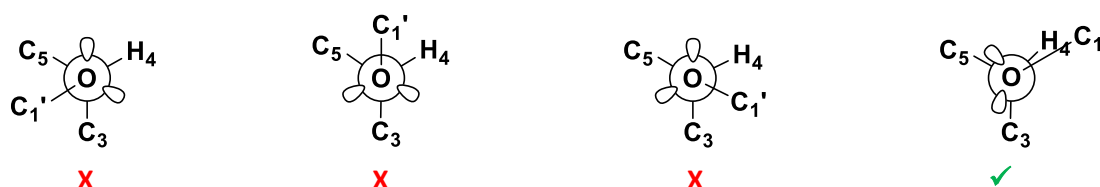


**Figure 11: Glycosidic torsion angles for  $\Psi$  angle in lactose**

Other important dihedral angles to consider in oligosaccharides are the  $\omega$  ( $O5-C5-C6-O6$ )<sup>64</sup> and  $\omega'$  ( $O'5-C'5-C'6-O'6$ ) torsional angles. Although three staggered rotamers are possible for

the  $\omega$ -angle [*gauche-trans* (*gt*) ( $\omega \sim 60^\circ$ ), *trans-gauche* (*tg*) ( $\omega \sim 180^\circ$ ) and *gauche-gauche* (*gg*) ( $\omega \sim 300^\circ$ )] (see Figure 12)

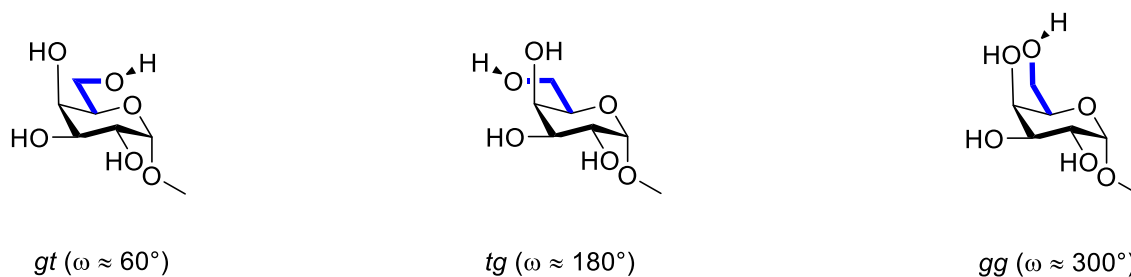


**Figure 12: The *gt*, *tg*, and *gg* rotamers of methyl- $\alpha$ -D-galactopyranoside<sup>64</sup>**

The conformational families about the C5-C6 bond display a bias for *gauche* orientations. The propensity for the  $\omega$ -angle to adopt *gauche* conformations in glucopyranosides has been attributed to the *gauche* effect. In structural terms, the *gauche* effect has been defined as the tendency for a molecule to adopt the structure that has the maximum number of *gauche* interactions between the adjacent electron pairs and/or polar bonds.<sup>64</sup> According to Woods et al, the *gt* rotamer is the preferred conformation for methyl- $\alpha$ -D-galactopyranoside, followed by *tg* and *gg* with rotamer populations of 47:39:14.<sup>64</sup> Table 3 provides examples from the literature where the  $\Phi$  (+g)  $\Psi$  (syn) and  $\omega$  (*gt*) torsional angles are consistent in a range of oligosaccharides binding to different proteins.

| Ligand  | Lectin     | Dihedral angle $\Phi$ ) H1-C1-O-C'X $\Psi$ )<br>H'X-C'X-O-C1 $\omega$ ) O5-C5-C6-O6<br>and $\omega'$ ) O'5-C'5-C'6-O'6 <sup>64</sup> |        |          |           | PDB<br>code | Conformation | Reference | Resolution | Method for<br>structure<br>determination | Method for<br>Obtaining Crystal |
|---------|------------|--|--------|----------|-----------|-------------|--------------|-----------|------------|--|---------------------------------|
|         |            | $\Phi$   | $\Psi$ | $\omega$ | $\omega'$ |             |              |           |            |  |                                 |
| Lactose | Galectin-3 | 54.06  | 8.5    | 61.3     | -65.8     | 3AYE        | gt           | 65        | 2.00       | x-ray                                    | Soaked Crystal                  |
| Lactose | Galectin-7 | 61.35  | 4      | 67.6     | -43.8     | 4GAL        | gt           | 66        | 1.95       | x-ray                                    | Soaked Crystal                  |
| TDG     | Galectin-1 | 62.25  | 18     | 63.2     | -16.9     | 3OYW        | gt           | 67        | 2.5        | x-ray                                    | Soaked Crystal                  |
| TDG     | Galectin-3 | 54.6   | 17     | 64       | 74.3      | 4JC1        | gt           | 68        | 1.5        | x-ray                                    | Soaked Crystal                  |
| LacNAc  | Galectin-3 | 52.62  | 12.3   | 65.3     | -71.7     | 1KJL        | gt           | 69        | 1.4        | x-ray                                    | Soaked Crystal                  |
| LacNAc  | Galectin-7 | 55.36  | 14     | 42.1     | -55.5     | 5GAL        | gt           | 66        | 2          | x-ray                                    | Soaked Crystal                  |

**Table 3: Dihedral angles of natural oligosaccharides in crystal structures.**



In the case of lactose with galectin-3<sup>65</sup> and -7,<sup>66</sup> a  $\Phi$  dihedral angle of  $54.2^\circ$  and  $61.4^\circ$  respectively can be seen. TDG, an *S*-disaccharide, in complex with galectin-1<sup>67</sup> shows a  $\Phi$  dihedral angle of  $62.2^\circ$  and  $54.6^\circ$  with galectin-3<sup>68</sup> (see Figure 13-Figure 15).

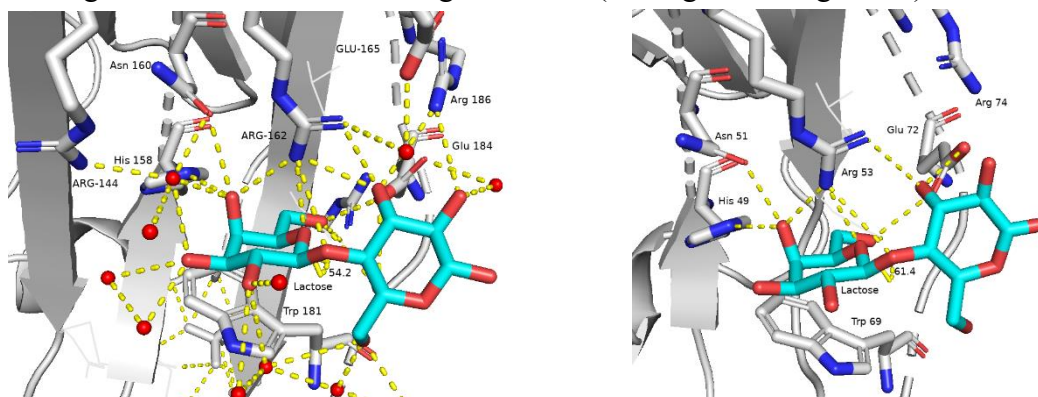


**Figure 13: Lactose in complex with CRD's of galectin-3 & galectin-7, exo-syn  $\Phi$  dihedral angles of  $54.2^\circ$  for galectin-3 and  $61.4^\circ$  for galectin-7 shown (PDB ID'S: 3AYE & 4GAL respectively)**

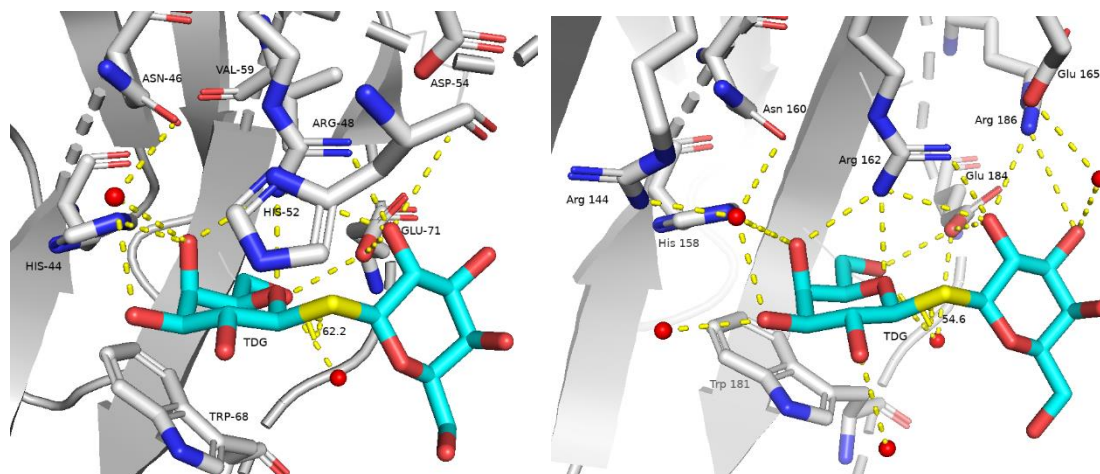


**Figure 14: TDG in complex with galectins -1 & -3 with  $\Phi$  dihedral angle of  $62.2^\circ$  for galectin-1 &  $54.6^\circ$  for galectin-3 shown. (PDB ID'S: 3OYW & 4JC1 respectively)**

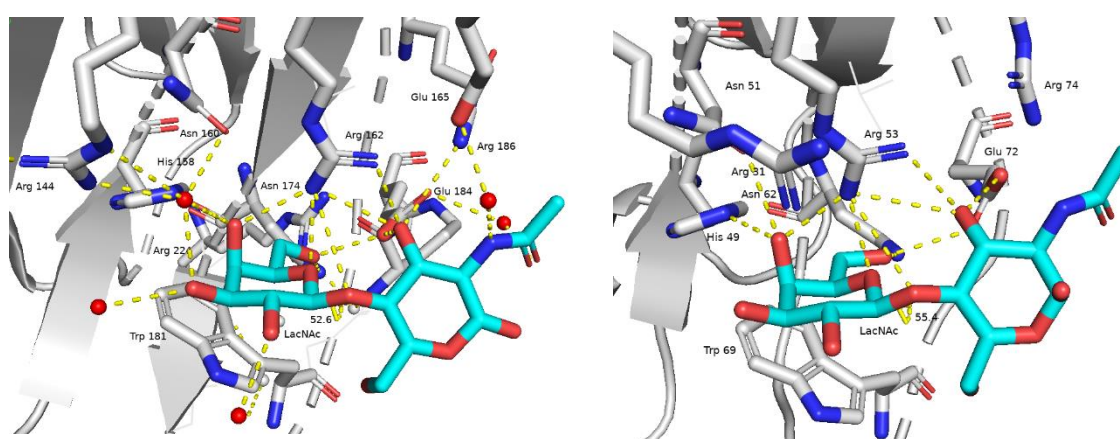


**Figure 15: LacNAc in complex with CRD's of galectin-3<sup>69</sup> & galectin-7,<sup>66</sup> exo-syn  $\Phi$  dihedral angles of  $52.6^\circ$  for galectin-3 and  $55.4^\circ$  for galectin-7 shown (PDB ID'S: 1KJL & 5GAL respectively)**

## Synthetic Modifications to Ligands- Development of Glycomimetics

In all the above examples, it is the motif amino acids from subsite C<sup>15</sup> (see Figure 7) that are involved in binding, proving the conserved nature of ligand binding and the orientation of amino acid residues in site C of the galectin CRD. The binding of a saccharide in site D is the second most conserved feature, but here the structure requirements for interaction are much less, hence the galectin specificity can vary, binding to lactose, TDG or LacNAc, among other saccharide ligands. Preference for one or the other of these is one source of variation in the specificity between galectins. Another major source of variation in specificity between galectins is their different ability to accommodate saccharides (eg. Sialic acid) or other functional groups (e.g. sulfate) in subsite B (and further extensions into subsite A). These are linked to the 3-OH of the galactose in subsite C and may strongly increase or decrease affinity. The structurally less defined Site E is included to summarize possible interactions with moieties linked at the reducing end of the saccharide in site D. Interactions in site E might help explain some proposed galectin binding activities that are not easily explained based on the properties of the well-defined sites A-D (see Figure 16).



**Figure 16: Artists Impression of subsites A-E of Galectin CRD. Reproduced with permission from ref<sup>15</sup>, Copyright © 2004 Kluwer Academic Publishers**

These features of galectins have enticed synthetic chemists to build upon or edit the structure of natural ligands in an effort to improve their binding affinity and produce more potent ligands as potential drug candidates. Mono- or oligosaccharides that are analogous to natural ligands but have some chemical modification made to their structure are called glycomimetics. Simple modifications to structure can result in vast improvements in binding data. As previously mentioned, modification of the 3-position of the galactose moiety in lactose- $\beta$ 1-*O*-*p*NP ( $K_D = 1.3 \times 10^{-4}$  M) with a sulfate group results in a 76-fold improvement in affinity for full length Galectin-8 ( $K_D = 1.7 \times 10^{-6}$  M) and a 68-fold improvement for Gal-8N ( $K_D = 1.9 \times 10^{-6}$  M).

Introduction of sialic acid at the 3-position results in a 54-fold improvement for full length Galectin-8 ( $K_D = 2.4 \times 10^{-6}$  M) and 48-fold for Gal-8*N* ( $K_D = 2.7 \times 10^{-6}$  M). Interestingly, no improvement is observed for Gal-8*C* in either case, suggesting that this increase in affinity is due to interactions with the *N*-domain. This was confirmed when the Gln47 residue of the *N*-domain was converted to Ala47. The specific affinity for sulfated or sialylated glycans was selectively lost, indicating that this Gln47 plays important roles for binding to Sia- $\alpha$ 2,3-Gal or SO<sub>3</sub><sup>-</sup>-3-Gal residues. These results were obtained using an ELISA and surface plasmon resonance assay.<sup>70</sup> Crystal structures compare the interactions between Lactose (PDB ID: 3AP4), SO<sub>3</sub><sup>-</sup>-3-Lac (PDB ID: 3AP6) and Sia- $\alpha$ 2,3-Lac (PDB ID: 3AP7) with Gal-8*N*. In the SO<sub>3</sub><sup>-</sup>-3-Lac complex, the residues involved in lactose recognition are nearly identical to those in the galectin-8*N*-lactose complex, and 4 residues are involved in sulfate recognition. Of the 3 oxygen molecules in the sulfate, O2S and O3S hydrogen bond directly with the protein. The O3S is positioned such that it directly hydrogen bonds with Arg45, Gln47, and Arg59, whereas O2S only hydrogen bonds with Arg59. Water molecules (W2 and W3) are well conserved in the SO<sub>3</sub><sup>-</sup>-3-Lac complex as in the lactose complex; however, W1 is substituted with O3S of the sulfate. Gln47 and Arg59 are important for sulfate recognition because the distance between these elements is short enough to permit interactions. Trp86 interacts with OS2 through W2-mediated hydrogen bonding. W2 is located at almost the same position as in the lactose complex and O1S forms a W3-mediated hydrogen bond with Gln47. W3 exists in all 4 molecules of the asymmetrical unit and W1, which is conserved in all lactose complexes, is substituted with O3S. Gln47 and Arg59 are important for sulfate recognition because they are located at a short distance from the ligand and are unique to galectin-8*N*, hence substitution of Gln47 with Ala resulted in selective loss of affinity.

In the Sia- $\alpha$ 2,3-Lac complex, the residues involved in lactose recognition are almost the same as those in the lactose complex, and the terminal sialic acid-recognizing residues are very similar to those involved in sulfate recognition. Only the carboxylate in sialic acid interacts directly with galectin-8*N* amino acids, forming hydrogen bonds with Gln47, Arg59, and Trp86. Of these, Arg59 forms 2 independent hydrogen bonds, suggesting that Arg59 is important for sialic acid recognition. Gln47 forms water mediated hydrogen bonds with the oxygen atom (O11) of the sialic acid moiety.<sup>71</sup>

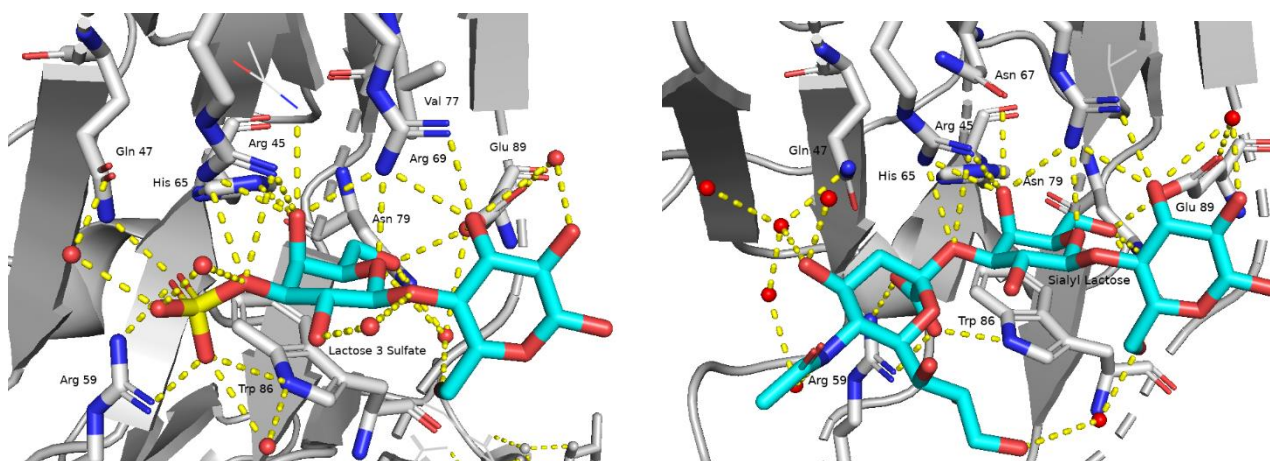


**Figure 17: Comparing H-bonding pattern in 3'-substituents in SO<sub>3</sub><sup>-</sup>-3-Lac & Sia- $\alpha$ 2,3-Lac (PDB ID'S: 3AP6 & 3AP7) respectively.**

The 3-position modifications are a common feature in the development of galectin inhibitors, particularly in the case of galectin-3. Although the identity and conformation of residues involved in binding the Lactose/LacNAc moiety in the primary binding site of galectin-1 and galectin-3 are very similar, they differ in the vicinity of the galactose O3. Galectin-3 has an arginine residue at position 144 which is well positioned to interact with other saccharide residues, or any functionality linked to the galactose O3. The serine found in galectin-1 is presumably unable to make similar interactions. In addition, the bulky leucine residue at position 31 in galectin-1 is reduced to an alanine (Ala-146) in galectin-3, creating an extended groove towards subsite B with more space for O3 substituents,<sup>58</sup> which would point directly into this groove, towards the arginine. By using this structural knowledge of the galectin-3 carbohydrate recognition site, Nilsson et al began a strategy for generating potential galectin inhibitors based on derivatization at the C-3' atom in 3'-amino-LacNAc. Derivatization of this position with diverse structural extensions was an attractive strategy for creation of additional favourable interactions with the protein and for discovery of high-affinity inhibitors for galectin-3. In 3'-amino-LacNAc, the 3-OH is replaced by an amino group, a versatile handle for the introduction of a wide variety of functional groups.<sup>72</sup> Amide coupling of aromatic acyl halides with the 3-NH<sub>2</sub> provided the most potent inhibitors, with a *p*-methoxy-tetra fluoro substituted benzamide (see Figure 18) averaging an IC<sub>50</sub> value of 4.4  $\mu$ M over three ELISA experiments.<sup>72</sup> This inhibitor was about 50 times more potent than the parent LacNAc derivative.

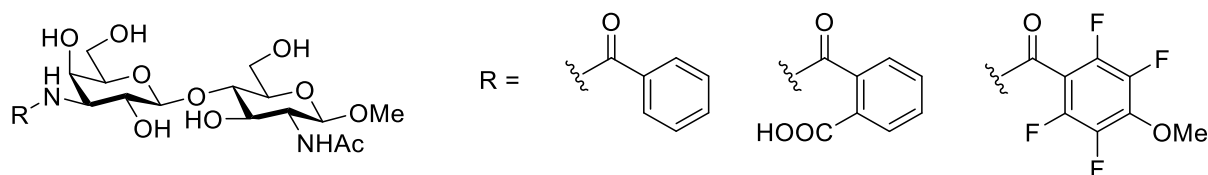


**Figure 18: Most potent 3-substituted aromatic LacNAc derivatives**<sup>72</sup>

Analysis of the *p*-methoxy-2,3,5,6-tetrafluorobenzamido- substituted LacNAc in complex with galectin-3 showed the benzamide substituent in the extended site as expected. Upon binding, a significant ligand induced conformational change occurred in the structure of galectin-3C, the monomeric C-terminal carbohydrate domain of galectin-3, where the side chain of Arg144 was moved 3.5 Å to interact with the benzamido ring in a cation- $\pi$  interaction. In the complex with LacNAc, the Arg144 guanidino group was involved in a H-bond with water molecules at the galectin-3C surface. The four fluorine atoms on the aromatic ring would be expected to withdraw electron density away from the phenyl, making it a relatively poor  $\pi$  electron system and thereby weakening the cation- $\pi$  interaction. However, a number of other factors must be considered to influence the affinity, such as  $\pi$ - $\pi$  interactions, charge-transfer, desolvation effects and electrostatic interactions of the methoxy group situated close to the guanidino group of Arg144.<sup>69</sup> The fluorine substituents on the C5 and C6 atoms of the aryl ring have dipolar C-F $\cdots$ H-N and C-F $\cdots$ C=O interactions with the side chain amide of Asp160.<sup>73</sup> A series of fifty-five 3'-C aromatic substituted LacNAc derivatives were synthesised and tested in a Competitive Fluorescence Polarization Assay. Results from the assay suggested that *para* and *meta* substitutions on the aromatic rings improve affinity, while *ortho* substitution was a hindrance. Four compounds stood out with better results than the *p*-methoxy-2,3,5,6-tetrafluorobenzamide, their structures can be seen in Figure 19.

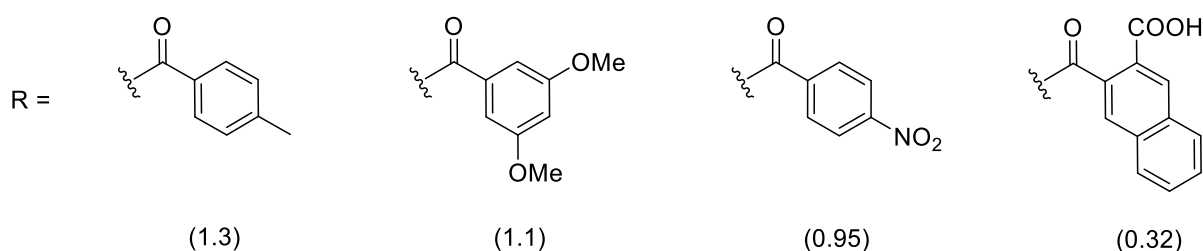


**Figure 19: Structures of aromatic 3-LacNAc substituents with improved affinity,  $K_D$  values ( $\mu\text{M}$ ) from FP assay with Gal-3 shown in brackets.**

The nitro-substituent is predicted to extend the  $\pi$ -system of the benzamide closer to Arg144, leading to an improved interaction with the guanidine group. Although one of the methoxy groups would point into bulk solution in complex with the protein, two symmetrically placed

methoxy groups are entropically favourable, because two degenerate conformers of the disubstituted *m*-methoxy ring would interact with galectin-3 with the same enthalpic contribution. The best result of the series was due to the larger more polarisable aromatic system of the substituted naphthalene ring which filled the hydrophobic cleft lined by Arg144 and resulted in better affinity due to the formation of a stronger cation- $\pi$  interaction with the guanidine group. The *ortho*-carboxy substituent on the naphthalene provided a means of increasing the solubility of the inhibitor.<sup>69</sup> Protein conformational entropy plays a significant role in protein-ligand interactions, through favourable contributions to the free energy of ligand binding.<sup>73</sup> A combination of NMR spectroscopy, ITC, and X-ray crystallography was used to study the energy of interactions between galectin-3 and free lactose, 3-benzamido-LacNAc- $\beta$ 1-OCH<sub>3</sub> and 3-(*p*-methoxy-2,3,5,6-tetrafluoro)-benzamido-LacNAc- $\beta$ 1-OCH<sub>3</sub> (see Figure 18). NMR relaxation provided information on the conformational flexibility of the protein complexes and the associated entropic contributions to the free energy of binding. It was used to verify that the flexibilities of both the ligand and the protein play significant roles in modulating the binding interactions in solution<sup>73</sup> and agreed with interactions observed in the crystal structures. Since no residues outside of the confirmed binding site (identified by crystallography) had significant backbone or side-chain chemical shift perturbations ( $\Delta\delta > 0.05$  ppm), it was confirmed that all the ligands bind to the same site.<sup>73</sup> ITC was used to characterize the thermodynamics of ligand binding. The ITC data were adequately fit to a single-site model for the binding of each ligand to Gal-3C, as expected from the NMR and X-ray data. Although a change was observed in the  $K_D$  values measured by ITC, the relative affinities remain consistent with those previously determined by FP.<sup>69</sup> For all three ligands, binding is driven by a large enthalpic contribution ( $\Delta H^\circ < 0$ ) but is entropically disfavoured ( $-T\Delta S^\circ > 0$ ) in keeping with previous results for other ligands.<sup>60, 69, 73 74</sup>

Building on these results, Nilsson proceeded to investigate TDG as a scaffold for inhibitor development, as TDG is known to have 1.6 fold better activity towards galectin-3 compared to LacNAc.<sup>75</sup> The 3-OH's in both galactose moieties of TDG were replaced by amino groups to incorporate functionality. Introduction of a phenyl amide at the 3- and 3'- positions resulted in a ~2-fold improvement (3  $\mu$ M) relative to the corresponding LacNAc derivative (6.7  $\mu$ M). This improvement is due to an additional cation- $\pi$  interaction with Arg186 in subsite D. A small number of substituted aromatic rings (see Figure 20) were subsequently investigated based on the results from ref<sup>69</sup>. The results were consistent with the previous study,<sup>69</sup> where di *m*-



methoxy and *p*-nitro substituents gave a 60 fold (50 nM) and ~91 fold (33 nM) improvement compared to the phenyl amide respectively.<sup>75</sup>

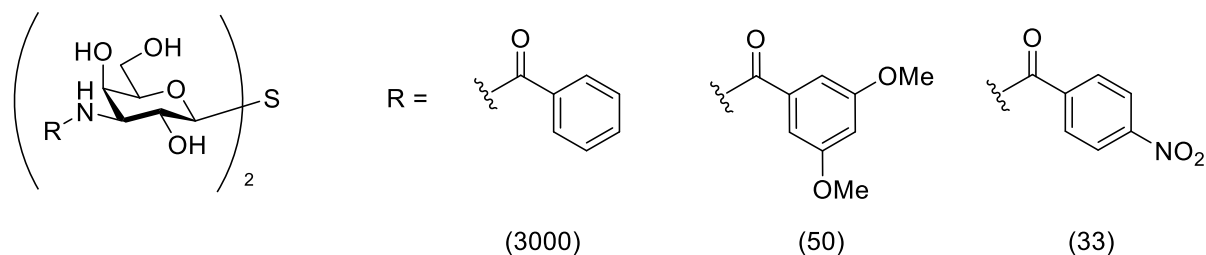


**Figure 20: TDG derivatives with  $K_D$  values (nM) from FP assay with Gal-3 shown in brackets.**

A series of ten mono-, unsymmetrical and symmetrical TDG 3- and 3'-diamides were evaluated for binding to address the specific interactions of Arg144 and Arg186 from galectin-3 and the corresponding residues in galectin-1, -7, -8*N*, and -9*N*.<sup>60</sup> An investigation into selective binding of the two residues allowed for tuning of ligand structure to give the best interactions. The absence of an arginine residue in galectin-1 in the vicinity of C3 in the galactose moiety of lactose or LacNAc meant very little enhancement was observed for ligands with aromatic functionality at this position relative to the unsubstituted reference LacNAc-OCH<sub>3</sub>. An enhancement was seen for reference lactose derivatives with aromatic esters at the 2-position of glucose, which corresponds to the 3'-position of TDG, suggesting that cation- $\pi$  interactions with Arg73 in galectin-1 (analogous to Arg186 in galectin-3) define the affinity. An expected trend was observed in the FP results for galectin-3, where the disubstituted 3- and 3'-diphenyl amide TDG gave the strongest inhibition (1.7  $\mu$ M) followed by the monosubstituted (3.2  $\mu$ M) followed by the reference unsubstituted TDG (49  $\mu$ M). Analysis of the binding modes of mono- and disubstituted ligands in the series suggest that Arg144 and Arg186 have binding preferences for different aromatics. Naphthyl- and 3,5-dimethoxybenzamide were found to give the best interactions with Arg144 and Arg186 respectively. These results were confirmed with low energy complexes obtained via computational methods.<sup>60</sup>

Nilsson and co-workers decided to replace amide couplings with 1,3-dipolar cycloaddition reactions to introduce functionality at the 3-position. These reactions, as initially proposed by Huisgen in 1969,<sup>76, 77</sup> involved the concerted formation of 5-membered heterocycles from a 1,3-dipole and a dipolarophile. This transformation required elevated temperature and, when using asymmetric alkynes, often produced mixtures of 1,4- and 1,5-regioisomers. The introduction of a copper(I) catalyst by Sharpless<sup>78</sup> and Meldal<sup>79</sup> lead to accelerated reaction

rates and regioselectivity, exclusively producing the 1,4-disubstituted-1,2,3-triazole. These reactions are advantageous from a synthetic perspective, given their easy synthesis, high stability, the mild conditions required, and versatility of alkynes used, without the need for either complex reagents or anhydrous conditions. A series of 3-substituted methyl- $\beta$ -thiogalactoside derivatives were developed. The unsubstituted triazole ring in the 3-position decreased inhibitory potency, giving lower affinity values in the FP assay than the parent  $\beta$ -Galactose. However, substitution at the C4 position of the triazole proved to enhance the affinity, with these affinity-enhancing effects surpassing the affinity-decreasing effects of the triazole ring by itself. Figure 21 shows the best three compounds from this study.<sup>80</sup>

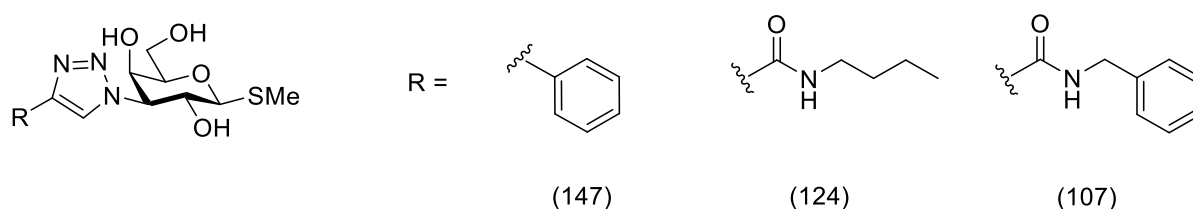


**Figure 21:  $\beta$ -Thiogalactoside derivatives with  $K_D$  values ( $\mu\text{M}$ ) from FP assay with Gal-3 shown in brackets.**

Replacing the  $\beta$ -thiogalactoside with an analogous TDG scaffold, while using the phenyl and butylamide substituents seen in Figure 21 resulted in compounds with  $K_D$  values of 44<sup>81</sup> and 29 nM<sup>82</sup> respectively for galectin-3. The phenyl compound also gave strong results for galectin-1, with a  $K_D$  value of 13 nM.<sup>81</sup> Modelling studies of a bulkier 4-phenoxyaryl substituent on the triazoles of TDG were performed to try and gain an insight into discrepancies in  $K_D$  values between galectin-1 and -3, with a 200-fold preference for the bulky aromatics being shown for galectin-3. Computational analysis suggested the ligand participated in three arginine-arene interactions with galectin-3 vs. one for galectin-1, while steric hindrance was also thought to be a factor.<sup>81</sup> Some of the other compounds to perform well in the galectin-3 FP assay included C4 triazole substituents of a methyl amide, propanolamide and a methoxyethamide, which gave  $K_D$  values of 120, 120 and 250 nM respectively (see Figure 22).<sup>82</sup> Conformational analysis of some 1,5-disubstituted triazoles via NOE and modelling studies suggested steric clashes occur between C5 triazole substituents and the conserved tryptophan residue at the  $\alpha$ -face of the sugar, blocking any potential CH- $\pi$  interactions with the sugar ring.



These clashes explain the relatively poor performance of ligands with substitution at this position.<sup>82</sup>

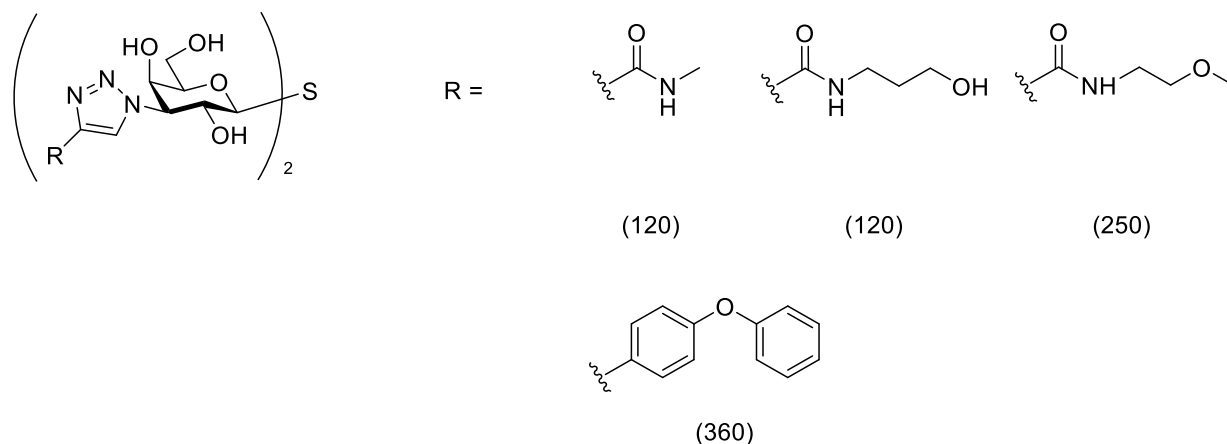


**Figure 22: 3,3'-Ditriazolyl TDG derivatives with  $K_D$  values (nM) from FP assay with Gal-3 shown in brackets.**

To date, among the most potent inhibitors developed in the Nilsson laboratory include 3,3'-bis-(4-haloaryl) and 3,3'-Bis-(4-heteroaryl)(triazol-1-yl)thiodigalactosides. Some of these inhibitors have reached single digit nM affinity and high selectivity for galectins. One selected compound, **GB 0139** (also known as TD139, see Figure 25) is currently involved in phase IIb clinical trials<sup>83</sup> and was demonstrated to function intracellularly in an amitriptyline-induced vesicle damage assay and to reduce fibrosis levels in a murine bleomycin lung fibrosis model.<sup>84</sup> From the series of nine aryl compounds made, 3- (2-3 nM)<sup>83</sup> and 4-fluorophenyl (34 nM) compounds turned out to be the only ones better than the unsubstituted phenyl compound and the 2-fluorophenyl (190 nM) derivative. The substitution position preference of the fluorophenyl derivatives agreed with the pattern meta > para > ortho from ref<sup>69</sup>. The thiophen-3-yl derivative seemed to show selectivity for galectin-1 with a  $K_D$  value of <10 nM. This is a sharp contrast to the 4-phenoxyaryl substituent previously discussed for galectin-3.<sup>81</sup> X-ray structures of the high-affinity 3-fluorophenyl, 4-fluorophenyl and thiophenyl derivatives in complex with galectin-3 proved that the TDG core of each of the ligands is in an identical binding mode to that observed in a previously reported galectin-3 TDG complex.<sup>68</sup> For all three ligands, a conformational change is induced in Arg144 similar to that already mentioned for the *p*-methoxy-2,3,5,6-tetrafluorobenzamido- substituted LacNAc.<sup>69</sup> For each ligand, the terminal ring sits into a pocket to participate in cation- $\pi$  interactions with the arginine residue. The 3-triazole linkers allow the rings to extend deeper into the pocket than the previous amide linkers, allowing more contacts with Ala146. For the 3-fluorophenyl, the fluorine is involved in multipolar interactions with the backbone carbonyl groups of Arg144 and Ile145. The

fluorine in *p*-fluorophenyl is directed towards Gly238 and Ser237 and contacts the  $\alpha$ -carbon of Gly238. An orthogonal dipolar interaction is also suggested with the Ser237 carbonyl group, due to the proximity. The second thiophene or fluorophenyl rings of the ligands are positioned above the salt bridge between Glu165 and Arg186. Although this interaction is poorly defined by the differences in electron density maps, the positioning of hydrophobic aromatic moieties close to salt bridges has been demonstrated in previous modelling studies to significantly enhance the salt bridge strength.<sup>85</sup> In galectin-3, Arg186 forms ion pairs with carboxylates from Glu165 and Glu184. The resulting  $\pi$ -electron surface from this interaction means no H-bonding with the surrounding media is required, as all H-bonding atoms are already coordinated. There will therefore not be a large entropic penalty by expelling hydrogen-bonded water molecules when ligands approach the binding site.<sup>86</sup> The interaction involves face-to-face stacking between the aryl triazole units and an extended surface of the  $\pi$ -system of the Glu165–Arg186 ion pair, which could allow for the aryl triazole units to position themselves over different segments of the large  $\pi$ -system with retained free energies of interaction.<sup>84</sup> The triazole rings located above His158 are each orientated with the nitrogen atoms positioned towards Trp181, allowing the formation of a water-mediated hydrogen bond between N2 of the triazole and the nitrogen atom of Trp181. The triazole rings of the ligands located near the in-plane Glu165–Arg186 salt bridge show two alternate conformations that stack face-to-face to the salt bridge. In the complexes with the thiophene and *p*-fluorophenyl derivatives, the triazole nitrogen atoms are directed towards Glu165. The orientation of one of the triazole rings in these cases results in contacts with both Glu184 and Arg186. In the complex with the 3-fluorophenyl, the ring is flipped, with the triazole nitrogen atoms close to Arg186, exclusively in contact with this residue.<sup>84</sup>

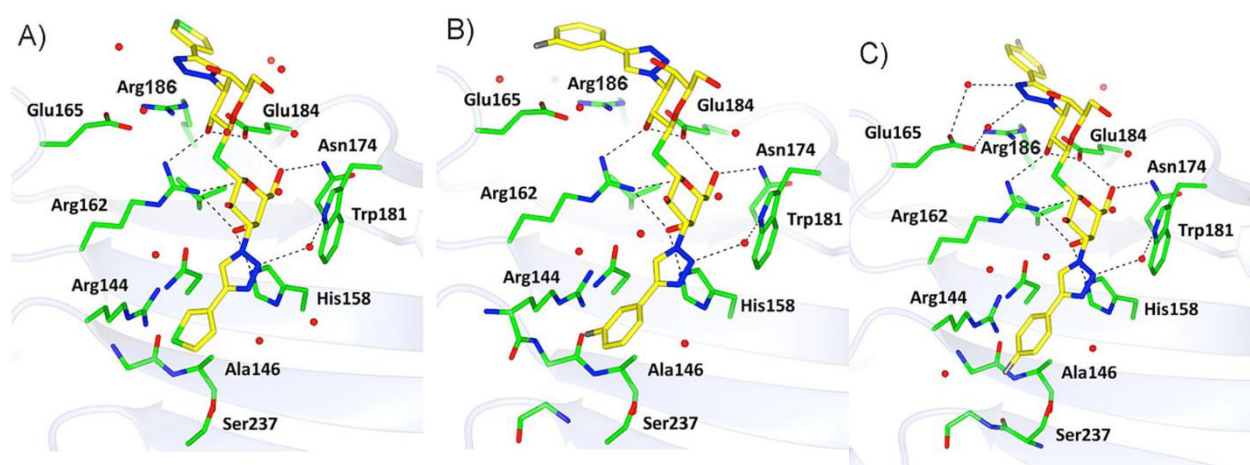


**Figure 23: Comparing the orientation of aromatic moieties in the TDG derivatives with Galectin-3 CRD.** Reproduced with permission from ref<sup>84</sup>, Copyright © 2016 WILEY-VCH Verlag GmbH & Co. KGaA, Weinheim

To optimize and study the glycoside cluster effect, Nilsson moved on from monovalent methyl- $\beta$ -thioglycosides to investigate lactose as a multivalent scaffold for a number of galectins. An ethyl azide was incorporated at the glycosidic oxygen of the glucose moiety as a linker, which was clicked to a few polyfunctional derivatives of unnatural amino acids such as phenyl-bis-alanine and phenyl-trisalanine (see Figure 24). The amino acids were functionalized by peptide couplings with acetylene groups for coupling with the sugar azides. Dissociation constants were determined for the synthesized ligands with galectin-1, -3, -4N, -4C, -4, -7, -8N and -9N by competitive fluorescence polarization. A pattern was observed in the structure of the linkers for galectin-1 inhibition, where a longer carbamate gave relatively more potency than its amide linker analogues. Interestingly, this effect was not seen in the other galectins. It is believed that the potency in the divalent molecules was due to cross-linking of two separate galectin-1 molecules leading to aggregation.<sup>87</sup> The divalent carbamate structure had a  $K_D$  of 3.2  $\mu$ M against galectin-1, reflecting a promising selectivity as this  $K_D$  was one order of magnitude or more lower than for any other galectin investigated.<sup>88</sup>

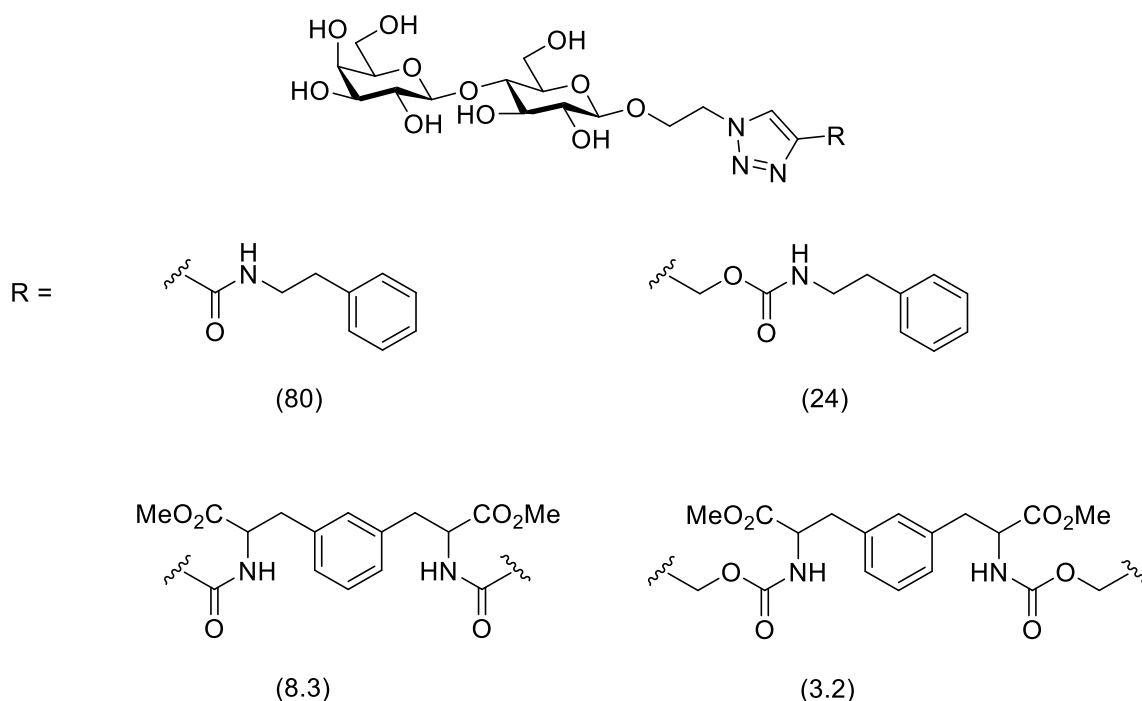


**Figure 24: Lactose derivatives with mono- and divalent ligands.  $K_D$  values ( $\mu$ M) from FP assay with galectin-1 shown in brackets.**

2-positions modifications were explored when Nilsson reasoned that the 2-position of the glucose moiety of lactose corresponds to the position of the *N*-acetyl group in LacNAc, or alternatively, the 3'-position of TDG, as already explored in ref. <sup>75</sup>. Functionalisation of lactose with 2-*O*-aromatic esters would orientate these substituents in a manner similar to those observed in the previously described TDG and LacNAc derivatives,<sup>72, 75</sup> resulting in compounds that can form beneficial interactions with the conserved arginines of galectins -1, -3, -7, and -9*N*.<sup>86</sup> The aromatic lactose esters showed the highest affinity enhancement for galectin-3. This enhancement is due in part to the beneficial interactions between the ester  $\pi$ -systems and the arginine guanidinium groups. All the aromatic esters had large increases in affinity giving a 25 to near 100-fold improvement over the reference lactose- $\beta$ 1-OCH<sub>3</sub>. A naphthoate giving the best results of the series for galectin-3 ( $K_D = 2.5 \pm 0.5 \mu\text{M}$ ) is consistent with the results observed in ref. <sup>69</sup>, although modelling studies revealed that in the conserved binding mode of galactose, the 2-*O*-naphthoate points towards Arg186 rather than Arg144. The previously described  $\pi$ -electron 'lid' effect between Arg186 and carboxylates from Glu165 and Glu184<sup>86</sup> is very important in the binding of 2-*O*-aromatic esters by galectin-3. This was proven when Arg186 was replaced with a serine, resulting in a decrease in affinity for all ligands in the series compared to the wild type protein.<sup>86</sup>

After discovering that C3- multifluorinated phenyl groups provided orthogonal multipolar fluorine–amide interactions which strongly enhanced affinity for galectin-3,<sup>84, 89</sup> development of a monosaccharide ligand that replaces the monosaccharide at the reducing side of galactose with a less polar aglycon with similar affinity and selectivity values to the TDG compounds became a goal of Nilsson and co-workers. Although **GB 0139** has outstanding affinity and specificity results for galectin-3, one drawback as a potential drug candidate is its route of administration. Inhalation is necessary as **GB 0139** has limited oral bioavailability due to its high polarity.<sup>90</sup> Efforts to develop a less polar oral galectin-3 inhibitor via derivatization of galactose, which already interacts with sidechains via multiple H-bonding and CH- $\pi$  stacking with aromatic amino acids, with unnatural structural elements that form multiple non-natural lectin–ligand interactions (orthogonal multipolar fluorine–amide, phenyl–arginine, sulfur- $\pi$ , and halogen bonds) provided inhibitors with low nanomolar affinity and high selectivity for galectin-3. Through much trial and error, a successful compound was developed (see Figure 25). Replacement of the galactose with a tolyl moiety resulted in micromolar affinity for galectin-3, however, this was a major decrease in affinity relative to the disaccharide. Epimerisation of the  $\beta$ -thiotolyl to the  $\alpha$ -anomer had a sixteen-fold enhanced affinity over the

corresponding  $\beta$ -anomer. The anomeric sulfur atom of the  $\alpha$ -galactoside is positioned near Trp181, suggesting a beneficial sulfur- $\pi$  interaction<sup>91, 92</sup> not shared by the  $\beta$ -galactosides. The anomeric *O*-analogue shows a relative decrease in affinity as no such interactions take place with the oxygen. Replacing the toluene with a phenyl ring provided a scaffold to investigate the influence of aromatic halogen substituents. The 3-chloro-phenyl substituent enhanced affinity for galectin-3 by ~six-fold relative to the  $\alpha$ -tolyl, leading to a  $K_D$  ~50 nM. Introduction of 4-chloro next to the 3-chloro group enhanced affinity further, giving a  $K_D$  of 37 nM. Due to the length and angle of the C-S bond, the 3-chloro substituent on the aromatic ring has the direction and position expected to form a halogen bond with the backbone carbonyl oxygen of Gly182 in the protein. The 4-chloro group points out in solution and cannot form a halogen bond with the protein, thereby unable to enhance affinity by itself. Introduction of electron withdrawing groups on the aryl aglycon enhances affinity due to its electron withdrawing effect, increasing the electropositive character of the halide  $\sigma$ -hole. Substitution at the 4-position is beneficial as there are no clashes with the protein surface, as are seen with 2-substitution and reflected in the affinity.<sup>93</sup>

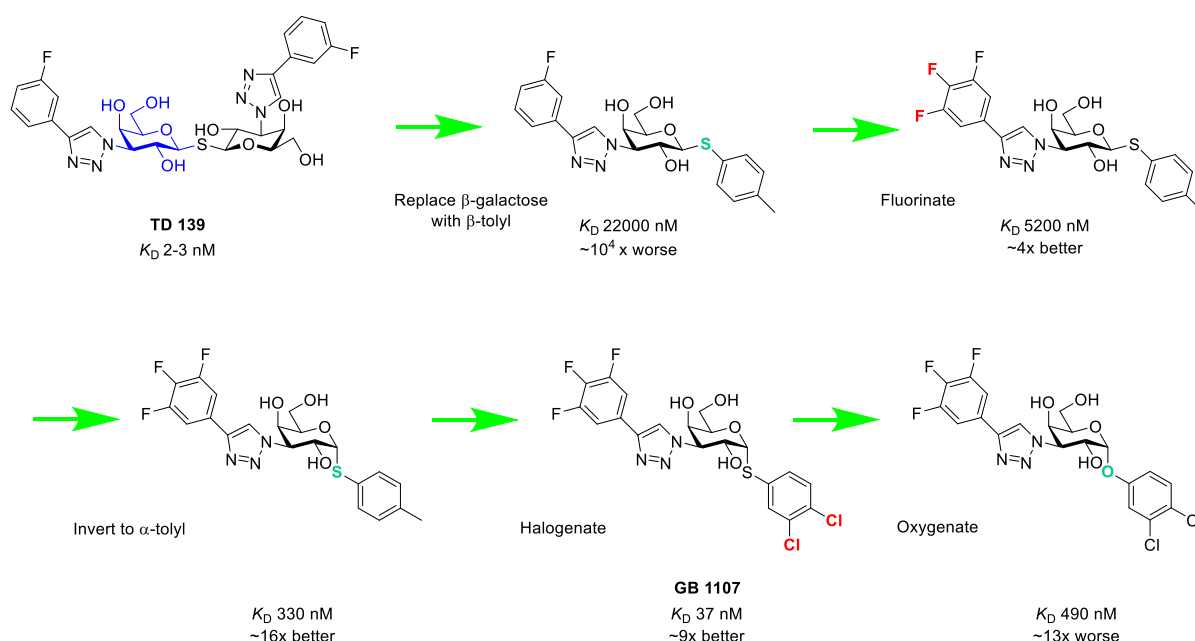


**Figure 25: Changes made to GB 0139 structure to identify the nM affinity monosaccharide ligand GB 1107.**

A strong monosaccharide drug candidate was developed in **GB 1107**, so development of additional analogues was subsequently performed aiming at optimizing the specific interactions while balancing polarity and lipophilicity. In vitro stability of four monosaccharide

derivatives, **GB 1107** and three other aryl aglycons were evaluated in human and mouse hepatocytes and pharmacokinetic properties of these compounds were assessed in mice following a single oral or intravenous administration.<sup>90</sup> A slight improvement in affinity was observed for **GB 1211** (25 nM), a structural analogue of **GB 1107** with a 5-bromo-3-pyridyl ring replacing the 3,4-dichlorophenyl moiety. Although there is not a drastic improvement in affinity, the lipophilicity range spans almost 2 log units (3–4.6), with **GB 1211** combining the highest affinity with the lowest lipophilicity; thus, **GB 1211** has the highest lipophilic efficiency. This suggests that lipophilicity is not the major contributor to affinity for this series of compounds. In vivo mouse clearance differed between the two compounds, with **GB 1211** having a 10-fold higher clearance than **GB 1107**, as well as relatively higher hepatic stability and a more favourable in vitro safety panel, resulting in its selection as a potential clinical candidate. **GB 1211** was found to be well tolerated in healthy subjects and is currently in clinical development as a novel, orally active therapy for liver fibrosis and cancer.<sup>90</sup>

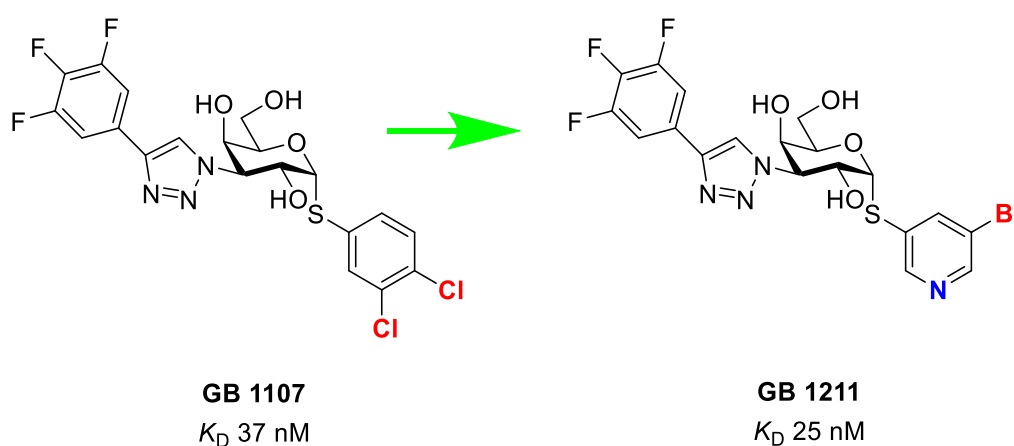


**Figure 26: Improvement in affinity for galectin-3 and pharmacokinetic profile going from GB 1107 to GB 1211**

The X-ray structure of **GB 1211** cocrystallized with human galectin-3 C-terminal domain (PDB ID 7ZQX) suggest a virtually identical ligand pose and interaction pattern to that of **GB 1107**.<sup>90</sup>

## Incorporation of Conformational Constraint into Glycomimetics

For pseudodisaccharides to be biologically useful, one of the requirements is that their conformational behaviour should be analogous to that of the natural compound, in order to minimize entropic costs of the recognition process when binding with the receptor.<sup>94</sup> Despite the exo-anomeric effect, which strongly influences the conformational preferences around the glycosidic linkages, binding events usually takes place with a loss of conformational entropy, especially for the ligand and as a consequence, large entropic penalties are generally observed.<sup>95</sup> It is important to determine how the synthetic derivatives are affected by such factors. The C-S bond length (1.78 Å) and C-S-C bond angle (99°) strongly differ from the values for C-O (1.41 Å) and C-O-C (116°). On the other hand, the C-N distance and C-N-C bond angle values are 1.47 Å and between 116.5-119.6°. In *S*- and *C*- analogues, the anomeric oxygen has been replaced by a sulfide- and methylene group respectively, with *C*-glycosides providing stability toward acid conditions.<sup>96</sup> However, the striking geometry differences between natural saccharides and their *C*-glycosyl analogues, owing to the differences in bond lengths and angles, as well as the lack of exo-anomeric effect which has little or no influence on *S*- and *C*-glycosides, results in higher flexibility than *O*-glycosides. Molecular modelling and NMR studies carried out by Montero et al.<sup>94</sup> investigated the conformational behaviour of *S*-lactose with respect to its *O*-analogue. They found that the global minima of *S*-lactose adopt exo-anomeric conformations around  $\Phi$  but the orientations around the aglyconic bond  $\Psi$  are different between *S*- and *O*-glycosyl compounds. The major conformer for *O*-glycosides is always centred at the syn- $\Psi$  region. However, for *S*-lactose, the anti-conformer is predominant. It is also noteworthy to emphasize the participation of anti-  $\Phi$  conformers for *S*-lactose, with a torsional variation of 120°, which is very unusual for  $\beta$ -*O*-glycosides.

Espinosa et al.<sup>97</sup> studied the conformations of  $\beta$ -1,3-linked lactose and its *C*-glycosyl derivative and found that binding to human galectin-1 selectively occurs in the syn- $\Phi$ / syn- $\Psi$  conformer, despite the global minimum of the *C*-disaccharide displaying an anti  $\Psi$  orientation. The orientation of the syn- $\psi_{(+)}$  conformer of the *C*-glycosyl analogue within the galectin-1 binding site is basically identical to that for the *O*-glycoside and lactose.<sup>98</sup> Potential energy maps were calculated for both compounds. The distribution map of the *C*-disaccharide (see Figure 27) predicted the presence of five low-energy conformations, suggesting that binding of the synthetic *C*-glycosyl molecule takes place with a conformational selection process, since binding of the *O*- and *C*-glycosides take place at the same binding site. These results are in

contrast with the predictions for the natural *O*-glycoside, for which about 98% of the population was located in the central low-energy region represented by the *syn*- $\Phi$ /*syn*- $\Psi$  global minimum.<sup>98</sup>

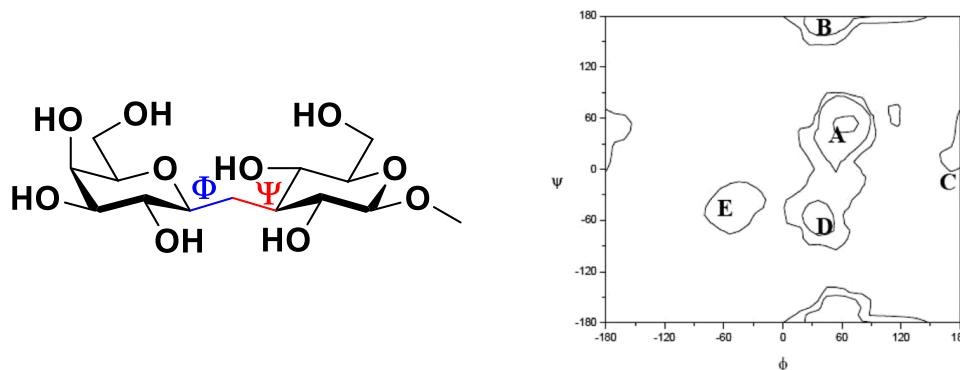


**Figure 27: Population distribution map for the C-glycosyl analogue of Gal- $\beta$ 1,3-Glc. Energy contours are given every 0.5 kcal mol<sup>-1</sup>. Distribution contours are given at 10, 1, and 0.1% of the population. A = *exo-syn*  $\Psi_{(+)}$ , B = *exo-anti*  $\Psi$ , D = *exo-syn*  $\Psi_{(-)}$**

The flexibility of these *C*-glycosides has a consequence in that preorganisation is necessary for binding, resulting in an entropic penalty, which is in turn reflected in the affinity. Although no  $K_D$  value could be found for binding of *C*-lactose with galectins, Titration NMR experiments reported in the literature suggest that when binding Ricin B, *C*-lactose competes with lactose for the same binding site and the affinity constant for *C*-lactose is smaller than that of its *O*-analogue, presumably due to entropic reasons since the flexibility of *C*-lactose in the free state is much higher.<sup>99, 100</sup> A strategy to overcome this entropic penalty is to lock the molecule into the desired conformation prior to binding using cyclic constraints. This technique was employed by Woods et al<sup>101</sup> in the design and synthesis of **FB 127**, a novel constrained Sia- $\alpha$ 2,3-Gal compound, that has subsequently been shown to inhibit infection by a broad range of influenza virus strains (see Figure 29). Conformational analysis of the population density of Sia- $\alpha$ 2,3-Gal glycosidic  $\Phi$  and  $\Psi$  angles from the GLYCAM simulation reflects that of *C*-lactose, showing three major populations: Cluster A, the *syn*-conformation ( $\Phi \sim -60^\circ$ ,  $\Psi \sim 0^\circ$ ), makes up 74.3% of the population. Cluster B, the *anti*-conformation ( $\Phi \sim -90^\circ$ ,  $\Psi \sim -60^\circ$  and  $\Phi \sim -170^\circ$ ,  $\Psi \sim -20^\circ$ ) has 25.3%. The third population in cluster C from  $0^\circ$  to  $+180^\circ$  makes up 0.3% (see Figure 28). Clusters A and B are widely reported in NMR studies of  $\alpha$ 2,3 linkages and have been shown to both be significantly populated in solution.



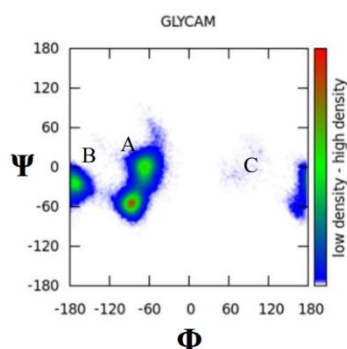


**Figure 28: GLYCAM Sia- $\alpha$ 2,3-Gal  $\Phi$  and  $\Psi$  angle population densities** <sup>102</sup>

The rationale behind **FB 127** was based on X-ray structural data for hemagglutinin-glycan complexes. MM-PBSA analysis in the PhD thesis of Hannah Smith, who carried out thesis work under the direction of Professor Robert J. Woods in Galway, <sup>102</sup> on a series of scaffolds lead to the prioritization of **FB 127** and structural analogues for synthesis and assay, as a result of their low reported  $\Delta G$  values. Table 4 compares the MM-PBSA results for Sia- $\alpha$ 2,3-Gal vs **FB 127**.

| Ligand                | $\Delta E_{\text{vdW}}^{\text{b}}$ | $\Delta E_{\text{elect}}^{\text{c}}$ | $\Delta G_{\text{PB}}^{\text{d}}$ | $\Delta G_{\text{NonPolar}}^{\text{e}}$ | $\Delta G^{\text{f}}$ | $\Delta \Delta G_{\text{rel}}^{\text{g}}$ |
|-----------------------|------------------------------------|--------------------------------------|-----------------------------------|---|-----------------------|---|
| Sia- $\alpha$ 2,3-Gal | $-28.1 \pm 3.6$                    | $-165.9 \pm 12.6$                    | $155.3 \pm 11.1$                  | $-2.6 \pm 0.1$                          | $-41.3 \pm 6.5$       | 0.0                                       |
| FB 127                | $-30.5 \pm 4.0$                    | $-165.1 \pm 14.3$                    | $152.9 \pm 13.3$                  | $-2.8 \pm 0.2$                          | $-45.4 \pm 5.6$       | 4.1                                       |

<sup>a</sup> All units in kcal mol<sup>-1</sup> <sup>b</sup> van der Waals contribution to the binding free energy. <sup>c</sup> Electrostatic contribution to the binding free energy. <sup>d</sup> Electrostatic contribution to the solvation free energy calculated using Poisson-Boltzmann method. <sup>e</sup> Non-polar contribution to the solvation free energy. <sup>f</sup>  $\Delta E_{\text{vdW}} + \Delta E_{\text{elect}} + \Delta G_{\text{NP}} + \Delta G_{\text{PB}}$ . <sup>g</sup>  $\Delta G$  relative to disaccharide  $\Delta G$ .

**Table 4: MM-PBSA results for proposed influenza inhibitors with standard deviation** <sup>a</sup>

102

An isopropylidene bridge introduced between the two saccharide units to constrain the glycosidic linkage into the exo-syn  $\Psi$  conformer. NMR and molecular dynamics showed that **FB 127** is rigid in solution and pre-organized into the exo-syn  $\Psi$  conformer for binding unlike the Sia- $\alpha$ 2,3-Gal linkage, which is much more flexible. Pre-organization of the Sia- $\alpha$ 2,3-Gal linkage via the cyclic constraint avoids an entropic penalty of  $\sim 3.5$  kcal mol<sup>-1</sup> and gave rise to an observed affinity enhancement of  $\sim 340$  fold <sup>101</sup> with this anti-adhesive relative to the native disaccharide for influenza hemagglutinin.

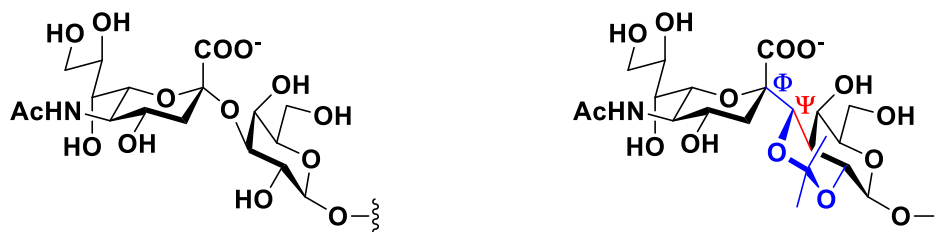


**Figure 29: Comparing the structure of natural Sia- $\alpha$ 2,3-Gal (left) with synthetic FB 127 (right) locked into the exo-syn  $\Psi$  conformation. The cyclic constraint is highlighted in blue**

### Aims of the Thesis

The first section of the thesis will focus on the development of galactosidase inhibitors. These inhibitors will be *C*-analogues of IPTG, where the *S*-linkage to the isopropyl aglycon moiety will be replaced with a carbon. Conformational constraint, as described above, will be analysed as a means to improve affinity towards galactosidase. Biological evaluation will be carried out via an inhibition assay.

The second section of the thesis will build on the galactosidase inhibitors to develop galectin inhibitors. The aim is to assess whether conformational constraint can be employed to develop a galectin inhibitor with inhibitory properties like those described in the introductory chapter. An effort will be made to gain an understanding into the protein-ligand interactions of both target proteins via molecular docking.

## References

- (1) Zhu, X.; Schmidt, R. R. New Principles for Glycoside-bond Formation. *Angew. Chemie Int. Ed.* **2009**, *48*, 1900–1934.
- (2) Reece, J.; Urry, L.; Cain, M.; Wasserman, S.; Minorsky, P.; Jackson, R. The Structure and Function of Large Biological Molecules. In *Campbell Biology*; Benjamin Cummings/ Pearson: Boston, 2011; pp 114–135.
- (3) Berg, J. M.; Tymoczko, J. L.; Gatto, G. J.; Stryer, L. Carbohydrates. In *Biochemistry*; W.H. Freeman & Co: New York, 2015; pp 315–336.
- (4) McMurry, J. E. Biomolecules: Carbohydrates. In *Organic Chemistry*; Brooks/Cole, Cengage Learning: Monterey, Calif., 2012; pp 1000–1043.
- (5) Nagae, M.; Nishi, N.; Murata, T.; Usui, T.; Nakamura, T.; Wakatsuki, S.; Kato, R. Crystal Structure of the Galectin-9 N-Terminal Carbohydrate Recognition Domain from *Mus Musculus* Reveals the Basic Mechanism of Carbohydrate Recognition \*. *J. Biol. Chem.* **2006**, *281*, 35884–35893.
- (6) Ruiz, F. M.; Gilles, U.; Lindner, I.; André, S.; Romero, A.; Reusch, D.; Gabius, H.-J. Combining Crystallography and Hydrogen–Deuterium Exchange to Study Galectin–Ligand Complexes. *Chem. – A Eur. J.* **2015**, *21*, 13558–13568.
- (7) Bianchet, M. A.; Ahmed, H.; Vasta, G. R.; Amzel, L. M. Soluble  $\beta$ -Galactosyl-Binding Lectin (Galectin) from Toad Ovary: Crystallographic Studies of Two Protein-Sugar Complexes. *Proteins Struct. Funct. Bioinforma.* **2000**, *40*, 378–388.
- (8) Leffler, H. Galectins Structure and Function—a Synopsis. *Mamm. Carbohydr. Recognit. Syst.* **2001**, 57–83.
- (9) Rabinovich, G. A.; Toscano, M. A.; Jackson, S. S.; Vasta, G. R. Functions of Cell Surface Galectin-Glycoprotein Lattices. *Curr. Opin. Struct. Biol.* **2007**, *17*, 513–520.
- (10) Ouellet, M.; Mercier, S.; Pelletier, I.; Bounou, S.; Roy, J.; Hirabayashi, J.; Sato, S.; Tremblay, M. J. Galectin-1 Acts as a Soluble Host Factor That Promotes HIV-1 Infectivity through Stabilization of Virus Attachment to Host Cells. *J. Immunol.* **2005**, *174*, 4120–4126.
- (11) Lagana, A.; Goetz, J. G.; Cheung, P.; Raz, A.; Dennis, J. W.; Nabi, I. R. Galectin Binding to Mgat5-Modified N-Glycans Regulates Fibronectin Matrix Remodeling in Tumor Cells. *Mol. Cell. Biol.* **2006**, *26*, 3181–3193.
- (12) Saghebasl, S.; Davaran, S.; Rahbarghazi, R.; Montaseri, A.; Salehi, R.; Ramazani, A. Synthesis and in Vitro Evaluation of Thermosensitive Hydrogel Scaffolds Based on (PNIPAAm-PCL-PEG-PCL-PNIPAAm)/Gelatin and (PCL-PEG-PCL)/Gelatin for Use in Cartilage Tissue Engineering. *J. Biomater. Sci. Polym. Ed.* **2018**, *29*, 1185–1206.
- (13) Modenutti, C. P.; Capurro, J. I. B.; Di Lella, S.; Martí, M. A. The Structural Biology of Galectin-Ligand Recognition: Current Advances in Modeling Tools, Protein Engineering, and Inhibitor Design . *Frontiers in Chemistry* . 2019.
- (14) Wang, L.; Zhao, Y.; Wang, Y.; Wu, X. The Role of Galectins in Cervical Cancer Biology and Progression. *Biomed Res. Int.* **2018**, *2018*, 2175927.

- (15) Leffler, H.; Carlsson, S.; Hedlund, M.; Qian, Y.; Poirier, F. Introduction to Galectins. *Glycoconj. J.* **2002**, *19*, 433–440.
- (16) Elad-Sfadia, G.; Haklai, R.; Ballan, E.; Gabius, H.-J.; Kloog, Y. Galectin-1 Augments Ras Activation and Diverts Ras Signals to Raf-1 at the Expense of Phosphoinositide 3-Kinase. *J. Biol. Chem.* **2002**, *277*, 37169–37175.
- (17) Elad-Sfadia, G.; Haklai, R.; Balan, E.; Kloog, Y. Galectin-3 Augments K-Ras Activation and Triggers a Ras Signal That Attenuates ERK but Not Phosphoinositide 3-Kinase Activity. *J. Biol. Chem.* **2004**, *279*, 34922–34930.
- (18) Strik, H. M.; Schmidt, K.; Lingor, P.; Tönges, L.; Kugler, W.; Nitsche, M.; Rabinovich, G. A.; Bähr, M. Galectin-1 Expression in Human Glioma Cells: Modulation by Ionizing Radiation and Effects on Tumor Cell Proliferation and Migration. *Oncol. Rep.* **2007**, *18*, 483–488.
- (19) Arcolia, V.; Journe, F.; Wattier, A.; Leteurtre, E.; Renaud, F.; Gabius, H.-J.; Remmelink, M.; Decaestecker, C.; Rodriguez, A.; Boutry, S. Galectin-1 Is a Diagnostic Marker Involved in Thyroid Cancer Progression. *Int. J. Oncol.* **2017**, *51*, 760–770.
- (20) Kobayashi, T.; Shimura, T.; Yajima, T.; Kubo, N.; Araki, K.; Tsutsumi, S.; Suzuki, H.; Kuwano, H.; Raz, A. Transient Gene Silencing of Galectin-3 Suppresses Pancreatic Cancer Cell Migration and Invasion through Degradation of  $\beta$ -Catenin. *Int. J. Cancer* **2011**, *129*, 2775–2786.
- (21) Mohafez, O. M. M.; Abd EL-Aziz, M. A.; Abd El-Ghany, A. A. The Expression Pattern of Galectin-3 in the Rat Hepatocellular Carcinoma. *Bull. Pharm. Sci. Assiut* **2011**, *34*, 181–187.
- (22) Ikemori, R. Y.; Machado, C. M. L.; Furuzawa, K. M.; Nonogaki, S.; Osinaga, E.; Umezawa, K.; de Carvalho, M. A.; Verinaud, L.; Chammas, R. Galectin-3 up-Regulation in Hypoxic and Nutrient Deprived Microenvironments Promotes Cell Survival. *PLoS One* **2014**, *9*, e111592.
- (23) Sanchez-Ruderisch, H.; Fischer, C.; Detjen, K. M.; Welzel, M.; Wimmel, A.; Manning, J. C.; André, S.; Gabius, H. Tumor Suppressor P16INK4a: Downregulation of Galectin-3, an Endogenous Competitor of the Pro-apoptosis Effector Galectin-1, in a Pancreatic Carcinoma Model. *FEBS J.* **2010**, *277*, 3552–3563.
- (24) Merlin, J.; Stechly, L.; de Beaucé, S.; Monté, D.; Leteurtre, E.; van Seuning, I.; Huet, G.; Pigny, P. Galectin-3 Regulates MUC1 and EGFR Cellular Distribution and EGFR Downstream Pathways in Pancreatic Cancer Cells. *Oncogene* **2011**, *30*, 2514–2525.
- (25) Thijssen, V. L. J. L.; Poirier, F.; Baum, L. G.; Griffioen, A. W. Galectins in the Tumor Endothelium: Opportunities for Combined Cancer Therapy. *Blood, J. Am. Soc. Hematol.* **2007**, *110*, 2819–2827.
- (26) Lange, F.; Brandt, B.; Tiedge, M.; Jonas, L.; Jeschke, U.; Pöhland, R.; Walzel, H. Galectin-1 Induced Activation of the Mitochondrial Apoptotic Pathway: Evidence for a Connection between Death-Receptor and Mitochondrial Pathways in Human Jurkat T Lymphocytes. *Histochem. Cell Biol.* **2009**, *132*, 211–223.
- (27) Chung, C. D.; Patel, V. P.; Moran, M.; Lewis, L. A.; Miceli, M. C. Galectin-1 Induces Partial TCR  $\zeta$ -Chain Phosphorylation and Antagonizes Processive TCR Signal Transduction. *J. Immunol.* **2000**, *165*, 3722–3729.

- (28) Akahani, S.; Nangia-Makker, P.; Inohara, H.; Kim, H.-R. C.; Raz, A. Galectin-3: A Novel Antiapoptotic Molecule with a Functional BH1 (NWGR) Domain of Bcl-2 Family. *Cancer Res.* **1997**, *57*, 5272–5276.
- (29) Fukumori, T.; Takenaka, Y.; Oka, N.; Yoshii, T.; Hogan, V.; Inohara, H.; Kanayama, H.; Kim, H.-R. C.; Raz, A. Endogenous Galectin-3 Determines the Routing of CD95 Apoptotic Signaling Pathways. *Cancer Res.* **2004**, *64*, 3376–3379.
- (30) Mazurek, N.; Conklin, J.; Byrd, J. C.; Raz, A.; Bresalier, R. S. Phosphorylation of the  $\beta$ -Galactoside-Binding Protein Galectin-3 Modulates Binding to Its Ligands. *J. Biol. Chem.* **2000**, *275*, 36311–36315.
- (31) Perillo, N. L.; Pace, K. E.; Seilhamer, J. J.; Baum, L. G. Apoptosis of T Cells Mediated by Galectin-1. *Nature* **1995**, *378*, 736–739.
- (32) Grigorian, A.; Torossian, S.; Demetriou, M. T-cell Growth, Cell Surface Organization, and the Galectin–Glycoprotein Lattice. *Immunol. Rev.* **2009**, *230*, 232–246.
- (33) Ito, K.; Ralph, S. J. Inhibiting Galectin-1 Reduces Murine Lung Metastasis with Increased CD4<sup>+</sup> and CD8<sup>+</sup> T Cells and Reduced Cancer Cell Adherence. *Clin. Exp. Metastasis* **2012**, *29*, 561–572.
- (34) Banh, A.; Zhang, J.; Cao, H.; Bouley, D. M.; Kwok, S.; Kong, C.; Giaccia, A. J.; Koong, A. C.; Le, Q.-T. Tumor Galectin-1 Mediates Tumor Growth and Metastasis through Regulation of T-Cell Apoptosis Gal-1 Regulates Tumor Growth and T-Cell Death. *Cancer Res.* **2011**, *71*, 4423–4431.
- (35) O’Driscoll, L.; Linehan, R.; Liang, Y. H.; Joyce, H.; Oglesby, I.; Clynes, M. Galectin-3 Expression Alters Adhesion, Motility and Invasion in a Lung Cell Line (DLKP), in Vitro. *Anticancer Res.* **2002**, *22*, 3117–3125.
- (36) Fukumori, T.; Oka, N.; Izaki, H.; Takahashi, M.; Kanayama, H. Galectin-3 Is Overexpressed in Renal Cell Carcinoma and It Regulates Immune Suppression through the Induction of Apoptosis of T Cells. *J. Urol.* **2008**, *179*, 91–92.
- (37) Nangia-Makker, P.; Honjo, Y.; Sarvis, R.; Akahani, S.; Hogan, V.; Pienta, K. J.; Raz, A. Galectin-3 Induces Endothelial Cell Morphogenesis and Angiogenesis. *Am. J. Pathol.* **2000**, *156*, 899–909.
- (38) Markowska, A. I.; Jefferies, K. C.; Panjwani, N. Galectin-3 Protein Modulates Cell Surface Expression and Activation of Vascular Endothelial Growth Factor Receptor 2 in Human Endothelial Cells \*. *J. Biol. Chem.* **2011**, *286*, 29913–29921.
- (39) Polyak, K.; Xia, Y.; Zweier, J. L.; Kinzler, K. W.; Vogelstein, B. A Model for P53-Induced Apoptosis. *Nature* **1997**, *389*, 300–305.
- (40) Lu, J.; Pei, H.; Kaeck, M.; Thompson, H. J. Gene Expression Changes Associated with Chemically Induced Rat Mammary Carcinogenesis. *Mol. Carcinog. Publ. Coop. with Univ. Texas MD Anderson Cancer Cent.* **1997**, *20*, 204–215.
- (41) Lahm, H.; André, S.; Hoeflich, A.; Fischer, J. R.; Sordat, B.; Kaltner, H.; Wolf, E.; Gabius, H.-J. Comprehensive Galectin Fingerprinting in a Panel of 61 Human Tumor Cell Lines by RT-PCR and Its Implications for Diagnostic and Therapeutic Procedures. *J. Cancer Res. Clin. Oncol.* **2001**, *127*, 375–386.
- (42) Toscano, M. A.; Bianco, G. A.; Ilarregui, J. M.; Croci, D. O.; Correale, J.; Hernandez,

- J. D.; Zwirner, N. W.; Poirier, F.; Riley, E. M.; Baum, L. G.; Rabinovich, G. A. Differential Glycosylation of TH1, TH2 and TH-17 Effector Cells Selectively Regulates Susceptibility to Cell Death. *Nat. Immunol.* **2007**, *8*, 825–834.
- (43) Zhu, C.; Anderson, A. C.; Schubart, A.; Xiong, H.; Imitola, J.; Khoury, S. J.; Zheng, X. X.; Strom, T. B.; Kuchroo, V. K. The Tim-3 Ligand Galectin-9 Negatively Regulates T Helper Type 1 Immunity. *Nat. Immunol.* **2005**, *6*, 1245–1252.
- (44) Flahaut, C.; Michalski, J. C.; Danel, T.; Humbert, M. H.; Klein, A. The Effects of Ethanol on the Glycosylation of Human Transferrin. *Glycobiology* **2003**, *13*, 191–198.
- (45) Carlsson, M. C.; Bengtson, P.; Cucak, H.; Leffler, H. Galectin-3 Guides Intracellular Trafficking of Some Human Serotransferrin Glycoforms \*. *J. Biol. Chem.* **2013**, *288*, 28398–28408.
- (46) Mizgerd, J. P.; Kubo, H.; Kutkoski, G. J.; Bhagwan, S. D.; Scharffetter-Kochanek, K.; Beaudet, A. L.; Doerschuk, C. M. Neutrophil Emigration in the Skin, Lungs, and Peritoneum: Different Requirements for CD11/CD18 Revealed by CD18-Deficient Mice. *J. Exp. Med.* **1997**, *186*, 1357–1364.
- (47) Mizgerd, J. P.; Horwitz, B. H.; Quillen, H. C.; Scott, M. L.; Doerschuk, C. M. Effects of CD18 Deficiency on the Emigration of Murine Neutrophils during Pneumonia. *J. Immunol.* **1999**, *163*, 995–999.
- (48) Sato, S.; Ouellet, N.; Pelletier, I.; Simard, M.; Rancourt, A.; Bergeron, M. G. Role of Galectin-3 as an Adhesion Molecule for Neutrophil Extravasation during Streptococcal Pneumonia. *J. Immunol.* **2002**, *168*, 1813–1822.
- (49) Colnot, C.; Fowles, D.; Ripoche, M.; Bouchaert, I.; Poirier, F. Embryonic Implantation in Galectin 1/Galectin 3 Double Mutant Mice. *Dev. Dyn. an Off. Publ. Am. Assoc. Anat.* **1998**, *211*, 306–313.
- (50) Hsu, D. K.; Yang, R.-Y.; Pan, Z.; Yu, L.; Salomon, D. R.; Fung-Leung, W.-P.; Liu, F.-T. Targeted Disruption of the Galectin-3 Gene Results in Attenuated Peritoneal Inflammatory Responses. *Am. J. Pathol.* **2000**, *156*, 1073–1083.
- (51) Colnot, C.; RIPOCHE, M.; Milon, G.; Montagutelli, X.; Crocker, P. R.; Poirier, F. Maintenance of Granulocyte Numbers during Acute Peritonitis Is Defective in Galectin-3-null Mutant Mice. *Immunology* **1998**, *94*, 290–296.
- (52) Kuwabara, I.; Liu, F.-T. Galectin-3 Promotes Adhesion of Human Neutrophils to Laminin. *J. Immunol.* **1996**, *156*, 3939–3944.
- (53) Massa, S. M.; Cooper, D. N. W.; Leffler, H.; Barondes, S. H. L-29, an Endogenous Lectin, Binds to Glycoconjugate Ligands with Positive Cooperativity. *Biochemistry* **1993**, *32*, 260–267.
- (54) Woo, H. J.; Shaw, L. M.; Messier, J. M.; Mercurio, A. M. The Major Non-Integrin Laminin Binding Protein of Macrophages Is Identical to Carbohydrate Binding Protein 35 (Mac-2). *J. Biol. Chem.* **1990**, *265*, 7097–7099.
- (55) Almkvist, J.; Karlsson, A. Galectins as Inflammatory Mediators. *Glycoconj. J.* **2002**, *19*, 575–581.
- (56) Jeng, K. C. G.; Frigeri, L. G.; Liu, F.-T. An Endogenous Lectin, Galectin-3 (EBP/Mac-2), Potentiates IL-1 Production by Human Monocytes. *Immunol. Lett.* **1994**, *42*, 113–

116.

- (57) Brewer, C. F. Thermodynamic Binding Studies of Galectin-1, -3 and -7. *Glycoconj. J.* **2002**, *19*, 459–465.
- (58) Seetharaman, J.; Kanigsberg, A.; Slaaby, R.; Leffler, H.; Barondes, S. H.; Rini, J. M. X-Ray Crystal Structure of the Human Galectin-3 Carbohydrate Recognition Domain at 2.1-Å Resolution. *J. Biol. Chem.* **1998**, *273*, 13047–13052.
- (59) Tejler, J. Synthetic Galectin Inhibitors Selective O-Galactosyl Aldoximes, Multivalent Lactosides and Galactose-Mimicking Mannosides, Lund University, 2006.
- (60) Cumpstey, I.; Salomonsson, E.; Sundin, A.; Leffler, H.; Nilsson, U. J. Double Affinity Amplification of Galectin–Ligand Interactions through Arginine–Arene Interactions: Synthetic, Thermodynamic, and Computational Studies with Aromatic Diamido Thiodigalactosides. *Chem. Eur. J.* **2008**, *14*, 4233–4245.
- (61) Cumpstey, I.; Carlsson, S.; Leffler, H.; Nilsson, U. J. Synthesis of a Phenyl Thio-β-d-Galactopyranoside Library from 1,5-Difluoro-2,4-Dinitrobenzene: Discovery of Efficient and Selective Monosaccharide Inhibitors of Galectin-7. *Org. Biomol. Chem.* **2005**, *3*, 1922–1932.
- (62) Karplus, M. Contact Electron-Spin Coupling of Nuclear Magnetic Moments. *J. Chem. Phys.* **1959**, *30*, 11–15.
- (63) Minch, M. J. Orientational Dependence of Vicinal Proton-Proton NMR Coupling Constants: The Karplus Relationship. *Concepts Magn. Reson.* **1994**, *6*, 41–56.
- (64) Kirschner, K. N.; Woods, R. J. Solvent Interactions Determine Carbohydrate Conformation. *Proc. Natl. Acad. Sci.* **2001**, *98*, 10541–10545.
- (65) Bian, C.-F.; Zhang, Y.; Sun, H.; Li, D.-F.; Wang, D.-C. Structural Basis for Distinct Binding Properties of the Human Galectins to Thomsen-Friedenreich Antigen. *PLoS One* **2011**, *6*, e25007.
- (66) Leonidas, D. D.; Vatzaki, E. H.; Vorum, H.; Celis, J. E.; Madsen, P.; Acharya, K. R. Structural Basis for the Recognition of Carbohydrates by Human Galectin-7. *Biochemistry* **1998**, *37* (40), 13930–13940.
- (67) Stannard, K. A.; Collins, P. M.; Ito, K.; Sullivan, E. M.; Scott, S. A.; Gabutero, E.; Grice, I. D.; Low, P.; Nilsson, U. J.; Leffler, H. Galectin Inhibitory Disaccharides Promote Tumour Immunity in a Breast Cancer Model. *Cancer Lett.* **2010**, *299*, 95–110.
- (68) Bum-Erdene, K.; Gagarinov, I. A.; Collins, P. M.; Winger, M.; Pearson, A. G.; Wilson, J. C.; Leffler, H.; Nilsson, U. J.; Grice, I. D.; Blanchard, H. Investigation into the Feasibility of Thioditaloside as a Novel Scaffold for Galectin-3-specific Inhibitors. *ChemBioChem* **2013**, *14*, 1331–1342.
- (69) Sörme, P.; Arnoux, P.; Kahl-Knutsson, B.; Leffler, H.; Rini, J. M.; Nilsson, U. J. Structural and Thermodynamic Studies on Cation–π Interactions in Lectin–Ligand Complexes: High-Affinity Galectin-3 Inhibitors through Fine-Tuning of an Arginine–Arene Interaction. *J. Am. Chem. Soc.* **2005**, *127*, 1737–1743.
- (70) Ideo, H.; Seko, A.; Ishizuka, I.; Yamashita, K. The N-Terminal Carbohydrate Recognition Domain of Galectin-8 Recognizes Specific Glycosphingolipids with High Affinity. *Glycobiology* **2003**, *13*, 713–723.

- (71) Ideo, H.; Matsuzaka, T.; Nonaka, T.; Seko, A.; Yamashita, K. Galectin-8-N-Domain Recognition Mechanism for Sialylated and Sulfated Glycans. *J. Biol. Chem.* **2011**, *286*, 11346–11355.
- (72) Sörme, P.; Qian, Y.; Nyholm, P.; Leffler, H.; Nilsson, U. J. Low Micromolar Inhibitors of Galectin-3 Based on 3'-derivatization of N-acetyllactosamine. *ChemBioChem* **2002**, *3*, 183–189.
- (73) Diehl, C.; Engström, O.; Delaine, T.; Håkansson, M.; Genheden, S.; Modig, K.; Leffler, H.; Ryde, U.; Nilsson, U. J.; Akke, M. Protein Flexibility and Conformational Entropy in Ligand Design Targeting the Carbohydrate Recognition Domain of Galectin-3. *J. Am. Chem. Soc.* **2010**, *132*, 14577–14589.
- (74) Ahmad, N.; Gabius, H.-J.; Sabesan, S.; Oscarson, S.; Brewer, C. F. Thermodynamic Binding Studies of Bivalent Oligosaccharides to Galectin-1, Galectin-3, and the Carbohydrate Recognition Domain of Galectin-3. *Glycobiology* **2004**, *14*, 817–825.
- (75) Cumpstey, I.; Sundin, A.; Leffler, H.; Nilsson, U. J. C2-symmetrical Thiodigalactoside Bis-benzamido Derivatives as High-affinity Inhibitors of Galectin-3: Efficient Lectin Inhibition through Double Arginine–Arene Interactions. *Angew. Chemie* **2005**, *117*, 5240–5242.
- (76) Huisgen, R. 1, 3-dipolar Cycloadditions. Past and Future. *Angew. Chemie Int. Ed. English* **1963**, *2*, 565–598.
- (77) Huisgen, R. Kinetics and Mechanism of 1, 3-dipolar Cycloadditions. *Angew. Chemie Int. Ed. English* **1963**, *2*, 633–645.
- (78) Rostovtsev, V. V.; Green, L. G.; Fokin, V. V.; Sharpless, K. B. A Stepwise Huisgen Cycloaddition Process: Copper(I)-Catalyzed Regioselective “Ligation” of Azides and Terminal Alkynes. *Angew. Chemie Int. Ed.* **2002**, *41*, 2596–2599.
- (79) Tornøe, C. W.; Christensen, C.; Meldal, M. Peptidotriazoles on Solid Phase:[1, 2, 3]-Triazoles by Regiospecific Copper (I)-Catalyzed 1, 3-Dipolar Cycloadditions of Terminal Alkynes to Azides. *J. Org. Chem.* **2002**, *67*, 3057–3064.
- (80) Salameh, B. A.; Leffler, H.; Nilsson, U. J. 3-(1,2,3-Triazol-1-Yl)-1-Thio-Galactosides as Small, Efficient, and Hydrolytically Stable Inhibitors of Galectin-3. *Bioorg. Med. Chem. Lett.* **2005**, *15*, 3344–3346.
- (81) van Hattum, H.; Branderhorst, H. M.; Moret, E. E.; Nilsson, U. J.; Leffler, H.; Pieters, R. J. Tuning the Preference of Thiodigalactoside-and Lactosamine-Based Ligands to Galectin-3 over Galectin-1. *J. Med. Chem.* **2013**, *56*, 1350–1354.
- (82) Salameh, B. A.; Cumpstey, I.; Sundin, A.; Leffler, H.; Nilsson, U. J. 1H-1,2,3-Triazol-1-Yl Thiodigalactoside Derivatives as High Affinity Galectin-3 Inhibitors. *Bioorg. Med. Chem.* **2010**, *18*, 5367–5378.
- (83) Sethi, A.; Sanam, S.; Alvala, R.; Alvala, M. An Updated Patent Review of Galectin-1 and Galectin-3 Inhibitors and Their Potential Therapeutic Applications (2016–Present). *Expert Opin. Ther. Pat.* **2021**, *31*, 709–721.
- (84) Delaine, T.; Collins, P.; MacKinnon, A.; Sharma, G.; Stegmayr, J.; Rajput, V. K.; Mandal, S.; Cumpstey, I.; Larumbe, A.; Salameh, B. A. Galectin-3-binding Glycomimetics That Strongly Reduce Bleomycin-induced Lung Fibrosis and Modulate Intracellular Glycan Recognition. *ChemBioChem* **2016**, *17*, 1759–1770.



- (85) Thompson, S. E.; Smithrud, D. B. Carboxylates Stacked over Aromatic Rings Promote Salt Bridge Formation in Water. *J. Am. Chem. Soc.* **2002**, *124*, 442–449.
- (86) Cumpstey, I.; Salomonsson, E.; Sundin, A.; Leffler, H.; Nilsson, U. J. Studies of Arginine–Arene Interactions through Synthesis and Evaluation of a Series of Galectin-binding Aromatic Lactose Esters. *ChemBioChem* **2007**, *8*, 1389–1398.
- (87) Sacchettini, J. C.; Baum, L. G.; Brewer, C. F. Multivalent Protein–Carbohydrate Interactions. A New Paradigm for Supermolecular Assembly and Signal Transduction. *Biochemistry* **2001**, *40*, 3009–3015.
- (88) Tejler, J.; Tullberg, E.; Frejd, T.; Leffler, H.; Nilsson, U. J. Synthesis of Multivalent Lactose Derivatives by 1, 3-Dipolar Cycloadditions: Selective Galectin-1 Inhibition. *Carbohydr. Res.* **2006**, *341*, 1353–1362.
- (89) Peterson, K.; Kumar, R.; Stenström, O.; Verma, P.; Verma, P. R.; Håkansson, M.; Kahl-Knutsson, B.; Zetterberg, F.; Leffler, H.; Akke, M.; Logan, D. T.; Nilsson, U. J. Systematic Tuning of Fluoro-Galectin-3 Interactions Provides Thiodigalactoside Derivatives with Single-Digit nM Affinity and High Selectivity. *J. Med. Chem.* **2018**, *61*, 1164–1175.
- (90) Zetterberg, F. R.; MacKinnon, A.; Brimert, T.; Gravelle, L.; Johnsson, R. E.; Kahl-Knutson, B.; Leffler, H.; Nilsson, U. J.; Pedersen, A.; Peterson, K.; Roper, J. A.; Schambye, H.; Slack, R. J.; Tantawi, S. Discovery and Optimization of the First Highly Effective and Orally Available Galectin-3 Inhibitors for Treatment of Fibrotic Disease. *J. Med. Chem.* **2022**, *65*, 12626–12638.
- (91) Forbes, C. R.; Sinha, S. K.; Ganguly, H. K.; Bai, S.; Yap, G. P. A.; Patel, S.; Zondlo, N. J. Insights into Thiol–Aromatic Interactions: A Stereoelectronic Basis for S–H/ $\pi$  Interactions. *J. Am. Chem. Soc.* **2017**, *139*, 1842–1855.
- (92) Beno, B. R.; Yeung, K.-S.; Bartberger, M. D.; Pennington, L. D.; Meanwell, N. A. A Survey of the Role of Noncovalent Sulfur Interactions in Drug Design. *J. Med. Chem.* **2015**, *58*, 4383–4438.
- (93) Zetterberg, F. R.; Peterson, K.; Johnsson, R. E.; Brimert, T.; Håkansson, M.; Logan, D. T.; Leffler, H.; Nilsson, U. J. Monosaccharide Derivatives with Low-nanomolar Lectin Affinity and High Selectivity Based on Combined Fluorine–Amide, Phenyl–Arginine, Sulfur– $\pi$ , and Halogen Bond Interactions. *ChemMedChem* **2018**, *13*, 133–137.
- (94) Montero, E.; García-Herrero, A.; Asensio, J. L.; Hirai, K.; Ogawa, S.; Santoyo-González, F.; Cañada, F. J.; Jiménez-Barbero, J. The Conformational Behaviour of Non-Hydrolyzable Lactose Analogues: The Thioglycoside, Carbaglycoside, and Carba-Iminoglycoside Cases. *European J. Org. Chem.* **2000**, *2000*, 1945–1952.
- (95) Gimeno, A.; Delgado, S.; Valverde, P.; Bertuzzi, S.; Berbís, M. A.; Echavarren, J.; Lacetera, A.; Martín-Santamaría, S.; Surolia, A.; Cañada, F. J. Minimizing the Entropy Penalty for Ligand Binding: Lessons from the Molecular Recognition of the Histo Blood-group Antigens by Human Galectin-3. *Angew. Chemie Int. Ed.* **2019**, *58*, 7268–7272.
- (96) Jimenez-Barbero, J.; Espinosa, J. F.; Asensio, J. L.; Canada, F. J.; Poveda, A. *Adv. Carbohydr. Chem. Biochem* **2001**, *56*, 56000–56006.
- (97) Vidal, P.; Roldós, V.; Fernández-Alonso, M. del C.; Vauzeilles, B.; Bleriot, Y.; Cañada,

- F. J.; André, S.; Gabius, H.; Jiménez-Barbero, J.; Espinosa, J. F. Conformational Selection in Glycomimetics: Human Galectin-1 Only Recognizes Syn- $\Psi$ -Type Conformations of B-1,3-Linked Lactose and Its C-Glycosyl Derivative. *Chem. Eur. J.* **2013**, *19*, 14581–14590.
- (98) Martín-Santamaría, S.; Gabius, H.-J.; Jiménez-Barbero, J. Structural Studies on the Interaction of Saccharides and Glycomimetics with Galectin-1: A 3D Perspective Using a Combined Molecular Modeling and NMR Approach. *Pure Appl. Chem.* **2011**, *84*, 49–64.
- (99) Espinosa, J.-F.; Cañada, F. J.; Asensio, J. L.; Martín-Pastor, M.; Dietrich, H.; Martín-Lomas, M.; Schmidt, R. R.; Jiménez-Barbero, J. Experimental Evidence of Conformational Differences between C-Glycosides and O-Glycosides in Solution and in the Protein-Bound State: The C-Lactose/O-Lactose Case. *J. Am. Chem. Soc.* **1996**, *118*, 10862–10871.
- (100) Poveda, A.; Jiménez-Barbero, J. NMR Studies of Carbohydrate–Protein Interactions in Solution. *Chem. Soc. Rev.* **1998**, *27*, 133–144.
- (101) Woods, R. J.; Murphy, P. V.; Yang, L.; Smith, H. M. K.; Hendel, J. Glycomimetics to Inhibit Pathogen-Host Interactions. WO2013US31238 20130314, 2015.
- (102) Smith, H. M. K. Computational Design of Glycomimetic Inhibitors of Influenza A Adhesion, National Univeristy of Ireland Galway, 2014.

**Chapter 2: Synthesis and Biological Activity of Galactosidase Inhibitors**

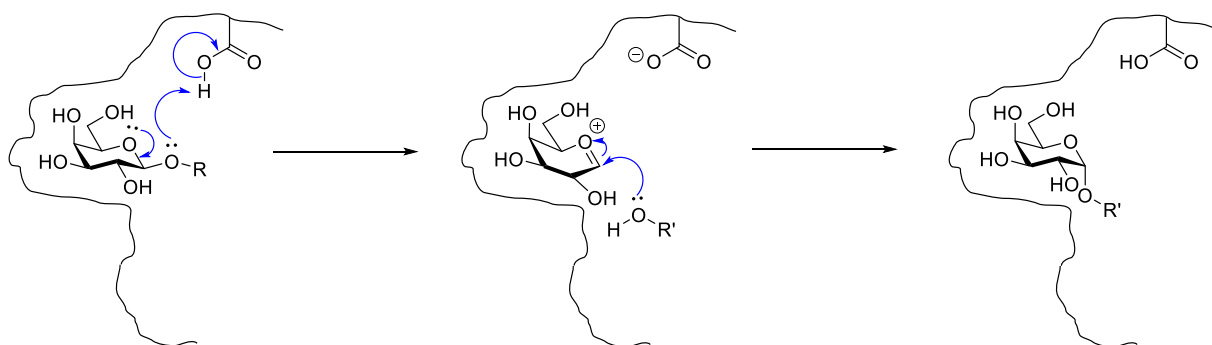
|  |           |
|--|-----------|
| <b>Glycosidases .....</b>  | <b>48</b> |
| <b>β-Galactosidase .....</b>   | <b>50</b> |
| <b>Isopropyl-β-D-1-thiogalactopyranoside (IPTG).....</b>             | <b>51</b> |
| <b>Synthesis.....</b>  | <b>53</b> |
| <b>β-Galactosidase Inhibition Assay- Procedure and Results .....</b> | <b>60</b> |
| <b>Discussion.....</b>   | <b>70</b> |
| <b>Molecular Docking of Selected Ligands .....</b>                   | <b>75</b> |
| <b>Conclusions.....</b>  | <b>80</b> |
| <b>References.....</b>   | <b>81</b> |

## Glycosidases

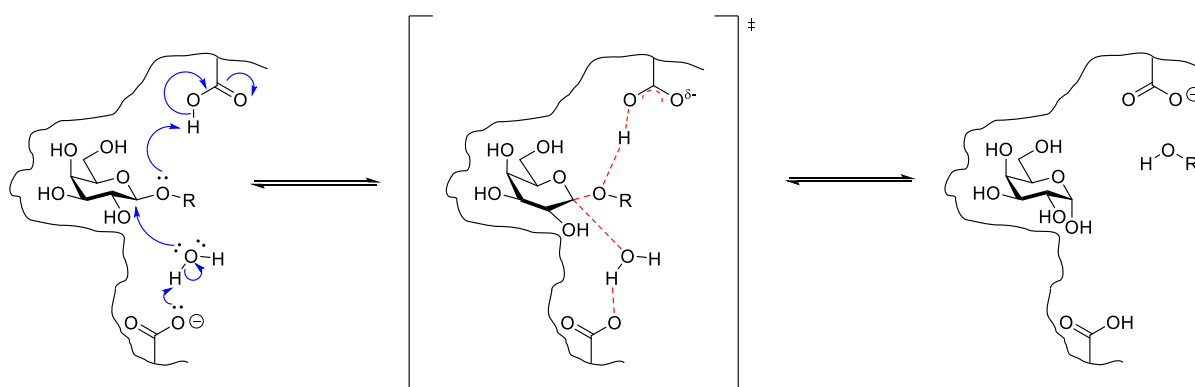
Glycosidases are a family of carbohydrate processing enzymes which can break and make glycosidic bonds. These enzymes can carry out their function using the active site, which is made up of two parts: The catalytic site, which increases the rate of the reaction and the binding site which holds the reactants in place and determines the selectivity of the reaction.<sup>1</sup> Certain amino acid residues in the catalytic site will aid in the hydrolysis of glycosidic bonds. Acidic sidechains can protonate the glycosidic oxygen to form an oxonium ion. Protonation improves the leaving group ability of the alcohol and so catalyses the formation of a glycosyl cation intermediate. This bond breaking is typically assisted by the involvement of the lone pair on the ring oxygen. The reactive intermediate is then attacked by water as a nucleophile, leading to the hydrolysis of the glycosidic bond. The transition state that leads to the formation of this reactive intermediate is stabilised by the catalytic site of the enzyme.

Glycosidases can be either retaining or inverting, depending on whether the initial product formed has the same stereo configuration as the reactant or if it is inverted. Inverting glycosidases epimerise the configuration of the products anomeric centre relative to the starting glycoside. The enzyme buries the glycoside to be hydrolysed in its folds allowing the water nucleophile to access the donor selectively from the opposite face to the leaving group, hence changing the stereochemistry of the product. The inverting glycosidase pathway can take place via a two-step  $S_N1$  pathway or an  $S_N2$  process (see Scheme 3).

Inverting Glycosidase ( $S_N1$  pathway):



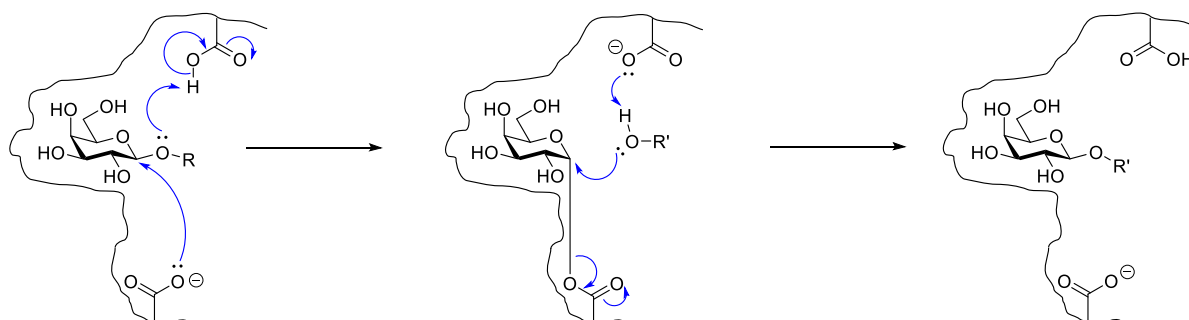
Inverting Glycosidase ( $S_N2$  pathway):



### Scheme 3: Comparing the possible reaction mechanisms for inverting glycosidases

A half chair is observed in the transition state of the  $S_N2$  pathway in Scheme 3 due to a change in hybridization of the anomeric carbon from  $sp^3$  to  $sp^2$ . Retaining glycosidases operate via a double inversion mechanism which gives products of the same stereochemistry. Two carboxylic acid sidechains are generally present in the enzyme active site, one to assist oxonium ion formation as previously mentioned and the other to intercept the glycosyl cation, forming a covalent glycosyl enzyme intermediate which is then attacked by a nucleophile from the same face as the departed nucleophile (see Scheme 4).<sup>1</sup>

Retaining Glycosidase ( $S_N2$  pathway):



### Scheme 4: Reaction mechanism for retaining glycosidases

The use of glycosidases in glycoside synthesis is possible if the reverse of the hydrolysis reaction can be promoted. Glycosidase enzymes tend to have strict binding specificity at the glycosyl donor position but are often less specific and in some cases non-existent in their shape requirements when binding to the aglycon. Such promiscuity results in poorer efficiency when they are used for oligosaccharide synthesis relative to glycosyltransferases, because of a

decrease in regioselectivity. This feature can also be seen as advantageous as it means these enzymes are more robust, easier to isolate than glycosyl transferases and provides scope for the use of a broader range of acceptors in the same enzymatic system.

### $\beta$ -Galactosidase

$\beta$ -Galactosidase is a glycosyl hydrolase enzyme which hydrolyzes lactose into galactose and glucose, for example. Operationally, it has fairly strict specificity at the galactosyl position but is adept at hydrolyzing galactopyranosides with a wide variety of aglycons.<sup>2</sup> Bacteria such as *E.coli* are known to rely on glucose as their primary source of carbon and energy even when other sugars are available.<sup>3</sup> When glucose is limited, *E.coli* expresses a gene encoding  $\beta$ -galactosidase to hydrolyze lactose.  $\beta$ -Galactosidase from *E.coli* is a 1023 amino acid polypeptide chain consisting of five sequential domains, with an extended segment of around 50 residues at the *N*-terminus.<sup>4</sup> The residues Glu461, Met502, Tyr503 and Glu537 are found close together and are highly conserved, relative to other homologous  $\beta$ -galactosidase sequences. This active site pocket is therefore identified as the substrate binding site (see Figure 30).<sup>2, 4</sup>

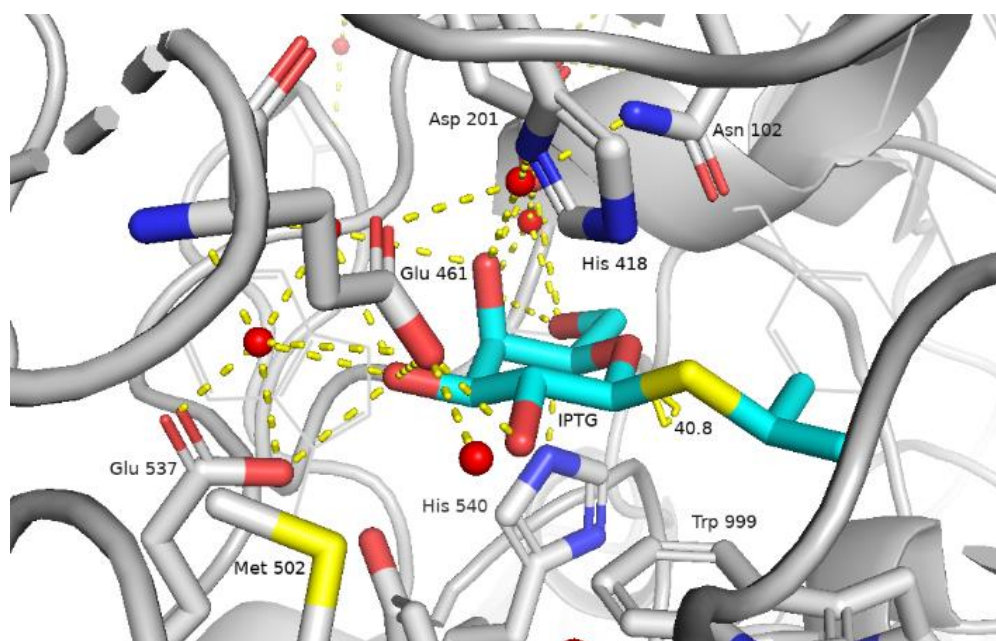


**Figure 30: IPTG ( $\Phi = 40.8^\circ$ ) in complex with amino acid residues in active site pocket of  $\beta$ -Galactosidase (PDB ID: 1JYX)**

The *E.Coli*  $\beta$ -galactosidase is a retaining glycosidase, catalysing hydrolysis of its substrates via the double inversion reaction described in Scheme 4, where the product retains the same stereochemistry as the starting state. In this case, Glu461, or a  $Mg^{2+}$  ion<sup>2</sup> acts as the general

acid catalyst, protonating the oxygen atom at the anomeric position to form an oxonium ion. Protonation improves the leaving group ability, providing an alcohol rather than alkoxide and cleavage of the glycosidic bond is the rate determining step towards the formation of the glycosyl cation intermediate. This reactive intermediate is attacked by nucleophilic water and subsequent carboxylate mediated proton removal from the oxonium results in formation of a hemiacetal. In a transglycosylation reaction catalysed by the glycosidase, with a lactose substrate, allolactose, a disaccharide isomer of lactose with  $\beta$ 1,6 glycosidic linkage instead of  $\beta$ 1,4 linkage, is the preferred product.

### **Isopropyl- $\beta$ -D-1-thiogalactopyranoside (IPTG)**

Isopropyl- $\beta$ -D-1-thiogalactopyranoside (**IPTG**) is a common molecular biology reagent which is useful in the laboratory as a tool for inducing protein expression in engineered bacterial strains where the gene is under the control of the lac operon, a gene cluster and promoter that functions together with additional sequences in regulation. The lac operon includes the genes for  $\beta$ -galactosidase as well as galactoside/ lactose permease, used to transport lactose into the cell.<sup>5</sup> The inducer triggers gene expression by preventing the lac repressor, a tetrameric protein of identical monomers, from binding the operator. The inducer binds to an allosteric site on the lac repressor and thereby results in a dissociation of the repressor from operator DNA. An inducer molecule binds in the centre of the large domain within each monomer. This binding leads to conformational changes that modify the relationship between the two small DNA-binding domains. These domains can no longer easily contact DNA simultaneously, leading to a dramatic reduction in DNA-binding affinity.<sup>5</sup>

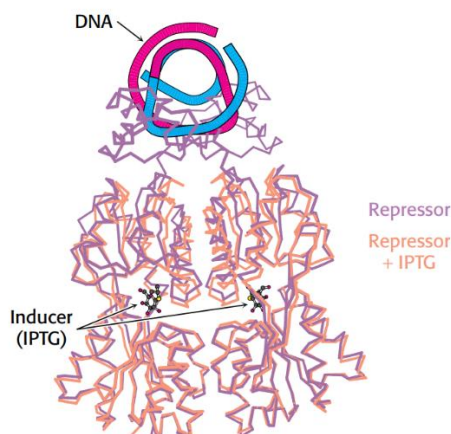


**Figure 31: Effects of IPTG on the structure of the Lac Repressor, with the Repressor (Purple) bound to DNA superimposed with the unbound repressor in contact with the inducer (orange). Structural changes in the presence and absence of the inducer can be compared. Reproduced with permission from ref <sup>5</sup> Copyright © 2015 W.H. Freeman & Co. Publishers**

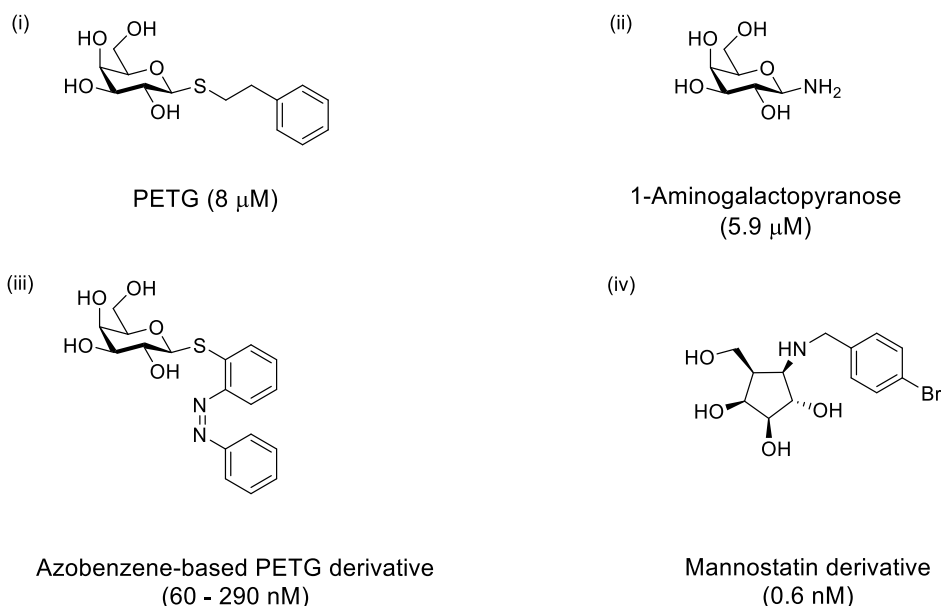
Lactose enters the *E.coli* cell via lactose permease and is converted to allolactose via one of the few existing  $\beta$ -galactosidase molecules. Allolactose is referred to as the inducer of the lac operon as it triggers the relief of repression and hence, expression of the lac operon genes, leading to a  $10^3$ -fold increase in the concentration of  $\beta$ -galactosidase.<sup>3</sup> IPTG is a mimic of allolactose and although it is a potent inducer of  $\beta$ -galactosidase expression, it is not a substrate of the enzyme.<sup>3</sup> IPTG is advantageous over allolactose as it is non-hydrolyzable due to its thioglycoside linkage, preventing the cell from metabolizing or degrading the inducer. Therefore, its concentration remains constant during experiments. An inducer that cannot be metabolized allows researchers to explore the physiological function of lactose as a carbon source for growth, separate from its function in the regulation of gene expression.<sup>3</sup>

As shown in Figure 30, IPTG binds to  $\beta$ -galactosidase in a “shallow” mode and “stack” with Trp999.<sup>6</sup> This residue has proven to be key in facilitating the action of  $\beta$ -galactosidases.<sup>7</sup> Several site-specific substitutions (Phe, Gly, Tyr, Leu) for Trp999 were made, with each substitution caused greatly decreasing affinities for substrates and inhibitors that bind in the “shallow” mode. The residue is also very important for binding glucose to the glycosyl enzyme intermediate when making/breaking glycosidic bonds.<sup>7</sup> IPTG is a well-established competitive inhibitor of *E.coli*  $\beta$ -galactosidase, with many reports<sup>6, 7, 8, 9</sup> of colorimetric assays performed to test its ability to inhibit the hydrolysis of glycosidic bonds in sugar molecules fitted with chromogenic aglycon moieties, such as X-Gal, ONPG and PNP. In an effort to make a more potent inhibitor than IPTG, synthesis of a series of C-analogues of IPTG was



performed and the inhibitory ability of these molecules was compared to **IPTG** in a galactosidase inhibition assay.

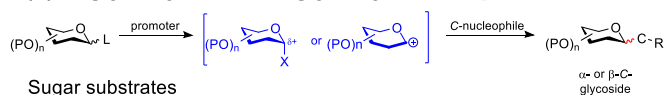
Some examples of  $\beta$ -galactosidase (*E. coli*) inhibitors with  $K_i$  values reported in the literature can be seen in Figure 32.<sup>10, 11, 12, 13</sup>



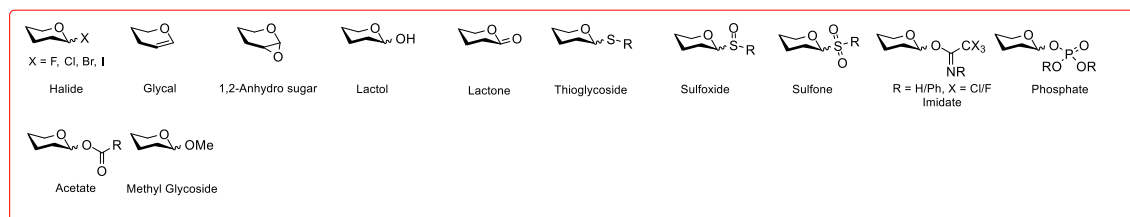
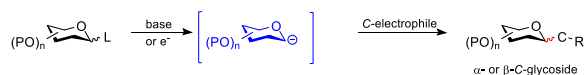
**Figure 32: Examples of competitive  $\beta$ -galactosidase (*E. coli*) inhibitors with  $K_i$  values shown.**

## Synthesis

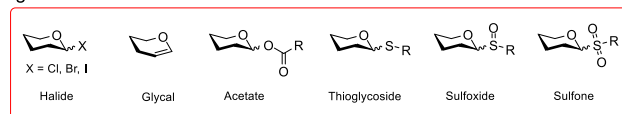
The investigation commenced with the synthesis of a series of *C*-analogues of **IPTG**, including conformationally constrained *C*-glycosides. Replacement of the C-O anomeric linkage in naturally occurring *O*-glycosides with a C-S or C-C bond is known to engender hydrolytic stability, providing derivatives that if capable of adopting similar conformations, should hence retain function, although they are not hydrolysed to provide galactose. The synthesis of *C*-glycosides has become an area of intense study among carbohydrate chemists and biochemists because the discovery of naturally occurring *C*-nucleosides with important pharmacological properties gave momentum to synthetic efforts for preparing active carbohydrate analogues. *C*-Glycosides are of interest as inhibitors of carbohydrate processing enzymes and are stable analogues of glycans involved in important intra- and inter-cellular processes.<sup>14</sup> Many approaches to *C*-glycoside synthesis have been reported in the literature (see Scheme 5 for selected examples).

**(a) C-glycosylation via glycosyl electrophilic/ cationic species**

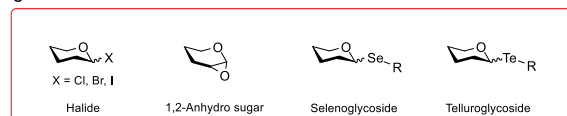
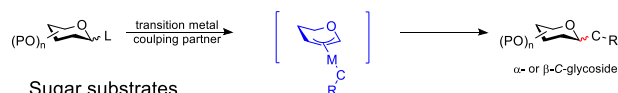
Sugar substrates

**(b) C-glycosylation via glycosyl anionic species**

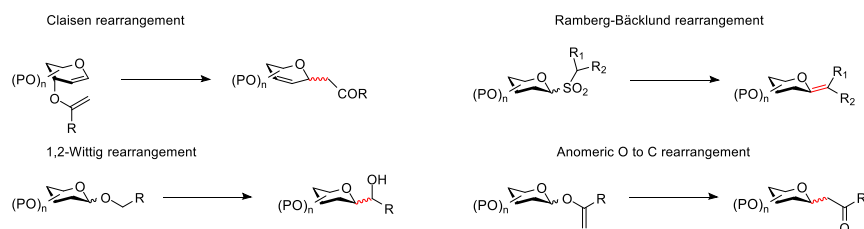
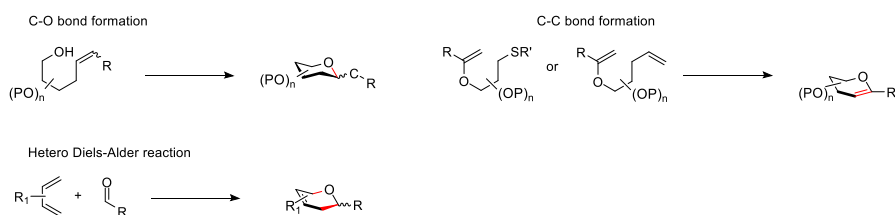
Sugar substrates

**(c) C-glycosylation via glycosyl radical species**

Sugar substrates

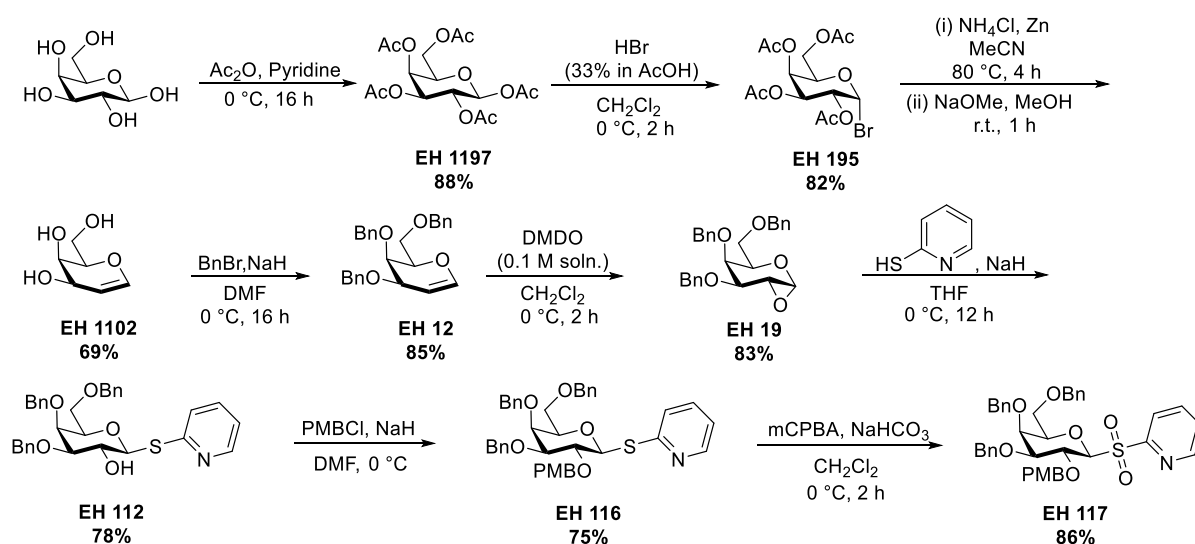
**(d) C-glycosylation via transition metal complexes**

Sugar substrates

**(e) Rearrangements****(f) Sugar ring formations**

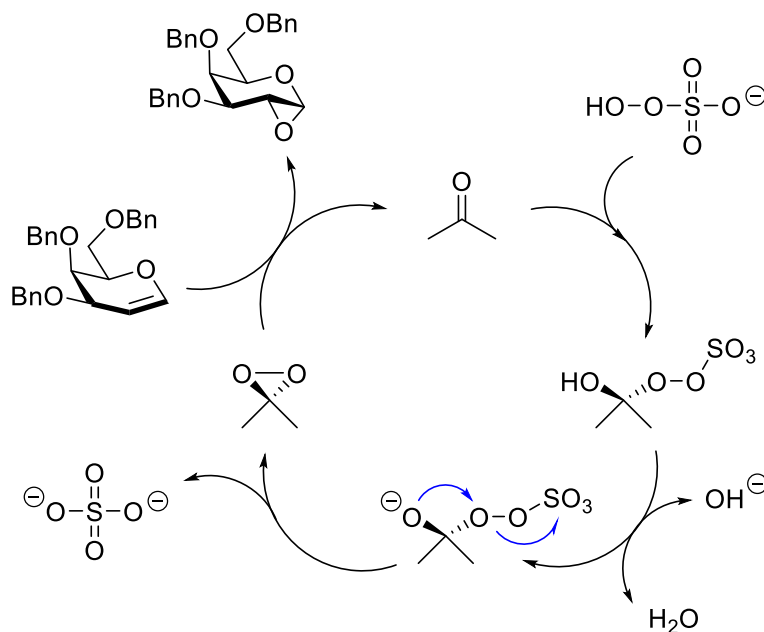
**Scheme 5: Major chemical methods for the synthesis of C-glycosides.** Adapted with permission from ref<sup>15</sup>, Copyright © 2017 American Chemical Society.

Glycosyl halides are perhaps the most versatile donors, as they can react with nucleophiles, electrophiles, form radical intermediates and transition metal complexes. The route chosen herein started with the synthesis of a galactosyl sulfone donor **EH 117** (Scheme 6) which is itself a versatile substrate for glycosylation reactions due to the presence of a good leaving group. Sulfones can react via anionic and cationic intermediates as well as undergoing rearrangements such as the Rämberg-Backlund reaction.  $\text{SmI}_2$  mediated C-C coupling with isobutyraldehyde was chosen due to the anomeric stereoretentive nature of the reaction and the resulting free secondary alcohol in the product **EH 122** which provided scope for synthesis of constrained C-glycosides. After the coupling, a methylene bridge was added between the adjacent free alcohols to form a cyclic constraint.



### Scheme 6: Synthesis of the Galactosyl Sulfone Donor

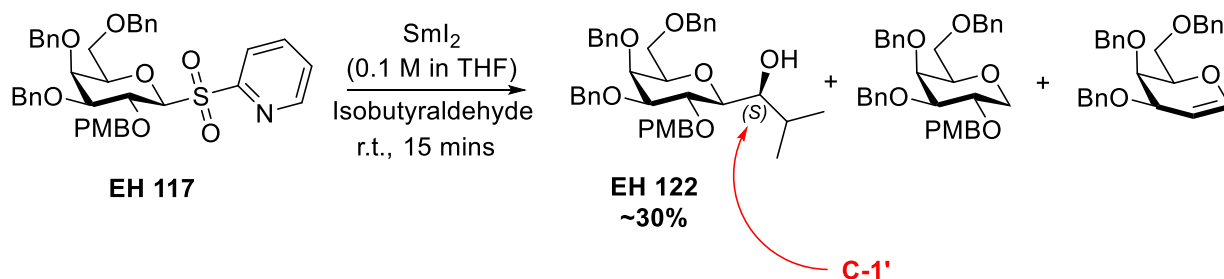
Free galactose was peracetylated using acetic anhydride and pyridine, giving the pentaacetylated product **EH 1197** in 88% yield. This compound was treated with a 33% hydrogen bromide solution in acetic acid to give **EH 195**. This  $\alpha$ -bromo derivative underwent an elimination reaction with ammonium chloride and zinc at 80 °C. Deacetylation under basic conditions gave the free galactal **EH 1102** in 69% yield. Perbenzylation using benzyl bromide and sodium hydride in DMF resulted in **EH 12**. A 0.1 M dimethyl dioxirane solution was generated in situ at 0 °C by dropwise addition of potassium peroxymonosulfate dissolved in water to a vigorously stirred round bottom containing acetone and sodium bicarbonate. **EH 12** dissolved in  $\text{CH}_2\text{Cl}_2$  was then added dropwise over 1 hour, resulting in epoxidation of the alkene to give **EH 19** (see Scheme 7).<sup>16</sup>



**Scheme 7: Catalytic cycle of epoxidation of Galactal**<sup>17</sup>

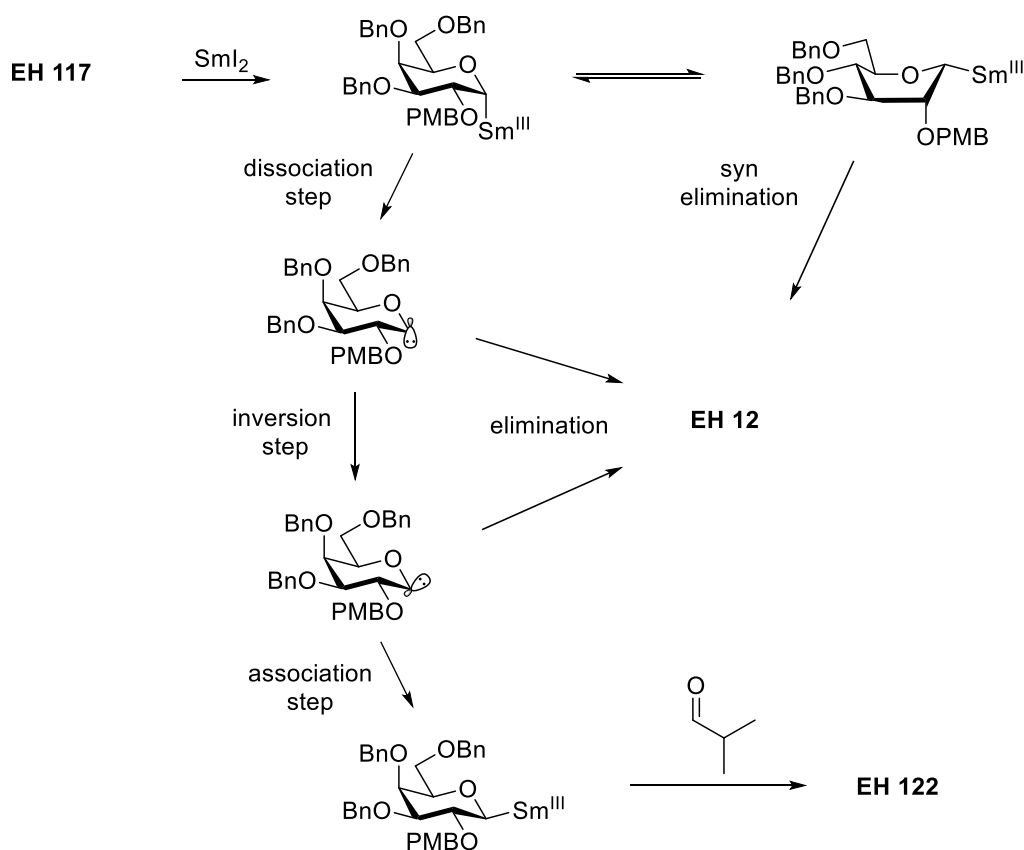
Treatment of 2-mercaptopyridine with sodium hydride generated a thiolate nucleophile which attacked **EH 19** upon dropwise addition at 0 °C, causing formation of the aromatic  $\beta$ -thioglycoside **EH 112** in 78% yield. Ring opening of the epoxide left the 2-position free, so protection of this alcohol using sodium hydride and paramethoxy benzyl chloride provided **EH 116** followed by oxidation of the thioglycosidic linkage with *m*CPBA and sodium bicarbonate<sup>18</sup> gave **EH 117**.

Beau et al have many reports<sup>18, 19, 20, 21</sup> on the use of Barbier-type conditions to form *C*-glycosides by reacting  $\alpha$ -chlorides or 2-pyridyl sulfones of neutral hexopyranoses with a carbonyl substrate. These reactions proceed via a mild room-temperature intermolecular addition of a glycosyl-samarium species onto a carbonyl and provide a rapid entry to 1,2-trans-*C*-glycosides. A 0.1 M solution of SmI<sub>2</sub> was generated in-situ by first activating Samarium metal via stirring under inert conditions for 24 h, followed by addition of excess iodine dissolved in dry, degassed THF and stirred for a further 18 h at 60 °C.<sup>22</sup> Once cooled, the SmI<sub>2</sub> solution was added to **EH 117** and aldehyde and an almost instantaneous reaction ensued (see scheme 8).



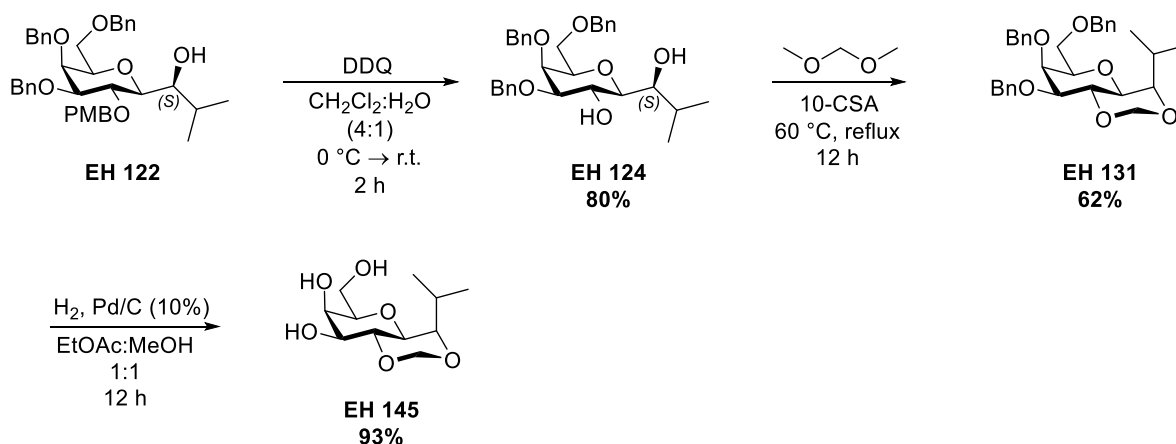
**Scheme 8: SmI<sub>2</sub> mediated C-C coupling reaction. Side products from reaction also shown.**

Scheme 8 shows side products from the reaction include the galactose moiety without the aglycon which results from C-S bond cleavage and galactal, the  $\beta$ -elimination product.<sup>23</sup> In the desired product **EH 122**, a  $\beta$ -C-galactoside was selectively observed while the low stereoselectivity at the newly created exocyclic stereocentre  $\alpha$  to the anomeric carbon (C-1') is in contrast with previous results reported for low-temperature coupling reactions with anomeric lithium reagents and shows that the major isomer has C-1'-(*S*)-configuration at the newly generated stereocentre (C-1').<sup>18, 24, 25, 26</sup> Mechanistically, it is thought that one-electron transfer from SmI<sub>2</sub> to the aryl sulfone LUMO of **EH 117** leads to homolytic C1-S bond cleavage and subsequent formation of the thermodynamically more stable  $\alpha$ -radical owing to favourable overlap between the singly occupied  $p_{C1}$  and  $n_{O5}$  orbitals.<sup>18, 27, 28</sup> A second reduction step then leads to a kinetic  $\alpha$ -oriented organosamarium. To relieve the energetically unfavoured interaction between the occupied  $\sigma_{C1-Sm}$  and  $n_{O5}$  orbitals, the organosamarium either undergoes a conformational ring flip to give a boat or skew-boat conformer or a configurational change affording a more sterically and energetically favoured diequatorial arrangement of the C1- and C2-substituents (see Scheme 9). The equatorially oriented C2-O2 bond must move through an eclipsed conformer with the C1-Sm bond, making this a higher energy process, hence configurational change to the  $\beta$ -organosamarium is the dominant pathway.



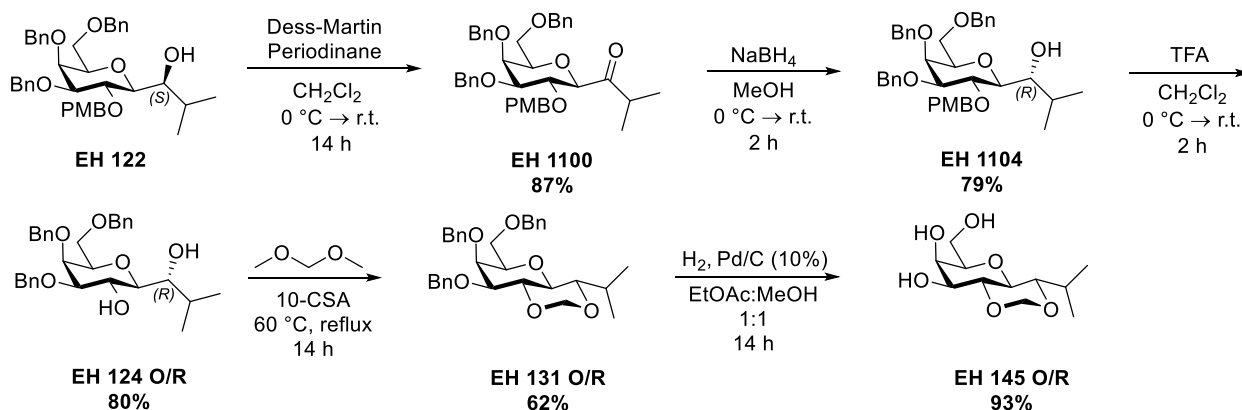
**Scheme 9: Mechanistic rationale for the highly stereoselective C-galactosylation reactions**<sup>25</sup>

The two naked anomeric anions following the dissociation and inversion steps in Scheme 9 are highly reactive and may undergo competitive  $\beta$ -elimination before recombination with the metal cation to the more stable  $\beta$  anomer, hence a greater facility for  $\beta$ -elimination to **EH 12**. The resulting mixture of **EH 122** and an uncharacterised elimination product was initially inseparable via chromatography, however, deprotection of the PMB group at the 2-position using DDQ<sup>29</sup> facilitated chromatographic separation of the mixture, with **EH 124** as the major product. The cyclic constraint was incorporated into the molecule when the isolated stereoisomer was refluxed overnight in neat dimethoxymethane in the presence of 10-CSA to form a methylene bridge between the two free hydroxyls, giving **EH 131**. Deprotection of the benzyl protecting groups via Hydrogenation in the presence of a 10% palladium on carbon catalyst provided **EH 145**, the final compound in 93% yield (see Scheme 10).



### Scheme 10: Introduction of cyclic constraint followed by global deprotection.

Epimerisation of the exocyclic secondary alcohol was achieved via Dess-Martin periodinane oxidation, stirring overnight at 0 °C to give **EH 1100**, followed by simultaneous reduction of the corresponding ketone. This was achieved with sodium borohydride in MeOH after addition at 0 °C, allowing the reaction to attain room temperature while stirring for 2 h, resulting in **EH 1104**. This stereoinverted product was reacted with trifluoroacetic acid in CH<sub>2</sub>Cl<sub>2</sub> to remove the PMB group at the 2- position<sup>30</sup> and underwent acetal formation and deprotection as previously described, giving **EH 145 O/R**.



### Scheme 11: Inversion of the isopropyl substituent, acetal formation and deprotection

Comparing *J* values of signals in <sup>1</sup>H-NMR spectra before and after oxidation-reduction indicate structural differences. A change in the coupling constant between H-1 and H-1' from 1.6 Hz to 5.2-5.8 Hz suggest stereoinversion. Signals representing H-1' before and after can be seen in Figure 33.

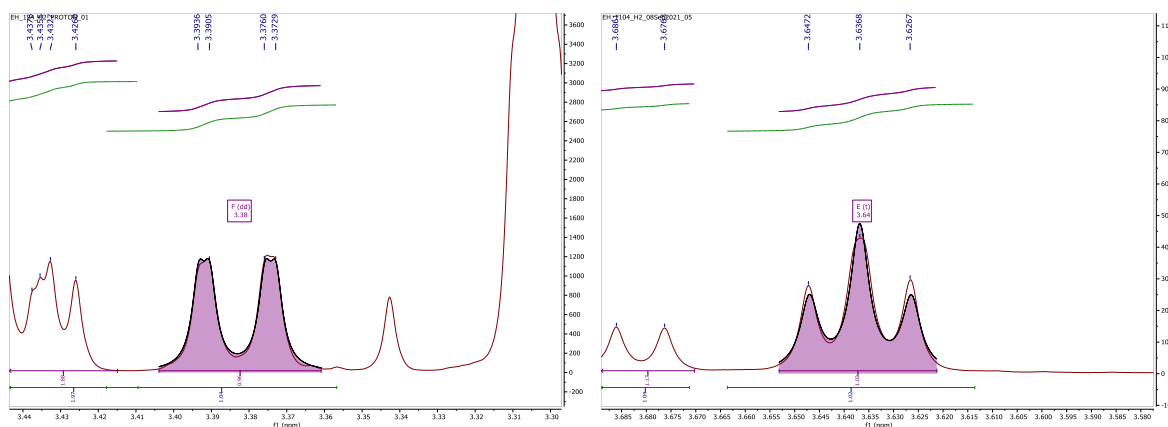
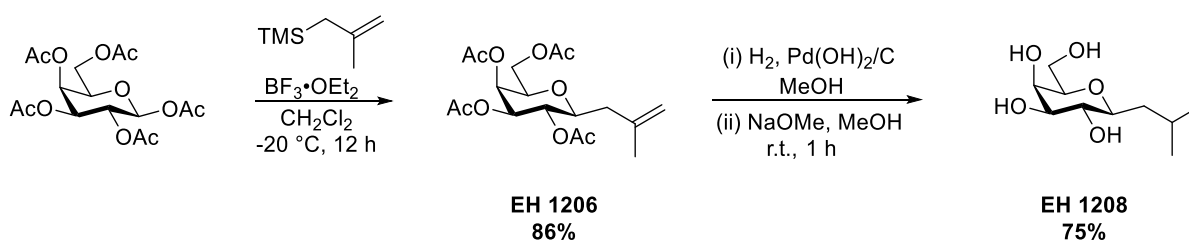


**Figure 33: Changes in the signals for H-1' (Attached to C-1') before (EH 122 on left) and after (EH 1104 on right) oxidation-reduction**

The unconstrained *C*-glycoside derivative **EH 1208** was synthesised according to a 3-step procedure by Pohl et al.<sup>31</sup> which started with **EH 1195** reacting with 2-methylallyl TMS in the presence of boron trifluoride diethyl etherate at -20 °C for 12 h. This reaction provided a 2:3 mixture of  $\alpha$ : $\beta$  anomers which were separable by chromatography. Hydrogenation of the alkene gave an acetylated isobutyl *C*-galactoside (IBCG) derivative **EH 1206** which was deprotected under basic conditions to yield **EH 1208** in 75% over two steps.



**Scheme 12: Route for preparation of IBCG (EH 1208)**

### $\beta$ -Galactosidase Inhibition Assay- Procedure and Results

With the galactosidase inhibitors in hand, an inhibition assay was carried out using three galactosidase enzymes,  $\beta$ -Galactosidase derived from *E. coli*,  $\beta$ -Galactosidase from *A. niger* and  $\alpha$ -galactosidase from *A. niger*. Enzyme inhibition can either be irreversible or reversible. An irreversible inhibitor will either destroy a functional group on an enzyme that is essential for the enzymes activity or dissociates very slowly from its target enzyme because it has become covalently bound to the enzyme. Irreversible inhibitors first form a reversible noncovalent complex with the enzyme (E·I). Subsequently, the enzyme and inhibitor produce



the covalently modified "dead-end complex" (E-I), an irreversible covalent complex. The reaction proceeds via the equation:



Where  $K_1$  defines the dissociation constant for the noncovalent complex, and  $k_{\text{inact}}$  the rate constant for covalent bond formation.<sup>32</sup> The noncovalent interactions in E·I complexes are much weaker than covalent bonds, which have energies between -50 and -110 kcal mol<sup>-1</sup>.<sup>33</sup> Irreversible inhibitors are useful for studying reactions mechanisms as they can identify key amino acid residues involved in catalytic functions in the active site by analysing which residue is bound to the inhibitor after inactivation.<sup>34</sup> Reversible inhibition, in contrast to irreversible inhibition, is characterized by noncovalent enzyme inhibitor interactions and a rapid dissociation of the enzyme inhibitor complex. Three types of possible reversible inhibition include competitive, uncompetitive, and non-competitive/mixed inhibition. Competitive inhibition is where the enzyme binds noncovalently to the substrate forming an enzyme substrate (E·S) complex or inhibitor (E·I) but not both (E·S·I, enzyme-substrate-inhibitor complex).<sup>33</sup> The competitive inhibitor is generally structurally similar to the substrate and binds to the active site of the enzyme, thereby preventing the substrate from binding to the same active site. The competitive inhibitor diminishes the rate of catalysis by reducing the proportion of enzyme molecules bound to a substrate. At any given inhibitor concentration, competitive inhibition can be relieved by increasing the substrate concentration. Under these conditions, the substrate successfully competes with the inhibitor for the active site.<sup>33</sup> Competitive inhibition can be analysed quantitatively by steady state kinetics. Uncompetitive inhibition is substrate dependent inhibition where the inhibitor binds only to the E·S complex. The binding site of an uncompetitive inhibitor is created only on interaction of the enzyme and substrate. Uncompetitive inhibition cannot be overcome by the addition of more substrate. In non-competitive inhibition, the inhibitor and substrate can bind simultaneously to an enzyme molecule at different binding sites. A non-competitive inhibitor can bind free enzyme or the E·S complex. It acts by decreasing the concentration of functional enzyme rather than diminishing the proportion of enzyme molecules bound to the substrate.<sup>33</sup> Non-competitive inhibition cannot be overcome by increasing the substrate concentration. The curve expressing the relationship between [S] and  $V_0$ , the initial rate of the reaction can be expressed algebraically by the Michaelis-Menten equation:

$$V_0 = \frac{V_{max}[S]}{K_M + [S]}$$

Where  $V_{max}$  is the maximum velocity of the enzyme reaction and  $K_M$  is the Michaelis constant, the  $[S]$  at which  $V_0$  is half maximal. The Michaelis Menten equation can be algebraically transformed into equations that are more useful in plotting experimental data. The double reciprocal of the equation, the Lineweaver-Burk equation (see equation below) is advantageous over the Michaelis-Menten equation as it gives a straight-line plot, allowing more accurate determination of  $V_{max}$ , which can only be approximated from a simple plot of  $V_0$  vs  $[S]$ .<sup>34</sup>

$$\frac{1}{V_0} = \frac{K_M}{V_{max}[S]} + \frac{1}{V_{max}}$$

$$Y = M \cdot X + C$$

When used for determining the type of enzyme inhibition, the double reciprocal Lineweaver–Burk plot can distinguish competitive, uncompetitive and noncompetitive (mixed) inhibitors. The various modes of inhibition can be compared to the uninhibited reaction (see Figure 34).<sup>33</sup>

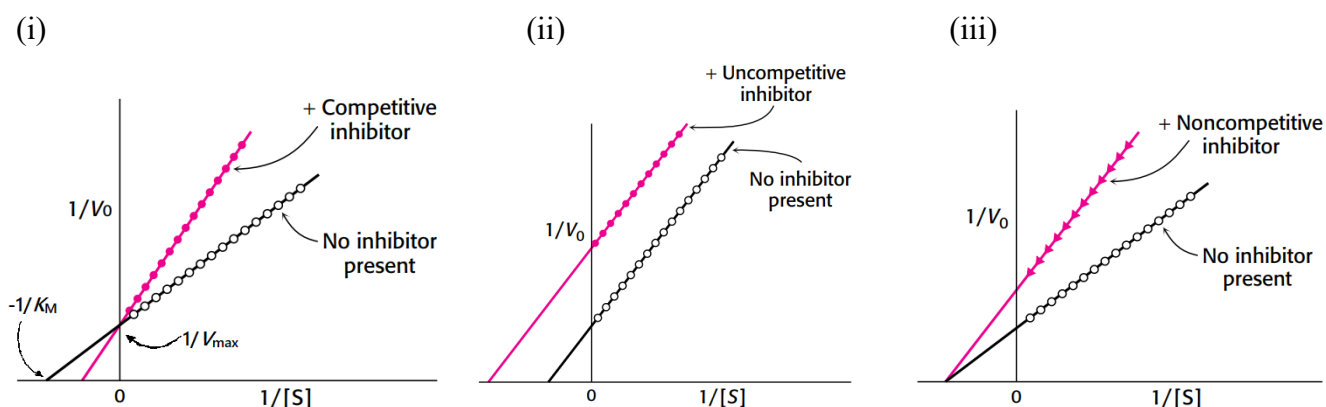


**Figure 34: Lineweaver Burk Plots representing various types of Enzyme inhibition (i) Competitive Inhibitors have no effect on  $V_{max}$  but increase  $K_M$  (ii) Uncompetitive Inhibitors have no effect on slope.  $V_{max}$  and  $K_M$  are reduced by equivalent amounts (iii) Noncompetitive (mixed) inhibitors show that  $K_M$  is unaltered and  $V_{max}$  is decreased.**

Preparation of Lineweaver-Burk plots using data from our kinetic experiments suggest that mixed inhibition is the predominant enzyme reaction (see Figure 35).

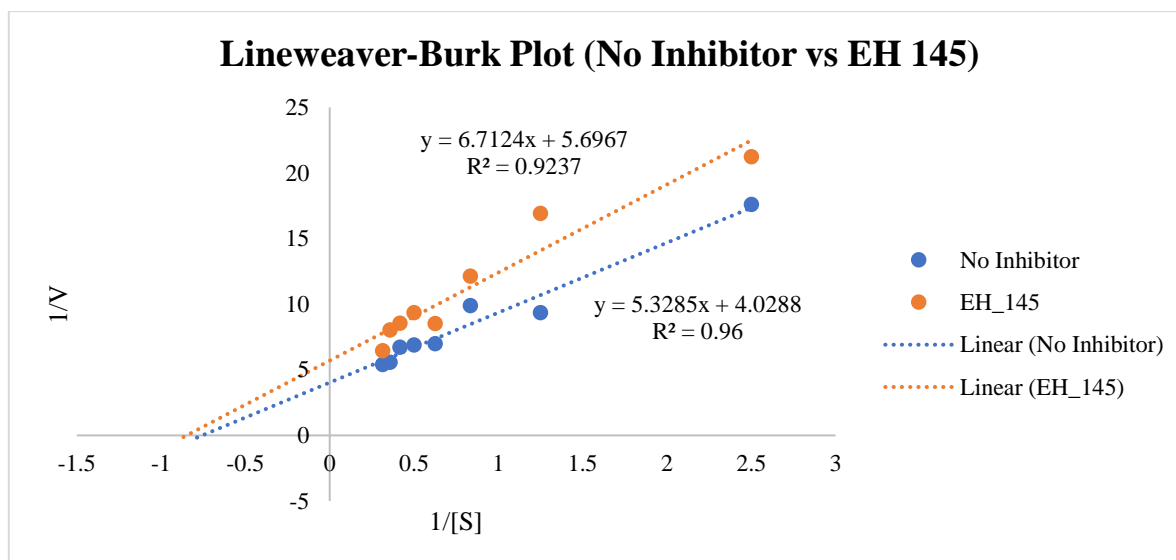
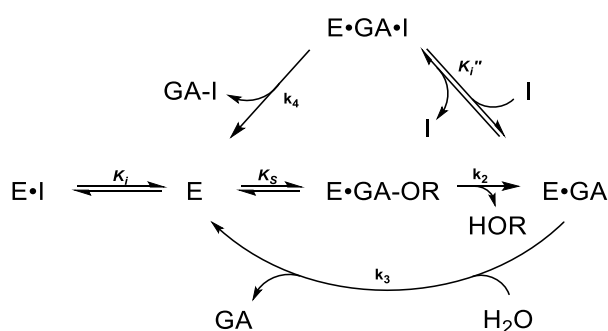


**Figure 35: Lineweaver-Burk Plot of No Inhibitor vs EH 145. No change in  $K_M$  and a decrease in  $V_{max}$  suggest mixed inhibition. Data produced from Abs (400 nM) readings obtained via a Fluorometric Enzyme Inhibition Assay.**

In the presence of an inhibitor, reactions involving  $\beta$ -galactosidase proceed via Scheme 13,<sup>6</sup> where E is the enzyme, I is the inhibitor, GA-OR is the galactose substrate with the chromophoric aglycon at the anomeric position, GA is the cleavage product of the enzyme reaction and HOR is the cleaved aglycon. Upon cleavage of the glycosidic bond, the aglycon moiety becomes UV active and a plot of Abs. vs time was prepared for a [substrate] range of 0.4 mM  $\rightarrow$  3.2 mM in the absence and presence of 1 mM inhibitor.



**Scheme 13: Reactions of  $\beta$ -Galactosidase in the presence of a mixed inhibitor,  $K_i$  (Not to be confused with  $K_I$ , the dissociation constant of the noncovalent E·I complex in irreversible inhibition) is the dissociation constant for the interaction of a competitive inhibitor with free enzyme.  $K_i''$  is the dissociation constant for binding to the “galactosylated” enzyme.  $K_s$  is the dissociation constant of the enzyme-substrate complex.  $k_2$  is the rate constant for the galactosylation step,  $k_3$  is the rate constant for the degalactosylation step,  $k_4$  is the rate constant for acceptors to form adducts.**

The slopes of these lines provided a range of velocity values, which were used to prepare a variation of the Lineweaver-Burk plot, the Hanes Woolf plot (see equation of line below):

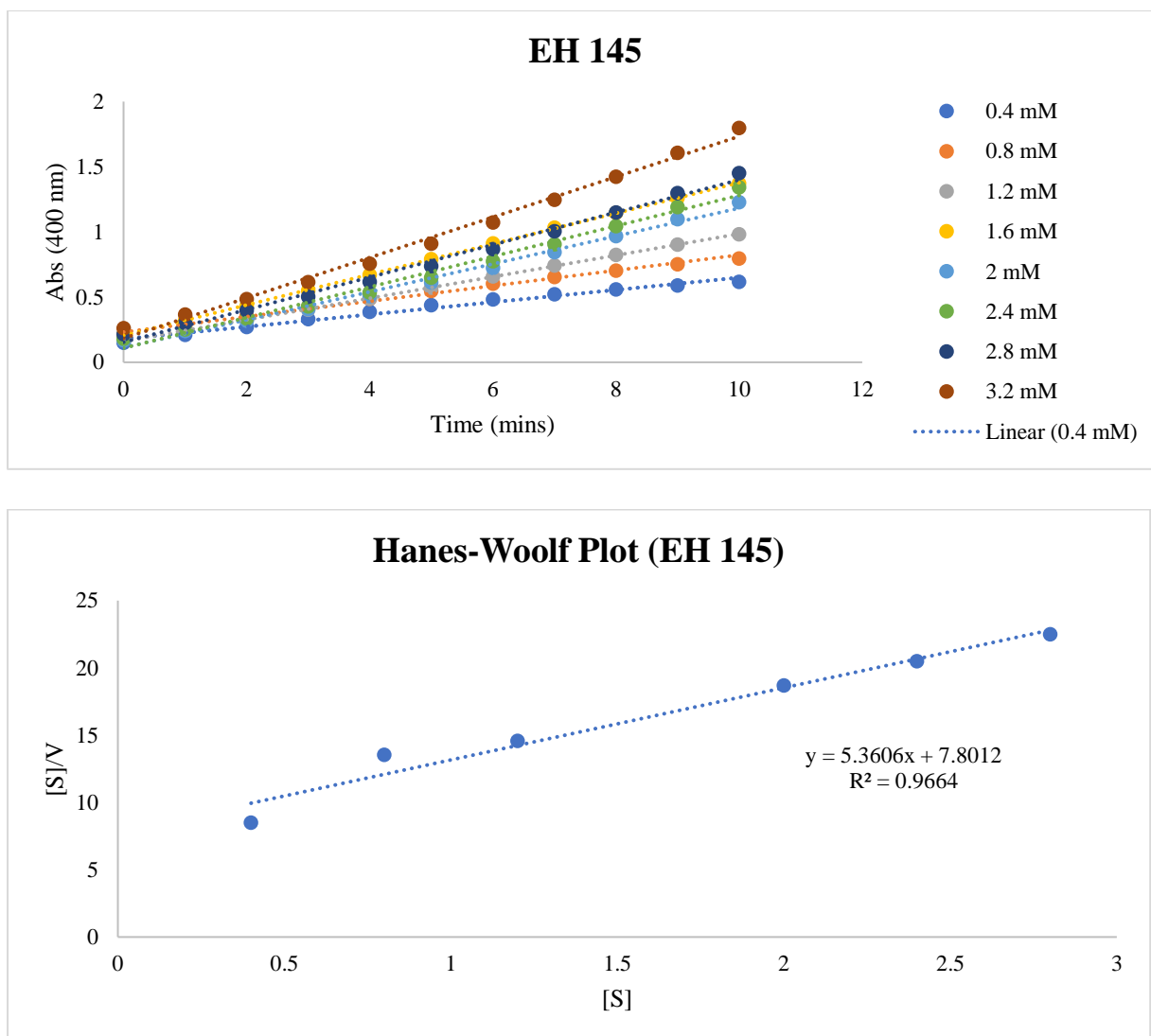


**Figure 36:(i) Plot of Abs. vs Time for EH 145 at different [substrate] (ii) Hanes-Woolf Plot generated from plot of Abs. vs Time.**

$$\frac{[S]}{V} = \frac{[S]}{V_{max}} + \frac{K_M}{V_{max}}$$

$$Y = M \cdot X + C$$

$K_M$  in the presence and  $K_M'$  in the absence of an inhibitor can be used to calculate  $K_i$  according to the equation:

$$\frac{K_M'}{K_M} = 1 + \frac{[I]}{K_i}$$

The results of the assay for the set of synthesised compounds are summarised in tables 5A-B.

Table 5A

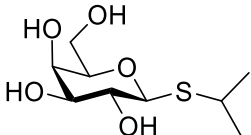
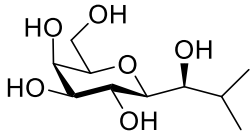
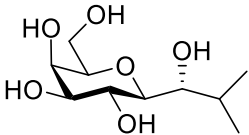
| Enzyme                                      | $K_i$ (mM)  |   |   |
|---|---|---|---|
|   | <br>IPTG | <br>EH 124 H2 | <br>EH 1104 H2 |
| $\beta$ -Galactosidase ( <i>E. coli</i> )   | 0.1988  | 0.3717  | 0.23  |
| $\beta$ -Galactosidase ( <i>A. niger</i> )  | 12.1  | No Inhibition   | 0.8318  |
| $\alpha$ -Galactosidase ( <i>A. niger</i> ) | No Inhibition   | No Inhibition   | No Inhibition   |

Table 5B

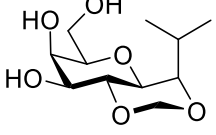
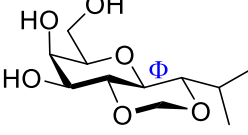
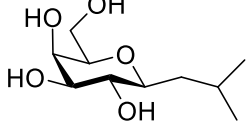
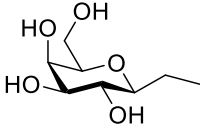
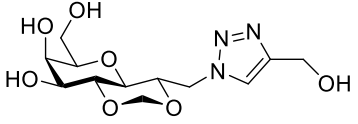
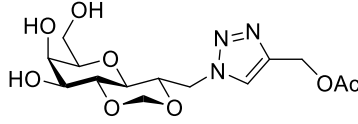
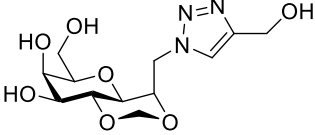
| Enzyme                                      | $K_i$ (mM)  |  |  |
|---|---|--|--|
|   | <br>EH 145 | <br>EH 145 O/R | <br>EH 1208 |
| $\beta$ -Galactosidase ( <i>E. coli</i> )   | 0.1975  | 0.176  | 0.0882   |
| $\beta$ -Galactosidase ( <i>A. niger</i> )  | No Inhibition   | 3.272  | 2  |
| $\alpha$ -Galactosidase ( <i>A. niger</i> ) | 2.915   | No Inhibition  | 24.75  |

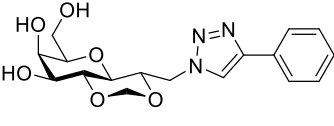
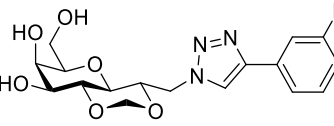
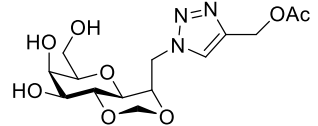
Table 6A &amp; 5B: Results of the Galactosidase Inhibition study with IPTG analogues

C-Galactose derivatives synthesised by Ashis Dhara and Dr. Saidulu Konda were also tested and these results can be seen in tables 6 and 7.

Table 6A

| Enzyme                                      | $K_i$ (mM)  |  |  |
|---|---|--|--|
|   | <br>AD 442 | <br>AD 585 | <br>AD556 |
| $\beta$ -Galactosidase ( <i>E. coli</i> )   | 0.95  | 1.4  | 1.2437   |
| $\beta$ -Galactosidase ( <i>A. niger</i> )  | 0.7039  | 0.78332  | 0.875  |
| $\alpha$ -Galactosidase ( <i>A. niger</i> ) | 2.6186  | 7.5277   | 2.1295   |

| Table 6B                                    |   |
|---|---|
| Enzyme                                      | $K_i$ (mM)  |
|   | <br>AD 584 |
| $\beta$ -Galactosidase ( <i>E. coli</i> )   | 21.27   |
| $\beta$ -Galactosidase ( <i>A. niger</i> )  | No Inhibition   |
| $\alpha$ -Galactosidase ( <i>A. niger</i> ) | 1.5484  |

| Table 6C                                    |  |   |  |
|---|--|---|--|
| Enzyme                                      | $K_i$ (mM)   |   |  |
|   | <br>AD 558 | <br>AD 433 | <br>AD 553 |
| $\beta$ -Galactosidase ( <i>E. coli</i> )   | 1.183  | 2.342   | 0.77685  |
| $\beta$ -Galactosidase ( <i>A. niger</i> )  | 0.648  | 2.7375  | 1.315  |
| $\alpha$ -Galactosidase ( <i>A. niger</i> ) | 8.44   | 4.369   | 9.5483   |

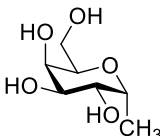
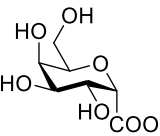
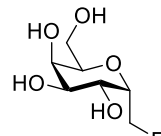
| Table 6D                                    |   |  |   |
|---|---|--|---|
| Enzyme                                      | $K_i$ (mM)  |  |   |
|   | <br>AD 500 | <br>AD 516 | <br>AD 525 |
| $\beta$ -Galactosidase ( <i>E. coli</i> )   | No Inhibition   | No Inhibition  | 0.9091  |
| $\beta$ -Galactosidase ( <i>A. niger</i> )  | 5.659   | No Inhibition  | 2.8374  |
| $\alpha$ -Galactosidase ( <i>A. niger</i> ) | No Inhibition   | 1.824  | No Inhibition   |

Table 6E

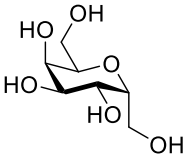
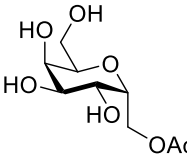
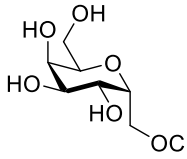
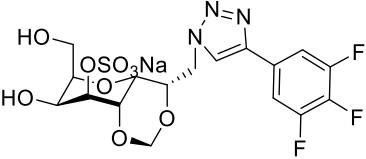
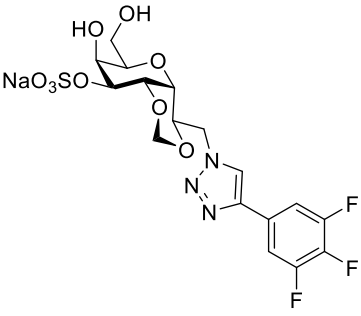
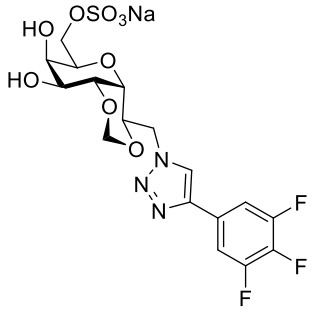
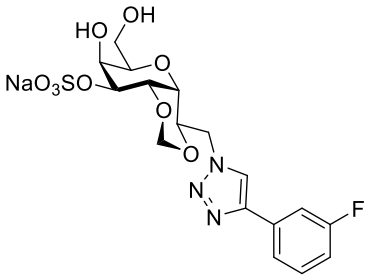
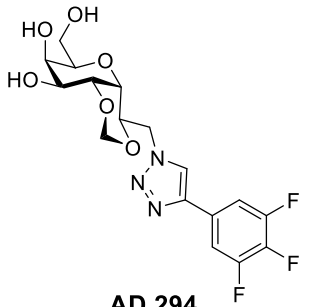
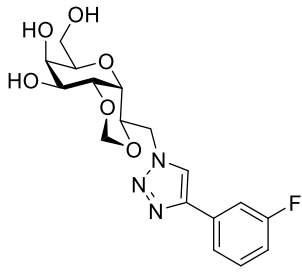
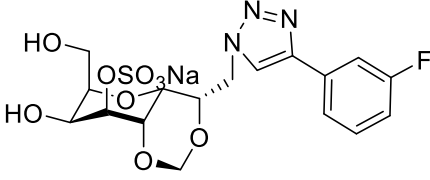
| Enzyme                                      | $K_i$ (mM)  |  |   |
|---|---|--|---|
|   |  |  |  |
|   | AD 452  | AD 466   | AD 511  |
| $\beta$ -Galactosidase ( <i>E. coli</i> )   | 0.5377  | 1.359  | No Inhibition   |
| $\beta$ -Galactosidase ( <i>A. niger</i> )  | 1719.3  | 1.317  | 5.008   |
| $\alpha$ -Galactosidase ( <i>A. niger</i> ) | 6.015   | No Inhibition  | No Inhibition   |

Table 6F

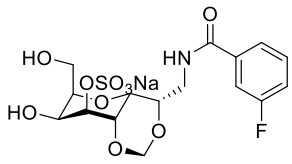
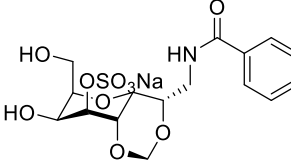
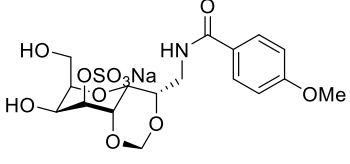
| Enzyme                                      | $K_i$ (mM)  |   |  |
|---|---|---|--|
|   |  |  |  |
|   | AD 301A   | AD 301B   | AD 304B  |
| $\beta$ -Galactosidase ( <i>E. coli</i> )   | 0.8523  | 1.5287  | 1.379  |
| $\beta$ -Galactosidase ( <i>A. niger</i> )  | 8.8938  | 1.65  | 1.6356   |
| $\alpha$ -Galactosidase ( <i>A. niger</i> ) | No Inhibition   | No Inhibition   | No Inhibition  |

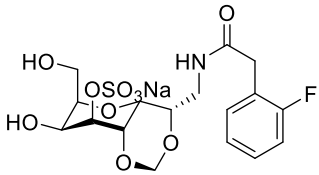
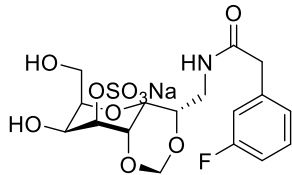
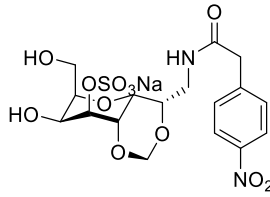
| <b>Table 6G</b>                             |  |   |   |
|---|--|---|---|
| <b>Enzyme</b>                               | <b><math>K_i</math> (mM)</b>   |   |   |
|   | <br><b>AD 309</b> | <br><b>AD 294</b> | <br><b>AD 287A</b> |
| $\beta$ -Galactosidase ( <i>E. coli</i> )   | 0.93   | 1.8405  | No Inhibition   |
| $\beta$ -Galactosidase ( <i>A. niger</i> )  | 6.902  | No Inhibition   | 2.2976  |
| $\alpha$ -Galactosidase ( <i>A. niger</i> ) | 5.173  | 14  | No Inhibition   |

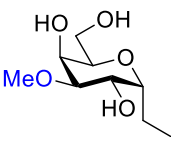
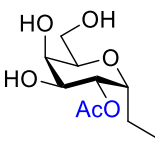
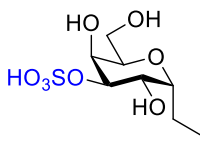
| <b>Table 6H</b>                             |  |
|---|--|
| <b>Enzyme</b>                               | <b><math>K_i</math> (mM)</b>   |
|   | <br><b>AD 307</b> |
| $\beta$ -Galactosidase ( <i>E. coli</i> )   | No Inhibition  |
| $\beta$ -Galactosidase ( <i>A. niger</i> )  | 33.5735  |
| $\alpha$ -Galactosidase ( <i>A. niger</i> ) | 376.727  |

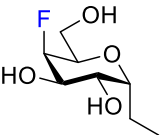
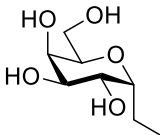
**Tables 6A-H: Results of the Galactosidase Inhibition study with Ashis Dhara's compounds**



| Table 7A                                    |   |  |   |
|---|---|--|---|
| Enzyme                                      | $K_i$ (mM)  |  |   |
|   | <br><b>SK 65</b> | <br><b>SK 81</b> | <br><b>SK 87</b> |
| $\beta$ -Galactosidase ( <i>E. coli</i> )   | 1.1764  | 0.557  | 0.7216  |
| $\beta$ -Galactosidase ( <i>A. niger</i> )  | 31.623  | 1.412  | 3.5573  |
| $\alpha$ -Galactosidase ( <i>A. niger</i> ) | 1.8288  | No Inhibition  | 3.5464  |

| Table 7B                                    |   |  |   |
|---|---|--|---|
| Enzyme                                      | $K_i$ (mM)  |  |   |
|   | <br><b>SK 84</b> | <br><b>SK 83</b> | <br><b>SK 79</b> |
| $\beta$ -Galactosidase ( <i>E. coli</i> )   | 0.6047  | 0.5357   | 0.515   |
| $\beta$ -Galactosidase ( <i>A. niger</i> )  | 1.055   | 21.59  | 4.97  |
| $\alpha$ -Galactosidase ( <i>A. niger</i> ) | 1.2825  | 17.088   | 1.8785  |

| Table 7C                                    |  |   |  |
|---|--|---|--|
| Enzyme                                      | $K_i$ (mM)   |   |  |
|   | <br><b>SK 167</b> | <br><b>SK 122</b> | <br><b>SK 284</b> |
| $\beta$ -Galactosidase ( <i>E. coli</i> )   | 0.7362   | 1.00  | 0.9677   |
| $\beta$ -Galactosidase ( <i>A. niger</i> )  | 1.8216   | 3.18  | 1.988  |
| $\alpha$ -Galactosidase ( <i>A. niger</i> ) | 1.53   | 5.16  | 1.5462   |

| Table 7D                                    |   |  |
|---|---|--|
| Enzyme                                      | $K_i$ (mM)  |  |
|   | <br><b>SK 198</b> | <br><b>SK 155</b> |
| $\beta$ -Galactosidase ( <i>E. coli</i> )   | 0.9449  | 2.727  |
| $\beta$ -Galactosidase ( <i>A. niger</i> )  | 2.88  | 5.6275   |
| $\alpha$ -Galactosidase ( <i>A. niger</i> ) | 3.4079  | 4.301  |

**Tables 7A-D: Results of the Galactosidase Inhibition study with Saidulu Konda's compounds**

### Discussion

Overall affinity was certainly lower than the inhibitors shown in Figure 32, however, in tables 5A and 5B, a structure-activity relationship can be inferred for inhibition of the  $\alpha$ -galactosidase enzyme. Only very weak to no inhibitory activity was observed for all the compounds, except **EH 145**, the constrained axial isopropyl derivative. The orientation of the isopropyl group is hypothesised to play a pivotal role in the binding activity. Interestingly, this compound did not make any major improvement compared to **IPTG** in the  $\beta$ -galactosidase from *E. coli*. The best inhibitor in this series for inhibition of the *E.Coli*  $\beta$ -galactosidase when comparing the 6

compounds in Tables 5A and 5B was **EH 1208**. A 2.2-fold improvement is seen relative to **IPTG** for  $\beta$ -galactosidase from *E. coli* for **EH 1208** (Table 5B), and a 6-fold improvement for  $\beta$ -galactosidase from *A. niger*. Although results are poor for  $\alpha$ -galactosidase from *A. niger*, the C-glycosyl compounds which are inhibitors are better than **IPTG** (Table 5A). There was a slight improvement when comparing **EH 145 O/R** (Table 5B) to **IPTG** for  $\beta$ -galactosidase from *E. coli*, although the unconstrained analogues, **EH 124 H2** and **EH 1104 H2** (both Table 5A) were poorer.

The constraint in **EH 145** (Table 5B) forces an axial orientation of the isopropyl group, which is unfavoured in the unconstrained analogues (see Figure 38). Constraint of **EH 145** and **EH 145 O/R** show a slight improvement compared to the unconstrained analogues **EH 124 H2** and **EH 1104 H2**, which supports a possible role for preorganisation of the isopropyl group. Results for **EH 145 O/R** are however 2 and 1.6-fold worse than **EH 1208** for  $\beta$ -Galactosidase (*E. coli*) and  $\beta$ -Galactosidase (*A. niger*) respectively. Although the constraint provides stability against entropic penalties due to preorganisation when binding, the possibility of a steric clash in the enzyme binding site cannot be ignored. There is a 1.6-fold difference between **EH 1104 H2** (*R*) and **EH 124 H2** (*S*) unconstrained analogues with  $\beta$ -Galactosidase (*E. coli*) (Table 5A). Prior to analysis of carbohydrate-protein interactions, it is important to try and rationalise a preference for these inhibitors based on their intramolecular steric and electronic repulsive interactions. To distinguish between **EH 124 H2** and **EH 1104 H2**, it is important to consider the corresponding *O*-glycosides, which are influenced by the exo-anomeric effect.

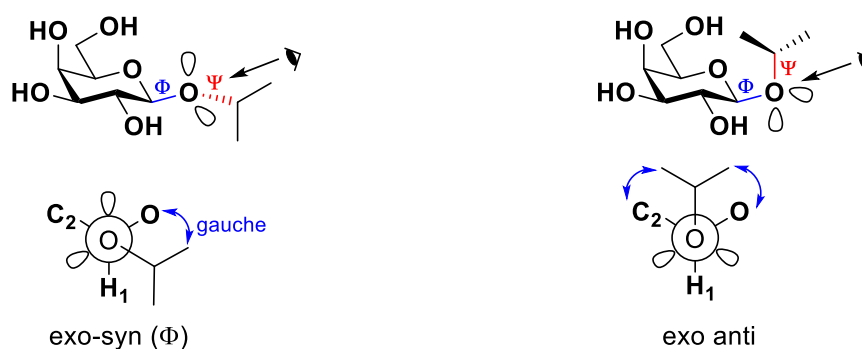


**Figure 37: Newman Projections of *O*-glycoside conformations corresponding to conformational C-glycoside mimetics **EH 124 H2** and **EH 1104 H2****

When looking along the O-C1 bond, both exo-syn and exo-anti conformers are stabilised by the exo-anomeric effect, with one lone pair of electrons anti-periplanar to the endocyclic oxygen in Figure 37. However, the exo-syn, which is mimicked by **EH 1104 H2**, has less steric interactions than the exo-anti, which is mimicked by **EH 124 H2** making **EH 1104 H2** a

mimetic of the more favoured *O*-glycoside exo-syn conformation. Due to the absence of electron lone pairs in *C*-glycosides, there is no stabilisation by the exo-anomeric effect, however the conformational preference about the glycoside bond shows similar preference to the *O*-glycoside in terms of steric gauche interactions placing the two largest substituents (iPr and gal C2) in an antiperiplanar arrangement (see Figure 38), as shown in a series of papers published by Kishi et al.<sup>35, 36, 37, 38, 39</sup> Newman projections looking along the C-1'-C1 bond like those in Figure 38 suggest less gauche interactions in **EH 1104 H2** and the absence of a 1,3-diaxial clash as observed in **EH 124 H2** (displayed in green). Blue arrows indicate gauche interactions of bulky groups. Less gauche interactions are observed in **EH 1104 H2** compared to **EH 124 H2**. There is a steric preference for when C2 is antiperiplanar to the isopropyl, this conformation is expected to be favoured in both compounds (see Figure 40 for docking pose of **EH 124 H2** and **EH 1104 H2**).

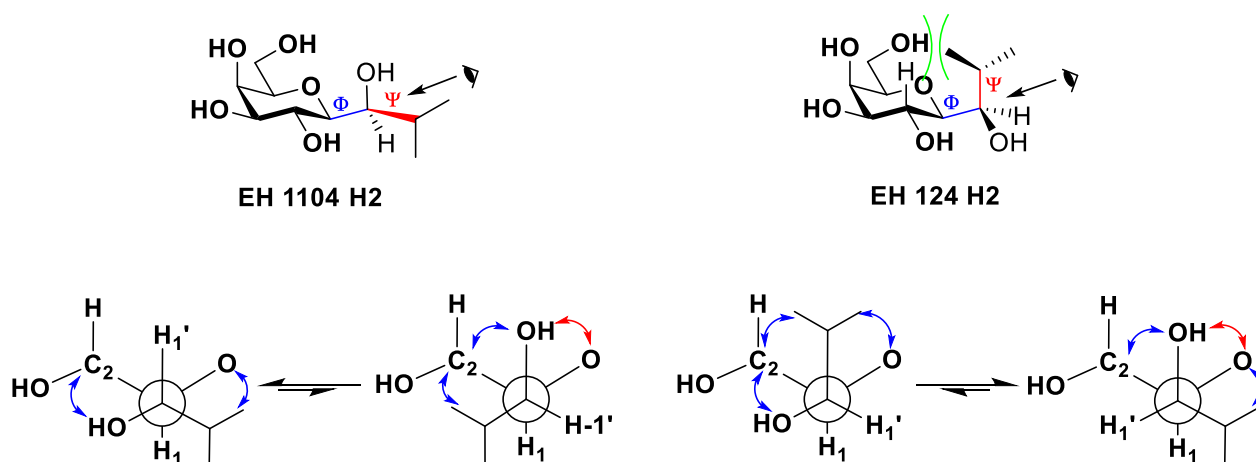


**Figure 38: Comparing the conformers of EH 1104 H2 vs EH 124 H2**

The red arrows in Figure 38 indicate the gauche effect, where two electron withdrawing substituents gauche ( $60^\circ$ ) to one another are more stable than the anti-conformation ( $180^\circ$ ) due to hyperconjugation. The electronegativity of the oxygen means electron density is pulled towards the oxygen in the C-O bond and as a result, stability is provided when electron density is donated from the adjacent C-H  $\sigma$  bonding orbital to the C-O  $\sigma^*$  antibonding orbital. Only the gauche conformation allows good overlap between the donor and the acceptor.



**Figure 39: Side view of C1-C1' bond of EH 1104 H2 and EH 124 H2 showing hyperconjugation model for explaining the gauche effect.**

**EH 1104 H2** also gives a better performance for the  $\beta$ -Galactosidase from *A. niger*, suggesting that the orientation of the alcohol has an influence on binding. This data is consistent with the constrained compounds that they precede for the  $\beta$ -Galactosidase enzymes, where **EH 145 O/R** (exo-syn) is better than **EH 145** (exo-anti) in both cases.

In tables 6A-C, all the  $\beta$ -derivatives, apart from **AD 584** (Table 6B), had  $K_i$  values less than 3 mM for  $\beta$ -galactosidase (*E. coli*), this should be a straightforward explanation, with the exo-anti orientation of the triazole substituent, although this reasoning is inconsistent with **AD 553** (Table 6C), which gave the strongest inhibition in this series of  $\beta$  derivatives for  $\beta$ -galactosidase (*E. coli*). The  $\beta$ -ethyl derivative **AD 442** (Table 6A) gave better inhibition than all except one of the constrained triazole substituted ligands for the two  $\beta$ -galactosidase enzymes. As already mentioned, **AD 553** gave better results for *E. coli*, while **AD 558** gave better results for *A. niger*. The slightly poorer results for the bulky triazole ligands are perhaps due to steric clashes in the binding pocket. This observation is supported by **AD 433** vs. **AD 558**, (both Table 6C, see Figure 41 for docking of **AD 433**). In the case of **AD 585** vs. **AD 556** (Table 6A) and **AD 584** vs. **AD 553**, the acetylated derivatives gave better results than the free alcohols with  $\beta$ -galactosidase from *E. coli*. The results for all the  $\beta$ -derivatives were generally poorer with  $\alpha$ -galactosidase. Surprisingly, **AD 584** gave the best results of the  $\beta$ -compounds for  $\alpha$ -galactosidase after giving the worst inhibition for the two  $\beta$ -galactosidases.

No inhibition was observed in a few unconstrained  $\alpha$ -derivatives with  $\beta$ -galactosidase from *E. coli*. The best inhibitor in this series was **AD 452** (Table 6E, see Figure 42 for docking), followed by **AD 525** (Table 6D), which was  $\sim 2$  fold weaker than **AD 452**. Contrary to the previous trend with the  $\beta$ -derivatives, the free alcohol of **AD 452** gave a 2.5 fold improvement over the acetylated **AD 466** (Table 6E). This ligand proved to be the best inhibitor for  $\beta$ -galactosidase from *A. niger* and was  $\sim 2$  fold stronger than **AD 525**, the next most potent.

Despite being the best inhibitor for  $\beta$ -galactosidase from *E. coli*, **AD 452** gave relatively low affinity results for  $\beta$ -galactosidase from *A. niger*. Results for this series with  $\alpha$ -galactosidase were generally poor, with four of the six compounds tested showing no inhibition. Despite showing no inhibition for either of the  $\beta$ -galactosidase enzymes, **AD 516** (Table 6D) was the best inhibitor for  $\alpha$ -galactosidase.

All the constrained derivatives in tables 7A and 7B underwent a conformational ring flip from  ${}^4C_1$  to  ${}^1C_4$ . Despite the ring flip, this series of compounds performed well in terms of inhibition of  $\beta$ -galactosidase from *E. coli*. The *para*-nitro derivative **SK 79** (Table 7B) was the best inhibitor for this enzyme in this series. The substitution pattern of the aromatic ring is a defining factor in the inhibition ability. With the fluorinated compounds **SK 65**, **SK 81** (Table 7A), **SK 83** and **SK 84** (Table 7B), inhibition ability appears to follow *para* > *meta* > *ortho*. This is in slight contrast however to  $\beta$ -galactosidase from *A. niger*, where *meta* > *ortho* in **SK 83** vs. **SK 84**. When comparing the results of **SK 65** vs. **SK 83**, the extra carbon appears to have an enhancing effect on the inhibition ability of the ligands (see Figure 43 for docking), although not a huge difference, a  $\sim 2$  fold and  $\sim 1.5$  fold improvement for **SK 83** in  $\beta$ -galactosidase from *E. coli* and  $\beta$ -galactosidase from *A. niger* respectively. Despite **SK 81** giving good results for both  $\beta$ -galactosidase enzymes, no inhibition was observed for  $\alpha$ -galactosidase. With  $\alpha$ -galactosidase, the extra carbon of **SK 83** compared to **SK 65** (Table 7A) has a negative effect on the inhibitory ability for this enzyme, with a  $\sim 9$  fold deterioration due to the extra carbon. In contrast to the  $\beta$ -galactosidases, the aromatic substitution pattern for this enzyme follows the trend *ortho* > *meta* > *para*, with *para* substituted **SK 84** giving the best inhibitory performance for this enzyme.

The unconstrained  $\alpha$ -derivatives from table 7 gave some interesting results for  $\beta$ -galactosidase from *E. coli*. 2-,3- and 4-position substituents were investigated for this series of compounds and compared to the free  $\alpha$ -ethyl C-glycoside **SK 155** (Table 7D). All of the substituents appeared to improve the affinity relative to **SK 155**, with this compound giving the poorest results for both  $\beta$ -galactosidases. The best inhibitor for all three of the enzymes tested was **SK 167** (Table 7C, see Figure 44 for docking). Only the 2-*O* acetylated **SK 122** (Table 7C) gave poorer results than **SK 155** for  $\alpha$ -galactosidase.

## Molecular Docking of Selected Ligands

To gain an understanding and explain the biological data in the galactosidase assay, the ligands were docked into the protein binding pocket to explore potential interactions between ligand and protein that may give a rationale for the results. Two X-ray crystal structures were retrieved from the Protein Data Bank, both were  $\beta$ -galactosidase derivatives bound to **IPTG**, one derived from *E. coli* (PDB ID: 3MUZ<sup>40</sup>) and one from *A. niger* (PDB ID: 5IFT<sup>41</sup>). A crystal structure for  $\alpha$ -galactosidase from *A. niger* with inhibitor could not be found at the protein databank (www.rcsb.org). Although the PDB structures obtained had mutations from the native enzymes (R599A for 3MUZ and E298Q for 5IFT) these were corrected via the docking software to give structures that matched the wild type proteins. The ligands were docked by editing the **IPTG** structure already present in the protein binding pocket to build the synthesized molecules. The 3-D structure of ligands were predicted based on  $J$ -values from <sup>1</sup>H-NMR signals and prepared using the Maestro software (see experimental section for details). For **EH 124 H2** vs **EH 1104 H2**, the  $\alpha$ -face of both sugar rings was predicted to engage in CH- $\pi$  interactions with Trp999 in the same way as **IPTG** in 1JYX.<sup>2</sup> The 4-OH and 6-OH of both are involved in H-bonding with the carboxylate of Asp201, while the 2-OH and 3-OH are both H-bonded to the carboxylate of Glu461. Incorporation of the constraint meant the loss of these 2-OH H-bond interactions, which likely leads to a reduction in affinity compared to **EH 1208** or **IPTG**, limiting gains made by the preorganisation strategy. The binding mode differed slightly due to the orientation of the isopropyl group and the free exocyclic alcohol. No significant difference between the  $K_i$  values for **EH 145** and **EH 145 O/R** suggest that the promiscuous nature of the enzyme allow it to tolerate different orientations of these groups For **EH 124 H2** orientation of 2'-OH allows H-bonding with Asn102, while the same alcohol on **EH 1104 H2** is involved in an OH- $\pi$  interaction with the indole nitrogen of Trp999. The H-2' in both **EH 124 H2** and **EH 1104 H2** participate in the same CH- $\pi$  interactions as the sugar ring with Trp999. In **EH 1104 H2**, H-1' and one of the terminal methyl groups of the isopropyl moiety are in close proximity (3.03 Å & 2.41 Å respectively) to the N-H of Asn102, while H-1' in **EH 124 H2** is orientated away from this residue (see Figure 40).

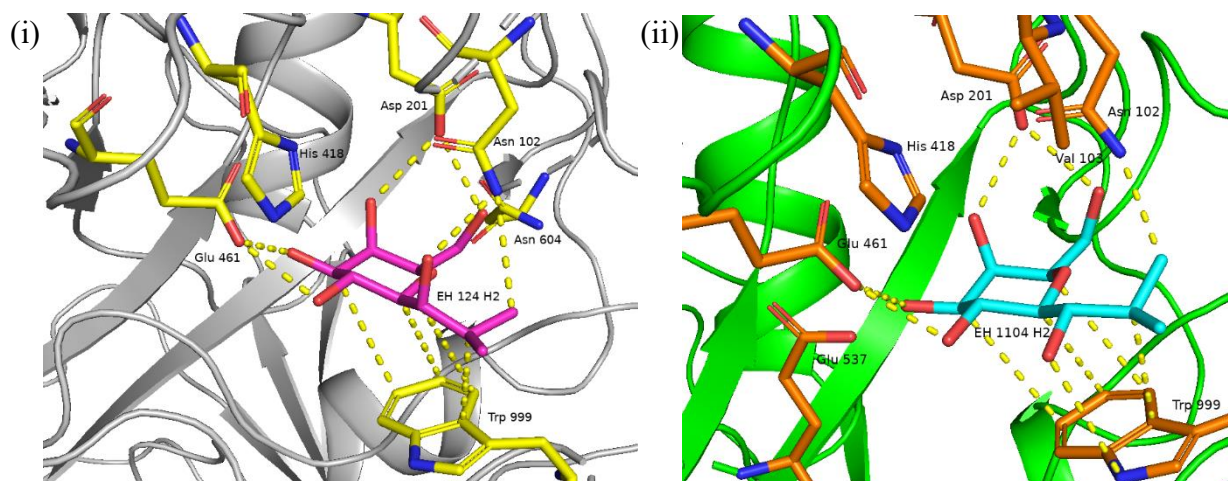


**Figure 40: Comparing the binding mode of (i) EH 124 H2 and (ii) EH 1104 H2 with  $\beta$ -Galactosidase from *E. coli* (PDB ID: 3MUZ)**

For the constrained compound **EH 145**, H-1' points towards Trp999, the distance of 2.49 Å suggests a CH- $\pi$  interaction. The axial orientation of the isopropyl moiety means H-2' and one of the terminal methyl's is within a 2.5 Å radius of Asn102. With **EH 145 O/R**, the equatorial orientation of the isopropyl means H-2' follows the unconstrained compounds in a CH- $\pi$  interaction with Trp999, an interaction that is more defined than with **EH 145**. From the docking studies it is difficult to see any steric clashes due to the methylene constraint, although the loss of the 2-OH H-bond is evident, which may explain the 2-fold difference in the results between **EH 145 O/R** and **EH 1208** for  $\beta$ -galactosidase from *E. coli*. The methylene linker to the aglycon in all the equatorial  $\beta$ -constrained derivatives in tables 6A-C have CH- $\pi$  interactions with Trp999, these interactions are missing in the axial  $\beta$ -constrained derivatives **AD 553** and **AD 584**. Analysis of the ligand interaction diagrams generated from Maestro suggest that the aglycon moiety of most of the axial and equatorial constrained compounds do not interact with amino acid residues but rather protrude out towards space, hence it is difficult to gain a rationale behind the discrepancy in results. Two exceptions are **AD 433** and **AD 558**, where Arg800 located 5.7 Å from the phenyl ring has the potential for a cation- $\pi$  interaction. Despite the conserved binding of **AD 433**, the fluorine substituent in on the phenyl ring is the potential cause of the decrease in affinity, due to the withdrawal of electron density causing a weaker cation- $\pi$  interaction (see Figure 41).



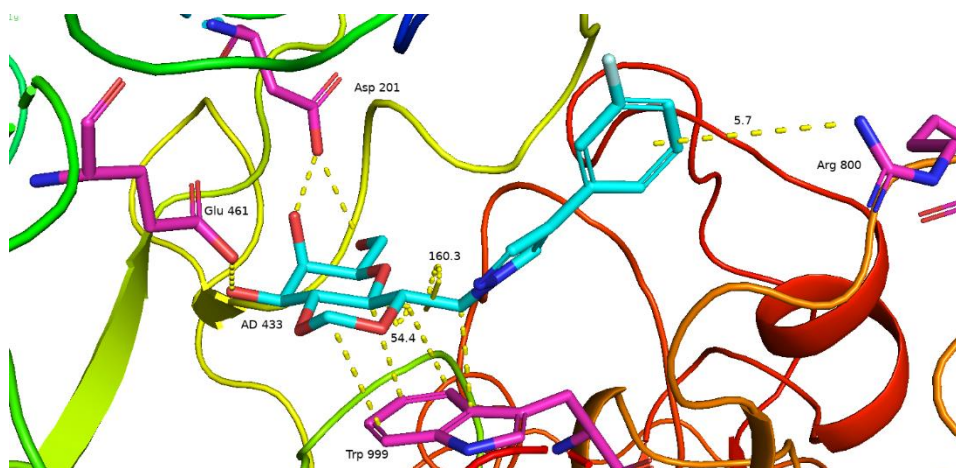


**Figure 41: Distance (Å) of phenyl ring in AD 433 from Arg800 in  $\beta$ -Galactosidase from *E. coli* (PDB ID: 3MUZ)**

To try and clarify the substantial difference in results of **AD 452** between the two  $\beta$ -galactosidase enzymes, the binding mode of each enzyme was examined (see Figure 42). **AD 452** with  $\beta$ -galactosidase from *E. coli* appears to take up a similar pose to **AD 433** in Figure 41, with both the methylene protons on the  $\alpha$ -anomeric moiety involved in CH- $\pi$  interactions and the hydroxyl in a H-bond with the indole nitrogen of Trp999.

Despite the low affinity inhibition results of **AD 452** with  $\beta$ -galactosidase from *A. niger*, docking of this protein-ligand complex suggests several non-covalent interactions. The binding predicted in the docking study for the galactose moiety is unconserved relative to the galactose moiety in 5IFT, which is not surprising considering the axial anomeric substituent. Docking shows the gal H-1 forms a hydrogen bond with the carboxylate of Glu142. The axial anomeric hydroxyl group also forms a H-bond with the same sidechain residue while simultaneously interacting with the phenol hydroxyl in Tyr364. These interactions of the axial anomeric substituent perhaps justify the unconserved binding mode. H-3 forms a CH- $\pi$  interaction with Tyr260, while 3-OH and 4-OH from the sugar ring H-bond to Glu200. 6-OH is involved in three H-bonding interactions with separate residues, the backbone carbonyl and nitrogen of Ile139 and Ala141 respectively and the phenol hydroxyl of Tyr96. C-6 has a CH- $\pi$  interaction with Tyr342 and the endocyclic oxygen is H-bonded to Asn140. One conserved feature of **AD 452** binding in *A. niger* is the  $\alpha$ -face of the sugar close enough to Tyr260 for CH- $\pi$  interactions. A study by Hudson et al.<sup>42</sup> examining the relative interaction strength of aromatic amino acid residue sidechains with carbohydrate C-H's follows the order Trp > Tyr > Phe > His. The Tyr residue in the *A. niger* structure replacing Trp999 means a weaker CH- $\pi$  interaction which might account for the affinity difference. Figure 42 illustrates docking of **AD 452** with the two enzymes.

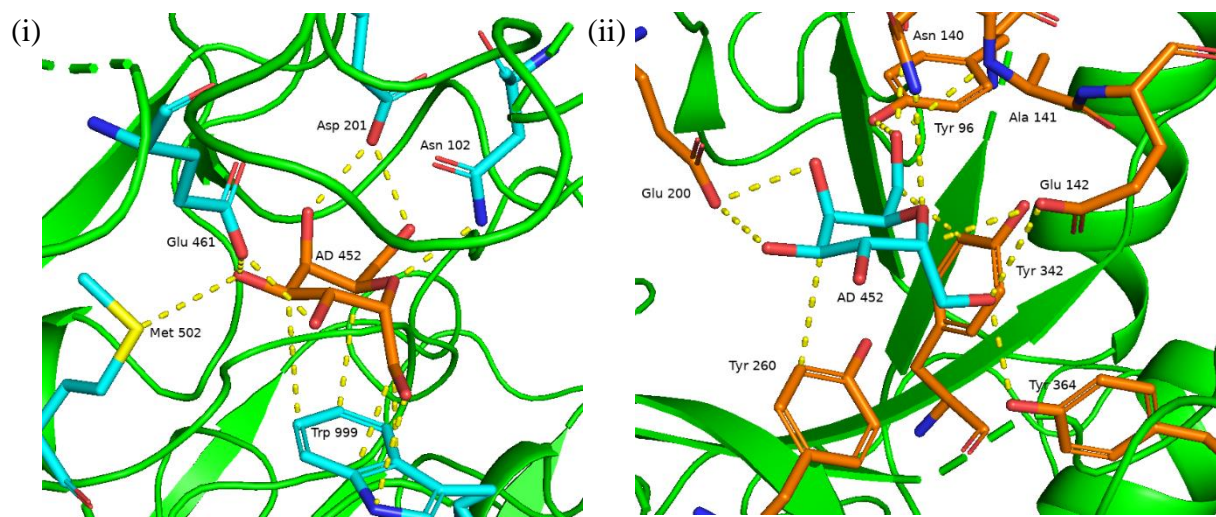


**Figure 42: Binding modes of AD 452 with (i)  $\beta$ -galactosidase from *E. coli* (PDB ID: 3MUZ) and (ii)  $\beta$ -galactosidase from *A. niger* (PDB ID: 5IFT)**

The aromatic amide substituents in **SK 65** – **SK 79** in table 7 are predicted to be involved in some interesting interactions with  $\beta$ -galactosidase from *E. coli*. The extra methylene in **SK 84** – **SK 79** compared to **SK 65** – **SK 87** was mentioned to be beneficial to binding, this group in all three compounds orientates the aromatic ring towards beneficial stacking interactions while itself having a CH- $\pi$  interaction with Trp999. **SK 79** gave the best performance of this series of compounds. Analysis of the docking suggests the substituted phenyl ring is involved in a  $\pi$ - $\pi$  stacking interaction with Trp999 and a CH- $\pi$  interaction with Phe601. The strong electron withdrawing nitro group at the *para* position of the ring may be responsible for the enhancement in affinity. **SK 84** has the same stacking with Trp999, while simultaneously stacking with Tyr503. The aromatic ring in **SK 83** is extended further into the pocket to stack with Tyr503 and His540, these interactions contrast with the analogous **SK 65** stacking exclusively with Trp999. The extra methylene in **SK 83** is involved in a CH- $\pi$  interaction with Trp999, while the 3-sulfate of **SK 65** and **SK 83** are both in a salt bridge with Arg800 (see Figure 43). The greater resonance stability due to the -I and +R effect of the *p*-fluoro and *p*-methoxy in **SK 81** and **SK 87** respectively increase the electron cloud in the aromatic ring relative to **SK 65**, resulting in stronger  $\pi$ - $\pi$  stacking interactions with Trp999. The methoxy oxygen in **SK 87** is 2.7 Å from the phenolic OH on Tyr503 for a potential H-bond and the terminal methyl is in a CH- $\pi$  interaction with Trp568. The unconserved nature of galactose binding for this series is not surprising considering the change in the sugar ring conformation and the relatively bulky aglycons. Docking suggests inhibition is driven by aglycon interactions

rather than those of the glycoside moiety. The Carbonyl or Nitrogen of the amide linker in each compound is H-bonded to Asn102.

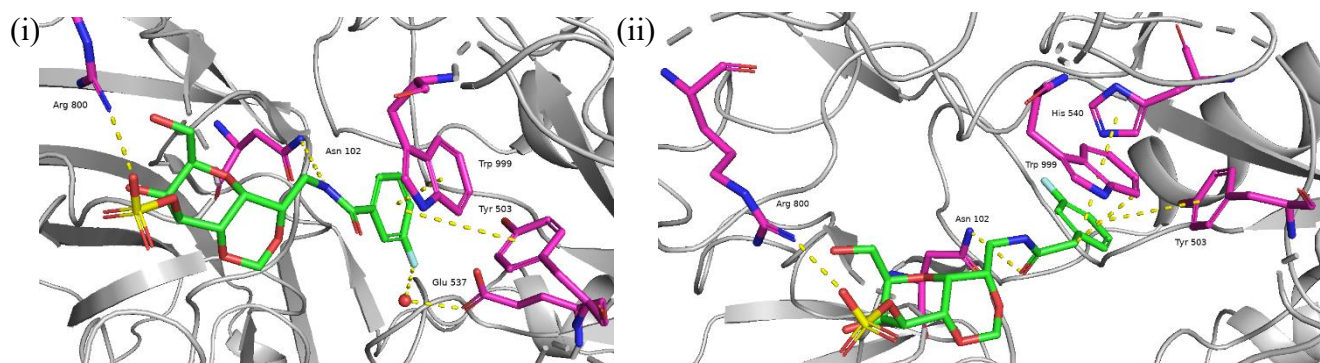


**Figure 43: Comparing the binding mode of (i) SK 65 and (ii) SK 83 in  $\beta$ -galactosidase from *E. coli* (PDB ID: 3MUZ)**

The lower affinity for **SK 65** with  $\beta$ -galactosidase from *A. niger* are somewhat reflected in the docking study, where the 3-*O*-sulfate is involved in a water mediated hydrogen bond with Ser238. 6-OH is simultaneously H-bonded to the backbone Nitrogen of Tyr260 and water mediated H-bonded to the backbone Carbonyl of Ala237. The Nitrogen in the amide linker is H-bonded to Glu200, the fluorophenyl ring is  $\pi$ - $\pi$  stacked with Tyr342, with the fluorine substituent on the phenyl ring H-bonded to the terminal sidechain Nitrogen of Asp199. Unlike the previous compounds analysed, docking suggests there are inconsistencies in the galactose binding for this enzyme.

The final series of  $\alpha$ -unconstrained *C*-derivatives in table 7 had a different substituent at each position in the sugar ring. **SK 167** gave the best results of this series for  $\beta$ -galactosidase from *E. coli* with a methoxy group at the 3-position. Docking of **SK 167** predicts unconserved binding relative to similar structures, such as **AD 452**, perhaps due to the 3-methoxy substituent on **SK 167**, placing it in the vicinity of a few aromatic sidechain residues that have potential for hydrophobic/CH- $\pi$  interactions. Trp999 and Phe601 are both within a 3 Å radius of the 3-methoxy, while C-6 of galactose is  $\sim$ 3.2 Å from Tyr503. The terminal carbon of the anomeric ethyl is within 3.1 Å of Trp568 while the methylene protons alpha to the anomeric carbon are within 3 Å of His540. 2-OH and 6-OH are H-bonded to the carboxylates of Asp201 and Glu461 respectively. The 2-*O*-Ac of **SK 122** does not appear to have any interactions with neighbouring residues while the 3-*O*-sulfate of **SK 284** forms a salt bridge with Arg800 (see Figure 44).

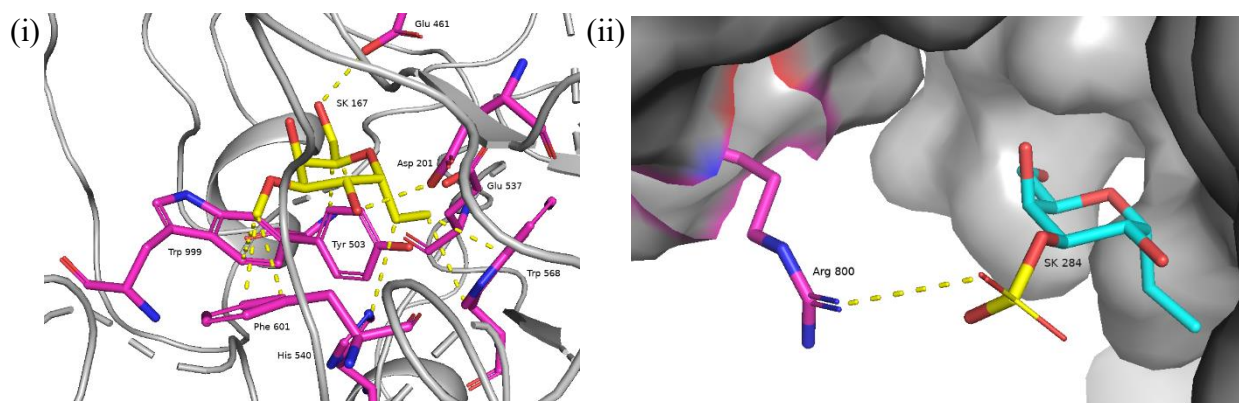


**Figure 44: Comparing the binding mode of the 3-position substituents in (i) SK 167 and (ii) SK 284 with  $\beta$ -galactosidase from *E. coli* (PDB ID: 3MUZ)**

The  $\sim$ 3-fold improvement of **SK 198** vs **SK 155** for  $\beta$ -galactosidase from *E. coli* is to be expected due to the withdrawal of electron density by the axial 4-fluorine of **SK 198** from the sugar ring, increasing its electrophilic character and thereby strengthening the CH- $\pi$  interactions of the  $\alpha$ -face sugar protons with Trp999. The two ligands bind to the enzyme at the same site, with the axial fluorine also involved in a water mediated H-bond with Glu537.

## Conclusions

The results of the inhibition assay suggest that **EH 1208** gave the best inhibitory performance for  $\beta$ -galactosidase from *E. coli*, giving a better result than its constrained analogues **EH 145** and **EH 145 O/R**. This improved affinity can be explained by the loss of a Hydrogen bond between the 2-OH of the sugar and Glu461 due to the incorporation of the methylene bridge in the constrained derivatives, as suggested by the docking study. Although the constrained compounds were outperformed by **EH 1208**, the incorporation of the constraint can be interpreted as having a positive impact on the inhibitory ability of **EH 145** and **EH 145 O/R**, due to their improved inhibitory performance compared to **EH 124 H2** and **EH 1104 H2**. Conserved binding of the glycosidic moieties of each of the relatively smaller inhibitors was observed in the docking study, matching that of IPTG. The derivatives in tables 7A – 7B did not have conserved binding in the docking study, due to their relatively bulky nature and the conformational ring flip observed, although it was interesting to analyse their binding modes.



## References

- (1) Davis, Benjamin G.; Fairbanks, A. J. Enzyme Disaccharide Formation. In *Carbohydrate Chemistry*; Oxford University Press: New York, 2002; pp 65–77.
- (2) Juers, D. H.; Heightman, T. D.; Vasella, A.; McCarter, J. D.; Mackenzie, L.; Withers, S. G.; Matthews, B. W. A Structural View of the Action of Escherichia Coli (LacZ)  $\beta$ -Galactosidase. *Biochemistry* **2001**, *40*, 14781–14794.
- (3) Nelson, David L.; Cox, M. M. Regulation of Gene Expression. In *Lehringer Principles of Biochemistry*; W.H. Freeman & Co: New York, 2013; pp 1155–1198.
- (4) Jacobson, R. H.; Zhang, X.-J.; DuBose, R. F.; Matthews, B. W. Three-Dimensional Structure of  $\beta$ -Galactosidase from E. Coli. *Nature* **1994**, *369*, 761–766.
- (5) Berg, J. M.; Tymoczko, J. L.; Gatto, G. J.; Stryer, L. The Control of Gene Expression in Prokaryotes. In *Biochemistry*; W.H. Freeman & Co: New York, 2015; pp 925–940.
- (6) Juers, D. H.; Hakda, S.; Matthews, B. W.; Huber, R. E. Structural Basis for the Altered Activity of Gly794 Variants of Escherichia Coli  $\beta$ -Galactosidase<sup>†</sup>. *Biochemistry* **2003**, *42*, 13505–13511.
- (7) Huber, R. E.; Hakda, S.; Cheng, C.; Cupples, C. G.; Edwards, R. A. Trp-999 of  $\beta$ -Galactosidase (Escherichia Coli) Is a Key Residue for Binding, Catalysis, and Synthesis of Allolactose, the Natural Lac Operon Inducer. *Biochemistry* **2003**, *42*, 1796–1803.
- (8) Martinez-Bilbao, M.; Huber, R. E. Substitutions for Gly-794 Show That Binding Interactions Are Important Determinants of the Catalytic Action of  $\beta$ -Galactosidase (Escherichia Coli). *Biochem. cell Biol.* **1994**, *72*, 313–319.
- (9) Martinez-Bilbao, M.; Holdsworth, R. E.; Edwards, L. A.; Huber, R. E. A Highly Reactive Beta-Galactosidase (Escherichia Coli) Resulting from a Substitution of an Aspartic Acid for Gly-794. *J. Biol. Chem.* **1991**, *266*, 4979–4986.
- (10) Huber, R. E.; Gaunt, M. T. The Inhibition of  $\beta$ -Galactosidase (Escherichia Coli) by Amino Sugars and Amino Alcohols. *Can. J. Biochem.* **1982**, *60*, 608–612.
- (11) Hadd, A. G.; Raymond, D. E.; Halliwell, J. W.; Jacobson, S. C.; Ramsey, J. M. Microchip Device for Performing Enzyme Assays. *Anal. Chem.* **1997**, *69*, 3407–3412.
- (12) Greul, J. N.; Kleban, M.; Schneider, B.; Picasso, S.; Jäger, V. Amino (Hydroxymethyl) Cyclopentanetriols, an Emerging Class of Potent Glycosidase Inhibitors—Part II: Synthesis, Evaluation, and Optimization of B-d-Galactopyranoside Analogues. *ChemBioChem* **2001**, *2*, 368–370.
- (13) Rustler, K.; Mickert, M. J.; Nazet, J.; Merkl, R.; Gorris, H. H.; König, B. Development of Photoswitchable Inhibitors for  $\beta$ -Galactosidase. *Org. Biomol. Chem.* **2018**, *16*, 7430–7437.
- (14) Du, Y.; Linhardt, R. J.; Vlahov, I. R. Recent Advances in Stereoselective C-Glycoside Synthesis. *Tetrahedron* **1998**, *54*, 9913–9960.
- (15) Yang, Y.; Yu, B. Recent Advances in the Chemical Synthesis of C-Glycosides. *Chem. Rev.* **2017**, *117*, 12281–12356.
- (16) Cheshev, P.; Marra, A.; Dondoni, A. Direct Epoxidation of D-Glucal and d-Galactal

- Derivatives with in Situ Generated DMDO. *Carbohydr. Res.* **2006**, *341*, 2714–2716.
- (17) Burke, C. P.; Shi, Y. Enantioselective Epoxidation of Conjugated Cis-Enynes by Chiral Dioxirane. *J. Org. Chem.* **2007**, *72*, 4093–4097.
- (18) Urban, D.; Skrydstrup, T.; Beau, J.-M. Stereocontrolled Synthesis of  $\alpha$ -C-Galactosamine Derivatives via Chelation-Controlled C-Glycosylation. *J. Org. Chem.* **1998**, *63*, 2507–2516.
- (19) Doisneau, G.; Beau, J.-M. Radical Dimerization of Glycosyl 2-Pyridylsulfones with Samarium (II) Iodide in the Presence of HMPA. *Tetrahedron Lett.* **1998**, *39*, 3477–3480.
- (20) Palmier, S.; Vauzeilles, B.; Beau, J.-M. A Highly Selective Route to  $\beta$ -C-Glycosides via Nonselective Samarium Iodide Induced Coupling Reactions. *Org. Biomol. Chem.* **2003**, *1*, 1097–1098.
- (21) Miquel, N.; Doisneau, G.; Beau, J.-M. Reductive Samarium of Anomeric 2-Pyridyl Sulfones with Catalytic Nickel: An Unexpected Improvement in the Synthesis of 1,2-Trans-Diequatorial C-Glycosyl Compounds. *Angew. Chemie Int. Ed.* **2000**, *39*, 4111–4114.
- (22) Szostak, M.; Spain, M.; Procter, D. J. Preparation of Samarium(II) Iodide: Quantitative Evaluation of the Effect of Water, Oxygen, and Peroxide Content, Preparative Methods, and the Activation of Samarium Metal. *J. Org. Chem.* **2012**, *77*, 3049–3059.
- (23) Chiara, J. L.; Sessler, E. Samarium Diiodide-Mediated Reductive Coupling of Epoxides and Carbonyl Compounds: A Stereocontrolled Synthesis of C-Glycosides from 1, 2-Anhydro Sugars. *Angew. Chemie Int. Ed.* **2002**, *41*, 3242–3246.
- (24) Wittmann, V.; Kessler, H. Stereoselective Synthesis of C-Glycosides with a Glycosyl Dianion. *Angew. Chemie/International Ed.* **1993**, *32*, 1091–1093.
- (25) Skrydstrup, T.; Jarreton, O.; Mazéas, D.; Urban, D.; Beau, J.-M. A General Approach to 1,2-Trans-C-Glycosides via Glycosyl Samarium(III) Compounds. *Chem. – A Eur. J.* **1998**, *4*, 655–671.
- (26) Lesimple, P.; Beau, J.-M. Stereocontrolled Synthesis of C-Glycosides: Further Studies on the Organolithium Reagents Derived from 2-Deoxy-D-Glucose and D-Glucose. *Bioorg. Med. Chem.* **1994**, *2*, 1319–1330.
- (27) Cohen, T.; Bhupathy, M. Organoalkali Compounds by Radical Anion Induced Reductive Metalation of Phenyl Thioethers. *Acc. Chem. Res.* **1989**, *22*, 152–161.
- (28) Rychnovsky, S. D.; Powers, J. P.; LePage, T. J. Conformation and Reactivity of Anomeric Radicals. *J. Am. Chem. Soc.* **1992**, *114*, 8375–8384.
- (29) Zhou, J.; Lv, S.; Zhang, D.; Xia, F.; Hu, W. Deactivating Influence of 3-O-Glycosyl Substituent on Anomeric Reactivity of Thiomannoside Observed in Oligomannoside Synthesis. *J. Org. Chem.* **2017**, *82*, 2599–2621.
- (30) Ohlsson, J.; Nilsson, U. J. A Galabiose-Based Two-Dimensional Scaffold for the Synthesis of Inhibitors Targeting Pk- and P-Antigen Binding Proteins. *Tetrahedron Lett.* **2003**, *44*, 2785–2787.
- (31) Ko, K.-S.; Kruse, J.; Pohl, N. L. Synthesis of Isobutyl-C-Galactoside (IBCG) as an Isopropylthiogalactoside (IPTG) Substitute for Increased Induction of Protein

- Expression. *Org. Lett.* **2003**, *5*, 1781–1783.
- (32) Tuley, A.; Fast, W. The Taxonomy of Covalent Inhibitors. *Biochemistry* **2018**, *57*, 3326–3337.
- (33) Berg, J. M.; Tymoczko, J. L.; Gatto, G. J.; Stryer, L. Enzymes: Basic Concepts and Kinetics. In *Biochemistry*; W.H. Freeman & Co: New York, 2015; pp 215–245.
- (34) Nelson, David L.; Cox, M. M. Enzymes. In *Lehringer Principles of Biochemistry*; W.H. Freeman & Co: New York, 2013; pp 189–242.
- (35) Wu, T. C.; Goekjian, P. G.; Kishi, Y. Preferred Conformation of C-Glycosides. 1. Conformational Similarity of Glycosides and Corresponding C-Glycosides. *J. Org. Chem.* **1987**, *52*, 4819–4823.
- (36) Goekjian, P. G.; Wu, T. C.; Kishi, Y. Preferred Conformation of C-Glycosides. 6. Conformational Similarity of Glycosides and Corresponding C-Glycosides. *J. Org. Chem.* **1991**, *56*, 6412–6422.
- (37) Goekjian, P. G.; Wu, T. C.; Kang, H. Y.; Kishi, Y. Preferred Conformation of C-Glycosides. 7. Preferred Conformation of Carbon Analogs of Isomaltose and Gentiobiose. *J. Org. Chem.* **1991**, *56*, 6422–6434.
- (38) Wang, Y.; Goekjian, P. G.; Ryckman, D. M.; Miller, W. H.; Babirad, S. A.; Kishi, Y. Preferred Conformation of C-Glycosides. 9. Conformational Analysis of 1,4-Linked Carbon Disaccharides. *J. Org. Chem.* **1992**, *57*, 482–489.
- (39) O’Leary, D. J.; Kishi, Y. Preferred Conformation of C-Glycosides. 13. A Comparison of the Conformational Behavior of Several C-, N-, and O-Furanosides. *J. Org. Chem.* **1994**, *59*, 6629–6636.
- (40) Dugdale, M. L.; Vance, M. L.; Wheatley, R. W.; Driedger, M. R.; Nibber, A.; Tran, A.; Huber, R. E. Importance of Arg-599 of  $\beta$ -Galactosidase (*Escherichia Coli*) as an Anchor for the Open Conformations of Phe-601 and the Active-Site Loop. *Biochem. Cell Biol.* **2010**, *88*, 969–979.
- (41) Rico-Díaz, A.; Ramírez-Escudero, M.; Vizoso-Vázquez, Á.; Cerdán, M. E.; Becerra, M.; Sanz-Aparicio, J. Structural Features of *Aspergillus Niger*  $\beta$ -Galactosidase Define Its Activity against Glycoside Linkages. *FEBS J.* **2017**, *284*, 1815–1829.
- (42) Hudson, K. L.; Bartlett, G. J.; Diehl, R. C.; Agirre, J.; Gallagher, T.; Kiessling, L. L.; Woolfson, D. N. Carbohydrate–Aromatic Interactions in Proteins. *J. Am. Chem. Soc.* **2015**, *137*, 15152–15160.

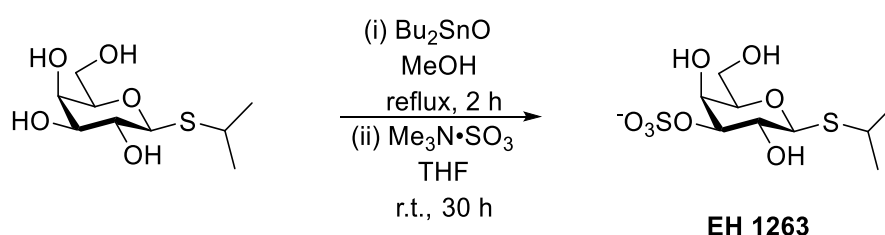
**Chapter 3: Galectin Inhibitors**

|  |     |
|--|-----|
| <b>Synthesis</b> .....                   | 85  |
| <b>Fluorescence Polarisation</b> .....   | 94  |
| <b>FP Experiment Design</b> .....        | 95  |
| <b>Method</b> .....                      | 96  |
| <b>Results</b> .....                     | 98  |
| <b>Discussion</b> .....                  | 104 |
| <b>Conclusions and Future Work</b> ..... | 117 |
| <b>References</b> .....                  | 118 |



## Synthesis

To further utilise the various galactopyranose derivatives synthesised in chapter 2, it was decided to prepare derivatives with 3-position modifications, like those discussed in chapter 1, and evaluate them as galectin inhibitors. The isopropyl derivatives **IPTG**, **EH 124 H2**, **EH 145**, **EH 145 O/R** and **EH 1208** from tables 5A and 5B in chapter 2 were functionalised with a sulfate group to provide the corresponding derivatives **EH 1263**, **EH 1265**, **EH 1260**, **EH 1266** and **EH 1264** respectively (see table 8 for structures). Thus, each of the compounds were heated at reflux with dibutyl tin oxide followed by treatment with sulfur trioxide trimethyl amine complex as indicated for formation of **EH 1263** as shown in Scheme 14.



**Scheme 14: Sulfation of IPTG to EH 1263**

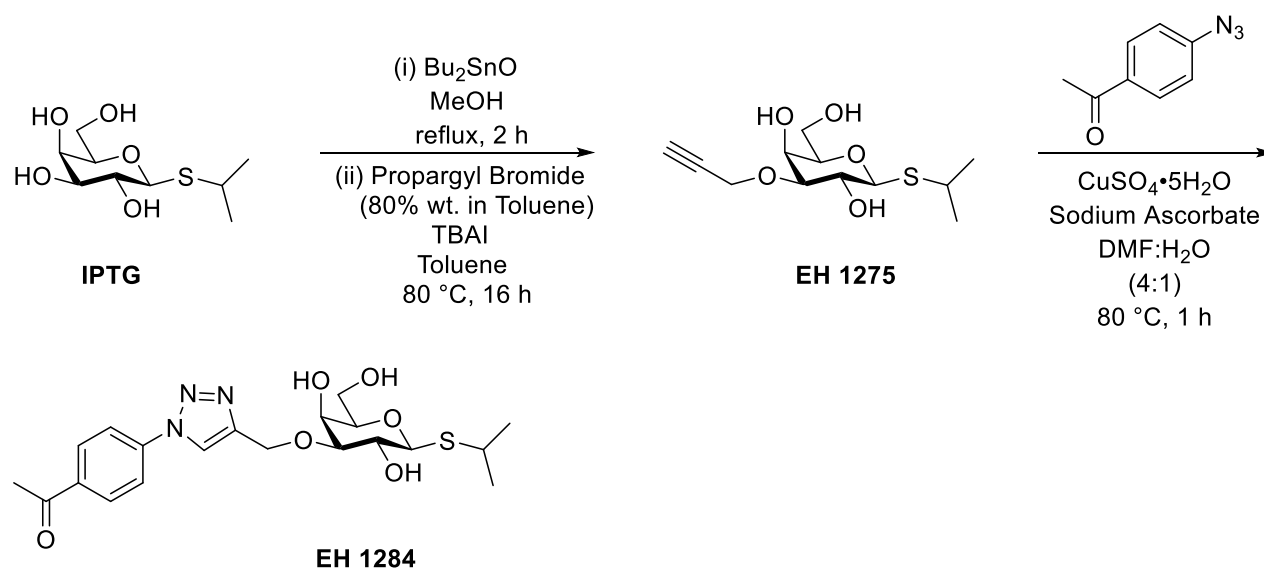
The downfield shift of H-3 signal from  $\delta$  3.45 (dd,  $J = 9.3, 3.3$  Hz, 1H) to  $\delta$  4.26 (dd,  $J = 9.3, 3.2$  Hz, 1H) was the only significant change in the  $^1\text{H-NMR}$  spectrum when comparing it to that of the reactant and the downfield shift is consistent with the sulfate group being introduced at the 3-position.<sup>1</sup>

**Table 8: Structures of sulfated derivatives synthesised from the relevant galactopyranose derivative under same conditions as Scheme 14**

| Lab Notebook Code | Structure |
|-------------------|-----------|
| <b>EH 1260</b>    |           |
| <b>EH 1263</b>    |           |
| <b>EH 1264</b>    |           |

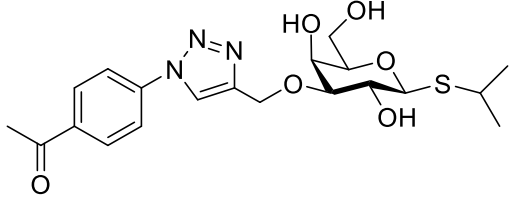
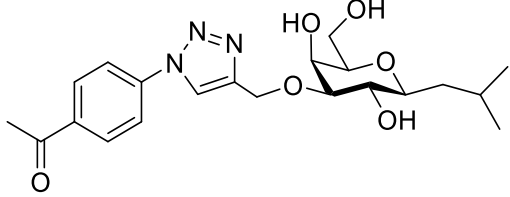
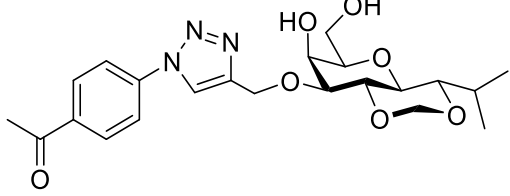
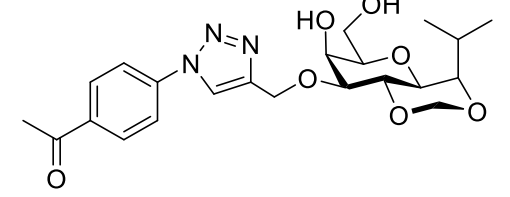
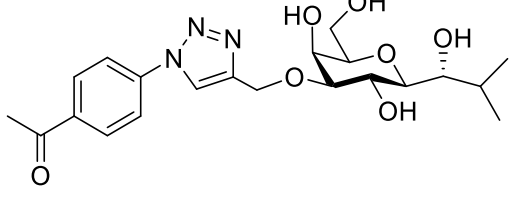
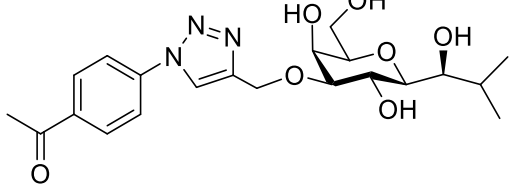
|                |  |
|----------------|--|
| <b>EH 1265</b> |  |
| <b>EH 1266</b> |  |

As previously mentioned, it is known that 3-sulfated galactose derivatives, such as 3-sulfolactose, have improved affinity compared to the unsulfated galactose derivative, such as for galectin-8N.<sup>2</sup> Another 3-position modification to the galactose isopropyl series carried out was regioselective *O*-propargylation and subsequent triazole formation via Click Chemistry. Like the sulfate addition, the propargylation was achieved by initially refluxing the reactant in methanol in the presence of dibutyl tin oxide followed by stirring at 80 °C with propargyl bromide in toluene for 16 h. Thus, regioselective propargylation of **IPTG** gave **EH 1275** (see Scheme 15). Click reactions, i.e., copper catalysed azide-alkyne cycloadditions (CuAAC), were then performed with various azides. The reaction of *p*-azidoacetophenone with **EH 1275** to give **EH 1284** is illustrative as shown in Scheme 15. Table 9 summarises the list of products prepared via the conditions shown in Scheme 15.



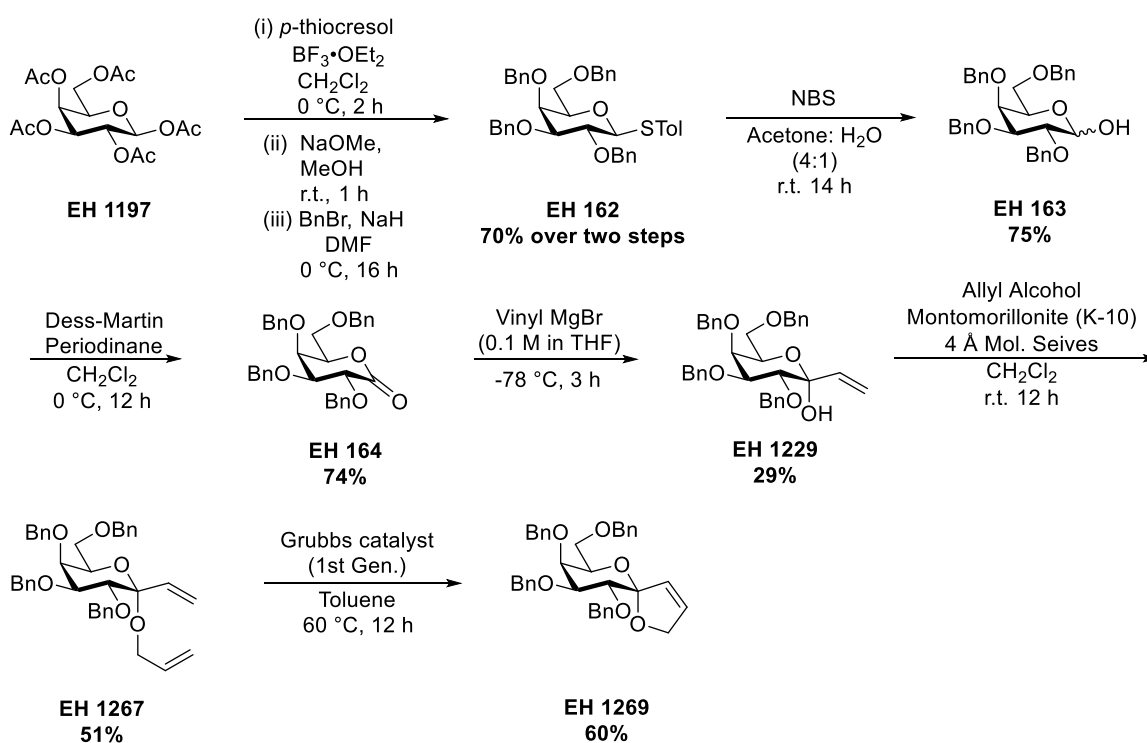
**Scheme 15: Synthesis of EH 1284, the *p*-acetophenone derivative from IPTG**

**Table 9: Structures of *p*-acetophenone derivatives, synthesised from appropriate galactopyranose derived precursor under same conditions as shown in Scheme 15.**

| Lab Notebook Code/Compound number | Structure  |
|-----------------------------------|--|
| EH 1284                           |    |
| EH 1285                           |    |
| EH 1286                           |   |
| EH 1287                           |  |
| EH 1288                           |  |
| EH 1289                           |  |

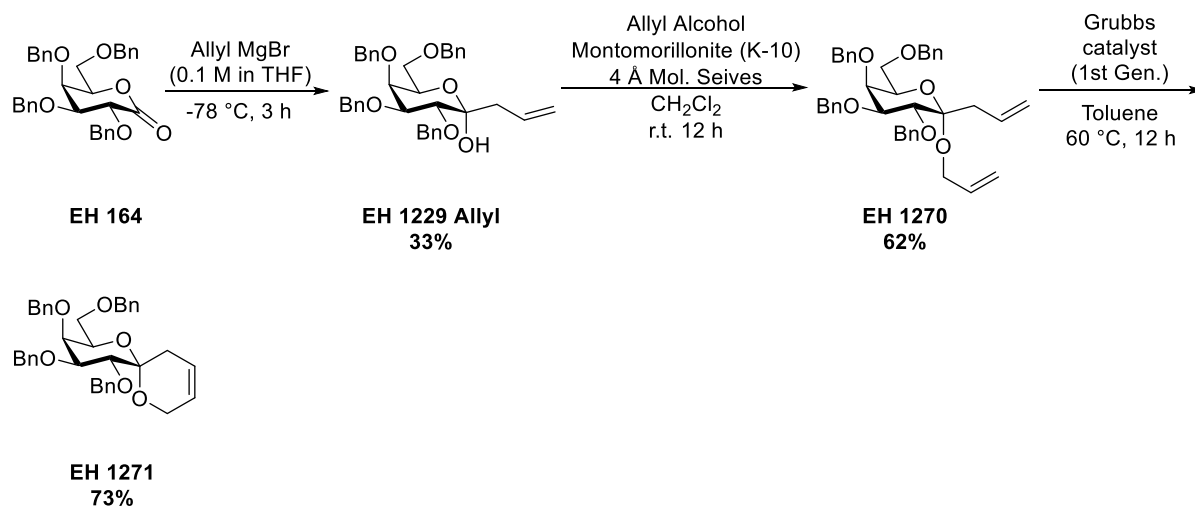
A series of 5-membered spiroketal compounds were then synthesised by adapting a procedure by Leeuwenburgh et al <sup>3</sup> (Scheme 16). Thus, penta-*O*-acetyl- $\beta$ -D-galactopyranose **EH 1197** was reacted with 4-methylbenzenethiol under Lewis acidic conditions to give the 2,3,4,6-tetra-

*O*-acetylated  $\beta$ -thiotoluene intermediate **EH 161**. Base promoted removal of the acetate protecting groups followed by benzylation using benzyl bromide and sodium hydride gave the per-*O*-benzylated  $\beta$ -STol derivative **EH 162** (70% yield over two steps). The thioglycoside **EH 162** was reacted with *N*-bromosuccinimide in a 4:1 mixture of acetone-H<sub>2</sub>O to give the hemiacetal product **EH 163**, which was then oxidised using Dess-Martin periodinane overnight to give a lactone product **EH 164**. Grignard reaction of **EH 164** at -78 °C with a 0.1 M solution of vinyl magnesium bromide in THF, gave the hemiketal **EH 1229**. The hemiketal **EH 1229** was reacted with allyl alcohol in the presence of acid activated Montmorillonite K-10 clay to give the ketal **EH 1267**. Subsequent reaction of **EH 1267** with the 1<sup>st</sup> generation Grubbs catalyst in toluene at 60 °C gave the spiro compound **EH 1269** in after ring closing metathesis.



### Scheme 16: Synthesis of EH 1269, the 5-membered Spiro derivative

The 6-membered spiroketal intermediate **EH 1271** (see Scheme 17) was synthesised using allyl magnesium bromide. The ketal forming reaction to make **EH 1270** the subsequent RCM were achieved using the same reagents and conditions as those shown in Scheme 16.



### Scheme 17: Synthesis of EH 1271

Crystal structures of **EH 1269** and **EH 1271** (Figure 45) confirmed that the oxygen atom was axial in both spiro compounds.

Single crystals of **EH 1269** were obtained by dissolving the sample in a minimum amount of  $\text{CH}_2\text{Cl}_2$  and allowing the solvent to evaporate at room temperature in the fumehood over 16 h. Single crystals of **EH 1271** were obtained by adding a minimum amount of ethanol and heating to boiling point until fully dissolved, allowing the solvent to then evaporate at room temperature in the fume hood over 48 h.

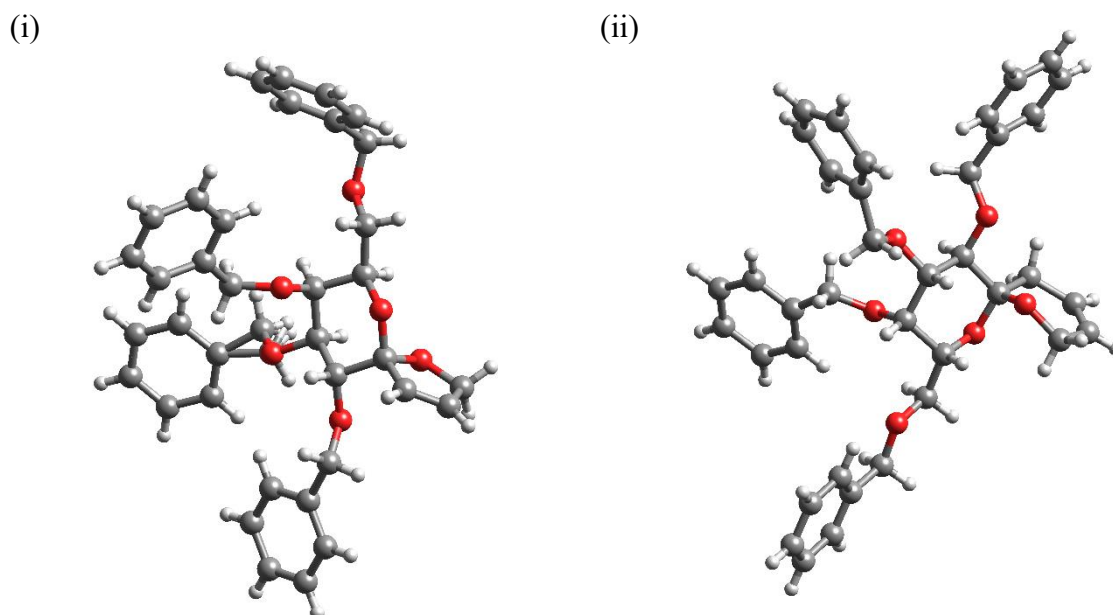
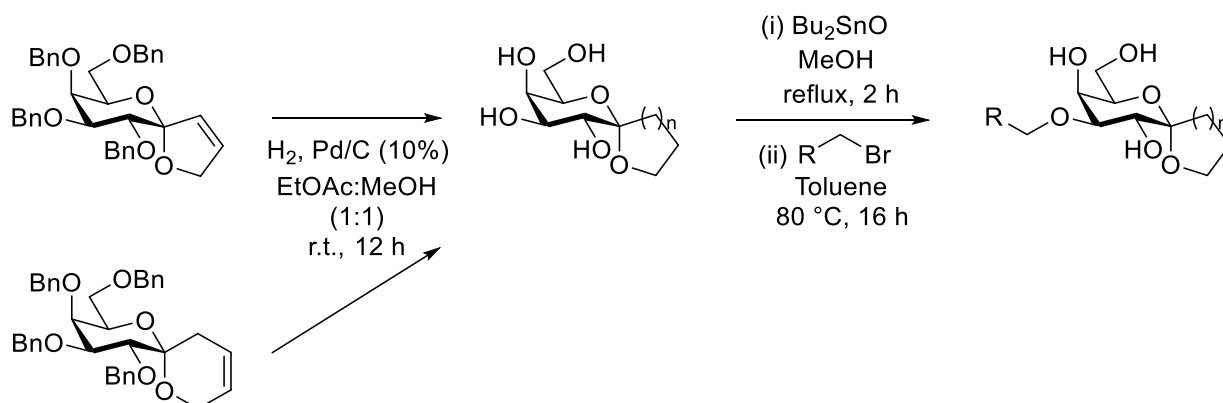


**Figure 45: Crystal structures of (i) EH 1269 (CCDC No: 2260436) and (ii) EH 1271 (CCDC No: 2260412) showing axial anomeric oxygen**

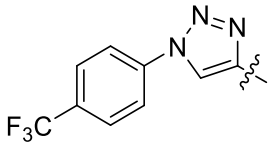
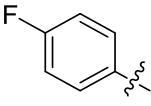
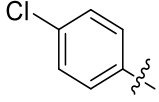
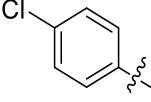
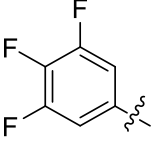
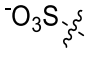
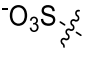
Both **EH1269** and **EH 1271** were subjected to hydrogenation in the presence of Pd/C (10%) to remove the benzyl protecting groups. The alkene in the aglycon was also hydrogenated during this reaction to give fully saturated 5- and 6-membered rings. The deprotected compounds were then functionalised at the 3-position with a series of aromatic rings (Scheme 18). Table 10 <sup>a, b</sup> shows the functionality introduced to **EH 1269** and **EH 1271**.



**Scheme 18: Removal of benzyl groups and introduction of 3-*O*-benzyl derivatives in spiro compounds**

**Table 10: Functionality introduced to Spiro compounds at 3-position <sup>a, b, c</sup>**

|                           |                    |                    |
|---------------------------|--------------------|--------------------|
| Carbohydrate Spiro Moiety |                    |                    |
| R =                       | <br><b>EH 1306</b> | <br><b>EH 1305</b> |
|                           | <br><b>EH 1307</b> | <br><b>EH 1308</b> |
|                           | <br><b>EH 1309</b> | <br><b>EH 1311</b> |

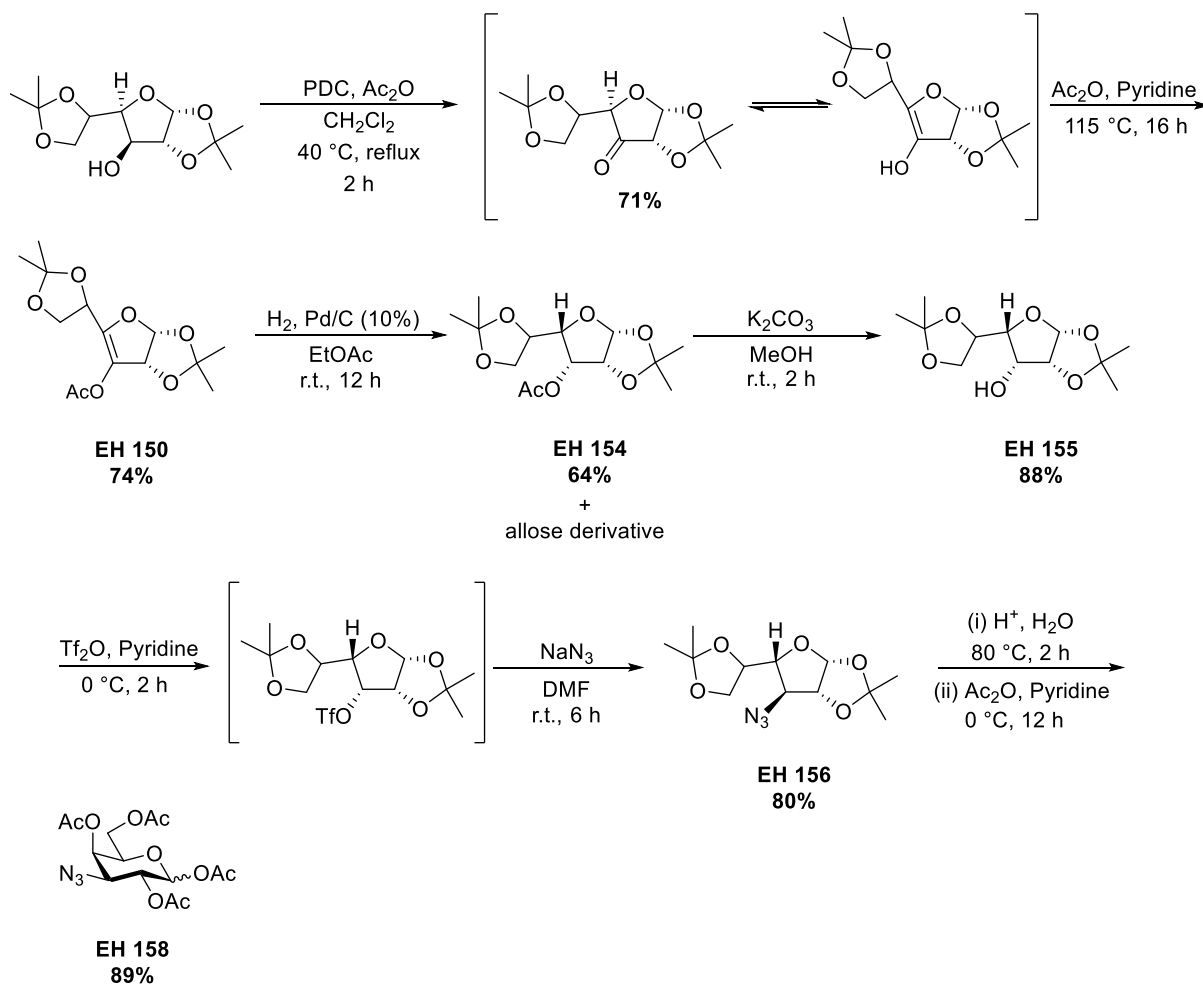
|  |   |   |
|--|---|---|
|  |  <p><b>EH 1310</b></p> |  <p><b>EH 1313</b></p> |
|  |  <p><b>EH 1317</b></p> |  <p><b>EH 1314</b></p> |
|  |   |  <p><b>EH 1315</b></p> |
|  |  <p><b>EH 1319</b></p> |  <p><b>EH 1293</b></p> |

<sup>a</sup> **EH 1305**, **EH 1306**, **EH1310** and **EH 1311** were synthesised via the two-step procedure shown in Scheme 15.

<sup>b</sup> **EH 1293** and **EH 1319** were synthesised via the procedure shown in Scheme 14.

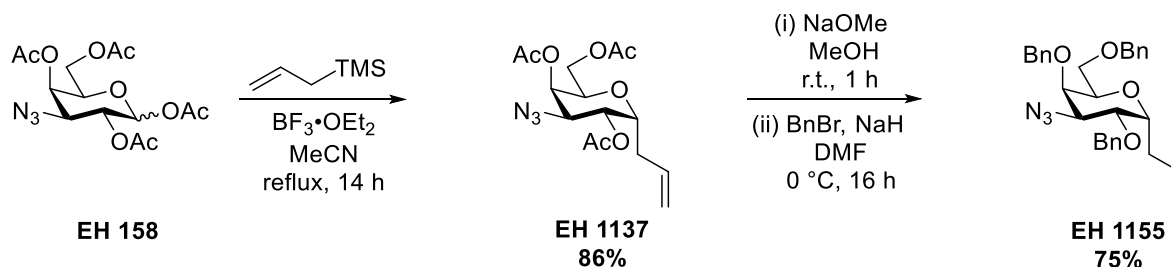
<sup>c</sup> For **EH 1308**, R' = Ac, for all other 6-membered spiro derivatives, R' = H.

A 5-membered bicyclic derivative was synthesised using 3-azido-galactose as a key intermediate. 3-Azido-galactose was synthesised according to a 9-step procedure developed by Hindsgaul et al.<sup>4</sup> and modified by Nilsson et al.<sup>5</sup> This process began with 1,2:5,6-di-*O*-isopropylidene- $\alpha$ -D-glucofuranose which underwent the pathway shown in Scheme 19 to both exchange the OH at C-3 for azide and to invert the stereochemistry at C-4 and produce the galactofuranose from glucofuranose. Thus, the reactant, diisopropylidene-D-glucofuranose (diacetone-D-glucose) was oxidised via pyridinium dichromate and acetic anhydride refluxing in CH<sub>2</sub>Cl<sub>2</sub> to give a ketone. The resulting ketone tautomerized to the corresponding enol which was trapped by acetylation achieved by heating in the presence of acetic anhydride and pyridine to give **EH 150**. The acetylated enol was hydrogenated with Pd/C (10%), providing **EH 154** and the acetate protecting group then removed to give **EH 155**, effectively inverting stereochemistry at C-3 and C-4. Triflation of the free alcohol with triflic anhydride and pyridine and subsequent S<sub>N</sub>2 reaction with sodium azide, resulted in **EH 156**. Removal of the isopropylidene protecting groups under acidic conditions and with heating converted the furanose to the pyranose structure. Subsequent peracetylation with acetic anhydride and pyridine gave a mixture of anomers (3:4  $\alpha$ : $\beta$ ) of **EH 158** in 89% yield.



### Scheme 19: Preparation of 3-azido-galactose (EH 158)

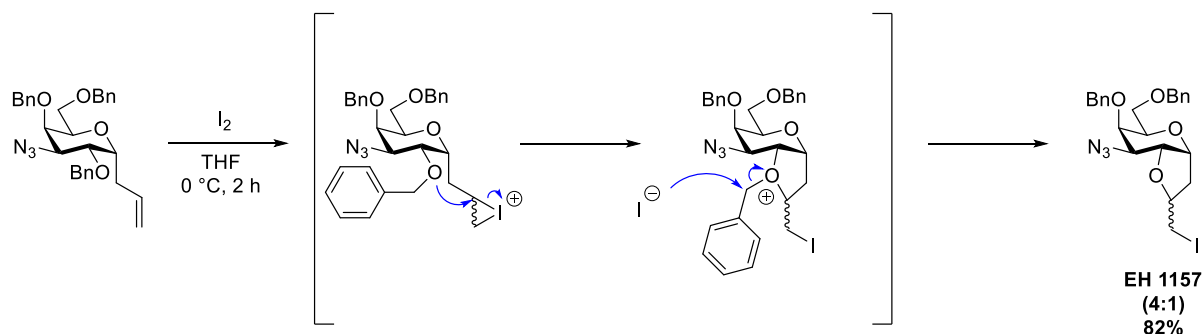
Allylation of **EH 158** was achieved through treatment with allyltrimethylsilane and 5 equivalents of BF<sub>3</sub>·Et<sub>2</sub>O via heating at reflux at 80 °C for 16 h to give **EH 1137** as an 11:1 mixture of anomers <sup>6</sup> (Scheme 20). De-*O*-acetylation, followed by benzylation allowed separation of the anomers via chromatography to give **EH 1155** in 75% yield over two steps.



### Scheme 20: Synthesis of allyl derivative EH 1155



Treatment of **EH 1155** with  $I_2$  affords an iodonium ion that reacts further to give a 4:1 mixture of diastereomers (Scheme 21) **EH1157**.<sup>7,8</sup> The iodoethers were separated via chromatography at this stage to give two separate stereoisomers, **EH 1157 US** and **EH 1157 LS** which followed the same subsequent synthetic route shown in Scheme 22.



**Scheme 21: Mechanism for the formation of EH 1157**

Although two different compounds were obtained, with their NMR spectra recorded, the stereochemistry of the two compounds could not be distinguished. Conformational studies on a related bicyclic galactopyranose scaffolds by Mari et al, through a combination of NMR analysis and molecular modelling suggest that the pyran ring in both diastereoisomers rapidly interconverts between three conformations, a  ${}^4C_1$  chair, a  ${}^1S_3$  skew boat and a  ${}^1C_4$  inverted chair, with the  ${}^4C_1$  chair representing about 50–60% of the total conformer population. Figure 46 represents the possible conformations of the bicyclic structures of the compounds studied by Mari et al.<sup>8</sup> Efforts to crystallise the final compounds in this route were also unsuccessful. Spectra for each of the diastereoisomers can be seen in the experimental section.

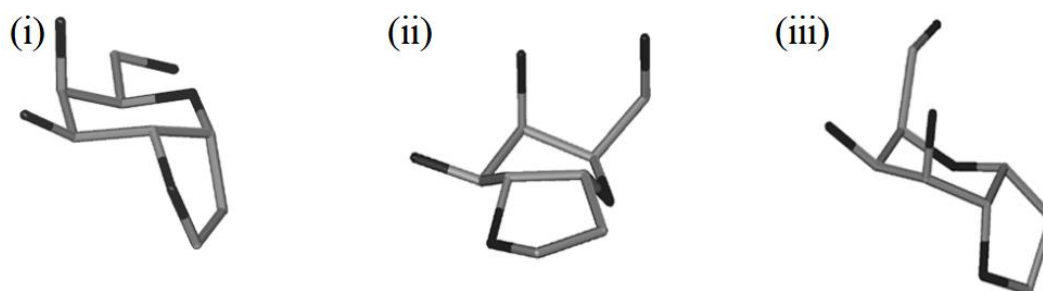
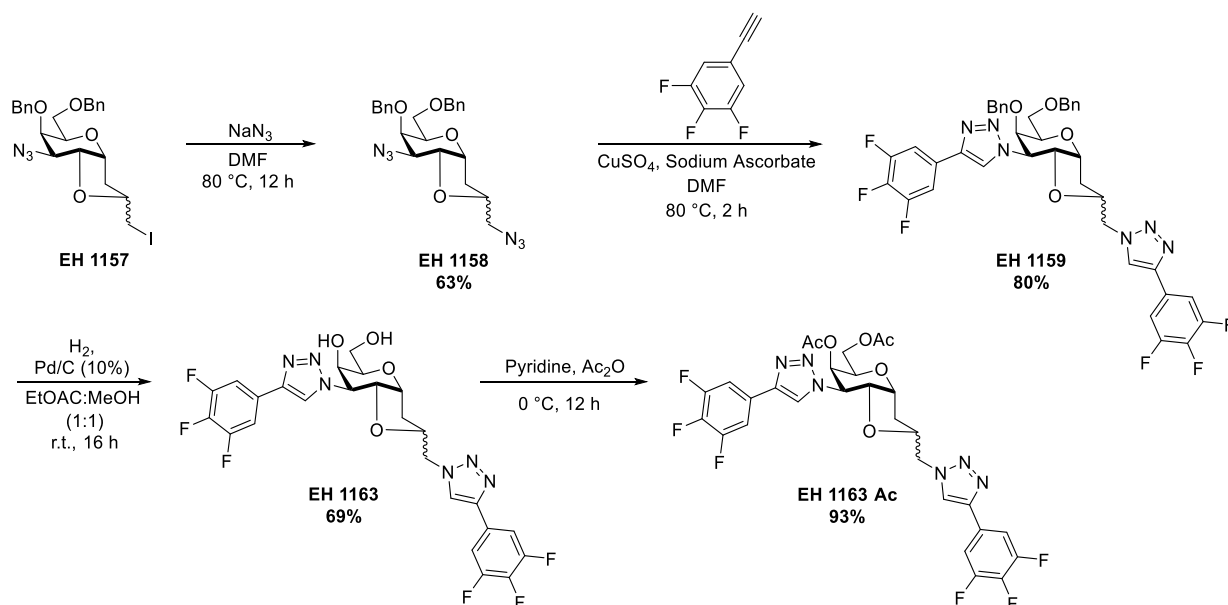


**Figure 46: Possible conformations of bicyclic scaffold (i)  ${}^4C_1$  cluster (ii)  ${}^1S_3$  cluster (iii)  ${}^1C_4$  cluster.** Reproduced with permission from ref<sup>8</sup>, Copyright © 2006 WILEY-VCH Verlag GmbH & Co. KGaA, Weinheim

Iodoether **EH 1157** was heated with 4 equivalents of sodium azide in DMF to 80 °C overnight displacing the iodine with an azide to give **EH 1158**. Two free azides in the structure provided

handles to introduce functionality. A double click reaction was performed with **EH 1158** using 3,4,5-trifluorophenylacetylene, allowing cycloaddition to occur at both azides, introducing the fluorophenyl ring to give **EH 1159**. Benzyl deprotection of **EH 1159** under hydrogenation conditions followed by acetylation and deacetylation provided **EH 1163 US** and **EH 1163 LS** as products (see Scheme 22). Acetylation was necessary to assign signals for the two compounds as there was a high degree of signal overlap in **EH 1163 US** and **EH 1163 LS**.



**Scheme 22: Synthesis of EH 1163 US and LS from EH 1157 (Both diastereoisomers follow the same scheme. Since stereochemistry is undefined for both, this scheme represents the two separate stereoisomers, which were separated after synthesis of EH 1157).**

With several *C*- and *S*-glycoside derivatives in hand, a fluorescence polarisation assay was performed to evaluate these compounds as galectin inhibitors.

### Fluorescence Polarisation

Fluorescence polarization (FP) is a well-established analytical technique to evaluate galectin–ligand interactions. FP is advantageous over other techniques such as isothermal titration calorimetry (ITC) which requires relatively high concentrations of interacting partners (typically more than 100  $\mu\text{M}$  for galectins), making it impractical for screening large numbers of compounds. The assay is based on measuring interactions of galectins with fluorescein-conjugated saccharides by FP which also permits calculation of  $K_D$  values for monovalent interactions between the galectin CRD's and their ligands.<sup>9,10</sup>

## FP Experiment Design

The principle of the assay is based on FP measurements where a fluorescein-tagged saccharide probe is excited with plane-polarized light and the degree of polarization remaining in the emitted light is measured (see Figure 47). This remaining polarization decreases in relation to the rotation speed of the fluorescent probe during the excited state lifetime. When the probe is bound to the galectin it rotates slower than when free, and the remaining fluorescence polarization is higher. The fluorescent anisotropy value for a probe-protein mixture is the average of the value for bound and free probe (weighted by their relative quantities) and hence, the amount of bound and free probe in solution can be estimated accurately. Each galectin has a specific optimal probe for inhibition studies (see Figure 48). Fixed amounts of galectin and selected probe are used to screen inhibitory potency of ligands. FP is measured by photomultipliers receiving light through perpendicularly polarized channels. The change in the FP measurement in the presence and absence of an inhibitor is indicative of ligand potency.

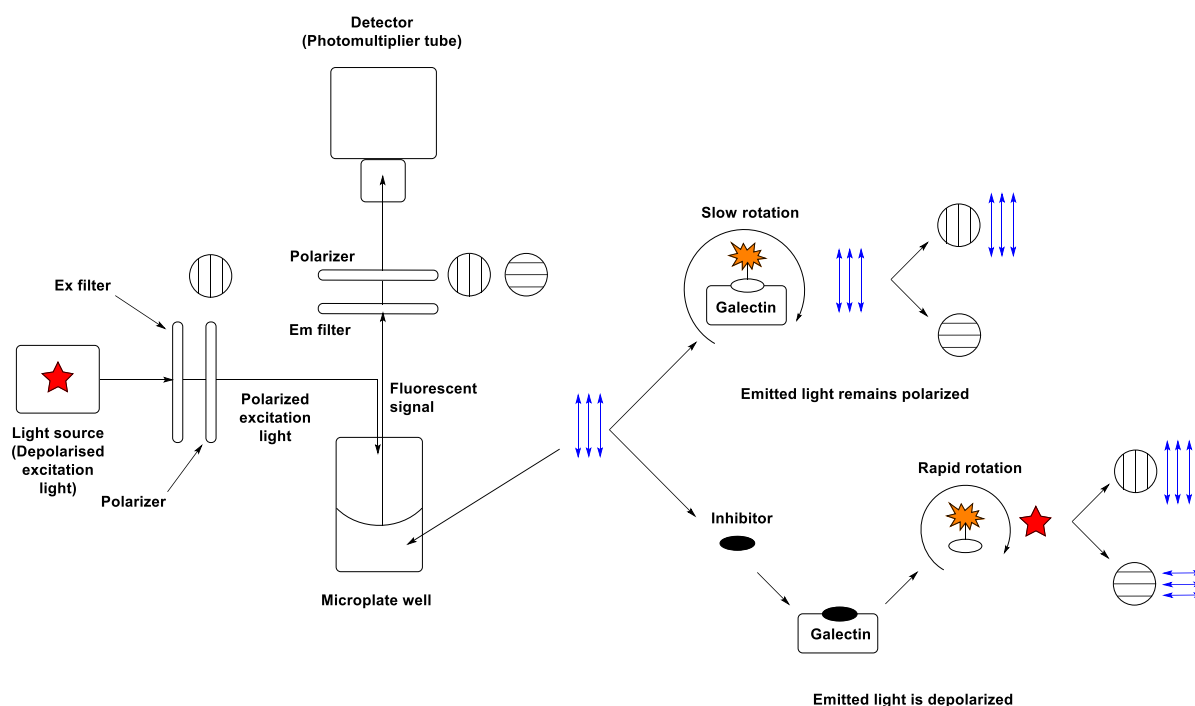


**Figure 47: Schematic Representation of FP detection on a microplate reader.**

$K_D$  values for galectin–inhibitor interactions are calculated based the assumption of a simple one-site competition. <sup>11</sup>

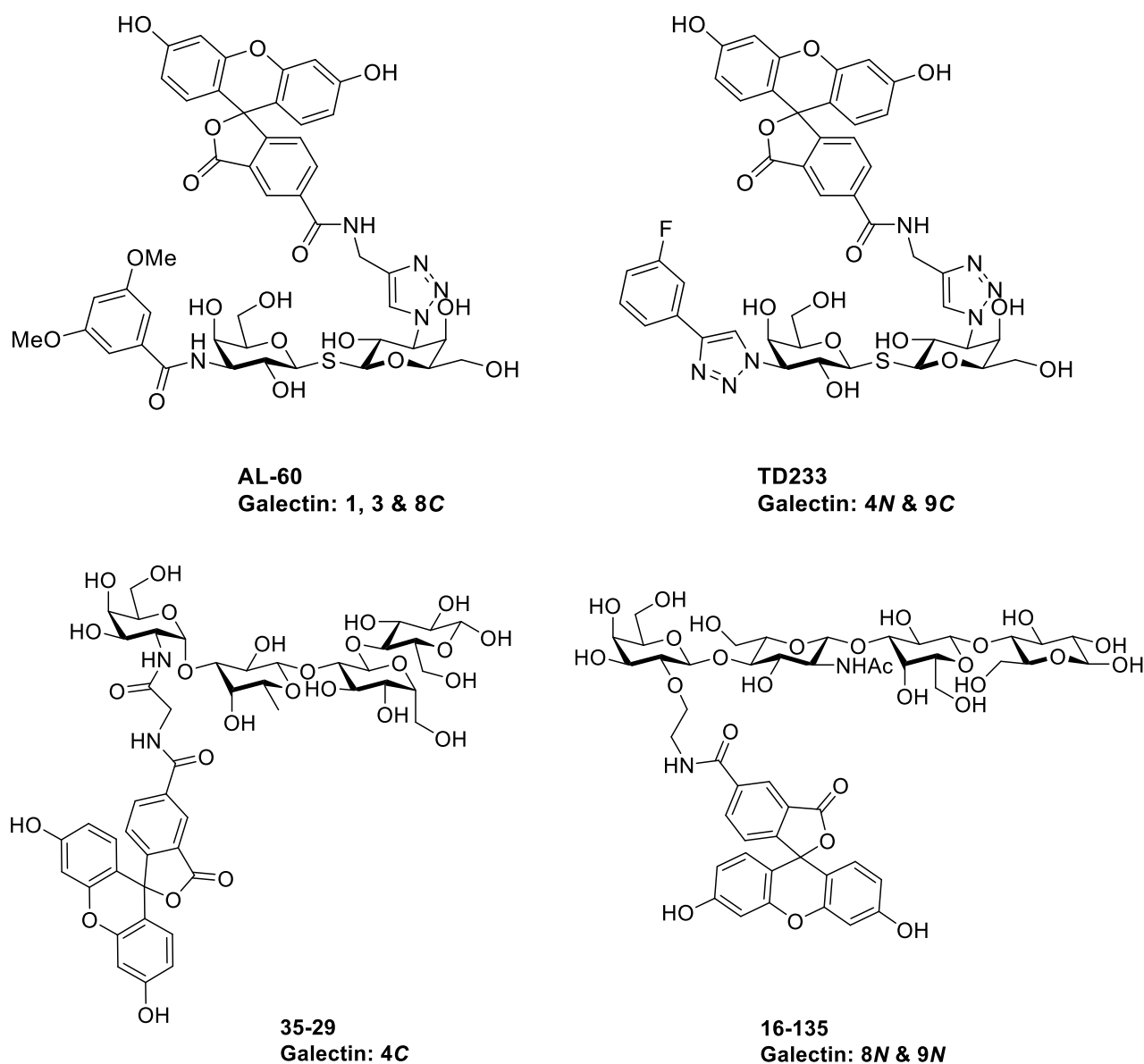


**Figure 48: Fluorescein linked probes used for different galectins (listed) to calculate  $K_D$  values of inhibitory ligands.**

## Method

FP was measured in 96-well microtiterplates (The final sample volume in each well was 120  $\mu\text{L}$ ). For direct binding, a solution of galectin was prepared in a microtiter plate (30  $\mu\text{L}$  per well, concentration was dependent on galectin used). Then 30  $\mu\text{L}$  of the fluorescent probe was added to give a final concentration of 0.02  $\mu\text{M}$  and the plate incubated under slow rotary shaking in the dark for 5 min. For the inhibition assay, 30  $\mu\text{L}$  of galectin and probe at fixed concentrations were mixed with 60  $\mu\text{L}$  of inhibitor solution and FP was measured. Inhibitor

concentration varied in a serial dilution from 0.074 to 2 mM. Control wells containing only fluorescent probe (0.02  $\mu\text{M}$ ) and fluorescein (0.02  $\mu\text{M}$ ) were included to first set the gain of the photomultipliers to avoid saturation and correct any imbalance in photomultiplier sensitivities. All dilutions and measurements were done in PBS. Incubation at room temperature and higher was achieved by using the thermostat of the instrument. The temperature was estimated by measuring selected wells with a mini thermometer. The  $K_D$  values for the galectin–inhibitor interaction were calculated directly from single data points by solving the two equations of mass action governing galectin–inhibitor interaction and galectin–probe interaction respectively:

$K_D(\text{inhibitor}) = [I] \times [G]/[IG]$  and  $K_D(\text{probe}) = [P] \times [G]/[PG]$ , where  $[I]$ ,  $[P]$  and  $[G]$  are the concentrations of free inhibitor, probe and galectin respectively and  $[IG]$  and  $[PG]$  are the concentrations of inhibitor–galectin complex and the probe–galectin complex, respectively. To solve the unknowns in these equations, the known parameters in the following equations were used. The known total concentrations of each component are as follows:

$$[I]_{\text{tot}} = [I] + [IG],$$

$$[P]_{\text{tot}} = [P] + [PG]$$

$$[G]_{\text{tot}} = [G] + [IG] + [PG]$$

The measured anisotropy value  $A$  is used to calculate the amount of bound probe, since the measured values are in units of polarization ( $P$ ) they were first converted to anisotropy as this correlates more directly with amount of bound probe:

$$[PG] = \frac{(A - A_0)}{(A_{\text{max}} - A_0)} \times [P]_{\text{tot}}$$

$A_{\text{max}}$  is obtained as the maximum value approached in a separate direct binding experiment as described above.  $A_0$  is the value for probe without galectin and inhibitor.  $K_D(\text{probe})$  is calculated from the control data point with probe and galectin but no inhibitor:

$$K_D(\text{probe}) = ([P]_{\text{tot}} - [PG]_{\text{no inh}}) \times ([G]_{\text{tot}} - [PG]_{\text{no inh}})/[PG]_{\text{no inh}}$$

$[PG]_{\text{no inh}}$  is calculated with  $A = A_{\text{no inh}}$ . The calculation is organized as a series of formulae (not shown) in Microsoft Excel where  $K_D(\text{inhibitor})$  and the other variables are calculated instantly as the measured  $A$  and the “fixed” values  $[I]_{\text{tot}}$ ,  $[P]_{\text{tot}}$ ,  $[G]_{\text{tot}}$ ,  $A_0$ ,  $A_{\text{no inh}}$ , and  $A_{\text{max}}$  were entered.

## Results

Synthesized compounds were tested against galectins -1, -3, -8C, -8N, -9C, -9N, -4C and -4N. An example of a binding curve for three selected compounds tested against galectin-3 can be seen in Figure 49.

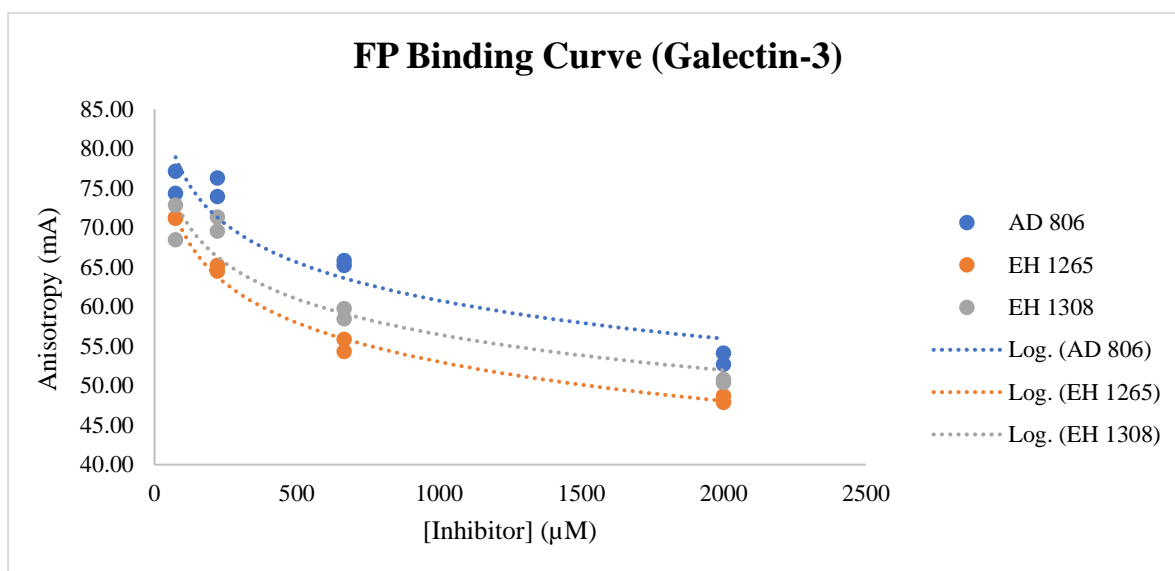


**Figure 49: Binding curves comparing inhibition of Galectin-3 by AD 806, EH 1265 and EH 1308**

Furthermore, 21 derivatives synthesised by Ashis Dhara (denoted with AD in compound numbers) were also tested in the FP assay, including those galactopyranose derivatives evaluated in the galactosidase inhibition study in chapter 2. The results of the assay are summarised in Tables 11 and 12. There were solubility issues with some of the compounds, where solubility was not achieved, even when dissolving in a 10% v/v solution of DMSO in PBS, denoted by an asterisk in the tables.

**Table 11: Dissociation constants ( $K_D$ ) for Ashis Dhara's (AD) compounds with galectins -1, -3, -8C-terminal domain, -8N-terminal domain, -9C-terminal domain, -9N-terminal domain, -4C-terminal domain and -4N-terminal domain**

| Lab Note book code | Structure | $K_D$ (mM) |       |        |        |        |        |        |        |
|--------------------|-----------|------------|-------|--------|--------|--------|--------|--------|--------|
|                    |           | Gal-1      | Gal-3 | Gal-8C | Gal-8N | Gal-9C | Gal-9N | Gal-4C | Gal-4N |
| <b>AD 553</b>      |           | 5.0        | 4.23  | 10.2   | 9.45   | 9.44   | >>4    | 14.26  | 1.64   |
| <b>AD 556</b>      |           | 2.28       | 1.71  | 6.3    | 5.2    | 5.69   | 7.33   | 2.25   | 1.43   |
| <b>AD 584</b>      |           | 3.55       | 3.81  | 8.42   | 8.82   | 9.68   | >>4    | 10.25  | 0.898  |
| <b>AD 433</b>      |           | 1.76       | 2.39  | 1.476  | 4.195  | >>4    | 7.95   | 8.42   | 0.89   |
| <b>AD 558</b>      |           | 2.47       | 1.74  | 8.276  | 5.87   | 2.32   | 5.9    | 16.15  | 1.09   |
| <b>AD 774</b>      |           | 0.93       | 1.4   | 1.7    | 2.31   | 0.304* | >>4    | 4.5    | 0.698  |
| <b>AD 776</b>      |           | 7.98       | 6.19  | 4.467  | 14.34  | >>4    | >>4    | 0.764  | 0.615  |
| <b>AD 791</b>      |           | 3.75       | 6     | 5.55   | 2.56   | >>4    | 6.394  | 0.962  | 1.27   |

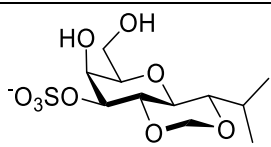
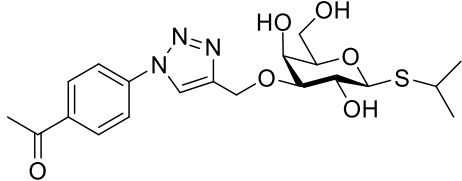
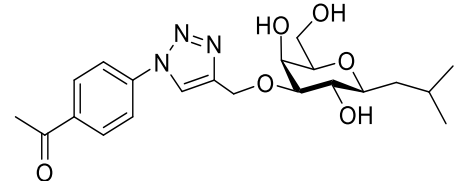
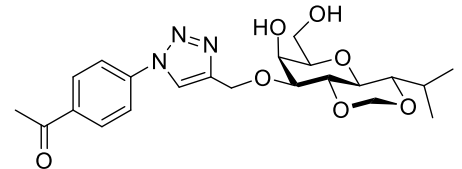
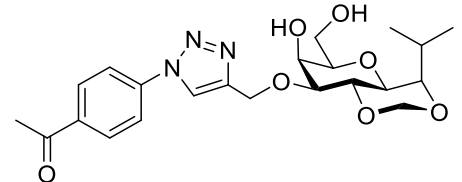
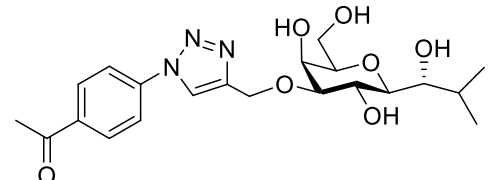
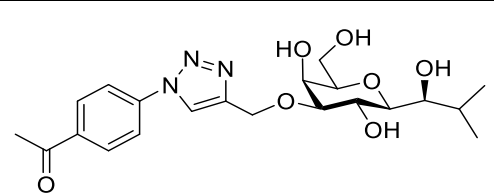
|               |  | Gal-1  | Gal-3  | Gal-8C | Gal-8N | Gal-9C | Gal-9N | Gal-4C | Gal-4N |
|---------------|--|--------|--------|--------|--------|--------|--------|--------|--------|
| <b>AD 799</b> |  | 2.73   | 5.88   | 1.31   | 1.8    | >>4    | 8.8    | 3.69   | 1.07   |
| <b>AD 801</b> |  | 7      | 2.89   | 5.382  | 3.97   | 6.77   | 5.025  | 16.38  | 0.795  |
| <b>AD 741</b> |  | 8.782  | 0.134  | 0.935* | 6.756  | 0.453* | >>4    | 2.00   | 4.15   |
| <b>AD 724</b> |  | 1.2    | 2.53   | 3.0    | 7.16   | 2.47   | 3.61   | 9.43   | 3.69   |
| <b>AD 736</b> |  | 4.03   | >>4    | 0.515  | 2.25   | 7.7    | >>4    | >>4    | 1.1    |
| <b>AD 784</b> |  | 3.64   | >>4    | 6.2    | 3.433  | >>4    | 1.757  | 0.577  | 2.29   |
| <b>AD 782</b> |  | 1.1    | 1.55   | 0.823* | 4.12   | 3.08   | 4.41   | 1.89   | 4.17   |
| <b>AD 779</b> |  | 0.24 * | 0.295* | 1.393  | 0.295  | 0.734  | 1.83   | 1.033  | 0.184* |
| <b>AD 786</b> |  | 0.627* | 0.278* | 0.766  | 3.12   | 1.7    | 0.807  | 1.427  | 0.403* |
| <b>AD 795</b> |  | 1.07   | 1.2    | 1.966  | 4.09   | 1.353  | 3.046  | 1.46   | 1.008  |
| <b>AD 804</b> |  | 1.39   | >>4    | 6.68   | 3.4    | >>4    | 3.644  | >>4    | 0.171  |



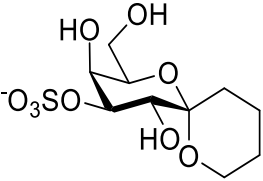
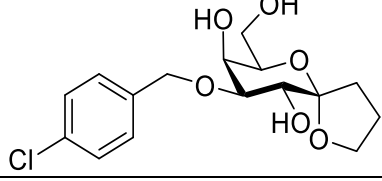
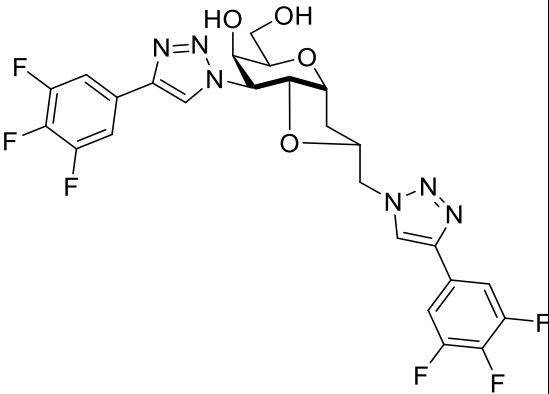
|               |  | Gal-1 | Gal-3 | Gal-8C | Gal-8N | Gal-9C | Gal-9N | Gal-4C | Gal-4N |
|---------------|--|-------|-------|--------|--------|--------|--------|--------|--------|
| <b>AD 806</b> |  | 1.82  | 0.63  | 3.17   | 0.793  | 1.111  | 0.767  | >>4    | 0.149  |
| <b>AD 794</b> |  | 2.14  | 1.61  | 1.78   | 0.449  | 5.94   | 3.227  | 4.056  | 1.135  |
| <b>AD 803</b> |  | 1.92  | 4.2   | 3.29   | 0.797  | >>4    | 7.873  | 16.38  | 4.46   |
| <b>AD 805</b> |  | 5.25  | 1.2   | 18.7   | 0.183  | 2.28   | 1.313  | 12.95  | 5.21   |

**Table 12: Dissociation constants ( $K_D$ ) for Eoin Hever's compounds with galectins -1, -3, -8C-terminal domain, -8N-terminal domain, -9C-terminal domain, -9N-terminal domain, -4C-terminal domain and -4N-terminal domain**

| Lab note book Code | Structure | $K_D$ (mM) |       |        |        |        |        |        |        |
|--------------------|-----------|------------|-------|--------|--------|--------|--------|--------|--------|
|                    |           | Gal-1      | Gal-3 | Gal-8C | Gal-8N | Gal-9C | Gal-9N | Gal-4C | Gal-4N |
| <b>EH 1260</b>     |           | 4.0        | >>4   | >>4    | 0.946  | 8.42   | >>4    | n.t.   | n.t.   |
| <b>EH 1263</b>     |           | 1.83       | 0.97  | 5.37   | 0.304  | 1.61   | 2.24   | 16.26  | 1.052  |
| <b>EH 1264</b>     |           | 4.53       | 4.74  | 5.88   | 0.906  | 7.1    | 11.96  | 2.576  | 12.32  |
| <b>EH 1265</b>     |           | 2.39       | 0.287 | 9.79   | 0.08   | 0.693  | 0.792  | 0.601  | 2.43   |

|                |   | Gal-1 | Gal-3 | Gal-8C | Gal-8N | Gal-9C | Gal-9N | Gal-4C | Gal-4N |
|----------------|---|-------|-------|--------|--------|--------|--------|--------|--------|
| <b>EH 1266</b> |    | 2.72  | 3.23  | 0.405  | 0.676  | 5.51   | 11.1   | 3.98   | 7.27   |
| <b>EH 1284</b> |    | 15.6  | 2.48  | >>4    | 5.81   | 0.351  | >>4    | >>4    | >>4    |
| <b>EH 1285</b> |    | 7.75  | >>4   | >>4    | 17.485 | 0.457  | >>4    | >>4    | >>4    |
| <b>EH 1286</b> |   | 4.92  | 4.9   | 1.4    | 6.38   | 0.345  | >>4    | >>4    | >>4    |
| <b>EH 1287</b> |  | 3.38  | 2.03  | 0.266  | 0.505  | n.t.   | >>4    | 2.19   | n.t.   |
| <b>EH 1288</b> |  | 5.4   | 1.38  | 12.55  | 3.222  | 3.404  | 7.26   | n.t.   | n.t.   |
| <b>EH 1289</b> |  | 4.78  | 0.73  | n.t.   | 0.828  | n.t.   | 3.065  | n.t.   | n.t.   |

|         |  | Gal-1 | Gal-3 | Gal-8C | Gal-8N | Gal-9C | Gal-9N | Gal-4C | Gal-4N |
|---------|--|-------|-------|--------|--------|--------|--------|--------|--------|
| EH 1305 |  | 2.43  | 0.803 | >>4    | 4.732  | >>4    | 6.75   | >>4    | 1.48   |
| EH 1307 |  | 4.33  | 1.3   | 16.68  | 6.25   | n.t.   | 2.108  | >>4    | 0.378  |
| EH 1308 |  | 6.18  | 0.35  | 3.8    | 4.194  | n.t.   | 0.751  | 6.43   | n.t.   |
| EH 1309 |  | 5.38  | 2.64  | n.t.   | 0.85   | n.t.   | 0.29   | n.t.   | n.t.   |
| EH 1310 |  | 4.99  | 0.845 | 12.1   | 7.17   | 12.6   | 0.159  | 0.73   | >>4    |
| EH 1311 |  | 3.25  | 0.608 | 3.09   | 0.756  | >>4    | 7.296  | 4.21   | 5.3    |
| EH 1313 |  | 16.22 | 2.98  | >>4    | 7.718  | 5.76   | 2.09   | 1.94   | >>4    |
| EH 1314 |  | 4.6   | 0.666 | 5.92   | 6.476  | 4.07   | 1.48   | 2.23   | 0.6    |
| EH 1315 |  | 6.38  | 1.07  | 11.05  | 6.97   | 2.73   | 0.836  | 4.47   | 1.85   |

|               |  | Gal-1 | Gal-3 | Gal-8C | Gal-8N | Gal-9C | Gal-9N | Gal-4C | Gal-4N |
|---------------|--|-------|-------|--------|--------|--------|--------|--------|--------|
| EH 1293       |   | 1.44  | 1.756 | >>4    | 0.348  | 12.49  | 10.26  | 4.6    | 7.87   |
| EH 1317       |   | 10.7  | 1.02  | 10.15  | 6.2    | 4.33   | 2.363  | 4.34   | 1.65   |
| EH 1163<br>US |  | 2.61  | 0.28* | 0.253* | 2.09   | 8.34   | 2.16   | 0.207  | 1.04   |

\* Precipitation after dissolving in 10% DMSO, so it is difficult to quantify the accuracy of these results,

n.t. = Not tested

## Discussion

The results from the testing using the FP assay showed that many compounds showed inhibition. Some compounds showed inhibition at low mM to high micromolar concentrations and showed selectivity, while others gave little to no inhibition. As the assay results are based on the degree of polarization remaining in the emitted light after excitation of the probe, it is essential that solubility of ligands is achieved to obtain reliable data, hence why it was difficult to quantify results in some cases.

In the same manner as in chapter 2, docking of selected ligands was carried out to try to establish a potential rationalisation for the FP results. X-ray crystal structures for all the galectins tested were obtained from the Protein Data Bank. All PDB structures consisted of the galectin in complex with ligands like those tested. The codes for the PDB files used were

3T2T<sup>12</sup> (galectin-1 with methyl 2-*O*-acetyl-3-*O*-toluoyl- $\beta$ -D-talopyranoside), 3T1L<sup>12</sup> (galectin-3 with methyl 2-*O*-acetyl-3-*O*-toluoyl- $\beta$ -D-talopyranoside), 3VKM<sup>13</sup> (galectin-8 with sialyllactose and lactose), 7P1M<sup>14</sup> (galectin-8*N* with benzimidazole-D-galactal), 3NV2<sup>15</sup> (galectin-9*C* with LacNAc), 2EAK<sup>16</sup> (galectin-9*N* with lactose), 4YM3<sup>17</sup> (galectin-4*C* with lactose), 5DUV<sup>18</sup> (galectin-4*N* with lactose). The ligands were docked by editing the lactose/LacNAc structure already present in the CRD to build the synthesized molecules. Ligands were prepared and docked using the Maestro software.

### Galectin-1

Galectin-1 bound some of the phenyl triazole derivatives such as **AD 774**, **AD 724**, **AD 782**, **AD 779**, **AD 786**, and **AD 795** with higher affinity than those without aromatic functionality, such as **AD 553** and **AD 584**.

There is no major selectivity for *C*- or *S*-glycosides with **AD 782**, **AD 795**, **AD 804** and **AD 806**, with all displaying similar inhibition for galectin-1. However, it appears that the presence of a cyclic constraint mimicking the exo-syn conformation has a favourable impact on binding relative to the mimic of the exo-anti conformer, with **AD 433** giving a 4-fold stronger affinity than **AD 776**, while **AD 556** gives 2-fold better affinity than **AD 553**. Although there is no exo-anomeric effect in *C*-glycosides, there are still conformational preferences in the  $\phi$  and  $\Psi$  angles. In contrast to *O*-disaccharides, like lactose, where staggered is preferred for  $\phi$  and eclipsed conformation is preferred for  $\Psi$  (aglycon torsion), staggered conformations are more favourable for both  $\phi$  and  $\Psi$  angles in *C*-disaccharides, as indicated by Espinosa and co-workers.<sup>19</sup> These conformational differences may be factors influencing binding affinity although no binding data could be found for *C*-lactose binding to a galectin, for example. The degree of fluorination of the phenyl ring has an impact on affinity, with the trifluorophenyl derivative **AD 774** binding nearly 2-fold stronger than monofluoro **AD 433** and ~2.5 fold stronger than unsubstituted **AD 558**. The 3-*O*-substituted derivatives are also beneficial, with ~4-fold improvement when comparing **AD 779** (see Figure 50) to **AD 774**, **AD 782** is ~1.5-fold better than **AD 433** and a ~12.5-fold difference between **AD 786** and **AD 776**. The bulkier 3-position substituents in **AD 741** and **AD 736** have a negative effect on binding compared to the 3-position unsubstituted analogue **AD 558**.

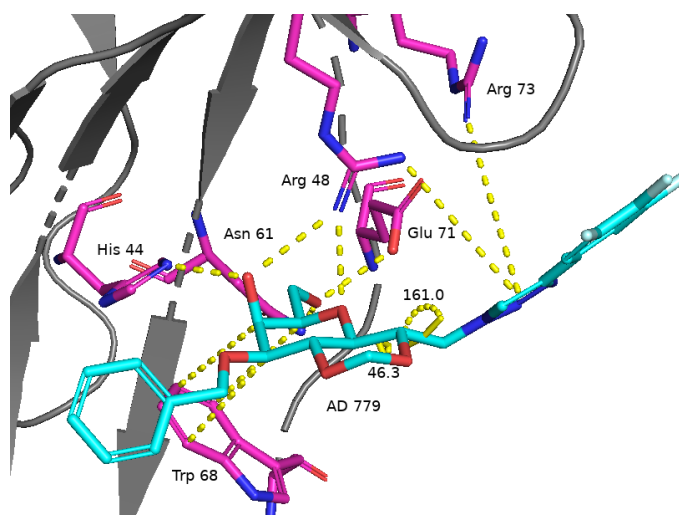


**Figure 50: AD 779 in complex with galectin-1 CRD**

Although dipolar  $C-F \cdots H-N$  and  $C-F \cdots C=O$  interactions were previously reported for fluorinated aromatic rings as a rationale for improved affinity relative to unsubstituted phenyl rings,<sup>20</sup> no such interactions are apparent after the docking of **AD 774** with galectin-1. Comparing the docking poses of conformational isomers **AD 433** and **AD 556** vs **AD 776** and **AD 553** in galectin-1 suggest **AD 433** and **AD 556** (both mimic *exo-syn*) have some favourable interactions with nearby residues while the aglycon moieties of the **AD 776** and **AD 553** (both may mimic *exo-anti* conformer), would point away from the protein towards solvent. A H-bond is apparent after docking between the fluorine on the phenyl ring of **AD 433** and the backbone amide N-H of Trp68. A water mediated H-bond between the acetate carbonyl of **AD 556** and the same amide N-H may be responsible for its improved affinity (see Figure 51).

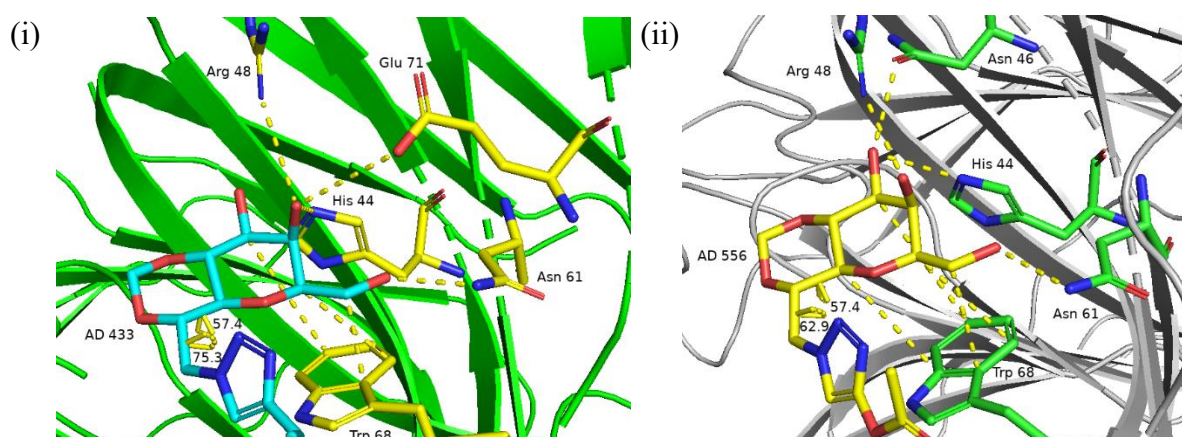


**Figure 51: Hydrogen bond formed between Trp68 backbone amide and *exo-syn* aglycons**  
**(i) Aromatic fluorine of AD 433 (ii) Water mediated with acetate carbonyl of AD 556**

Although the improved inhibition of 3-benzyl substituted derivatives, when compared to unsubstituted 3-OH derivatives, was beneficial, it was not possible based on docking to explain the affinity enhancement. Previous studies with galectin-1 have shown that a 3-position triazole substituted with thiophene can be beneficial as it is further extended into the binding pocket, allowing the heteroatoms to form close contacts with Val31 and Asp123,<sup>21</sup> however phenyl substituents at this position showed little benefit from such interactions<sup>22</sup> and the docking studies performed did not account for the change in affinity observed.

### Galectin-3

Evaluation of the ligands via galectin-3 based assays revealed some increases in affinity compared to methyl  $\beta$ -galactopyranoside, but with rather different selectivity compared to galectin-1. **AD 741**, which showed low affinity for galectin-1, was the best inhibitor in the series for galectin-3 and showed strong selectivity for galectin-3 over all other galectins tested. A 13-fold improvement in affinity was observed between **AD 741** and **AD 558**. These results indicate the acetophenone moiety of **AD 741** has some beneficial interactions with neighbouring residues. This agrees with work by Kren and co-workers,<sup>23</sup> where an analogous *p*-acetophenyl moiety at the 3-position of a TDG scaffold gave a 22-fold improved potency ( $IC_{50} = 3.8 \pm 1.1 \mu M$ ) for galectin-3 compared to a galactopyranose ligand ( $IC_{50} = 82 \pm 12 \mu M$ ). An unsubstituted phenyl ring attached via a methylene triazole to the 3-position of TDG has a 12-fold potency ( $IC_{50} = 6.7 \pm 1.7 \mu M$ ) improvement compared to TDG, suggesting a benefit due to the ketone.<sup>23</sup> The relatively poor inhibitory performance of the trifluoromethyl substituted **AD 736** suggest that the improved inhibition is not primarily due to the electron withdrawing nature of the ketone. The 3-position modifications with benzyl groups were generally beneficial for galectin-3 with a 3-fold improvement between **AD 779** and **AD 774** and ~22-fold from **AD 776** to **AD 786**. These trends are to be somewhat expected based on previous SAR studies with galectin-3, due to the conserved arginine residue in close proximity to these substituents.<sup>9, 10</sup> **AD 806** gave surprisingly good inhibitory results, ~2 and ~2.5 fold better than the corresponding thioglycoside **AD 795** and constrained exo-syn conformer **AD 782** respectively. The relatively poor results of **AD 804** with galectin-3 suggest a beneficial interaction occurs with the aglyconic alcohol. This trend is repeated when comparing **AD 801** with **AD 791** (*S*-glycoside) and **AD 799** (*C*-glycoside), as well as **EH 1265** with **EH 1263** and **EH 1264**. Comparing the results of **AD 741** with **EH 1286** suggest that the extra aromatic moiety has a beneficial interaction in the binding pocket. Despite this, some of the isopropyl

derivatives performed surprisingly well, with **EH 1265** and **EH 1289**, the 3-sulfate substituted and 3-azidoacetophenone substituted isopropyl derivatives respectively, displaying the best inhibition in the series. With the 5- and 6-membered spiro compounds, the axial anomeric oxygen is potentially beneficial to binding as it is orientated close to Trp181 in the CRD, suggesting an interaction between the oxygen lone pair and the  $\pi$ -system of the indole ring, not shared by an equatorial heteroatom.<sup>24</sup> **EH 1308** was the best performing of the spiro derivatives, with good selectivity for galectin-3. It is interesting to note that all the 6-membered spiro compounds performed better than their 5-membered analogues for galectin-3.

Docking of **AD 741** shows involvement of both the aryl triazole and the acetophenone rings in a cation- $\pi$  interaction with Arg144. The carbonyl group of the acetophenone appears to participate in a water mediated H-bond with the amide backbone N-H of Gly238. Arg162 is H-bonded to the axial 4-OH and the endocyclic oxygen. The  $\Psi$  angle in this complex is not in the preferred conformation ( $\Psi = 108.4^\circ$ ), however  $\Psi$  orientates the aromatic functionality towards the protein surface, allowing for cation- $\pi$  interactions with Arg162 and Arg186 (see Figure 52). Interactions with this aromatic functionality might explain the improved performance of **AD 741** relative to **EH 1286**.

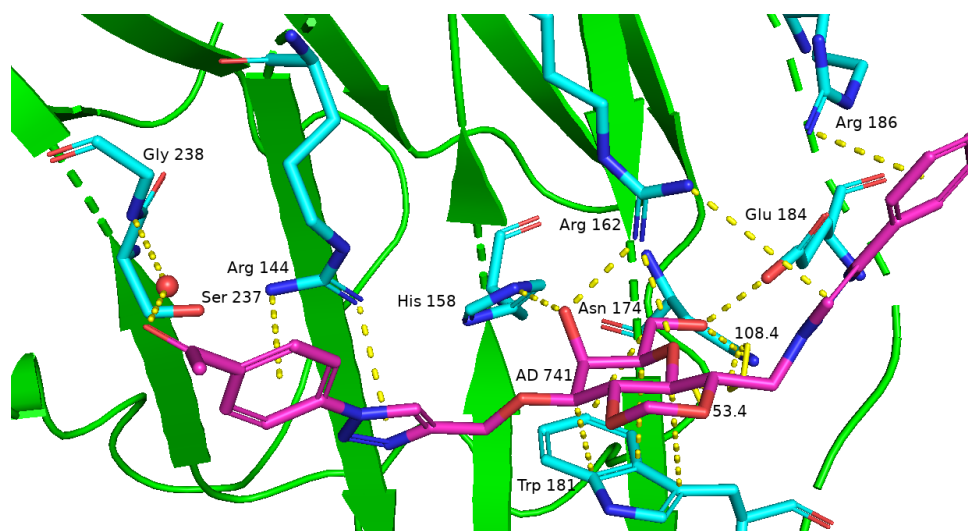


**Figure 52: AD 741 in complex with Galectin-3, showing interactions of Arg144 with the triazole and acetophenone moieties and Gly238 with the carbonyl. Interactions involving Arg162 and Arg186 can also be seen.**

The enhanced affinity of **AD 806** relative to **AD 804** can be explained by the H-bond interaction of the aglyconic alcohol with Arg162. Docking also suggests a water mediated H-bond with Glu184 and Arg186. A H-bond between the thioglycosidic linkage *S* atom in **AD 795** and



Arg162 is possible (see Figure 53),<sup>25, 26, 27</sup> but not in *C*-glycoside **AD 804**. The orientation of the aromatic moiety is different in both compounds due to the bond angle and atom size of *S* vs *C* in **AD 795** and **AD 806**.

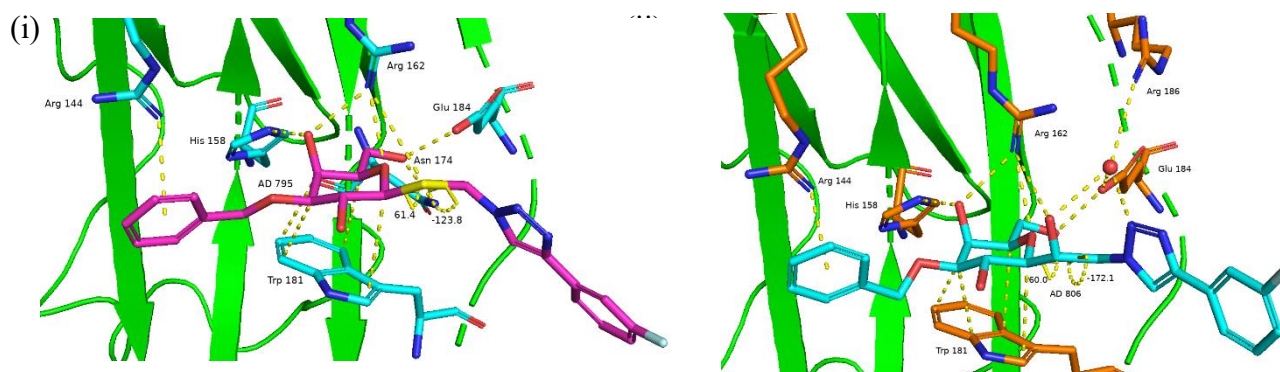


**Figure 53: H-bond interactions of glycosidic linkage of (i) AD 795 with  $\phi$  and  $\Psi$  dihedral angles shown and (ii) AD 806 with neighbouring residues.**

There are 3 possible conformations of the  $\phi$  angle in **AD 806**. The conformation bound in Figure 53 (ii) corresponds to energy minimum C in Figure 55 (iii), one of two stable  $\phi$  conformers. The formation of a H-bond with Arg162 is perhaps a factor influencing the conformation. In the other stable conformation, the aromatic moiety is too far from Glu184, preventing the water mediated H-bond between the triazole nitrogen and the sidechain carboxylate of Glu184. The three possible  $\phi$  conformations are represented as Newman projections in Figure 54. In the bound  $\phi$  conformation,  $\Psi \sim 180^\circ$ .

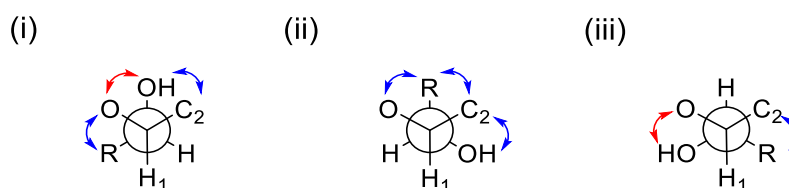
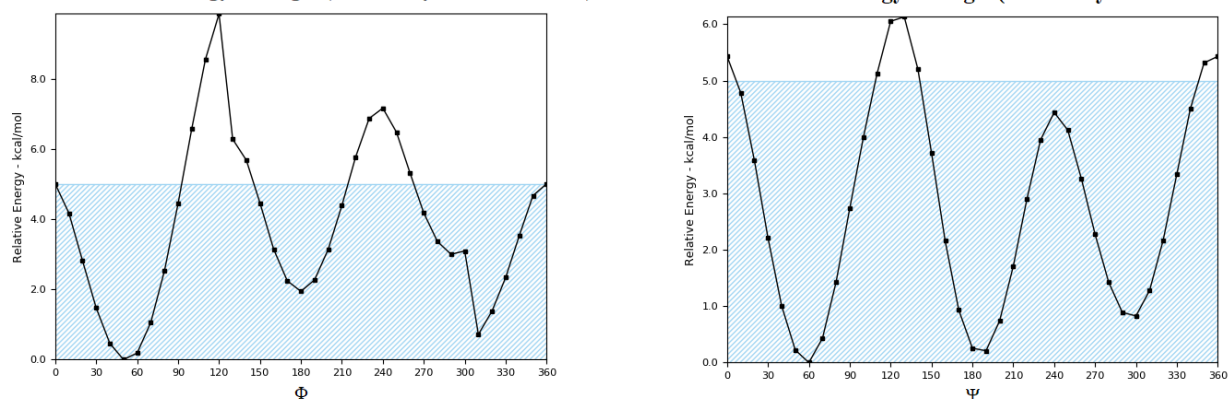


**Figure 54: Possible conformations of the  $\phi$  angle with steric Gauche interactions represented with blue arrows and the favourable Gauche effect shown with red arrows (i) Bound ligand conformation showing two steric clashes and stabilisation by the Gauche effect (ii) Three steric clashes and no stabilisation by the Gauche effect (iii) One steric clash and Gauche stabilization**

Conformational analysis (relaxed coordinate scan plotting energy as a function of the  $\phi$  and  $\Psi$  dihedrals) of **AD 806** suggest two minimum energy conformers for each dihedral angle. Relative energy plots generated using MacroModel for  $\phi$  (Figure 55 (i)) show an even distribution of Figure 54 (i) and Figure 54 (iii). These two different  $\phi$  conformations are seen in **AD 806** binding to galectin-3 ( $\phi \sim 60^\circ$ , Figure 53 (ii)) and **AD 806** binding to galectin-4N ( $\phi$

$\sim -70^\circ$ , Figure 61). For the  $\Psi$  angle (Figure 55 (ii)), AD 806 adopts the same minimum ( $\Psi \sim 180^\circ$ ) in both complexes.

(i) AD 806 Relative Energy  $\Phi$  Angle (defined by H1-C1-C1'-C2') (ii) AD 806 Relative Energy  $\Psi$  Angle (defined by C1-C1'-C2'-N)



(iii)

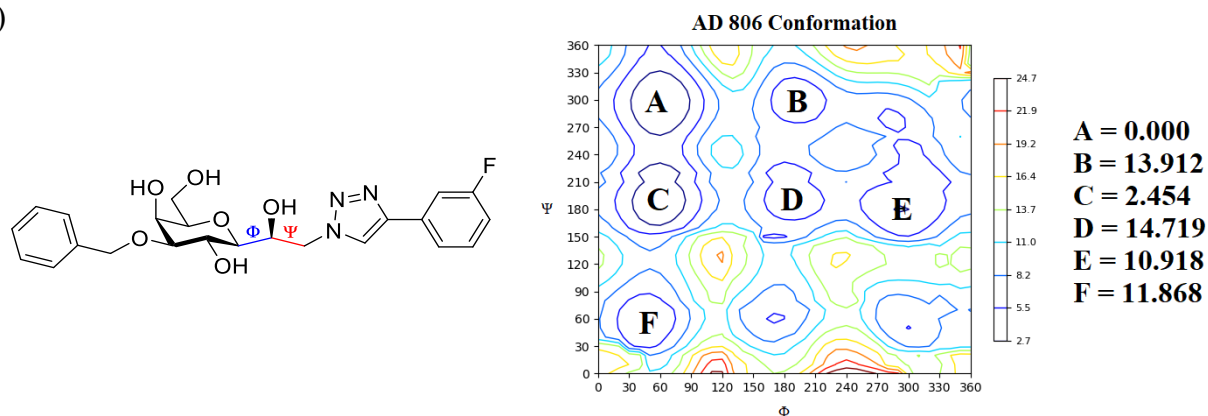


Figure 55: Relative Energy plots of (i)  $\Phi$  and (ii)  $\Psi$  angles in AD 806 (iii) Energy Contour plot of  $\Phi$  vs  $\Psi$  with relative energy minima (kcal mol<sup>-1</sup>) given. C and E are the energy minima corresponding to AD 806 in figure 50 (ii) and figure 58 respectively

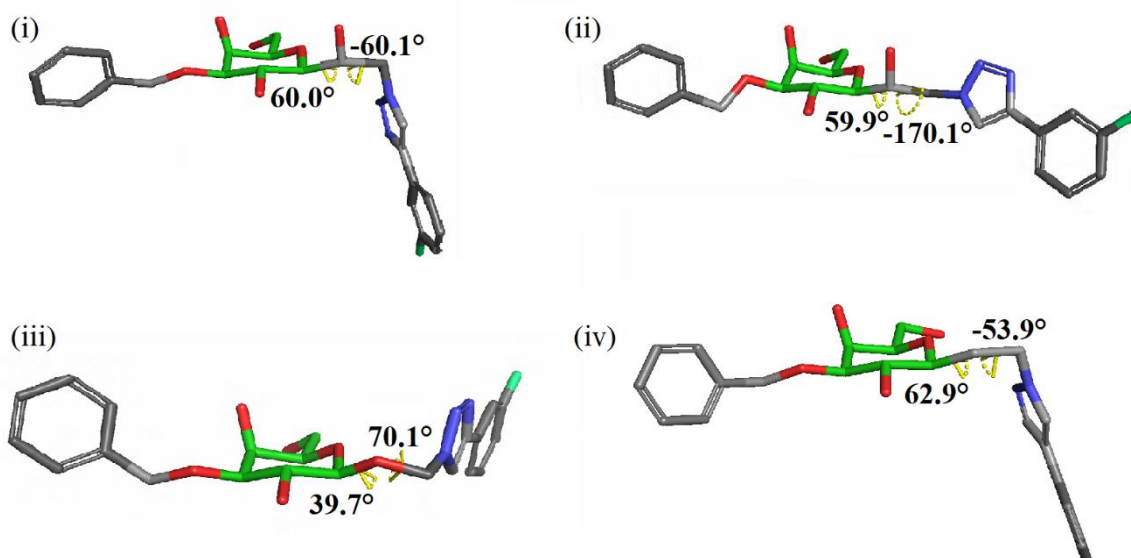


Figure 56: Comparing structure and minimum energy  $\Phi$  and  $\Psi$  dihedral angles of (i) AD 806 minimum A (absolute minimum) (ii) AD 806 minimum C (bound to galectin-3) (iii) O-glycoside analogue (iv) AD 804 (C-glycoside analogue)

### Galectin-8C and Galectin-8N

The compounds showed inhibition in the mM range mostly for galectin-8N/8C inhibition. One aspect of particular interest is that **AD 736** showed selectivity between galectin-8C and -8N. The cyclically constrained **EH 1287** was the best inhibition of the series. All compounds substituted with a sulfate at the 3-position gave better inhibition for galectin-8N than for those without the sulfate. This data is in good agreement with previous studies.<sup>2, 28</sup> All but one of the sulfated derivatives showing significant selectivity for gal-8N. The best inhibitor of the series was **EH 1265**, which gave an 8.5-fold improvement over **EH 1266** and an 11-fold improvement over **EH 1264**. The *S*-glycoside **EH 1263** was 3-fold better than both its *C*-analogue **EH 1264** and the constrained exo-anti mimic **EH 1260**. Noncyclic constrained **AD 806** gives a 4-fold better affinity than the constrained exo-anti **AD 786** and the same pattern was observed for the final three compounds in table 11, with **AD 805** giving the best performance for these compounds, inhibiting ~2.5-fold and 4.3-fold better than **AD 794** and **AD 803** respectively. It is interesting to note a ~10-fold improvement between **EH 1311** and **EH 1310**, possibly due to the change in ring size. An improvement is likewise seen comparing **EH 1293** and **EH 1319**.

Comparing the binding modes, predicted by docking, of **EH 1265** and **EH 1266** in complex with galectin-8N show that the loss of a H-bond may result in the difference in affinity (see Figure 57), which is consistent with the trend also seen for **AD 806** and **AD 804** with galectin-3. The galactopyranosyl moiety of both ligands display the characteristic galectin-carbohydrate interactions in the binding mode. The  $\alpha$ -face of the galactose ring of both ligands are involved in CH- $\pi$  interactions with Trp86 and the axial 4-OH is H-bonded to His65, Arg45 and Arg69, with the endocyclic oxygen also H-bonded to Arg69. The saccharide 6-OH is H-bonded to both the carboxylate sidechain of Glu89 and the sidechain N-H of Asn79. The Arg45 at the  $\beta$ -face of the sugar ring is involved in H-bonds to the 3-oxygen while the sulfate group at this position is H-bonded to the N-H of Gln47, a distance of 3.0 Å between oxygen on the sulfate group and the indole N-H of Trp86 suggests another H-bond, while a salt bridge and H-bond are predicted between the oxygen atoms on the sulfate group and the guanidium N-H's of Arg59. The difference in affinities can hence be rationalised by the exocyclic alcohol in **EH 1265** 3.3 and 2.8 Å from the N-H groups of Arg45 and Arg69 respectively. The H-bonds formed with these residues (Arg45 and Arg69) are lost in **EH 1266** due to the absence of this alcohol and in **EH 1264**. Although **EH 1263** performed 3-fold better than **EH 1264**, the relative strength of the H-bond formed with the exocyclic oxygen of **EH 1265** and its proximity to the arginine sidechains

compared to the sulfur in **EH 1263** leads to a potentially stronger interaction for **EH 1265**. The predicted docking modes of **EH 1265** and **EH 1266** bound to galectin-8*N* can be seen in Figure 57.

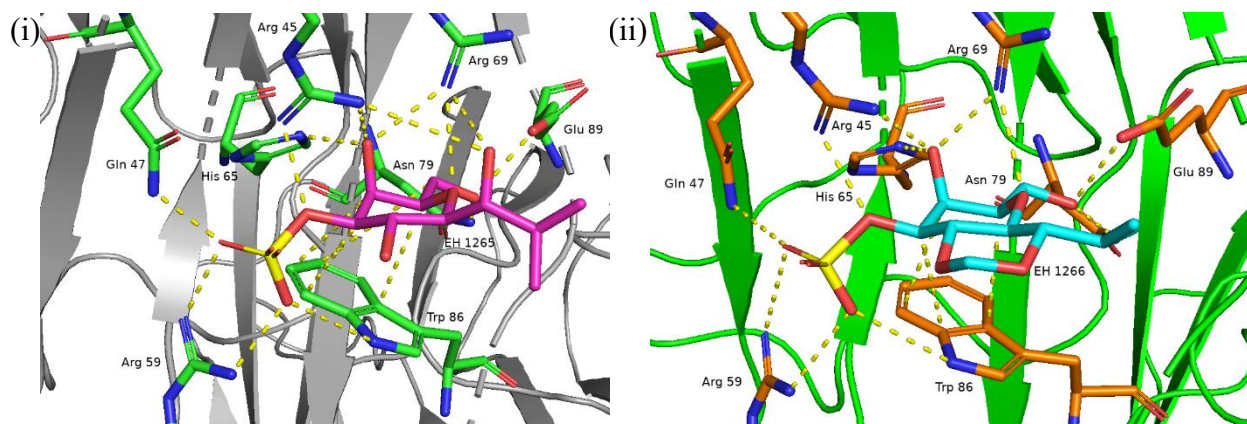


**Figure 57: Comparing the binding modes of (i) EH 1265 and (ii) EH 1266 with galectin-8*N***

The 10-fold improvement of **EH 1311** compared to **EH 1310** for galectin-8*N* can be rationalised due to the loss of a H-bond between the axial anomeric oxygen and the N-H of Trp86. Docking gives a distance of 3.1 Å between the **EH 1311** axial oxygen and the indole N-H, compared to 5.0 Å for **EH 1310**, a distance too great to form a H-bond. The docking pose of both compounds suggest a  $\pi$ - $\pi$  stacking interaction between the trifluoromethyl phenyl ring and the phenol sidechain of Tyr141 (see Figure 58). There is a difference in the distance between the two rings, 3.5 and 4.5 Å for **EH 1311** and **EH 1310** respectively. A combination of the variations in binding results in a weaker interaction.

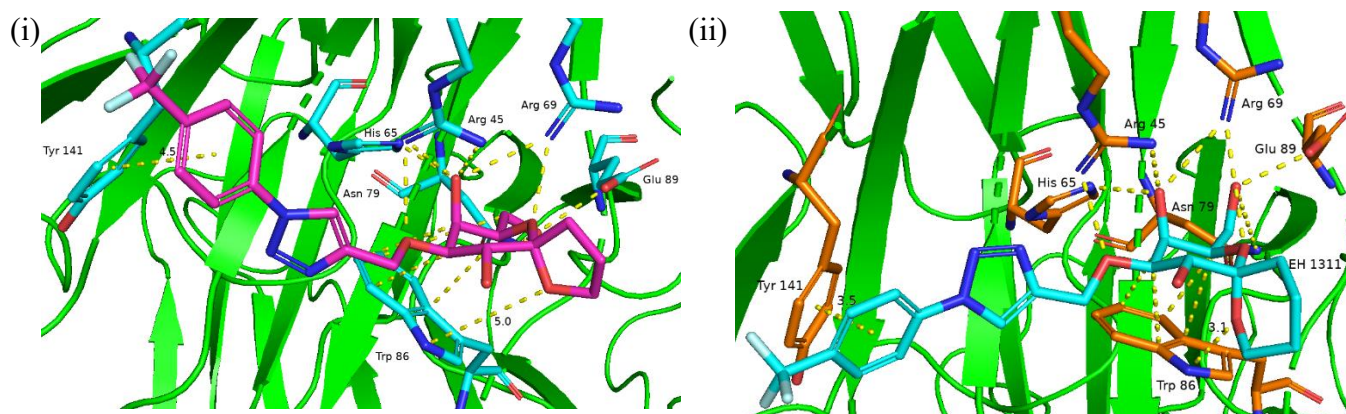


**Figure 58: Binding of (i) EH 1310 and (ii) EH 1311 to galectin-8*N* showing differences in H-bonding and  $\pi$ - $\pi$  stacking**



### Galectin-9C and Galectin-9N

AD 774 proved to be the most potent inhibitor for galectin-9C, binding with good selectivity. The results suggest that the extra fluorines on the aromatic ring are beneficial, especially when data is compared with AD 433 – AD 801. The pattern was repeated for AD 779, giving the best inhibition of the 3-benzyl substituted derivatives (AD 724 – AD 806). It is interesting to compare the results of AD 736 and AD 741, which have a similar trend as for galectin-3. Compounds AD 805, AD 806 and EH 1265 outperformed thioglycosides AD 794, AD 795 and EH 1263, which were in turn better than C-glycosides AD 803, AD 804 and EH 1264. EH 1284, EH 1285 and EH 1286 all bound to galectin-9C selectively, when comparing with all the other galectins tested.

Docking poses of Galectin-9C in complex with AD 774 shows that when the  $\Psi$  angle is  $\sim 180^\circ$ , the aromatic moiety is orientated away from the protein into space, so it is too far from the neighbouring residues to have any considerable interactions. Although the staggered conformation is preferred for  $\Psi$ ,<sup>6</sup> the eclipsed conformation ( $\Psi = 115.5^\circ$ ) may be adopted in this case in order to allow the trifluorophenyl triazole moiety to interact with two neighbouring arginine residues via cation- $\pi$  interactions. Despite the conformational energy penalty, the triazole is involved with Arg239 and the trifluorophenyl with Arg260. The *para* and *meta* fluorine substituents on the aromatic ring both participate in a dipolar interaction with the same guanidine N-H of Arg260, while the *meta* fluorine is also in a dipolar interaction with the sidechain carbonyl of Glu258. These interactions as well as the two possible conformations of the sugar can be seen in Figure 59.

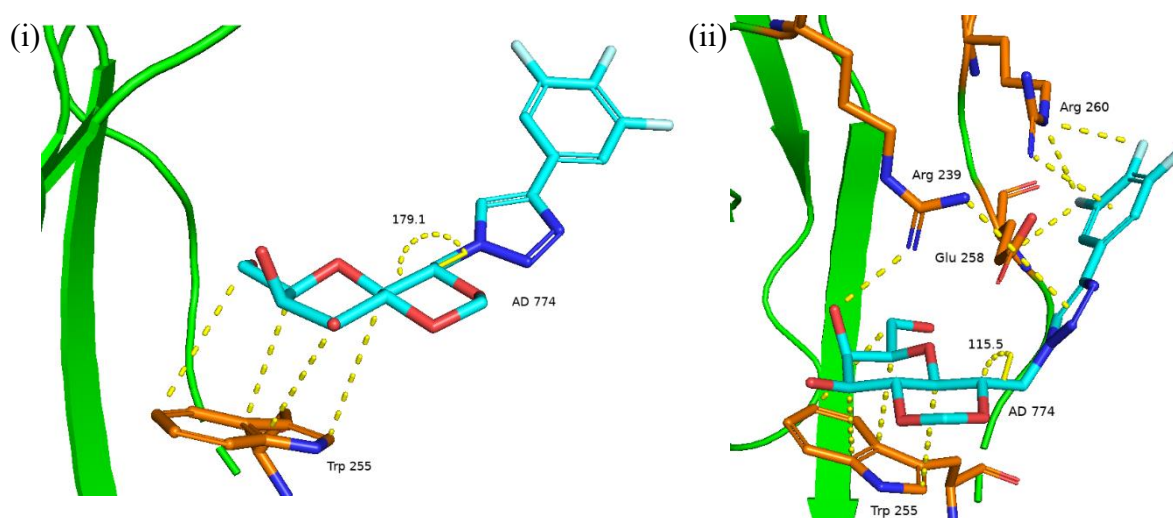


**Figure 59: (i) Staggered conformation of  $\Psi$  glycosidic torsion angle in AD 774 showing  $\Psi$  dihedral angle (ii) Eclipsed conformation of  $\Psi$  glycosidic torsion angle ( $\Psi = 115.5^\circ$ ) in AD 774 showing cation- $\pi$  and hydrogen bonding interactions with neighbouring amino acid residue sidechains in galectin-9C**

For 3-benzyl substituted derivatives, there are no amino acid residues in a close enough proximity to the benzyl substituents to make any beneficial interactions. His223 is just outside of the range of a potential  $\pi$ - $\pi$  stacking, located 6.8 Å from the 3-benzyl of **AD 724**.

Some of the ligands bound well to galectin-9*N*, the best being **EH 1310**, binding with good selectivity. **EH 1310** gave a 45-fold improvement over its corresponding 6-membered spiro **EH 1311**. In contrast to galectin-3, there was a recurring trend of 5-membered spiro compounds giving better results than their 6-membered analogues with a 1.7-fold improvement between **EH 1306** and **EH 1305**, 2.6-fold between **EH 1309** and **EH 1308** and 3.8-fold between **EH 1319** and **EH 1293**. A 2-fold improvement was seen between **EH 1315** and **EH 1313**, possibly due to solvation effects of the extra fluorines and the possible withdrawal of electron density from the sugar ring by the fluorines, increasing the strength of the CH- $\pi$  interactions with the Trp255, as suggested in a study by Woolfson et al.<sup>29</sup> This trend between these two ligands was also observed for galectin-9*C*, galectin-3 and galectin-1. The cyclic constrained **AD 786** and its non-cyclic constrained analogue **AD 806** gave similar binding results, ~4-fold better than both **AD 795** and **AD 804**.

### Galectin-4*C* and Galectin-4*N*

Although the results were not outstanding for galectin-4*C*, two ligands, **AD 791** and **AD 784**, bound with a good degree of selectivity. Other ligands to perform well for this protein included **AD 776** which interestingly bound with 2-fold greater affinity than **AD 786**. A few of the derivatives unsubstituted at the 3-position performed better than their 3-benzylated analogues (**AD 791** vs **AD 795** and **AD 799** vs **AD 804**), a feature of binding similar to galectin-9*C*. Analysis of docking poses of the 3-benzylated derivatives **AD 795** and **AD 804** do not show any obvious favourable interactions with neighbouring residues, suggesting 3-position substituents are of no benefit for binding to galectin-4*C*.

**AD 791** in complex with galectin-4*C* shows the aromatic part of the ligand takes part in a few interactions. Arg240, which is H-bonded to the axial 4-OH and the endocyclic oxygen, is also H-bonded to the thioglycosidic link to the aglycon in the same manner discussed for **AD 795** with galectin-3. Arg240 is involved in a cation- $\pi$  interaction with the triazole ring. The fluorophenyl ring is also involved in a cation- $\pi$  interaction with Lys261 while the fluorine is H-bonded to the sidechain N-H of Gln292 (see Figure 60).

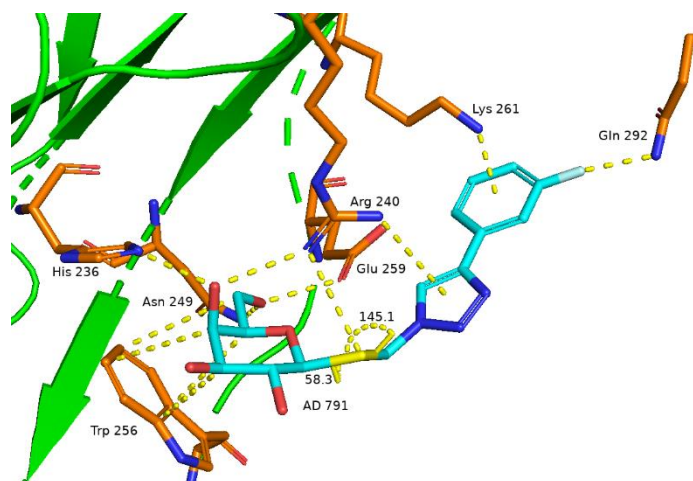


**Figure 60: Interactions of aromatic portions of AD 791 with neighbouring residues in CRD of Galectin-4C**

Results for galectin-4 $N$  were somewhat better, with some ligands binding selectively with high affinity. **AD 806** gave the best inhibition, while **AD 584**, **AD 433**, **AD 801**, **AD 804**, **EH 1306**, **EH1307**, and **EH 1314** all showed relatively good inhibition having bound poorly to all the other galectins. Both exo-syn (**AD 433** and **AD 774**) and exo-anti (**AD 584** and **AD 776**) cyclic constrained derivatives bound as well as the non-cyclic constrained **AD 801**, suggesting no outstanding conformational preference for galectin-4 $N$ . An advantage of the cyclic constraint is that it locks ligands into conformations which are not energetically favourable, ie Figure 54 (ii) overcoming energy penalties associated with these conformations and allowing their binding properties to be explored (Figure 62 (ii)). 3-benzyl substituents had mixed results, enhancing affinity for **AD 774** vs **AD 779**, **AD 776** vs **AD 786**, **AD 799** vs **AD 804**, **AD 801** vs **AD 806** and marginally for **AD 791** vs **AD 795**. Affinity was decreased for **AD 584** vs **AD 784**, **AD 433** vs **AD 782** and **AD 558** vs **AD 724**. As was the case with galectins -1, -8 $N$  and -4 $C$ , there was a preference for trifluorophenyl (**AD 774**) over monofluorophenyl (**AD 433**) over phenyl (**AD 558**) substituents. With the 3-benzyl substituted compounds, there was a slight contrast to this trend with the phenyl substituted **AD 724** giving marginally better inhibition than fluorophenyl **AD 782**. Although not selective for galectin-4 $N$ , the aryl trifluoromethyl substituent of **AD 736** appears to improve affinity relative to the ketone in **AD 741**, following the same trend as galectins -1, -8 $C$  and -8 $N$ .

**AD 806** in complex with galectin-4 $N$  binds via minimum E from Figure 55 (iii). Figure 61 shows the exocyclic aglyconic alcohol H-bonded to Arg67 and to the carbonyl of Glu87. The fluorophenyl ring points away from the protein into space, while the triazole is involved in cation- $\pi$  interactions with two arginine residues, Arg45 and Arg67. The 3-benzyl substituent is

involved in a  $\pi$ - $\pi$  stacking interaction with Phe47. With galectin-4N,  $\phi$  in **AD 806** adopts conformation (iii) from Figure 54.

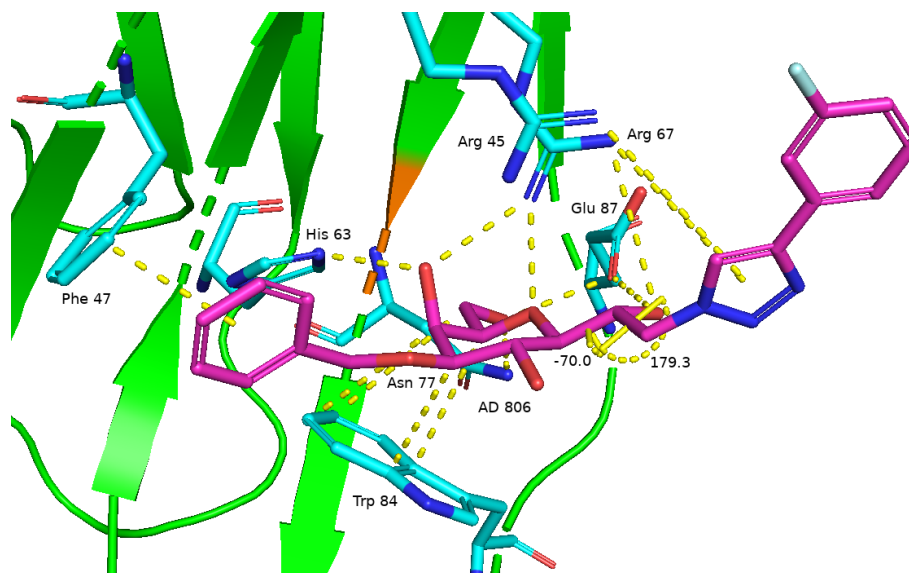


**Figure 61: AD 806 in complex with galectin-4N with  $\phi$  and  $\Psi$  angles shown**

**AD 433** has the same staggered conformation as **AD 806**, with a dihedral torsion angle of  $\sim -60^\circ$  for  $\phi$ , however **AD 433** is an *erythro* diastereomer compared to the *threo* isomer **AD 806**. The staggered conformation allows the same cation- $\pi$  interactions as those mentioned for **AD 806**, but in contrast to **AD 806**, the orientation of the fluorophenyl ring towards the protein allows a cation- $\pi$  interaction with Arg89 (Figure 62 (i)). The loss of a H-bond with Glu87 and the  $\pi$ - $\pi$  stacking with Phe47 may explain the 6-fold affinity loss of **AD 433** relative to **AD 806**. The cyclic constraint in **AD 776** forces the ligand to adopt conformation (ii) from Figure 54. Although sterically and electronically less energy favourable than **AD 433**, it orientates the triazole ring closer to Arg45 and Arg67 for cation- $\pi$  interactions.



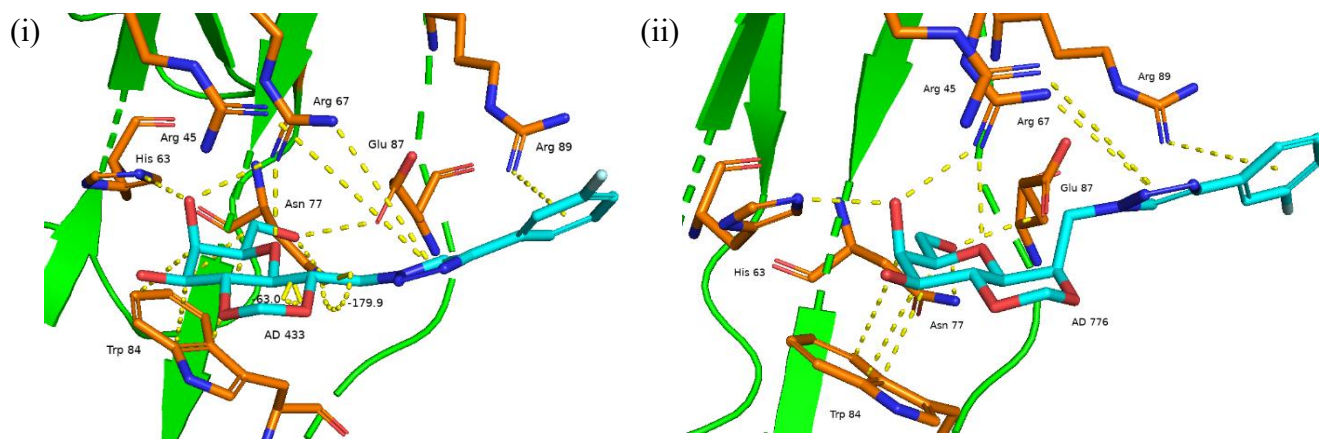


**Figure 62: (i) Staggered exo-syn conformer AD 433 with  $\Psi$  angle shown in complex with galectin-4N (ii) Exo-anti conformer AD 776 in complex with galectin-4N**

### Conclusions and Future Work

Most of the synthesised galectin inhibitors bound in the low millimolar to high micromolar range. Conformational constraint generally had a positive impact on binding, although in some cases, for example **EH 1265** vs **EH 1266** in complex with galectin-8N, the unconstrained derivative outperformed its constrained analogue due to the exocyclic OH participating in electrostatic interactions with neighbouring residues in the CRD. 3-position modifications were beneficial for binding to galectin-3, interacting with neighbouring residues via cation- $\pi$  and dipole-dipole interactions. For the spiroketal derivatives, the 6-membered ring performed better than their 5-membered analogues in most cases, with the docking study predicting a closer proximity of the axial anomeric oxygen to the indole nitrogen of the tryptophan residue at the  $\alpha$ -face of the sugar. Unconstrained derivatives, such as **AD 806** have a number of different possible conformations, as shown in the relaxed coordinate scan and in Figure 53 and Figure 61. The lack of constraint in this derivative means that the binding mode can be influenced by the amino acid residues present in the CRD. Future work on this project could employ a different heteroatom other than an oxygen in the spiroketal scaffold. Sulfur would be a suitable replacement for oxygen due to its relatively large size and less electronegative nature which could provide potential for sulfur- $\pi$  interactions with the  $\alpha$ -face tryptophan residue across the series of galectins.

## References

- (1) Guilbert, B.; Davis, N. J.; Pearce, M.; Aplin, R. T.; Flitsch, S. L. Dibutylstannylene Acetals: Useful Intermediates for the Regioselective Sulfation of Glycosides. *Tetrahedron: Asymmetry* **1994**, *5*, 2163–2178.
- (2) Ideo, H.; Seko, A.; Ishizuka, I.; Yamashita, K. The N-Terminal Carbohydrate Recognition Domain of Galectin-8 Recognizes Specific Glycosphingolipids with High Affinity. *Glycobiology* **2003**, *13*, 713–723.
- (3) van Hooff, P. A. V.; El Oualid, F.; Overkleeft, H. S.; van der Marel, G. A.; van Boom, J. H.; Leeuwenburgh, M. A. Synthesis and Elaboration of Functionalised Carbohydrate-Derived Spiroketal. *Org. Biomol. Chem.* **2004**, *2*, 1395–1403.
- (4) Lowary, T. L.; Hindsgaul, O. Recognition of Synthetic O-Methyl, Epimeric, and Amino Analogues of the Acceptor  $\alpha$ -L-Fucp-(1  $\rightarrow$  2)- $\beta$ -D-Galp-OR Glycosyltransferases. *Carbohydr. Res.* **1994**, *251*, 33–67.
- (5) Sörme, P.; Qian, Y.; Nyholm, P.; Leffler, H.; Nilsson, U. J. Low Micromolar Inhibitors of Galectin-3 Based on 3'-derivatization of N-acetyllactosamine. *ChemBioChem* **2002**, *3*, 183–189.
- (6) Goekjian, P. G.; Wu, T. C.; Kishi, Y. Preferred Conformation of C-Glycosides. 6. Conformational Similarity of Glycosides and Corresponding C-Glycosides. *J. Org. Chem.* **1991**, *56*, 6412–6422.
- (7) Cipolla, L.; Lay, L.; Nicotra, F. New and Easy Access to C-Glycosides of Glucosamine and Mannosamine. *J. Org. Chem.* **1997**, *62*, 6678–6681.
- (8) Mari, S.; Cañada, F. J.; Jiménez-Barbero, J.; Bernardi, A.; Marcou, G.; Motto, I.; Velter, I.; Nicotra, F.; La Ferla, B. Synthesis and Conformational Analysis of Galactose-Derived Bicyclic Scaffolds. *European J. Org. Chem.* **2006**, *2006*, 2925–2933.
- (9) Delaine, T.; Collins, P.; MacKinnon, A.; Sharma, G.; Stegmayr, J.; Rajput, V. K.; Mandal, S.; Cumpstey, I.; Larumbe, A.; Salameh, B. A. Galectin-3-binding Glycomimetics That Strongly Reduce Bleomycin-induced Lung Fibrosis and Modulate Intracellular Glycan Recognition. *ChemBioChem* **2016**, *17*, 1759–1770.
- (10) Peterson, K.; Kumar, R.; Stenström, O.; Verma, P.; Verma, P. R.; Håkansson, M.; Kahl-Knutsson, B.; Zetterberg, F.; Leffler, H.; Akke, M.; Logan, D. T.; Nilsson, U. J. Systematic Tuning of Fluoro-Galectin-3 Interactions Provides Thiodigalactoside Derivatives with Single-Digit nM Affinity and High Selectivity. *J. Med. Chem.* **2018**, *61*, 1164–1175.
- (11) Sörme, P.; Kahl-Knutsson, B.; Huflejt, M.; Nilsson, U. J.; Leffler, H. Fluorescence Polarization as an Analytical Tool to Evaluate Galectin–Ligand Interactions. *Anal. Biochem.* **2004**, *334*, 36–47.
- (12) Collins, P. M.; Öberg, C. T.; Leffler, H.; Nilsson, U. J.; Blanchard, H. Taloside Inhibitors of Galectin-1 and Galectin-3. *Chem. Biol. Drug Des.* **2012**, *79*, 339–346.
- (13) Yoshida, H.; Yamashita, S.; Teraoka, M.; Itoh, A.; Nakakita, S.; Nishi, N.; Kamitori, S. X-Ray Structure of a Protease-Resistant Mutant Form of Human Galectin-8 with Two Carbohydrate Recognition Domains. *FEBS J.* **2012**, *279*, 3937–3951.

- (14) Hassan, M.; Baussière, F.; Guzelj, S.; Sundin, A. P.; Håkansson, M.; Kovačič, R.; Leffler, H.; Tomašič, T.; Anderluh, M.; Jakopin, Ž.; Nilsson, U. J. Structure-Guided Design of d-Galactal Derivatives with High Affinity and Selectivity for the Galectin-8 N-Terminal Domain. *ACS Med. Chem. Lett.* **2021**, *12*, 1745–1752.
- (15) Yoshida, H.; Teraoka, M.; Nishi, N.; Nakakita, S.; Nakamura, T.; Hirashima, M.; Kamitori, S. X-Ray Structures of Human Galectin-9 C-Terminal Domain in Complexes with a Biantennary Oligosaccharide and Sialyllactose\*. *J. Biol. Chem.* **2010**, *285*, 36969–36976.
- (16) Nagae, M.; Nishi, N.; Nakamura-Tsuruta, S.; Hirabayashi, J.; Wakatsuki, S.; Kato, R. Structural Analysis of the Human Galectin-9 N-Terminal Carbohydrate Recognition Domain Reveals Unexpected Properties That Differ from the Mouse Orthologue. *J. Mol. Biol.* **2008**, *375*, 119–135.
- (17) Bum-Erdene, K.; Leffler, H.; Nilsson, U. J.; Blanchard, H. Structural Characterization of Human Galectin-4 C-Terminal Domain: Elucidating the Molecular Basis for Recognition of Glycosphingolipids, Sulfated Saccharides and Blood Group Antigens. *FEBS J.* **2015**, *282*, 3348–3367.
- (18) Bum-Erdene, K.; Leffler, H.; Nilsson, U. J.; Blanchard, H. Structural Characterisation of Human Galectin-4 N-Terminal Carbohydrate Recognition Domain in Complex with Glycerol, Lactose, 3'-Sulfo-Lactose and 2'-Fucosyllactose. *Sci. Rep.* **2016**, *6*, 20289.
- (19) Espinosa, J.-F.; Cañada, F. J.; Asensio, J. L.; Martín-Pastor, M.; Dietrich, H.; Martín-Lomas, M.; Schmidt, R. R.; Jiménez-Barbero, J. Experimental Evidence of Conformational Differences between C-Glycosides and O-Glycosides in Solution and in the Protein-Bound State: The C-Lactose/O-Lactose Case. *J. Am. Chem. Soc.* **1996**, *118*, 10862–10871.
- (20) Diehl, C.; Engström, O.; Delaine, T.; Håkansson, M.; Genheden, S.; Modig, K.; Leffler, H.; Ryde, U.; Nilsson, U. J.; Akke, M. Protein Flexibility and Conformational Entropy in Ligand Design Targeting the Carbohydrate Recognition Domain of Galectin-3. *J. Am. Chem. Soc.* **2010**, *132*, 14577–14589.
- (21) Peterson, K.; Collins, P. M.; Huang, X.; Kahl-Knutsson, B.; Essén, S.; Zetterberg, F. R.; Oredsson, S.; Leffler, H.; Blanchard, H.; Nilsson, U. J. Aromatic Heterocycle Galectin-1 Interactions for Selective Single-Digit NM Affinity Ligands. *RSC Adv.* **2018**, *8*, 24913–24922.
- (22) van Hattum, H.; Branderhorst, H. M.; Moret, E. E.; Nilsson, U. J.; Leffler, H.; Pieters, R. J. Tuning the Preference of Thiodigalactoside- and Lactosamine-Based Ligands to Galectin-3 over Galectin-1. *J. Med. Chem.* **2013**, *56*, 1350–1354.
- (23) Vrbata, D.; Filipová, M.; Tavares, M. R.; Červený, J.; Vlachová, M.; Šírová, M.; Pelantová, H.; Petrásková, L.; Bumba, L.; Konefał, R.; Etrych, T.; Křen, V.; Chytil, P.; Bojarová, P. Glycopolymers Decorated with 3-O-Substituted Thiodigalactosides as Potent Multivalent Inhibitors of Galectin-3. *J. Med. Chem.* **2022**, *65*, 3866–3878.
- (24) Zetterberg, F. R.; Peterson, K.; Johnsson, R. E.; Brimert, T.; Håkansson, M.; Logan, D. T.; Leffler, H.; Nilsson, U. J. Monosaccharide Derivatives with Low-nanomolar Lectin Affinity and High Selectivity Based on Combined Fluorine–Amide, Phenyl–Arginine, Sulfur– $\pi$ , and Halogen Bond Interactions. *ChemMedChem* **2018**, *13*, 133–137.
- (25) Zhou, P.; Tian, F.; Lv, F.; Shang, Z. Geometric Characteristics of Hydrogen Bonds

- Involving Sulfur Atoms in Proteins. *Proteins Struct. Funct. Bioinforma.* **2009**, *76*, 151–163.
- (26) Biswal, H. S.; Gloaguen, E.; Loquais, Y.; Tardivel, B.; Mons, M. Strength of NH $\cdots$ S Hydrogen Bonds in Methionine Residues Revealed by Gas-Phase IR/UV Spectroscopy. *J. Phys. Chem. Lett.* **2012**, *3*, 755–759.
- (27) Lu, T.; Zhang, J.; Xu, Y.; Wang, Z.; Feng, G.; Zeng, Z. Hydrogen Bond Interactions between Thioethers and Amides: A Joint Rotational Spectroscopic and Theoretical Study of the Formamide $\cdots$ dimethyl Sulfide Adduct. *Spectrochim. Acta Part A Mol. Biomol. Spectrosc.* **2023**, *288*, 122199.
- (28) Ideo, H.; Matsuzaka, T.; Nonaka, T.; Seko, A.; Yamashita, K. Galectin-8-N-Domain Recognition Mechanism for Sialylated and Sulfated Glycans. *J. Biol. Chem.* **2011**, *286*, 11346–11355.
- (29) Hudson, K. L.; Bartlett, G. J.; Diehl, R. C.; Agirre, J.; Gallagher, T.; Kiessling, L. L.; Woolfson, D. N. Carbohydrate–Aromatic Interactions in Proteins. *J. Am. Chem. Soc.* **2015**, *137*, 15152–15160.

**Chapter 4: Experimental Section**

|   |     |
|---|-----|
| <b>General Experimental Methods</b> ..... | 122 |
| <b>Materials and Reagents</b> .....       | 122 |
| <b>Instrumentation</b> .....              | 122 |
| <b>Molecular Docking</b> .....            | 123 |
| <b>Relaxed coordinate scans</b> .....     | 123 |
| <b>Chapter 2-Experimental</b> .....       | 125 |
| <b>Chapter 3-Experimental</b> .....       | 141 |
| <b>References</b> .....                   | 189 |

## General Experimental Methods

Reactions were performed under an inert atmosphere. Air and/or moisture sensitive liquids were transferred via cannula or plastic syringes fitted with stainless steel needles. Reactions were monitored by thin-layer chromatography (TLC) performed on aluminium sheets precoated with silica gel using the solvents indicated. Spots were visualized by UV light (254 nm) and charred with H<sub>2</sub>SO<sub>4</sub>-MeOH (1:20). During work-up, solutions in organic solvents were dried over Na<sub>2</sub>SO<sub>4</sub>. Removal of volatile organic solvents was carried out under reduced pressure on a Heidolph and/or Buchi rotary evaporator with the water bath temperature set between 40-50 °C. Chromatography was carried out with silica gel 60 (0.040-0.630 mm) using the solvent indicated via a stepwise solvent polarity gradient correlated with TLC mobility.

## Materials and Reagents

Unless otherwise noted, all commercially available reagents were used as obtained from suppliers without further purification. Chemicals were purchased from Sigma-Aldrich (Merck), Fisher-Scientific, Alfa-Aeser, Fluorochem, Carbosynth, or TCI. Solvents used in work up procedures and chromatography were either reagent or HPLC grade and were used without any further purification. Dichloromethane, methanol, toluene, acetonitrile, and tetrahydrofuran were obtained from commercial sources and dried using a Grubbs-Type (Puresolv) dry solvent purification system before performing reactions. Deuterated solvents CDCl<sub>3</sub>, CD<sub>3</sub>OD, Acetone-d<sub>6</sub> were obtained from suppliers and used without purification.

## Instrumentation

Proton nuclear magnetic resonance (<sup>1</sup>H-NMR) spectra and proton-decoupled carbon nuclear magnetic resonance (<sup>13</sup>C-NMR) spectra were recorded at 25 °C with 400 and 500 MHz Joel spectrometers. Data are reported in the following order: Chemical shift (δ) in ppm relative to internal standard Me<sub>4</sub>Si in CDCl<sub>3</sub> (δ 0.0) for <sup>1</sup>H and CDCl<sub>3</sub> (δ 77.0) or CD<sub>3</sub>OD (δ 47.59) for <sup>13</sup>C; multiplicities indicated as b (broad), s (singlet), d (doublet), t (triplet), q (quartet), p (pentet), hept (heptet), m (multiplet); Coupling constants (*J*) are given in Hertz (Hz). <sup>1</sup>H-NMR spectral signals were assigned with the aid of COSY, <sup>13</sup>C-NMR spectral signals using DEPT, gHSQCAD and/or gHMBCAD. Assignments of sugar protons are reported in a clockwise fashion from H-1 to H-6a/b, with H-1 as the anomeric proton and H-6a & H-6b as the two exocyclic methylene protons. Carbon assignments follow the same numbering pattern. H-1'

refers to protons  $\alpha$  to the anomeric carbon in the aglycon moiety, H-2' refers to protons  $\beta$  to the anomeric carbon. NMR data for known compounds was in good agreement with previously published data. High resolution mass spectra were measured in positive and/or negative mode as indicated using an Agilent Accurate Mass Q-TOF LC/MS Mass Spectrometry instrument using MeCN (acetonitrile) or MeOH as solvent. All HRMS data reported is within 5 ppm of the calculated mass. Known compounds are cited in references 10-19 in this section.

### Molecular Docking

Atomic coordinates for X-ray crystal structures for all the galectins used in docking were obtained from the Protein Data Bank ([www.rcsb.org](http://www.rcsb.org)). The codes for the PDB files used were 3T2T<sup>1</sup> (galectin-1 with methyl 2-*O*-acetyl-3-*O*-toluoyl- $\beta$ -D-talopyranoside), 3T1L<sup>1</sup> (galectin-3 with methyl 2-*O*-acetyl-3-*O*-toluoyl- $\beta$ -D-talopyranoside), 3VKM<sup>2</sup> (galectin-8 with sialyllactose and lactose), 7P1M<sup>3</sup> (galectin-8N with benzimidazole-D-galactal), 3NV2<sup>4</sup> (galectin-9C with LacNAc), 2EAK<sup>5</sup> (galectin-9N with lactose), 4YM3<sup>6</sup> (galectin-4C with lactose), 5DUV<sup>7</sup> (galectin-4N with lactose). The program Maestro (Version 2019.12.2, Schrödinger Release 2019-4, LLC, New York, NY, 2019) was used as the interface for performing of local docking experiments. In this procedure proteins were first prepared, after download, by adding missing sidechains using Prime, ligands in the co-crystal structure were stripped and hydrogens added as required and this was followed by optimization and minimization using the OPLS3e forcefield, necessary to correct the covalent geometry. Ligands for docking were built in Maestro based on lactose in the 5DUV PDB file, followed by minimization with OPLS3e using the LigPrep script. A receptor grid with 0.375 Å grid-spacing was constructed. Ligands and protein side chains within 15 Å were subjected to glide standard precision flexible docking with Maestro, employing positional constraints to the galactose C-1 and axial 4-OH to instigate conserved galactose binding. Docking runs were performed using Glide, with 400 runs per molecule from initial populations of 5000. The local search parameter was optimized to 100 steps, and all other parameters were kept at default. Docking results were clustered at a root-mean-squared deviation (RMSD) of <0.5 Å.<sup>8,9</sup>

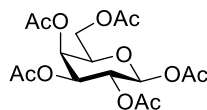
### Relaxed coordinate scans

Conformational analysis studies on unbound ligands were performed using the coordinate scan function from MacroModel. The OPLS3e forcefield was employed and water chosen as the solvent.  $\Phi$  and  $\Psi$  dihedral angles were defined as mentioned in figures 52 (i) and (ii) and

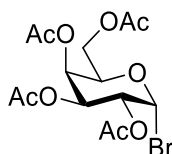
relative energy values calculated at increments of  $10^\circ$  for each dihedral. Coordinate scan plots were generated from relative energy results ( $\text{kcal mol}^{-1}$ ) using MacroModel. Images shown were generated using PyMol (Version 2.5.4, Schrödinger, LLC, New York, NY).



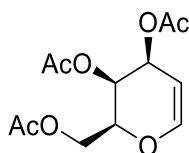
## Chapter 2-Experimental

**1,2,3,4,6-Penta-O-acetyl- $\beta$ -D-galactopyranose (EH 1197)**

Galactose (15.00 g, 83.26 mmol) was dissolved in acetic anhydride (100 mL) and heated to reflux. NaOAc (6.86 g, 83.6 mmol) was added portion wise to the reaction mixture, which was then allowed to heat under reflux for 3 h. The reaction was poured onto ice and stirred for 15 mins. The mixture was filtered and the solid collected. This solid was recrystallized from MeOH to give a white solid as the title compound (28.6 g, 88%). NMR data obtained was in good agreement with the literature.<sup>10</sup> HRMS calcd. for  $C_{16}H_{22}O_{11}Na [M+Na]^+$  413.1054, found  $m/z$  413.1054.

**2,3,4,6-Tetra-O-acetyl- $\alpha$ -D-galactopyranosyl bromide (EH 1195)<sup>11</sup>**

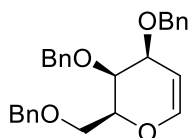
**EH 1197** (12.6 g, 32.3 mmol) was dissolved in anhydrous  $CH_2Cl_2$  (21 mL) and cooled to 0 °C. HBr (33% in AcOH, 12 mL) was added and the reaction mixture was allowed to for 2 h. The reaction was poured onto an ice-water mixture and stirred for 15 mins. The mixture was diluted with  $CH_2Cl_2$  and separated. The organic layer was washed with satd. Aq.  $NaHCO_3$  and brine, dried over  $Na_2SO_4$ , filtered and the solvent was removed under reduced pressure to give a viscous oil as the title compound (11.7 g, 88%). <sup>1</sup>H-NMR (500 MHz,  $CDCl_3$ )  $\delta$  6.69 (d,  $J$  = 4.0 Hz, 1H, H-1), 5.51 (dd,  $J$  = 3.3, 1.4 Hz, 1H, H-4), 5.40 (dd,  $J$  = 10.7, 3.4 Hz, 1H, H-3), 5.04 (dd,  $J$  = 10.6, 4.0 Hz, 1H, H-2), 4.48 (t,  $J$  = 6.7 Hz, 1H, H-5), 4.18 (dd,  $J$  = 11.4, 6.3 Hz, 1H, H-6a), 4.10 (dd,  $J$  = 11.3, 6.8 Hz, 1H, H-6b), 2.14 (s, 3H), 2.10 (s, 3H), 2.05 (s, 3H), 2.00 (s, 3H) (each OAc); <sup>13</sup>C-NMR (126 MHz,  $CDCl_3$ )  $\delta$  170.5, 170.2, 170.0 169.9 (each C=O), 88.2 (C-1), 71.2 (C-5), 68.1 (C-3), 67.9 (C-4), 67.1 (C-2), 60.9 (C-6), 20.9, 20.8, 20.7, 20.7 (each OAc).



### 3,4,6-Tri-*O*-acetyl-D-galactal (EH 11)

**EH 195** (11.7 g, 28.4 mmol) was dissolved in acetonitrile (150 mL). Zinc (11.14 g, 170.4 mmol) and  $\text{NH}_4\text{Cl}$  (9.12 g, 170.4 mmol) were added and the reaction mixture was stirred at 80 °C for 4 h. The reaction mixture was then filtered, extracted with EtOAc and the solvent was removed under reduced pressure. Chromatography (cyclohexane-EtOAc 3:2) gave the product as a white solid (5.34 g, 69%).  $R_f$  0.42 (cyclohexane-EtOAc: 4:1);  $^1\text{H-NMR}$  (500 MHz,  $\text{CDCl}_3$ )  $\delta$  6.46 (dd,  $J = 6.3, 1.8$  Hz, 1H, H-1), 5.56 (ddt,  $J = 4.4, 2.8, 1.8$  Hz, 1H, H-4), 5.43 (dt,  $J = 4.7, 1.9$  Hz, 1H, H-3), 4.73 (ddd,  $J = 6.3, 2.7, 1.5$  Hz, 1H, H-2), 4.32 (tt,  $J = 6.1, 1.5$  Hz, 1H, H-5), 4.27 (dd,  $J = 11.4, 7.3$  Hz, 1H, H-6a), 4.22 (dd,  $J = 11.4, 5.3$  Hz, 1H, H-6b), 2.13 (s, 3H), 2.09 (s, 3H), 2.03 (s, 3H) (each OAc);  $^{13}\text{C-NMR}$  (126 MHz,  $\text{CDCl}_3$ )  $\delta$  170.6, 170.3, 170.1 (each C=O), 145.4 (C-1), 98.8 (C-2), 72.8 (C-5), 63.9 (C-4), 63.8 (C-3), 61.9 (C-6), 20.8, 20.8, 20.6 (each OAc); HRMS calcd. for  $\text{C}_{12}\text{H}_{20}\text{NO}_7$  [ $\text{M}+\text{NH}_4$ ] $^+$  290.1240, found  $m/z$  290.1217.

NMR data obtained was in good agreement with the literature.<sup>12</sup>

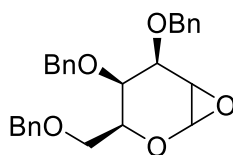


### 3,4,6-Tri-*O*-benzyl-D-galactal (EH 12)

**EH 11** (4.76 g, 17.5 mmol) was dissolved in dry MeOH (100 mL). NaOMe was added (330 mg, 6.12 mmol) and the reaction mixture was allowed to stir for 15 mins, after which time, TLC analysis indicated disappearance of the starting material. Amberlite ( $\text{H}^+$ ) was added to neutralise the reaction mixture, which was concentrated to give free galactal. The crude galactal (2.00 g, 13.7 mmol) was dissolved in DMF and cooled to 0 °C. NaH (2.18 g, 54.5 mmol) was added slowly, causing liberation of  $\text{H}_2$  and fizzing. The reaction was stirred for 10 mins followed by addition of BnBr (6.47 mL, 54.5 mmol). The reaction was allowed to attain room temperature and stirred overnight and was eventually quenched with MeOH following indication of product formation via TLC. The reaction mixture was extracted with EtOAc and the combined organic layers were washed with water, dried with  $\text{Na}_2\text{SO}_4$  and the solvent was

removed under reduced pressure. Chromatography (cyclohexane-EtOAc 4:1) afforded the product as a white solid (4.85 g, 85%).  $R_f$  0.51 (cyclohexane-EtOAc 4:1);  $^1\text{H-NMR}$  (500 MHz,  $\text{CDCl}_3$ )  $\delta$  7.44 – 7.16 (overlapping signals, 16H, each Ar-H), 6.37 (dd,  $J = 6.3, 1.5$  Hz, 1H, H-1), 4.88 (d,  $J = 12.0$  Hz, 1H, Bn- $\text{CH}_2$ ), 4.86 (ddd,  $J = 6.3, 2.9, 1.3$  Hz, 1H, H-2), 4.66 (d,  $J = 12.2$  Hz, 1H), 4.65 (d,  $J = 12.0$  Hz, 1H), 4.62 (d,  $J = 12.2$  Hz, 1H), 4.51 (d,  $J = 11.9$  Hz, 1H), 4.43 (d,  $J = 11.9$  Hz, 1H) (each Bn- $\text{CH}_2$ ), 4.23 – 4.16 (overlapping signals, 2H, H-3 & H-5), 3.95 (bt,  $J = 4.1$  Hz, 1H, H-4), 3.79 (dd,  $J = 10.3, 7.2$  Hz, 1H, H-6a), 3.66 (dd,  $J = 10.3, 5.1$  Hz, 1H, H-6b);  $^{13}\text{C-NMR}$  (126 MHz,  $\text{CDCl}_3$ )  $\delta$  144.2 (C-1), 138.5, 138.4, 138.0, 128.4, 128.3, 128.1, 127.9, 127.7, 127.6, 127.4 (each Ar-C/ C-H) 100.0 (C-2), 75.7 (C-5), 73.4 ( $\text{CH}_2$ ), 73.3 ( $\text{CH}_2$ ), 71.3 (C-4), 70.9 (C-3), 70.7 ( $\text{CH}_2$ ), 68.4 (C-6); HRMS calcd. for  $\text{C}_{27}\text{H}_{32}\text{NO}_4$  [ $\text{M}+\text{NH}_4$ ] $^+$  434.2331, found  $m/z$  434.2323.

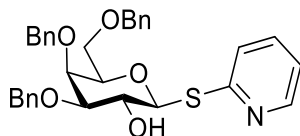
NMR data obtained was in good agreement with the literature.<sup>13</sup>



### 1,2-Anhydro-3,4,6-tri-*O*-benzyl-*D*-galactopyranose (EH 19)

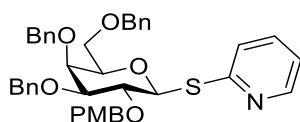
**EH 12** (500 mg, 1.2 mmol) was dissolved in  $\text{CH}_2\text{Cl}_2$  and cooled to 0 °C, followed by slow addition of a solution of dimethyldioxirane (20 mL of a 0.08 M solution, 1.6 mmol). The reaction mixture was stirred for 20 mins, after which TLC analysis indicated complete consumption of the starting material. The reaction mixture was extracted with  $\text{CH}_2\text{Cl}_2$  and the combined organic layers were dried with  $\text{Na}_2\text{SO}_4$ , filtered and the solvent was removed by rotary evaporation at 26 °C. The crude product (430 mg, 83%) was dried under vacuum for 1 h and used without any further purification.  $^1\text{H-NMR}$  (500 MHz,  $\text{CDCl}_3$ )  $\delta$  7.44 – 7.28 (15H, overlapping signals, each Ar-H), 6.39 (1H, d,  $J=2.0$  Hz, H-1), 5.01 (1H, d,  $J=10.8$  Hz, Bn- $\text{CH}_2$ ), 4.84 (1H, d,  $J=11.9$  Hz, Bn- $\text{CH}_2$ ), 4.65 (1H, d,  $J=11.9$  Hz, Bn- $\text{CH}_2$ ), 4.60 (1H, d,  $J=10.8$  Hz, Bn- $\text{CH}_2$ ), 4.47 (1H, d,  $J=11.7$  Hz, Bn- $\text{CH}_2$ ), 4.42 (1H, d,  $J=11.4$  Hz, Bn- $\text{CH}_2$ ), 4.15 – 4.00 (3H, overlapping signals, H-2, H-3, H-4), 3.82 (1H, t,  $J=3.0$  Hz, H-5), 3.71 (1H, t,  $J=8.6$  Hz, H-6a), 3.58 (1H, dd,  $J=8.9, 5.2$  Hz, H-6b);  $^{13}\text{C-NMR}$  (126 MHz,  $\text{CDCl}_3$ )  $\delta$  163.0, 137.6, 137.5, 137.4, 134.7, 133.6, 131.2, 129.8, 129.6, 128.6, 128.5, 128.5, 128.3, 128.1, 128.1, 128.0, 128.0, 127.9 (each Ar-C/ CH), 95.8 (C-1), 75.8 (Bn- $\text{CH}_2$ ), 75.4 (C-4), 73.7 (Bn- $\text{CH}_2$ ), 72.2 (C-3), 72.1

(C-5), 69.6 (Bn-CH<sub>2</sub>), 68.0 (C-2), 67.6 (C-6); HRMS calcd. for C<sub>27</sub>H<sub>28</sub>O<sub>5</sub>Na [M+Na]<sup>+</sup> 455.1834 found m/z 455.1815.



### 3,4,6-Tri-*O*-benzyl- $\beta$ -thiopyridine-D-galactopyranose (EH 112)

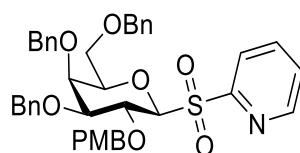
2-mercaptopyridine (58.8 mg, 0.53 mmol) was dissolved in dry THF and NaH (21.1 mg, 0.53 mmol) was added to it. The reaction was stirred at 0 °C for 15 min. A solution of **EH 12** (100 mg, 0.23 mmol) dissolved in THF was added slowly via cannula to the reaction mixture, which was then stirred for 2 h at 0 °C. The reaction was quenched by the addition of 1 M HCl solution. The reaction mixture was extracted with CH<sub>2</sub>Cl<sub>2</sub> and the combined organic layers were washed with 1 M HCl, water, dried with Na<sub>2</sub>SO<sub>4</sub> and the solvent was removed under reduced pressure. Chromatography (cyclohexane-EtOAc 4:1 → 1:1) afforded the product (98 mg, 78%) as a white solid; R<sub>f</sub> 0.71 (cyclohexane-EtOAc 1:1); <sup>1</sup>H-NMR (500 MHz, CDCl<sub>3</sub>)  $\delta$  8.42 (d, *J* = 4.5 Hz, 1H), 7.47 – 7.22 (m, 17H), 7.04 (td, *J* = 5.7, 1.6 Hz, 1H) (each Ar-H), 5.22 (d, *J* = 9.8 Hz, 1H, H-1), 4.94 (d, *J* = 11.4 Hz, 1H), 4.81 (d, *J* = 12.7 Hz, 1H), 4.78 (d, *J* = 12.7 Hz, 1H), 4.62 (d, *J* = 11.4 Hz, 1H), 4.49 (d, *J* = 11.8 Hz, 1H), 4.43 (d, *J* = 11.7 Hz, 1H) (each Bn-CH<sub>2</sub>), 4.20 (t, *J* = 9.5 Hz, 1H, H-2), 4.02 (d, *J* = 2.8 Hz, 1H, H-4), 3.76 (t, *J* = 6.5 Hz, 1H, H-5), 3.63 (d, *J* = 6.4 Hz, 2H, H-6a & H-6b), 3.58 (dd, *J* = 9.3, 2.8 Hz, 1H, H-3); <sup>13</sup>C-NMR (126 MHz, CDCl<sub>3</sub>)  $\delta$  156.6, 149.4, 138.6, 138.3, 137.8, 136.7, 128.5, 128.4, 128.2, 128.1, 128.0, 127.8, 127.7, 127.7, 127.6, 124.4, 120.8 (each Ar-C/ C-H), 85.4 (C-1), 83.6 (C-3), 78.0 (H-5), 74.6 (Bn-CH<sub>2</sub>), 73.6 (C-4), 73.5, 72.7 (each Bn-CH<sub>2</sub>), 70.3 (C-2), 68.6 (C-6). HRMS calcd. for C<sub>32</sub>H<sub>33</sub>NO<sub>5</sub>NaS [M+Na]<sup>+</sup> 566.1977 found m/z 566.1959.



### 2-*para*-Methoxybenzyl-3,4,6-tri-*O*-benzyl- $\beta$ -thiopyridine-D-galactopyranose (EH 116)

**EH 112** (250 mg, 0.46 mmol) was dissolved in DMF and cooled to 0 °C. NaH (55.2 mg, 1.38 mmol) was added slowly, causing liberation of H<sub>2</sub> and fizzing. The reaction was stirred for 10

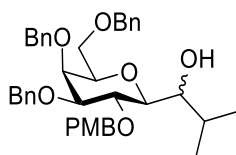
mins followed by addition of PMBCl (0.19 mL, 1.38 mmol). The reaction was allowed to warm to room temperature overnight and was eventually quenched with MeOH following indication of product formation via TLC. The reaction mixture was extracted with EtOAc and the combined organic layers were washed with water, dried with Na<sub>2</sub>SO<sub>4</sub> and the solvent was removed under reduced pressure. Chromatography (cyclohexane-EtOAc 4:1) afforded the product (228 mg, 75%) as a white solid.; R<sub>f</sub> 0.83 (cyclohexane-EtOAc 1:1); <sup>1</sup>H-NMR (500 MHz, CDCl<sub>3</sub>) δ 8.42 (dd, *J* = 5.0, 1.9 Hz, 1H), 7.47 – 7.21 (m, 19H), 6.99 (bt, *J* = 6.1 Hz, 1H), 6.80 (d, *J* = 8.6 Hz, 2H) (each Ar-H), 5.31 (d, *J* = 9.9 Hz, 1H, H-1), 5.00 (d, *J* = 11.4 Hz, 1H), 4.79 (d, *J* = 9.6 Hz, 3H), 4.73 (d, *J* = 9.9 Hz, 1H), 4.64 (d, *J* = 11.4 Hz, 1H), 4.48 (d, *J* = 11.7 Hz, 1H), 4.42 (d, *J* = 11.4 Hz, 1H) (each Bn-CH<sub>2</sub>), 4.06 (t, *J* = 9.5 Hz, 1H, H-2), 4.04 (d, *J* = 2.6 Hz, 1H, H-4), 3.78 (s, 3H, OCH<sub>3</sub>), 3.74 (t, *J* = 6.6 Hz, 1H, H-5), 3.69 (dd, *J* = 9.2, 2.7 Hz, 1H, H-3), 3.65 (d, *J* = 6.4 Hz, 2H, H-6a & H-6b); <sup>13</sup>C-NMR (126 MHz, CDCl<sub>3</sub>) δ 159.2, 157.8, 149.5, 138.7, 138.4, 137.9, 136.4, 130.3, 130.1, 128.4, 128.4, 128.2, 128.1, 127.9, 127.8, 127.7, 127.6, 127.5, 123.3, 120.2, 113.7 (each Ar-C/ C-H), 84.2 (C-1), 77.5 (C-5), 77.0 (C-2), 75.4 (Bn-CH<sub>2</sub>), 74.6 (Bn-CH<sub>2</sub>), 73.8 (C-4), 73.5 (Bn-CH<sub>2</sub>), 72.8 (Bn-CH<sub>2</sub>), 68.7 (C-6), 55.3 (OCH<sub>3</sub>); HRMS calcd. for C<sub>40</sub>H<sub>41</sub>NO<sub>6</sub>NaS [M+Na]<sup>+</sup> 686.2552 found *m/z* 686.2539.



**2-*para*-Methoxybenzyl-3,4,6-tri-*O*-benzyl-β-sulfonylpyridine-D-galactopyranose (EH 117)**

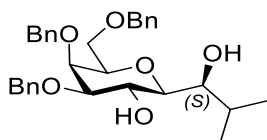
**EH 116** (280 mg, 0.42 mmol) was dissolved in dry CH<sub>2</sub>Cl<sub>2</sub> and cooled to 0 °C. NaHCO<sub>3</sub> (213 mg, 2.53 mmol) was added, followed by slow addition of mCPBA (182 mg, 1.05 mmol) over 30 min. The reaction mixture was left to stir for 2 h at 0 °C. The reaction was quenched with H<sub>2</sub>O following indication of product formation via TLC. The reaction mixture was subsequently washed with brine, dried over MgSO<sub>4</sub> and the solvent was removed under reduced pressure. Chromatography (cyclohexane-EtOAc 6:1) afforded the product (252 mg, 86%) as a white solid.; R<sub>f</sub> 0.37 (cyclohexane-EtOAc 3:2); <sup>1</sup>H-NMR (500 MHz, CDCl<sub>3</sub>) δ 8.62 (ddd, *J* = 4.8, 1.8, 0.9 Hz, 1H), 8.02 (bd, *J* = 7.8 Hz, 1H), 7.73 (td, *J* = 7.8, 1.7 Hz, 1H), 7.38 – 7.11 (m, 19H), 6.81 (d, *J* = 8.7 Hz, 2H) (each Ar-H), 4.98 (d, *J* = 9.6 Hz, 1H), 4.91 (d, *J* = 10.3 Hz, 1H) (each Bn-CH<sub>2</sub>), 4.89 (d, *J* = 8.4 Hz, 1H, H-1), 4.82 (d, *J* = 9.7 Hz, 1H, Bn-CH<sub>2</sub>), 4.72

(s, 2H, each Bn-CH<sub>2</sub>), 4.55 (d,  $J = 7.9$  Hz, 1H, H-2), 4.53 (d,  $J = 9.9$  Hz, 2H), 4.23 (s, 2H) (each Bn-CH<sub>2</sub>), 3.87 (d,  $J = 2.6$  Hz, 1H, H-4), 3.79 (s, 3H, OCH<sub>3</sub>), 3.66 (dd,  $J = 9.4, 2.7$  Hz, 1H, H-3), 3.58 (t,  $J = 6.3$  Hz, 1H, H-5), 3.42 (dd,  $J = 9.7, 6.7$  Hz, 1H, H-6a), 3.37 (dd,  $J = 9.7, 5.8$  Hz, 1H, H-6b); <sup>13</sup>C-NMR (126 MHz, CDCl<sub>3</sub>)  $\delta$  159.2, 156.1, 149.9, 138.4, 138.0, 137.7, 137.3, 130.3, 130.0, 129.8, 128.5, 128.4, 128.2, 127.9, 127.5, 127.0, 123.9, 113.6 (each Ar-C/C-H), 89.5 (C-1), 83.9 (C-3), 78.2 (C-5), 74.9 (Bn-CH<sub>2</sub>), 74.4 (Bn-CH<sub>2</sub>), 73.9 (C-2), 73.4 (Bn-CH<sub>2</sub>), 73.1 (C-4), 72.9 (Bn-CH<sub>2</sub>), 68.4 (C-6), 55.3 (OCH<sub>3</sub>); HRMS calcd. for C<sub>40</sub>H<sub>41</sub>NO<sub>8</sub>NaS [M+Na]<sup>+</sup> 718.2451 found m/z 718.2433.



**1-((2*S*,3*R*,4*S*,5*S*,6*R*)-4,5-bis(benzyloxy)-6-((benzyloxy)methyl)-3-((*para*-Methoxybenzyl)oxy)tetrahydro-2*H*-pyran-2-yl)-2-methylpropan-1-ol (EH 122)**

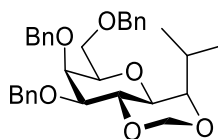
**EH 117** (150 mg, 0.22 mmol) and isobutyraldehyde (0.08 mL, 0.86 mmol) were added to a flame dried flask under N<sub>2</sub> atmosphere. A SmI<sub>2</sub> solution (0.1 M in THF, 15.1 mL, 1.51 mmol) was added to the flask via cannula. The reaction mixture was stirred for 15 mins at room temperature. A colour change of dark blue to yellow was observed during the reaction. A 10:1 mixture of satd. potassium sodium tartrate and satd. NaHCO<sub>3</sub> was added and the mixture was extracted with EtOAc. The combined organic phases were washed with brine, dried over MgSO<sub>4</sub>, and the solvent was removed under reduced pressure. Chromatography (cyclohexane-EtOAc 8:1) afforded the product as a mixture of inseparable stereoisomers (5:2, calculated from relative integrals of <sup>1</sup>H-NMR signals ( $\delta$  3.97 (d,  $J = 2.7$  Hz, 1H, H-4 major), 3.94 (d,  $J = 2.9$  Hz, 0.4H, H-4 minor)) (41.3 mg, 31%).; HRMS calcd. for C<sub>41</sub>H<sub>52</sub>O<sub>7</sub>Na [M+Na]<sup>+</sup> 541.2595 found m/z 541.2566.



**(2*S*,3*R*,4*R*,5*S*,6*R*)-4,5-Bis(benzyloxy)-6-((benzyloxy)methyl)-2-((*R*)-1-hydroxy-2-methylpropyl)tetrahydro-2*H*-pyran-3-ol (EH 124)**

**EH 122** (110 mg, 0.17 mmol) was dissolved in CH<sub>2</sub>Cl<sub>2</sub> and cooled to 0 °C. DDQ (51.8 mg, 0.23 mmol) was added and the mixture was allowed to stir for 2 hrs, after which time TLC

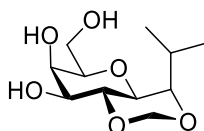
analysis indicated complete consumption of the starting material. The reaction was then quenched with NaHCO<sub>3</sub> solution, washed with brine, dried over MgSO<sub>4</sub> and the solvent removed under reduced pressure. Column chromatography (cyclohexane-EtOAc 3:2) afforded the product (72 mg, 81%) as a white solid.; R<sub>f</sub> 0.55 (cyclohexane-EtOAc 3:2); <sup>1</sup>H-NMR (500 MHz, CDCl<sub>3</sub>) δ 7.43 – 7.21 (overlapping signals, 15H, each Ar-H), 4.88 (d, *J* = 11.5 Hz, 1H), 4.76 (d, *J* = 11.8 Hz, 1H), 4.57 (d, *J* = 12.2 Hz, 1H), 4.55 (d, *J* = 12.6 Hz, 1H), 4.50 (d, *J* = 11.7 Hz, 1H), 4.46 (d, *J* = 11.7 Hz, 1H) (each Bn-CH<sub>2</sub>), 4.22 (t, *J* = 9.4 Hz, 1H, H-1), 4.01 (d, *J* = 2.8 Hz, 1H, H-4), 3.67 – 3.54 (overlapping signals, 3H, H-5, H-6a & H-6b), 3.47 – 3.41 (overlapping signals, 2H, H-3 & H-1'), 3.31 (bd, *J* = 9.4 Hz, 1H, H-2), 1.86 (h, *J* = 7.1 Hz, 1H, isopropyl CH), 1.02 (d, *J* = 6.7 Hz, 3H), 0.89 (d, *J* = 6.8 Hz, 3H) (each CH<sub>3</sub>); <sup>13</sup>C-NMR (126 MHz, CDCl<sub>3</sub>) δ 138.6, 137.9, 137.9, 128.6, 128.4, 128.2, 127.9, 127.9, 127.9, 127.8, 127.7, 127.6 (each Ar-C/ C-H), 84.4 (C-1'), 79.0 (C-2), 77.2 (C-5), 74.5 (C-3), 74.4 (Bn-CH<sub>2</sub>), 73.6 (Bn-CH<sub>2</sub>), 72.8 (C-4), 71.8 (Bn-CH<sub>2</sub>), 68.9 (C-6), 66.7 (C-1), 31.2 (C-2'), 19.3, 19.2 (each CH<sub>3</sub>).; HRMS calcd. for C<sub>31</sub>H<sub>38</sub>O<sub>6</sub>Na [M+Na]<sup>+</sup> 529.2566 found m/z 529.2571.



**(4*S*,4*aS*,6*R*,7*S*,8*S*,8*aR*)-7,8-Bis(benzyloxy)-6-((benzyloxy)methyl)-4-isopropylhexahydropyrano[3,2-*d*][1,3]dioxine (EH 131)**

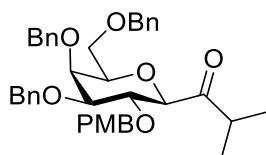
**EH 124** (180 mg, 0.35 mmol) was dissolved in dimethoxymethane (4.00 mL, 45.6 mmol), camphorsulfonic acid (165 mg, 0.71 mmol) was added and the reaction was allowed reflux overnight while stirring vigorously. After 18 hrs, TLC analysis indicated product formation. The solvent was removed under reduced pressure. Flash chromatography (cyclohexane-EtOAc 6:1) provided the product (110 mg, 60%) as a colourless oil.; R<sub>f</sub> 0.88 (cyclohexane-EtOAc 3:2); <sup>1</sup>H-NMR (500 MHz, CDCl<sub>3</sub>) δ 7.46 – 7.22 (overlapping signals, 15H, each Ar-H), 4.96 (d, *J* = 11.8 Hz, 1H), 4.89 – 4.79 (overlapping signals, 3H), 4.71 (d, *J* = 12.2 Hz, 1H), 4.59 (d, *J* = 11.7 Hz, 1H) (each Bn-CH<sub>2</sub>), 4.45 (s, 2H, acetal CH<sub>2</sub>), 4.21 (t, *J* = 9.2 Hz, 1H, H-2), 3.92 (d, *J* = 3.0 Hz, 1H, H-4), 3.69 (overlapping signals, 2H, H-1 & H-1'), 3.63 – 3.48 (overlapping signals, 4H, H-3, H-5, H-6a & H-6b), 2.42 (doublet of heptets, *J* = 6.6, 2.5 Hz, 1H, isopropyl CH), 1.03 (d, *J* = 6.4 Hz, 3H), 0.98 (d, *J* = 6.5 Hz, 3H) (each CH<sub>3</sub>); <sup>13</sup>C-NMR (126 MHz, CDCl<sub>3</sub>) δ 139.0, 138.5, 138.0, 128.5, 128.4, 128.4, 128.2, 128.1, 127.8, 127.8, 127.7, 127.7,

127.6, 127.5, 127.4 (each Ar-C/ C-H), 87.9 (Bn-CH<sub>2</sub>), 81.2 (C-3), 78.8 (C-1'), 78.0 (C-5), 76.3 (C-1), 75.1 (C-4), 74.6 (Bn-CH<sub>2</sub>), 73.5 (methylene CH<sub>2</sub>), 73.4 (C-2), 72.8 (Bn-CH<sub>2</sub>), 69.1 (C-6), 25.0 (C-2'), 20.6, 19.7 (each CH<sub>3</sub>).; HRMS calcd. for C<sub>32</sub>H<sub>38</sub>O<sub>6</sub>Na [M+Na]<sup>+</sup> 541.2566 found m/z 541.2595.



**(4*S*,4*aS*,6*R*,7*R*,8*S*,8*aR*)-6-(Hydroxymethyl)-4-isopropylhexahydropyrano[3,2-*d*][1,3]dioxine-7,8-diol (EH 145)**

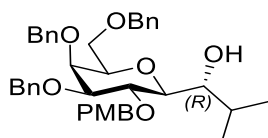
**EH 131** (30 mg, 0.06 mmol) was dissolved in EtOAc:MeOH (1:1) and Pd/C (10%) was added to the reaction mixture. The flask was fitted with a H<sub>2</sub> balloon and left to stir overnight. TLC analysis indicated complete consumption of the starting material. The reaction mixture was then filtered through celite and the solvent removed under reduced pressure. Flash chromatography (CH<sub>2</sub>Cl<sub>2</sub>-MeOH 9:1) provided the product (14 mg, 91%) as a white solid.; R<sub>f</sub> 0.4 (CH<sub>2</sub>Cl<sub>2</sub>-MeOH 9:1); <sup>1</sup>H-NMR (500 MHz, CD<sub>3</sub>OD) δ 4.82 (d, *J* = 6.5 Hz, 1H), 4.74 (d, *J* = 6.4 Hz, 1H) (each methylene CH<sub>2</sub>), 3.91 (dd, *J* = 3.5, 1.3 Hz, 1H, H-4), 3.86 (t, *J* = 9.3 Hz, 1H, H-2), 3.69 (dd, *J* = 11.2, 6.5 Hz, 1H, H-6a), 3.66 (dd, *J* = 11.3, 5.5 Hz, 1H, H-6b), 3.65 – 3.59 (overlapping signals, 3H, H-1, H-3 & H-1'), 3.48 (td, *J* = 6.6, 5.4, 1.2 Hz, 1H, H-5), 2.45 (ddt, *J* = 13.1, 10.1, 6.5 Hz, 1H, isopropyl CH), 1.05 (d, *J* = 6.3 Hz, 3H), 0.95 (d, *J* = 6.6 Hz, 3H) (each CH<sub>3</sub>); <sup>13</sup>C-NMR (126 MHz, CD<sub>3</sub>OD) δ 87.57 (methylene CH<sub>2</sub>), 79.72 (C-5), 78.82 (C-1'), 75.88 (C-1), 72.90 (C-2), 72.53 (C-3), 69.50 (C-4), 61.40 (C-6), 24.57 (C-2'), 19.86, 18.64 (each CH<sub>3</sub>).; HRMS calcd. for C<sub>12</sub>H<sub>23</sub>O<sub>6</sub>Na [M+Na]<sup>+</sup> 271.1152 found m/z 271.1154.



**1-((2*R*,3*R*,4*S*,5*S*,6*R*)-4,5-Bis(benzyloxy)-6-((benzyloxy)methyl)-3-((4-methoxybenzyl)oxy)tetrahydro-2*H*-pyran-2-yl)-2-methylpropan-1-one (EH 1100)** **EH 122** (750 mg, 1.2 mmol) was dissolved in CH<sub>2</sub>Cl<sub>2</sub> and cooled to 0 °C. Dess Martin Periodinane (1.14 g, 2.69 mmol) was added to the reaction mixture and allowed to stir overnight, after



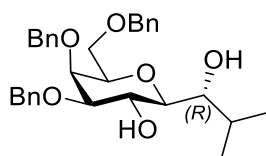
which TLC analysis indicated complete consumption of the starting material. The reaction mixture was filtered through celite, washed with satd. Na<sub>2</sub>S<sub>2</sub>O<sub>3</sub> solution, satd. NaHCO<sub>3</sub> solution, water, and brine. The organic layer was dried over MgSO<sub>4</sub>, filtered and the solvent removed under reduced pressure. The resulting ketone product (305 mg, 41%) was purified by column chromatography (cyclohexane-EtOAc 6:1); R<sub>f</sub> 0.66 (cyclohexane-EtOAc 6:1); <sup>1</sup>H-NMR (500 MHz, CDCl<sub>3</sub>) δ 7.45 – 7.24 (overlapping signals, 17H), 7.18 (d, *J* = 8.6 Hz, 1H), 6.83 (d, *J* = 8.6 Hz, 1H) (each Ar-H), 4.98 (d, *J* = 11.8 Hz, 1H), 4.81 – 4.76 (overlapping signals, 2H), 4.73 (d, *J* = 11.7 Hz, 1H), 4.64 (d, *J* = 11.7 Hz, 1H), 4.59 (d, *J* = 10.1 Hz, 1H), 4.48 (d, *J* = 11.8 Hz, 1H), 4.44 (d, *J* = 11.6 Hz, 1H) (each Bn-CH<sub>2</sub>), 4.18 (t, *J* = 9.6 Hz, 1H, H-2), 3.98 (d, *J* = 2.8 Hz, 1H, H-4), 3.91 (d, *J* = 9.6 Hz, 1H, H-1), 3.79 (s, 3H, OCH<sub>3</sub>), 3.65 (dd, *J* = 9.5, 2.8 Hz, 1H, H-3), 3.63 – 3.56 (overlapping signals, 3H, H-5, H-6a & H-6b), 3.00 (hept, *J* = 7.0 Hz, 1H, isopropyl CH), 1.14 (d, *J* = 7.0 Hz, 3H), 1.12 (d, *J* = 7.0 Hz, 3H) (each isopropyl CH<sub>3</sub>); <sup>13</sup>C-NMR (126 MHz, CDCl<sub>3</sub>) δ 209.36 (C=O), 159.24, 138.68, 138.32, 137.87, 130.55, 129.90, 129.50, 128.48, 128.47, 128.44, 128.43, 128.41, 128.34, 128.27, 128.24, 128.14, 128.02, 128.01, 127.97, 127.95, 127.89, 127.83, 127.80, 127.77, 127.69, 127.62, 127.60, 127.57, 127.55, 127.52, 127.48, 127.36, 113.82, 113.74 (each Ar-C/ C-H), 84.52 (C-3), 81.01 (C-1), 77.88 (C-5), 77.32, 77.06, 76.81, 75.39 (C-2), 74.90, 74.43, 73.57 (each Bn-CH<sub>2</sub>), 73.51 (C-4), 72.50 (Bn-CH<sub>2</sub>), 69.04 (C-6), 55.27 (OCH<sub>3</sub>), 38.55 (isopropyl CH), 18.23, 17.82 (each isopropyl CH<sub>3</sub>).



**(S)-1-((2S,3R,4S,5S,6R)-4,5-Bis(benzyloxy)-6-((benzyloxy)methyl)-3-((4-methoxybenzyl)oxy)tetrahydro-2H-pyran-2-yl)-2-methylpropan-1-ol (EH 1104)**

**EH 1100** (269 mg, 0.43 mmol) was dissolved in CH<sub>2</sub>Cl<sub>2</sub>-MeOH (1:1) and NaBH<sub>4</sub> (22 mg, 0.59 mmol) was added to the reaction mixture and allowed to stir for 30 mins, after which TLC analysis indicated complete consumption of the starting material. The solvent was then removed under reduced pressure. Flash chromatography (cyclohexane-EtOAc 6:1) provided the product (230 mg, 85%) as a white solid.; R<sub>f</sub> 0.29 (cyclohexane-EtOAc 4:1); <sup>1</sup>H-NMR (400 MHz, CDCl<sub>3</sub>) δ 7.44 – 7.15 (overlapping signals, 17H, aromatic H), 6.90 – 6.75 (overlapping signals, 2H, Ar-H), 5.01 (d, *J* = 10.3 Hz, 1H), 4.94 (d, *J* = 11.6 Hz, 1H), 4.78 (d, *J* = 11.7 Hz,

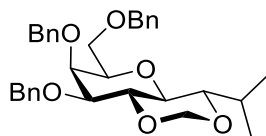
1H), 4.67 (d,  $J = 10.4$  Hz, 1H), 4.67 (d,  $J = 11.6$  Hz, 1H), 4.62 (d,  $J = 11.6$  Hz, 1H), 4.48 (d,  $J = 11.7$  Hz, 1H), 4.42 (d,  $J = 11.6$  Hz, 1H) (each Bn-CH<sub>2</sub>), 4.04 (t,  $J = 9.4$  Hz, 1H, H-2), 3.99 (d,  $J = 2.7$  Hz, 1H, H-4), 3.78 (s, 3H, OCH<sub>3</sub>), 3.68 (dd,  $J = 9.4, 2.7$  Hz, 1H, H-3), 3.64 (dd,  $J = 6.7, 3.7$  Hz, 1H, H-1'), 3.55 (s, 3H, H-5, H-6a & H-6b), 3.23 (dd,  $J = 9.2, 6.8$  Hz, 1H, H-2), 2.02 (tdd,  $J = 10.5, 5.2, 2.6$  Hz, 1H, isopropyl CH), 0.95 (d,  $J = 7.0$  Hz, 3H), 0.87 (d,  $J = 6.8$  Hz, 3H) (each CH<sub>3</sub>); <sup>13</sup>C-NMR (101 MHz, CDCl<sub>3</sub>)  $\delta$  130.02, 129.93, 128.65, 128.55, 128.37, 128.19, 127.97, 127.92, 127.89, 127.74, 127.69, 114.03 (each Ar-C/ C-H), 85.49 (C-3), 78.72 (C-1), 78.48 (C-2), 77.54 (C-1'), 77.51 (C-5), 77.47, 77.15, 76.84 (each CDCl<sub>3</sub>), 75.08, 74.65, 73.63 (each Bn-CH<sub>2</sub>), 73.61 (C-4), 72.19 (Bn-CH<sub>2</sub>), 69.08 (C-6), 55.38 (OCH<sub>3</sub>), 28.83 (C-2'), 19.66, 15.64 (each CH<sub>3</sub>); HRMS calcd. for C<sub>41</sub>H<sub>52</sub>O<sub>7</sub>Na [M+Na]<sup>+</sup> 649.3136 found  $m/z$  649.3134.



**(2*S*,3*R*,4*R*,5*S*,6*R*)-4,5-Bis(benzyloxy)-6-((benzyloxy)methyl)-2-((*S*)-1-hydroxy-2-methylpropyl)tetrahydro-2*H*-pyran-3-ol (EH 124 O/R)**

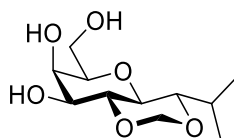
**EH 1104** (200 mg, 0.32 mmol) was dissolved in CH<sub>2</sub>Cl<sub>2</sub> and cooled to 0 °C. Trifluoroacetic acid (0.32 mL, 4.23 mmol) was added to the reaction mixture and allowed to stir for 30 mins, after which time TLC analysis indicated complete consumption of the starting material. The solvent was then removed under reduced pressure. Flash chromatography (cyclohexane-EtOAc 4:1) provided the product (126 mg, 78%) as a white solid.;  $R_f$  0.3 (cyclohexane-EtOAc 3:2); <sup>1</sup>H-NMR (500 MHz, CDCl<sub>3</sub>)  $\delta$  7.41 – 7.24 (overlapping signals, 15H, each Ar-H) 4.86 (d,  $J = 11.6$  Hz, 1H), 4.74 (d,  $J = 11.7$  Hz, 1H), 4.62 (d,  $J = 11.6$  Hz, 1H), 4.56 (d,  $J = 11.8$  Hz, 1H), 4.50 (d,  $J = 11.7$  Hz, 1H), 4.45 (d,  $J = 11.8$  Hz, 1H) (each Bn-CH<sub>2</sub>), 4.13 (t,  $J = 9.3$  Hz, 1H, H-2), 3.99 (d,  $J = 2.8$  Hz, 1H, H-4), 3.72 (dd,  $J = 7.7, 3.1$  Hz, 1H, H-1'), 3.46 (dd,  $J = 9.4, 2.9$  Hz, 1H, H-3), 3.19 (dd,  $J = 9.1, 7.6$  Hz, 1H, H-1), 2.09 (pd,  $J = 6.9, 3.1$  Hz, 1H, isopropyl CH), 0.98 (d,  $J = 7.0$  Hz, 3H), 0.89 (d,  $J = 6.8$  Hz, 3H) (each CH<sub>3</sub>); <sup>13</sup>C-NMR (126 MHz, CDCl<sub>3</sub>)  $\delta$  138.47, 137.91, 137.87, 128.64, 128.60, 128.44, 128.27, 128.18, 127.96, 127.87, 127.82, 127.76, 127.67, 113.96 (each Ar-C/ C-H), 83.86 (C-3), 78.29(C-1), 78.27 (C-1'), 77.42 (C-5), 77.28, 77.03, 76.77 (each CDCl<sub>3</sub>), 74.46, 73.55 (each Bn-CH<sub>2</sub>), 72.69 (C-4), 72.02 (Bn-CH<sub>2</sub>),

71.61 (C-2), 68.96 (C-6), 28.74 (C-2'), 19.30, 15.02 (each CH<sub>3</sub>); HRMS calcd. for C<sub>32</sub>H<sub>41</sub>O<sub>6</sub>Na [M+Na]<sup>+</sup> 529.2560 found m/z 529.2563.



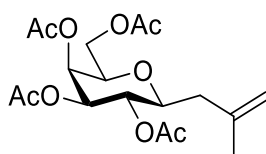
**(4*S*,4*aS*,6*R*,7*S*,8*S*,8*aR*)-7,8-Bis(benzyloxy)-6-((benzyloxy)methyl)-4-isopropylhexahydropyrano[3,2-*d*][1,3]dioxine (EH 131 O/R)**

**EH 124 O/R** (126 mg, 0.25 mmol) was dissolved in dimethoxymethane (4.00 mL, 45.6 mmol), camphorsulfonic acid (115 mg, 0.49 mmol) was added and the reaction was allowed to reflux overnight while stirring vigorously. After 18 hrs, TLC analysis indicated product formation. The solvent was removed under reduced pressure. Flash chromatography (cyclohexane-EtOAc 6:1) provided the product (81 mg, 63%) as a colourless oil.; R<sub>f</sub> 0.88 (cyclohexane-EtOAc 3:2); <sup>1</sup>H-NMR (500 MHz, CDCl<sub>3</sub>) δ 7.44 – 7.23 (overlapping signals, 15H, Ar-H), 5.13 (d, *J* = 6.2 Hz, 1H, methylene *CHH*), 4.96 (d, *J* = 11.4 Hz, 1H), 4.84 (d, *J* = 12.2 Hz, 1H) (each Bn-CH<sub>2</sub>), 4.77 (d, *J* = 6.3 Hz, 1H, methylene *CHH*), 4.71 (d, *J* = 12.3 Hz, 1H), 4.63 (d, *J* = 11.4 Hz, 1H), 4.47 (d, *J* = 11.8 Hz, 1H), 4.42 (d, *J* = 11.8 Hz, 1H) (each Bn-CH<sub>2</sub>), 4.00 – 3.93 (m, 2H, H-2 & H-4), 3.65 (dd, *J* = 9.8, 3.0 Hz, 1H, H-3), 3.61 (dd, *J* = 12.4, 5.4 Hz, 1H, H-5), 3.57 – 3.53 (overlapping signals, 2H, H-6a & H-6b), 3.44 (dd, *J* = 9.3, 2.9 Hz, 1H, H-3), 3.12 (t, *J* = 9.2 Hz, 1H, H-2), 2.05 (pd, *J* = 7.0, 2.8 Hz, 1H, isopropyl CH), 1.00 (d, *J* = 7.0 Hz, 3H), 0.93 (d, *J* = 6.8 Hz, 3H) (each CH<sub>3</sub>); <sup>13</sup>C-NMR (126 MHz, CDCl<sub>3</sub>) δ 138.47, 137.93, 128.50, 128.42, 128.23, 127.85, 127.78, 127.67, 127.59, 127.53 (each Ar-C/ C-H), 93.82 (methylene CH<sub>2</sub>), 82.50 (C-1'), 80.51 (C-3), 78.59 (C-2), 78.30 (C-5), 77.29, 77.04, 76.78 (each CDCl<sub>3</sub>), 74.99 (Bn-CH<sub>2</sub>), 74.88 (C-4), 74.26 (C-1), 73.52, 72.81 (each Bn-CH<sub>2</sub>), 68.87 (C-6), 27.99 (C-2'), 19.11, 15.71 (each CH<sub>3</sub>).



**(4*S*,4*aS*,6*R*,7*R*,8*S*,8*aR*)-6-(Hydroxymethyl)-4-isopropylhexahydropyrano[3,2-*d*][1,3]dioxine-7,8-diol (EH 145 O/R)**

**EH 131 O/R** (80 mg, 0.15 mmol) was dissolved in EtOAc:MeOH (1:1) and Pd/C (10%) was added to the reaction mixture. The flask was fitted with a H<sub>2</sub> balloon and left to stir overnight. TLC analysis indicated complete consumption of the starting material. The reaction mixture was then filtered through celite and the solvent removed under reduced pressure. Flash chromatography (CH<sub>2</sub>Cl<sub>2</sub>-MeOH 9:1) provided the product (36 mg, 93%) as a white solid.; R<sub>f</sub> 0.4 (CH<sub>2</sub>Cl<sub>2</sub>-MeOH 9:1); <sup>1</sup>H-NMR (500 MHz, CD<sub>3</sub>OD) δ 5.03 (d, *J* = 6.1 Hz, 1H), 4.70 (d, *J* = 6.1 Hz, 1H) (each methylene CH<sub>2</sub>), 3.91 (dd, *J* = 3.5, 1.3 Hz, 1H, H-4), 3.73 – 3.64 (overlapping signals, 3H, H-3, H-6*a* & H-6*b*), 3.56 (t, *J* = 9.5 Hz, 1H, H-2), 3.53 (ddd, *J* = 6.6, 5.3, 1.3 Hz, 1H, H-5), 3.37 (dd, *J* = 9.3, 2.8 Hz, 1H, H-3), 3.08 (t, *J* = 9.1 Hz, 1H, H-2), 2.08 (pd, *J* = 7.0, 2.8 Hz, 1H, isopropyl CH), 1.00 (d, *J* = 7.0 Hz, 3H), 0.92 (d, *J* = 7.0 Hz, 3H) (each CH<sub>3</sub>); <sup>13</sup>C-NMR (126 MHz, CD<sub>3</sub>OD) δ 93.45 (methylene CH<sub>2</sub>), 82.61 (C-1'), 79.60 (C-5), 78.19 (C-2), 73.56 (C-1), 71.74 (C-3), 69.61 (C-4), 61.24 (C-6), 27.77 (C-2'), 18.23, 14.70 (each CH<sub>3</sub>); HRMS calcd. for C<sub>12</sub>H<sub>23</sub>O<sub>6</sub>Na [M+Na]<sup>+</sup> 271.1152 found *m/z* 271.1154.

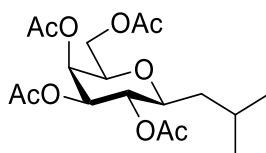


**1-(2'-Methylallyl)-2,3,4,6-tetra-*O*-acetyl-β-D-galactopyranose (EH 1206)**

**EH 1197** (1.00 g, 2.56 mmol) was dissolved in CH<sub>2</sub>Cl<sub>2</sub> and cooled to -20 °C. Methylallyl trimethylsilane (1.80 mL, 10.3 mmol) was added followed by the dropwise addition of BF<sub>3</sub>·OEt<sub>2</sub> (0.81 mL, 6.57 mmol). The reaction mixture was allowed to stir overnight under an inert atmosphere. The reaction mixture was then washed with a satd. NaHCO<sub>3</sub> solution, dried over MgSO<sub>4</sub> and the solvent removed under reduced pressure. Flash chromatography (cyclohexane-EtOAc 4:1) provided the product (851 mg, 86%) as a white solid.; R<sub>f</sub> 0.32 (cyclohexane-EtOAc 3:2); <sup>1</sup>H-NMR (500 MHz, CDCl<sub>3</sub>) δ 5.40 (dd, *J* = 3.4, 1.2 Hz, 1H, H-4),

5.10 (t,  $J = 9.8$  Hz, 1H, H-2), 5.02 (dd,  $J = 10.1, 3.4$  Hz, 1H, H-3), 4.79 (t,  $J = 1.8$  Hz, 1H, C=CHH), 4.73 (q,  $J = 1.2$  Hz, 1H, C=CHH), 4.13 (dd,  $J = 11.3, 6.9$  Hz, 1H, H-6a), 4.04 (dd,  $J = 11.3, 6.5$  Hz, 1H, H-6b), 3.84 (td,  $J = 6.8, 1.3$  Hz, 1H, H-5), 3.57 (td,  $J = 9.5, 8.1, 4.0$  Hz, 1H, H-1), 2.27 (dd,  $J = 14.9, 8.1$  Hz, 1H, CHH), 2.22 (dd,  $J = 15.1, 4.1$  Hz, 1H, CHH), 2.15 (s, 3H), 2.02 (s, 3H), 2.02 (s, 3H), 1.97 (s, 3H), 1.75 (s, 3H, CH<sub>3</sub>).; <sup>13</sup>C-NMR (126 MHz, CDCl<sub>3</sub>)  $\delta$  170.43, 170.32, 170.23, 169.79 (each C=O), 141.41 (C=CH<sub>2</sub>), 112.67 (C=CH<sub>2</sub>), 77.26 (CDCl<sub>3</sub>), 77.07 (C-1), 77.01, 76.75 (each CDCl<sub>3</sub>), 74.12 (C-5), 72.25 (C-3), 69.52 (C-2), 67.73 (C-4), 61.64 (C-6), 39.80 (CHH), 22.77 (CH<sub>3</sub>), 20.79, 20.69, 20.64, 20.60 (each OCH<sub>3</sub>).

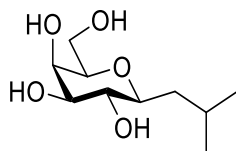
NMR data obtained was in good agreement with the literature <sup>14</sup>



### 1-(Isobutyl)-2,3,4,6-tetra-O-acetyl- $\beta$ -D-galactopyranose (EH 1206 H<sub>2</sub>)

**EH 1206** (350 mg, 0.90 mmol) was dissolved in MeOH and Pd/C (10%) was added to the reaction mixture. The flask was fitted with a H<sub>2</sub> balloon and left to stir overnight. TLC analysis indicated complete consumption of the starting material. The reaction mixture was then filtered through celite and the solvent removed under reduced pressure. Flash chromatography (cyclohexane-EtOAc 4:1) provided the product (327 mg, 93%) as a white solid.;  $R_f$  0.56 (cyclohexane-EtOAc 4:1); <sup>1</sup>H-NMR (500 MHz, CDCl<sub>3</sub>)  $\delta$  5.41 (dd,  $J = 3.3, 1.3$  Hz, 1H, H-4), 5.06 (t,  $J = 9.6$  Hz, 1H, H-2), 5.00 (dd,  $J = 10.1, 3.4$  Hz, 1H, H-3), 4.15 (dd,  $J = 11.3, 6.8$  Hz, 1H, H-6a), 4.04 (dd,  $J = 11.2, 6.6$  Hz, 1H, H-6b), 3.83 (td,  $J = 6.8, 1.1$  Hz, 1H, H-5), 3.42 (td,  $J = 9.8, 2.3$  Hz, 1H, H-1), 2.15 (s, 3H), 2.04 (s, 3H), 2.03 (s, 3H), 1.97 (s, 3H) (each OAc), 1.83 (dtd,  $J = 13.8, 9.4, 7.1, 3.1$  Hz, 1H, isopropyl CH), 1.53 (ddd,  $J = 14.3, 10.1, 4.5$  Hz, 1H, CHH), 1.20 (ddd,  $J = 14.2, 9.6, 2.3$  Hz, 1H, CHH), 0.92 (d,  $J = 6.8$  Hz, 3H), 0.87 (d,  $J = 6.6$  Hz, 3H) (each CH<sub>3</sub>); <sup>13</sup>C-NMR (101 MHz, CDCl<sub>3</sub>)  $\delta$  170.51, 170.42, 170.31, 169.96 (each C=O), 77.48, 77.16, 76.84 (each CDCl<sub>3</sub>), 76.74 (C-1), 74.19 (C-5), 72.34 (C-3), 69.87 (C-4), 67.85 (C-4), 61.73 (C-6), 40.25 (CHH), 24.31 (C-2'), 23.53 (CH<sub>3</sub>), 21.48 (CH<sub>3</sub>), 20.87, 20.77, 20.71, 20.68 (each OCH<sub>3</sub>); HRMS calcd. for C<sub>18</sub>H<sub>32</sub>NO<sub>9</sub> [M+NH<sub>4</sub>]<sup>+</sup> 406.2071 found  $m/z$  406.2021.

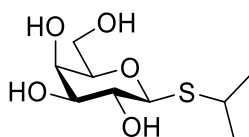
NMR data obtained was in good agreement with the literature <sup>14</sup>



### 1-(Isobutyl)-β-D-galactopyranose (EH 1208)

**EH 1206 H<sub>2</sub>** (65 mg, 0.17 mmol) was dissolved in dry MeOH and NaOMe was added (5 mg, 0.09 mmol). The reaction mixture was allowed to stir for 15 mins, after which time, TLC analysis indicated disappearance of the starting material. Amberlite (H<sup>+</sup>) was added to neutralise the reaction mixture, which was concentrated to give the deprotected compound. Flash chromatography (CH<sub>2</sub>Cl<sub>2</sub>-MeOH 9:1) provided the product (28 mg, 75%) as a white solid.; R<sub>f</sub> 0.3 (CH<sub>2</sub>Cl<sub>2</sub>-MeOH 9:1); <sup>1</sup>H-NMR (400 MHz, CD<sub>3</sub>OD) δ 3.84 (dd, *J* = 3.3, 1.1 Hz, 1H, H-4), 3.66 (dd, *J* = 11.3, 6.7 Hz, 1H, H-6a), 3.63 (dd, *J* = 11.2, 5.8 Hz, 1H, H-6b), 3.41 – 3.36 (overlapping signals, 2H, H-3 & H-5), 3.31 (d, *J* = 9.2 Hz, 1H, H-2), 3.11 (td, *J* = 10.0, 9.1, 2.1 Hz, 1H, H-1), 1.89 (ddtd, *J* = 13.4, 9.8, 6.6, 4.2 Hz, 1H, isopropyl CH), 1.59 (ddd, *J* = 14.0, 9.7, 2.1 Hz, 1H, CHH), 1.39 (ddd, *J* = 14.2, 10.0, 4.3 Hz, 1H, CHH), 0.91 (d, *J* = 6.8 Hz, 3H), 0.88 (d, *J* = 6.6 Hz, 3H) (each CH<sub>3</sub>); <sup>13</sup>C-NMR (126 MHz, CD<sub>3</sub>OD) δ 78.61 (C-5), 78.34 (C-1), 75.08 (C-3), 71.80 (C-2), 69.36 (C-4), 61.26 (C-6), 40.67 (CHH), 24.12 (C-2'), 22.91, 20.69 (each CH<sub>3</sub>).

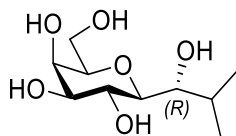
NMR data obtained was in good agreement with the literature <sup>14</sup>



### 1-Isopropyl-β-D-thiogalactopyranose (IPTG)

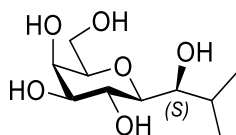
This compound was purchased from Carbosynth

<sup>1</sup>H-NMR (500 MHz, CD<sub>3</sub>OD) δ 4.39 (d, *J* = 9.4 Hz, 1H, H-1), 3.87 (dd, *J* = 3.3, 1.1 Hz, 1H, H-4), 3.72 (dd, *J* = 11.4, 6.8 Hz, 1H, H-6a), 3.68 (dd, *J* = 11.4, 5.5 Hz, 1H, H-6b), 3.53 – 3.48 (overlapping signals, 2H, H-2 & H-5), 3.45 (dd, *J* = 9.3, 3.3 Hz, 1H, H-3), 3.23 (hept, *J* = 6.8 Hz, 1H, isopropyl CH), 1.31 (d, *J* = 7.1 Hz, 3H), 1.30 (d, *J* = 7.2 Hz, 3H) (each CH<sub>3</sub>); <sup>13</sup>C-NMR (126 MHz, CD<sub>3</sub>OD) δ 85.71 (C-1), 79.08, 74.92 (C-3), 70.20, 69.04 (C-4), 61.18 (C-6), 48.08, 47.91, 47.74, 47.57, 47.40, 47.23, 47.06, 34.39 (C-1'), 22.98, 22.88 (each CH<sub>3</sub>).



**(2*S*,3*R*,4*S*,5*R*,6*R*)-2-((*S*)-1-Hydroxy-2-methylpropyl)-6-(hydroxymethyl)tetrahydro-2*H*-pyran-3,4,5-triol (EH 1104 H<sub>2</sub>)**

**EH 1104** (100 mg, 0.16 mmol) was dissolved in EtOAc:MeOH (1:1) and Pd/C (10%) was added to the reaction mixture. The flask was fitted with a H<sub>2</sub> balloon and left to stir overnight. TLC analysis indicated complete consumption of the starting material. The reaction mixture was then filtered through celite and the solvent removed under reduced pressure. Flash chromatography (CH<sub>2</sub>Cl<sub>2</sub>-MeOH 9:1) provided the product (25 mg, 67%) as a white solid.; <sup>1</sup>H-NMR (500 MHz, CD<sub>3</sub>OD) δ 3.89 (d, *J* = 3.2 Hz, 1H, H-4), 3.78 (t, *J* = 9.3 Hz, 1H, H-2), 3.74 (dd, *J* = 11.5, 6.7 Hz, 1H, H-6a), 3.69 (dd, *J* = 11.3, 4.9 Hz, 1H, H-6b), 3.64 (t, *J* = 5.2 Hz, 1H, H-1'), 3.53 – 3.46 (overlapping signals, 2H, H-3 & H-5), 3.28 (dd, *J* = 9.4, 5.8 Hz, 1H, H-1), 2.09 (pentet of doublets, *J* = 6.8, 4.6 Hz, 1H, isopropyl CH), 0.97 (d, *J* = 6.9 Hz, 3H), 0.94 (d, *J* = 6.7 Hz, 3H) (each CH<sub>3</sub>); <sup>13</sup>C-NMR (126 MHz, CD<sub>3</sub>OD) δ 79.10 (C-1), 78.58 (C-5), 77.94 (C-1'), 75.00 (C-3), 70.04 (C-2), 69.55 (C-4), 61.66 (C-6), 29.11 (C-2'), 18.89, 15.80 (each CH<sub>3</sub>).



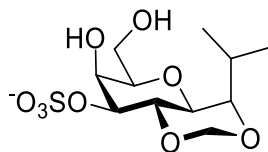
**(2*S*,3*R*,4*S*,5*R*,6*R*)-2-((*R*)-1-Hydroxy-2-methylpropyl)-6-(hydroxymethyl)tetrahydro-2*H*-pyran-3,4,5-triol (EH 124 H<sub>2</sub>)**

**EH 124** (81 mg, 0.13 mmol) was dissolved in EtOAc:MeOH (1:1) and Pd/C (10%) was added to the reaction mixture. The flask was fitted with a H<sub>2</sub> balloon and left to stir overnight. TLC analysis indicated complete consumption of the starting material. The reaction mixture was then filtered through celite and the solvent removed under reduced pressure. Flash chromatography (CH<sub>2</sub>Cl<sub>2</sub>-MeOH 9:1) provided the product (15 mg, 48%) as a white solid.; <sup>1</sup>H-NMR (500 MHz, CD<sub>3</sub>OD) δ 3.85 (dd, *J* = 3.3, 1.1 Hz, 1H, H-4), 3.79 (t, *J* = 9.6 Hz, 1H, H-2), 3.70 (dd, *J* = 11.4, 6.6 Hz, 1H, H-6a), 3.67 (dd, *J* = 11.4, 5.6 Hz, 1H, H-6b), 3.47 – 3.41 (m, 2H, H-3 & H-5), 3.38 (dd, *J* = 8.8, 1.6 Hz, 1H, H-1'), 3.22 (dd, *J* = 9.5, 1.6 Hz, 1H, H-1), 1.94 (doublet of heptets, *J* = 8.7, 6.7 Hz, 1H, isopropyl CH), 1.02 (d, *J* = 6.8 Hz, 3H), 0.89 (d, *J* = 6.7 Hz, 3H) (each CH<sub>3</sub>); <sup>13</sup>C NMR (126 MHz, CD<sub>3</sub>OD) δ 79.16 (C-2), 78.80 (C-5), 75.46 (C-

3), 74.15 (C-1'), 69.66 (C-4), 67.10 (C-2), 61.25 (C-6), 30.60 (C-2'), 18.80, 18.12 (each CH<sub>3</sub>);  
HRMS calcd. for C<sub>10</sub>H<sub>20</sub>O<sub>6</sub>Na [M+Na]<sup>+</sup> 259.1152 found m/z 259.1153.

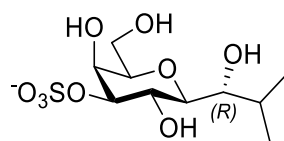


## Chapter 3-Experimental



**(4*R*,4*aS*,6*R*,7*S*,8*S*,8*aS*)-7-Hydroxy-6-(hydroxymethyl)-4-isopropylhexahydropyrano[3,2-*d*][1,3]dioxin-8-yl sulfate (EH 1260)**

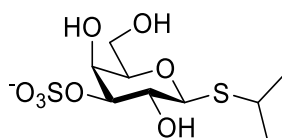
**EH 145** (20 mg, 0.08 mmol) was stirred in refluxing MeOH (20 mL), with Bu<sub>2</sub>SnO (40 mg, 0.16 mmol) for 2 h under nitrogen. The solvent was removed under reduced pressure and the dry dibutylstannylene complex was treated with Me<sub>3</sub>N·SO<sub>3</sub> (22 mg, 0.16 mmol) in THF (4 mL) at room temperature for 30 h. The reaction mixture was diluted with MeOH (3 mL), filtered and the solvent removed under reduced pressure. Flash chromatography (CH<sub>2</sub>Cl<sub>2</sub>-MeOH 4:1) provided the product (13 mg, 47%) as a colourless oil.; <sup>1</sup>H-NMR (500 MHz, CD<sub>3</sub>OD) δ 4.80 (d, *J* = 6.5 Hz, 1H), 4.72 (d, *J* = 6.4 Hz, 1H) (each methylene CH<sub>2</sub>), 4.38 (dd, *J* = 3.3, 1.1 Hz, 1H, H-4), 4.35 (dd, *J* = 9.4, 3.2 Hz, 1H, H-3), 4.01 (t, *J* = 9.7 Hz, 1H, H-2), 3.71 (dd, *J* = 9.8, 5.6 Hz, 1H, H-1), 3.69 – 3.67 (overlapping signals, 2H, H-6a & H-6b), 3.64 (dd, *J* = 10.3, 5.7 Hz, 1H, H-1'), 3.53 (td, *J* = 6.7, 5.5, 1.2 Hz, 1H, H-5), 2.45 (doublet of pentets, *J* = 10.3, 6.5 Hz, 1H, isopropyl CH), 1.05 (d, *J* = 6.4 Hz, 3H), 0.95 (d, *J* = 6.6 Hz, 3H) (each CH<sub>3</sub>); <sup>13</sup>C-NMR (126 MHz, CD<sub>3</sub>OD) δ 87.49 (methylene CH<sub>2</sub>), 79.54 (C-5), 79.36 (C-3), 78.77 (C-1'), 76.19 (C-1), 70.72 (C-2), 67.60 (C-4), 61.35 (C-6), 24.56 (C-2'), 19.81, 18.62 (each CH<sub>3</sub>).



**(2*S*,3*S*,4*S*,5*S*,6*R*)-3,5-Dihydroxy-2-((*S*)-1-hydroxy-2-methylpropyl)-6-(hydroxymethyl)tetrahydro-2*H*-pyran-4-yl sulfate (EH 1261)**

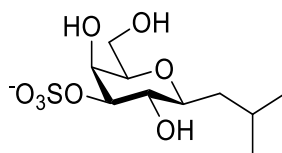
**(EH 1104 H<sub>2</sub>)** (20 mg, 0.08 mmol) was stirred in refluxing MeOH (3 mL), with Bu<sub>2</sub>SnO (42 mg, 0.17 mmol) for 2 h under nitrogen. The solvent was removed under reduced pressure and the dry dibutylstannylene complex was treated with Me<sub>3</sub>N·SO<sub>3</sub> (24 mg, 0.15 mmol) in THF (4 mL) at room temperature for 30h. The reaction mixture was diluted with MeOH (3 mL), filtered and the solvent removed under reduced pressure. Flash chromatography (CH<sub>2</sub>Cl<sub>2</sub>-MeOH 4:1)

provided the product (16 mg, 59%) as a colourless oil;  $^1\text{H-NMR}$  (500 MHz,  $\text{CD}_3\text{OD}$ )  $\delta$  4.28 – 4.22 (overlapping signals, 2H, H-3 & H-4), 3.96 (t,  $J = 9.9$  Hz, 1H, H-2), 3.73 (dd,  $J = 11.4$ , 6.8 Hz, 1H, H-6a), 3.67 (dd,  $J = 11.5$ , 4.9 Hz, 1H, H-6b), 3.64 (t,  $J = 5.0$  Hz, 1H, H-1'), 3.51 (t,  $J = 6.0$  Hz, 1H, H-5), 3.35 (dd,  $J = 9.4$ , 5.4 Hz, 1H, H-1), 2.09 (pd,  $J = 6.8$ , 4.7 Hz, 1H, isopropyl CH), 0.97 (d,  $J = 6.9$  Hz, 3H), 0.95 (d,  $J = 6.8$  Hz, 3H) (each  $\text{CH}_3$ );  $^{13}\text{C-NMR}$  (126 MHz,  $\text{CD}_3\text{OD}$ )  $\delta$  82.24 (C-3), 79.59 (C-1), 78.68 (C-5), 77.59 (C-1'), 68.06 (C-2), 67.66 (C-4), 61.51 (C-6), 29.02 (C-2'), 18.96, 15.88 (each  $\text{CH}_3$ ).



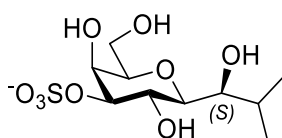
**(2*R*,3*S*,4*S*,5*R*,6*S*)-3,5-Dihydroxy-2-(hydroxymethyl)-6-(isopropylthio)tetrahydro-2*H*-pyran-4-yl sulfate (EH 1263)**

1-Isopropyl- $\beta$ -D-thiogalactopyranose (200 mg, 0.84 mmol) was stirred in refluxing MeOH (30 mL), with  $\text{Bu}_2\text{SnO}$  (418 mg, 1.68 mmol) for 2 h under nitrogen. The solvent was removed under reduced pressure and the dry dibutylstannylene complex was treated with  $\text{Me}_3\text{N}\cdot\text{SO}_3$  (234 mg, 1.68 mmol) in THF (40 mL) at room temperature for 30 h. The reaction mixture was diluted with MeOH (20 mL), filtered and the solvent removed under reduced pressure. Flash chromatography ( $\text{CH}_2\text{Cl}_2$ -MeOH 4:1) provided the product (150 mg, 56%) as a colourless oil.;  $^1\text{H-NMR}$  (500 MHz,  $\text{CD}_3\text{OD}$ )  $\delta$  4.50 (d,  $J = 9.7$  Hz, 1H, H-1), 4.30 (d,  $J = 3.3$  Hz, 1H, H-4), 4.26 (dd,  $J = 9.3$ , 3.2 Hz, 1H, H-3), 3.76 – 3.65 (overlapping signals, 3H, H-2, H-6a & H-6b), 3.58 (t,  $J = 6.2$  Hz, 1H, H-5), 3.25 (p,  $J = 6.8$  Hz, 1H, isopropyl CH), 1.31 (d,  $J = 6.8$  Hz, 3H), 1.29 (d,  $J = 6.9$  Hz, 3H) (each  $\text{CH}_3$ );  $^{13}\text{C-NMR}$  (126 MHz,  $\text{CD}_3\text{OD}$ )  $\delta$  85.39 (C-1), 81.78 (C-3), 78.69 (C-5), 68.39 (C-2), 67.38 (C-4), 61.02 (C-6), 34.37 (C-1'), 23.00, 22.93 (each  $\text{CH}_3$ ).



**(2*R*,3*S*,4*R*,5*S*,6*S*)-3,5-Dihydroxy-2-(hydroxymethyl)-6-isobutyltetrahydro-2*H*-pyran-4-yl sulfate (EH 1264)**

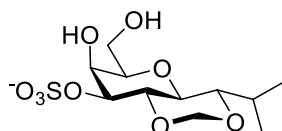
**EH 1208** (110 mg, 0.5 mmol) was stirred in refluxing MeOH (20 mL), with Bu<sub>2</sub>SnO (249 mg, 1.0 mmol) for 2 h under nitrogen. The solvent was removed under reduced pressure and the dry dibutylstannylene complex was treated with Me<sub>3</sub>N·SO<sub>3</sub> (139 mg, 1.0 mmol) in THF (20 mL) at room temperature for 30h. The reaction mixture was diluted with MeOH (10 mL), filtered and the solvent removed under reduced pressure. Flash chromatography (CH<sub>2</sub>Cl<sub>2</sub>-MeOH 4:1) provided the product (71 mg, 47%) as a colourless oil.; <sup>1</sup>H-NMR (500 MHz, CD<sub>3</sub>OD) δ 4.26 (dd, *J* = 3.3, 1.1 Hz, 1H, H-4), 4.20 (dd, *J* = 9.4, 3.2 Hz, 1H, H-3), 3.69 (dd, *J* = 11.2, 6.5 Hz, 1H, H-6a), 3.66 (dd, *J* = 11.3, 5.8 Hz, 1H, H-6b), 3.53 (t, *J* = 9.3 Hz, 1H, H-2), 3.46 (td, *J* = 6.3, 1.1 Hz, 1H, H-5), 3.23 (td, *J* = 9.7, 2.1 Hz, 1H, H-1), 1.91 (m, *J* = 9.7, 6.7, 4.3 Hz, 1H, isopropyl CH), 1.64 (ddd, *J* = 14.0, 9.8, 2.1 Hz, 1H, CHH), 1.42 (ddd, *J* = 14.2, 9.9, 4.3 Hz, 1H, CHH), 0.93 (d, *J* = 6.8 Hz, 3H), 0.90 (d, *J* = 6.6 Hz, 3H) (each CH<sub>3</sub>); <sup>13</sup>C-NMR (126 MHz, CD<sub>3</sub>OD) δ 82.45 (C-3), 78.44 (C1 & C-5), 69.80 (C-2), 67.65 (C-4), 61.16 (C-6), 40.69 (CHH), 24.08 (C-2'), 22.86, 20.67 (each CH<sub>3</sub>).



**(2*S*,3*S*,4*S*,5*S*,6*R*)-3,5-Dihydroxy-2-((*R*)-1-hydroxy-2-methylpropyl)-6-(hydroxymethyl)tetrahydro-2*H*-pyran-4-yl sulfate (EH 1265)**

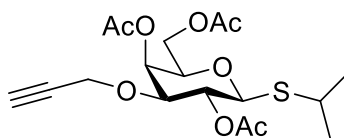
**EH 124 H<sub>2</sub>** (26 mg, 0.11 mmol) was stirred in refluxing MeOH (2 mL), with Bu<sub>2</sub>SnO (56 mg, 0.22 mmol) for 2 h under nitrogen. The solvent was removed under reduced pressure and the dry dibutylstannylene complex was treated with Me<sub>3</sub>N·SO<sub>3</sub> (31 mg, 0.22 mmol) in THF (3 mL) at room temperature for 30h. The reaction mixture was diluted with MeOH (5 mL), filtered and the solvent removed under reduced pressure. Flash chromatography (CH<sub>2</sub>Cl<sub>2</sub>-MeOH 4:1) provided the product (16 mg, 47%) as a colourless oil.; <sup>1</sup>H-NMR (500 MHz, CD<sub>3</sub>OD) δ 4.32 (d, *J* = 3.0, 1H, H-4), 4.27 (dd, *J* = 9.4, 3.0 Hz, 1H, H-3), 4.02 (t, *J* = 9.5 Hz, 1H, H-2), 3.76

(dd,  $J = 11.4, 5.8$  Hz, 1H, H-6a), 3.73 (dd,  $J = 11.3, 5.3$  Hz, 1H, H-6b), 3.57 (t,  $J = 5.4$  Hz, 1H, H-5), 3.44 (dd,  $J = 9.0, 1.3$  Hz, 1H, H-1'), 3.41 (dd,  $J = 9.5, 1.3$  Hz, 1H, H-1), 1.96 (doublet of heptets,  $J = 9.1, 6.8$  Hz, 1H, isopropyl CH), 1.03 (d,  $J = 6.7$  Hz, 3H), 0.91 (d,  $J = 6.7$  Hz, 3H) (each CH<sub>3</sub>); <sup>13</sup>C-NMR (126 MHz, CD<sub>3</sub>OD)  $\delta$  82.43 (C-3), 79.30 (C-1), 78.00 (C-5), 74.16 (C-1'), 68.44 (C-4), 65.21 (C-2), 61.35 (C-6), 30.37 (C-2'), 18.86, 18.07 (each CH<sub>3</sub>).



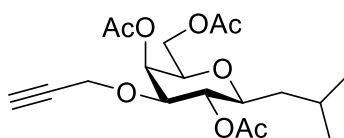
**(4*S*,4*aS*,6*R*,7*S*,8*S*,8*aS*)-7-Hydroxy-6-(hydroxymethyl)-4-isopropylhexahydropyrano[3,2-*d*][1,3]dioxin-8-yl sulfate (EH 1266)**

**EH 145 O/R** (30 mg, 0.12 mmol) was stirred in refluxing MeOH (3 mL), with Bu<sub>2</sub>SnO (60 mg, 0.24 mmol) for 2 h under nitrogen. The solvent was removed under reduced pressure and the dry dibutylstannylene complex was treated with Me<sub>3</sub>N·SO<sub>3</sub> (34 mg, 0.24 mmol) in THF (4 mL) at room temperature for 30h. The reaction mixture was diluted with MeOH (3 mL), filtered and the solvent removed under reduced pressure. Flash chromatography (CH<sub>2</sub>Cl<sub>2</sub>-MeOH 4:1) provided the product (19 mg, 47%) as a colourless oil.; <sup>1</sup>H-NMR (500 MHz, CD<sub>3</sub>OD)  $\delta$  5.02 (d,  $J = 6.2$  Hz, 1H), 4.67 (d,  $J = 6.2$  Hz, 1H) (each methylene CH<sub>2</sub>), 4.4 - 4.37 (overlapping signals, 2H, H-3 & H-4), 3.74 - 3.64 (overlapping signals, 3H, H-2, H-6a & H-6b), 3.58 (td,  $J = 6.6, 5.3, 1.1$  Hz, 1H, H-5), 3.38 (dd,  $J = 9.3, 2.8$  Hz, 1H, H-3), 3.17 (t,  $J = 9.2$  Hz, 1H, H-2), 2.09 (heptet of doublets,  $J = 7.0, 2.7$  Hz, 1H, isopropyl CH), 1.00 (d,  $J = 7.0$  Hz, 3H), 0.93 (d,  $J = 6.9$  Hz, 3H) (each CH<sub>3</sub>); <sup>13</sup>C-NMR (126 MHz, CD<sub>3</sub>OD)  $\delta$  93.32 (methylene CH<sub>2</sub>), 82.54 (C-1'), 79.44 (C-5), 78.38 (C-3), 75.92 (C-2), 73.84 (C-1), 67.75 (C-4), 61.19 (C-6), 27.69 (C-2'), 18.20, 14.62 (each CH<sub>3</sub>).



**(2*R*,3*S*,4*S*,5*R*,6*S*)-2-(Acetoxymethyl)-6-(isopropylthio)-4-(prop-2-yn-1-yloxy)tetrahydro-2*H*-pyran-3,5-diy l diacetate (EH 1275 Ac)**

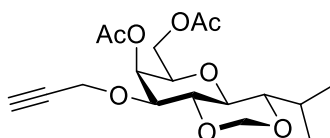
1-Isopropyl- $\beta$ -D-thiogalactopyranose (100 mg, 0.42 mmol) was stirred in refluxing MeOH (3 mL), with Bu<sub>2</sub>SnO (209 mg, 0.84 mmol) for 2 h under nitrogen. The solvent was removed under reduced pressure and the dry dibutylstannylene complex was treated with tetra butyl ammonium iodide (155 mg, 0.42 mmol) and propargyl bromide (80% wt. in toluene) (0.22 mL, 2.37 mmol) in toluene (4 mL) at 80°C for 30h. The solvent was then removed under reduced pressure. The crude reaction mixture was dissolved in Ac<sub>2</sub>O (3 mL) and pyridine (3 mL) and stirred overnight. The reaction mixture was diluted with EtOAc, washed with 1 M HCl, water and brine, dried over Na<sub>2</sub>SO<sub>4</sub>, filtered and concentrated. Flash chromatography (cyclohexane-EtOAc 3:2) provided the product (80 mg, 47% over two steps) as a white solid.; <sup>1</sup>H-NMR (400 MHz, CDCl<sub>3</sub>)  $\delta$  5.42 (dd,  $J$  = 3.5, 1.2 Hz, 1H, H-4), 5.06 (t,  $J$  = 9.8 Hz, 1H, H-2), 4.55 (d,  $J$  = 10.1 Hz, 1H, H-1), 4.18 (d,  $J$  = 2.4 Hz, 2H, CHH & CHH), 4.15 (dd,  $J$  = 11.6, 7.2 Hz, 1H, H-6a), 4.11 (dd,  $J$  = 11.6, 6.1 Hz, 1H, H-6b), 3.87 – 3.80 (overlapping signals, 2H, H-3 & H-5), 3.17 (hept,  $J$  = 6.7 Hz, 1H, isopropyl CH), 2.43 (t,  $J$  = 2.3 Hz, 1H, C $\equiv$ C-*H*), 2.12 (s, 3H), 2.08 (s, 3H), 2.04 (s, 3H) (each OAc), 1.30 (d,  $J$  = 5.2 Hz, 3H), 1.29 (d,  $J$  = 5.4 Hz, 3H) (each CH<sub>3</sub>); <sup>13</sup>C NMR (101 MHz, CDCl<sub>3</sub>)  $\delta$  170.62, 170.57, 169.75 (each C=O), 83.78 (H-1), 79.21 (C $\equiv$ C-H), 77.42, 77.10, 76.88 (C-3), 76.78, 75.12 (C $\equiv$ C-H), 74.58 (C-5), 68.70 (C-2), 65.88 (C-4), 62.25 (C-6), 56.55 (CH<sub>2</sub>-C $\equiv$ C-H), 35.49 (C-2'), 24.09, 23.82 (each CH<sub>3</sub>), 21.08, 20.89, 20.80 (each OCH<sub>3</sub>).



**(2*R*,3*S*,4*R*,5*S*,6*S*)-2-(Acetoxymethyl)-6-isobutyl-4-(prop-2-yn-1-yloxy)tetrahydro-2*H*-pyran-3,5-diy l diacetate (EH 1278 Ac)**

**EH 1208** (430 mg, 1.95 mmol) was stirred in refluxing MeOH (10 mL), with Bu<sub>2</sub>SnO (973 mg, 3.9 mmol) for 2 h under nitrogen. The solvent was removed under reduced pressure and the dry dibutylstannylene complex was treated with tetra butyl ammonium iodide (722 mg,

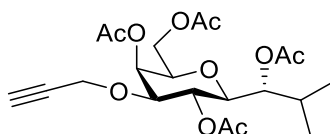
1.95 mmol) and propargyl bromide (80% wt. in toluene) (1.05 mL, 11.1 mmol) in toluene (10 mL) at 80°C for 30h. The solvent was then removed under reduced pressure. The crude reaction mixture was dissolved in Ac<sub>2</sub>O (5 mL) and pyridine (5 mL) and stirred overnight. The reaction mixture was diluted with EtOAc, washed with 1 M HCl, water and brine, dried over Na<sub>2</sub>SO<sub>4</sub>, filtered and concentrated. Flash chromatography (cyclohexane-EtOAc 3:2) provided the product (300 mg, 40% over two steps) as a white solid.; <sup>1</sup>H-NMR (400 MHz, CDCl<sub>3</sub>) δ 5.39 (dd, *J* = 3.5, 1.2 Hz, 1H, H-4), 4.89 (t, *J* = 9.6 Hz, 1H, H-2), 4.16 (d, *J* = 2.4 Hz, 2H, CHH & CHH), 4.12 (dd, *J* = 11.3, 7.1 Hz, 1H, H-6a), 4.05 (dd, *J* = 11.3, 6.2 Hz, 1H, H-6b), 3.77 – 3.72 (overlapping signals, 2H, H-3 & H-5), 3.37 (td, *J* = 10.0, 2.4 Hz, 1H, H-1), 2.40 (t, *J* = 2.4 Hz, 1H, C≡C-H), 2.11 (s, 3H), 2.07 (s, 3H), 2.03 (s, 3H) (each OAc), 1.81 (dddd, *J* = 16.2, 9.6, 7.8, 3.4 Hz, 1H, isopropyl CH), 1.50 (ddd, *J* = 14.4, 10.1, 4.5 Hz, 1H, CHH), 1.20 (ddd, *J* = 14.2, 9.6, 2.4 Hz, 1H, CHH), 0.89 (d, *J* = 6.7 Hz, 3H), 0.85 (d, *J* = 6.6 Hz, 3H) (each CH<sub>3</sub>); <sup>13</sup>C-NMR (101 MHz, CDCl<sub>3</sub>) δ 170.65, 170.22 (each C=O), 79.48 (C≡C-H), 77.43, 77.11, 77.09 (C-3), 76.79, 76.70 (C-1), 74.83 (C≡C-H), 74.37 (C-5), 71.00 (C-2), 66.21 (C-4), 62.32 (C-6), 56.33 (CH<sub>2</sub>-C≡C-H), 40.37 (C-1'), 24.37 (C-2'), 23.56, 21.54 (each CH<sub>3</sub>), 21.11, 20.93, 20.80 (each OCH<sub>3</sub>); HRMS calcd. for C<sub>19</sub>H<sub>28</sub>O<sub>8</sub>Na [M+Na]<sup>+</sup> 407.1676 found *m/z* 407.1676.



**((4*S*,4*aS*,6*R*,7*S*,8*R*,8*aR*)-7-Acetoxy-4-isopropyl-8-(prop-2-yn-1-yloxy)hexahydropyrano[3,2-*d*][1,3]dioxin-6-yl)methyl acetate (EH 1280 Ac)**

**EH 145 O/R** (30 mg, 0.11 mmol) was stirred in refluxing MeOH (20 mL), with Bu<sub>2</sub>SnO (42 mg, 0.17 mmol) for 2 h under nitrogen. The solvent was removed under reduced pressure and the dry dibutylstannylene complex was treated with tetra butyl ammonium iodide (42 mg, 0.11 mmol) and propargyl bromide (80% wt. in toluene) (0.05 mL, 0.68 mmol) in toluene (3 mL) at 80°C for 30h. The solvent was then removed under reduced pressure. The crude reaction mixture was dissolved in Ac<sub>2</sub>O (2 mL) and pyridine (2 mL) and stirred overnight. The reaction mixture was diluted with EtOAc, washed with 1 M HCl, water and brine, dried over Na<sub>2</sub>SO<sub>4</sub>, filtered and concentrated. Flash chromatography (cyclohexane-EtOAc 3:2) provided the

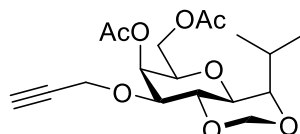
product (26 mg, 59% over two steps) as a white solid.;  $^1\text{H-NMR}$  (500 MHz,  $\text{CDCl}_3$ )  $\delta$  5.45 (dd,  $J = 3.5, 1.3$  Hz, 1H, H-4), 5.09 (d,  $J = 6.3$  Hz, 1H), 4.70 (d,  $J = 6.3$  Hz, 1H) (each methylene  $\text{CH}_2$ ), 4.30 (dd,  $J = 16.1, 2.5$  Hz, 1H,  $\text{CHH}$ ), 4.27 (dd,  $J = 16.2, 2.4$  Hz, 1H,  $\text{CHH}$ ), 4.10 (dd,  $J = 11.4, 7.2$  Hz, 1H, H-6a), 4.04 (dd,  $J = 11.4, 6.0$  Hz, 1H, H-6b), 3.89 (dd,  $J = 9.8, 3.5$  Hz, 1H, H-3), 3.85 (td,  $J = 7.2, 6.0, 1.3$  Hz, 1H, H-5), 3.65 (t,  $J = 9.5$  Hz, 1H, H-2), 3.39 (dd,  $J = 9.3, 3.1$  Hz, 1H, H-1'), 3.18 (t,  $J = 9.2$  Hz, 1H, H-1), 2.47 (t,  $J = 2.4$  Hz, 1H,  $\text{C}\equiv\text{C-H}$ ), 2.12 (s, 3H), 2.04 (s, 3H) (each OAc), 2.02 (dddd,  $J = 13.9, 10.1, 7.0, 3.0$  Hz, 1H, isopropyl CH), 0.99 (d,  $J = 7.1$  Hz, 3H), 0.93 (d,  $J = 6.9$  Hz, 3H) (each  $\text{CH}_3$ );  $^{13}\text{C-NMR}$  (126 MHz,  $\text{CDCl}_3$ )  $\delta$  170.47, 170.20 (each  $\text{C}=\text{O}$ ), 93.84 (methylene  $\text{CH}_2$ ), 82.36 ( $\text{C-1}'$ ), 78.96 ( $\text{C}\equiv\text{C-H}$ ), 77.27, 77.02, 76.84 ( $\text{C-2}$ ), 76.77 (each  $\text{CDCl}_3$ ), 75.65 ( $\text{C}\equiv\text{C-H}$ ), 75.43 ( $\text{C-3}$ ), 75.24 ( $\text{C-5}$ ), 74.05 ( $\text{C-1}$ ), 66.88 ( $\text{C-4}$ ), 62.00 ( $\text{C-6}$ ), 56.84 ( $\text{CHH}$ ), 28.41 ( $\text{C-1}'$ ), 20.73, 20.67 (each  $\text{OCH}_3$ ), 18.85, 15.98 (each  $\text{CH}_3$ ); HRMS calcd. for  $\text{C}_{18}\text{H}_{26}\text{O}_8\text{Na}$   $[\text{M}+\text{Na}]^+$  393.1520 found  $m/z$  393.1524.



**(2*S*,3*R*,4*S*,5*S*,6*R*)-2-((*S*)-1-Acetoxy-2-methylpropyl)-6-(acetoxymethyl)-4-(prop-2-yn-1-yloxy)tetrahydro-2*H*-pyran-3,5-diyl diacetate (EH 1281 Ac)**

**EH 1104 H<sub>2</sub>** (65 mg, 0.27 mmol) was stirred in refluxing MeOH (3 mL), with  $\text{Bu}_2\text{SnO}$  (137 mg, 0.55 mmol) for 2 h under nitrogen. The solvent was removed under reduced pressure and the dry dibutylstannylene complex was treated with tetra butyl ammonium iodide (102 mg, 0.27 mmol) and propargyl bromide (80% wt. in toluene) (0.15 mL, 1.55 mmol) in toluene (3 mL) at  $80^\circ\text{C}$  for 30h. The solvent was then removed under reduced pressure. The crude reaction mixture was dissolved in  $\text{Ac}_2\text{O}$  (3 mL) and pyridine (3 mL) and stirred overnight. The reaction mixture was diluted with EtOAc, washed with 1 M HCl, water and brine, dried over  $\text{Na}_2\text{SO}_4$ , filtered and concentrated. Flash chromatography (cyclohexane-EtOAc 3:2) provided the product (40 mg, 36% over two steps) as a white solid.;  $^1\text{H-NMR}$  (500 MHz,  $\text{CDCl}_3$ )  $\delta$  5.39 (dd,  $J = 3.4, 1.1$  Hz, 1H, H-4), 5.17 (t,  $J = 9.8$  Hz, 1H, H-2), 4.80 (dd,  $J = 6.5, 3.2$  Hz, 1H, H-1'), 4.18 (d,  $J = 2.4$  Hz, 2H,  $\text{CHH}$  &  $\text{CHH}$ ), 4.12 (dd,  $J = 11.3, 6.7$  Hz, 1H, H-6a), 4.07 (dd,  $J = 11.3, 6.6$  Hz, 1H, H-6b), 3.79 – 3.73 (overlapping signals, 2H, H-3 & H-5), 3.60 (dd,  $J = 10.2, 3.2$  Hz, 1H, H-1), 2.42 (t,  $J = 2.4$  Hz, 1H,  $\text{C}\equiv\text{C-H}$ ), 2.12 (s, 3H), 2.10 (s, 3H), 2.07 (s,

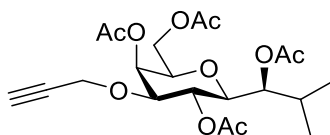
3H), 2.05 (s, 3H) (each OAc), 0.98 (d,  $J = 6.8$  Hz, 3H), 0.91 (d,  $J = 6.8$  Hz, 3H) (each CH<sub>3</sub>); <sup>13</sup>C-NMR (126 MHz, CDCl<sub>3</sub>)  $\delta$  170.50, 170.40, 170.36, 169.95 (each C=O), 78.45 (C-1), 77.26, 77.19 (C-3), 77.00, 76.94 (C-1'), 76.75 (each CDCl<sub>3</sub>), 74.91 (C $\equiv$ C-H), 74.07 (C-5), 68.00 (C-2), 65.61 (C-4), 61.93 (C-6), 56.17 (CHH), 28.83 (C-2'), 21.02, 20.93, 20.77, 20.71 (each OCH<sub>3</sub>), 19.27, 18.21 (each CH<sub>3</sub>).



**((4R,4aS,6R,7S,8R,8aR)-7-Acetoxy-4-isopropyl-8-(prop-2-yn-1-yloxy)hexahydropyrano[3,2-d][1,3]dioxin-6-yl)methyl acetate (EH 1282 Ac)**

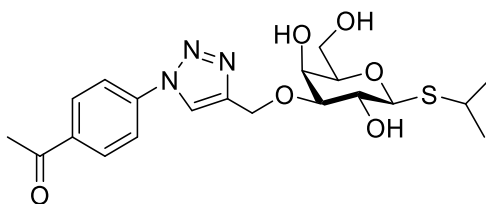
**EH 145** (20 mg, 0.08 mmol) was stirred in refluxing MeOH (3 mL), with Bu<sub>2</sub>SnO (40 mg, 0.16 mmol) for 2 h under nitrogen. The solvent was removed under reduced pressure and the dry dibutylstannylene complex was treated with tetra butyl ammonium iodide (30 mg, 0.08 mmol) and propargyl bromide (80% wt. in toluene) (0.04 mL, 0.45 mmol) in toluene (3 mL) at 80°C for 30h. The solvent was then removed under reduced pressure. The crude reaction mixture was dissolved in Ac<sub>2</sub>O (3 mL) and pyridine (3 mL) and stirred overnight. The reaction mixture was diluted with EtOAc, washed with 1 M HCl, water and brine, dried over Na<sub>2</sub>SO<sub>4</sub>, filtered and concentrated. Flash chromatography (cyclohexane-EtOAc 3:2) provided the product (15 mg, 52% over two steps) as a white solid; <sup>1</sup>H-NMR (500 MHz, CDCl<sub>3</sub>)  $\delta$  5.44 (dd,  $J = 3.5, 1.3$  Hz, 1H, H-4), 4.82 (d,  $J = 7.3$  Hz, 1H), 4.81 (d,  $J = 7.3$  Hz, 1H) (each methylene CH<sub>2</sub>), 4.31 (dd,  $J = 16.1, 2.5$  Hz, 1H, CHH), 4.27 (dd,  $J = 16.1, 2.3$  Hz, 1H, CHH), 4.07 (dd,  $J = 11.3, 6.7$  Hz, 1H, H-6a), 4.05 (dd,  $J = 11.3, 6.3$  Hz, 1H, H-6b), 3.93 (t,  $J = 9.6$  Hz, 1H, H-2), 3.84 (dd,  $J = 9.4, 3.4$  Hz, 1H, H-3), 3.81 (td,  $J = 6.6, 1.3$  Hz, 1H, H-5), 3.76 (dd,  $J = 9.8, 5.7$  Hz, 1H, H-1), 3.70 (dd,  $J = 10.2, 5.7$  Hz, 1H, H-1'), 2.47 (t,  $J = 2.4$  Hz, 1H, C $\equiv$ C-H), 2.39 (m, 1H, isopropyl CH), 2.12 (s, 3H), 2.05 (s, 3H) (each OAc), 1.01 (d,  $J = 6.5$  Hz, 3H), 0.98 (d,  $J = 6.6$  Hz, 3H) (each CH<sub>3</sub>); <sup>13</sup>C-NMR (126 MHz, CDCl<sub>3</sub>)  $\delta$  170.54, 170.21 (each C=O), 87.96 (methylene CH<sub>2</sub>), 78.95 (C $\equiv$ C-H), 78.42 (C-1'), 77.26, 77.01, 76.75, 76.36 (C-3), 75.98 (C-1), 75.41 (C $\equiv$ C-H), 75.05 (C-5), 71.68 (C-2), 66.77 (C-4), 62.03 (C-6), 56.77 (CH<sub>2</sub>), 24.91 (C-2'), 20.72, 20.71 (each OCH<sub>3</sub>), 20.33, 19.57 (each CH<sub>3</sub>); HRMS calcd. for C<sub>18</sub>H<sub>26</sub>O<sub>8</sub>Na [M+Na]<sup>+</sup> 393.1520 found m/z 393.1521.





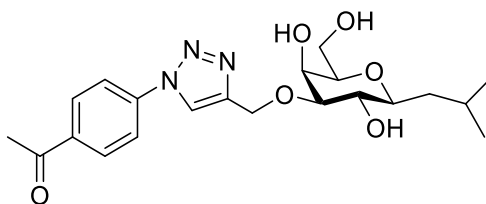
**(2*S*,3*R*,4*S*,5*S*,6*R*)-2-((*R*)-1-Acetoxy-2-methylpropyl)-6-(acetoxymethyl)-4-(prop-2-yn-1-yloxy)tetrahydro-2*H*-pyran-3,5-diyl diacetate (EH 1283 Ac)**

**EH 124 H<sub>2</sub>** (25 mg, 0.11 mmol) was stirred in refluxing MeOH (3 mL), with Bu<sub>2</sub>SnO (53 mg, 0.21 mmol) for 2 h under nitrogen. The solvent was removed under reduced pressure and the dry dibutylstannylene complex was treated with tetra butyl ammonium iodide (40 mg, 0.11 mmol) and propargyl bromide (80% wt. in toluene) (0.06 mL, 0.61 mmol) in toluene (3 mL) at 80°C for 30 h. The solvent was then removed under reduced pressure. The crude reaction mixture was dissolved in Ac<sub>2</sub>O (3 mL) and pyridine (3 mL) and stirred overnight. The reaction mixture was diluted with EtOAc, washed with 1 M HCl, water and brine, dried over Na<sub>2</sub>SO<sub>4</sub>, filtered and concentrated. Flash chromatography (cyclohexane-EtOAc 3:2) provided the product (17 mg, 36% over two steps) as a white solid.; <sup>1</sup>H-NMR (500 MHz, CDCl<sub>3</sub>) δ 5.43 (dd, *J* = 3.5, 1.1 Hz, 1H, H-4), 5.12 (t, *J* = 9.8 Hz, 1H, H-2), 4.80 (dd, *J* = 9.8, 2.5 Hz, 1H, H-3), 4.24 – 4.04 (overlapping signals, 4H, *CHH*, *CHH*. H-6a & H-6b), 3.84 – 3.74 (overlapping signals, 2H, H-3 & H-5), 3.62 (dd, *J* = 10.0, 2.6 Hz, 1H, H-1), 2.42 (t, *J* = 2.3 Hz, 1H, C≡C-*H*), 2.16 (s, 3H), 2.10 (s, 3H), 2.05 (s, 3H), 2.04 (s, 3H) (each OAc), 0.95 (d, *J* = 6.8 Hz, 3H), 0.88 (d, *J* = 6.8 Hz, 3H) (each CH<sub>3</sub>); <sup>13</sup>C-NMR (126 MHz, CDCl<sub>3</sub>) δ 170.95, 170.55, 170.50, 169.75 (each C=O), 79.20 (C≡C-H), 77.48 (C-3), 77.29 (C-1), 77.26, 77.00, 76.75 (each CDCl<sub>3</sub>), 75.63 (C-5), 74.91 ((C≡C-H), 74.23 (C-1'), 65.99 (C-4), 65.95 (C-2), 62.25 (C-6), 56.33 (CH<sub>2</sub>), 29.68, 28.56 (C-2'), 20.93, 20.89, 20.66 (each OCH<sub>3</sub>), 19.27, 18.39 (each CH<sub>3</sub>).



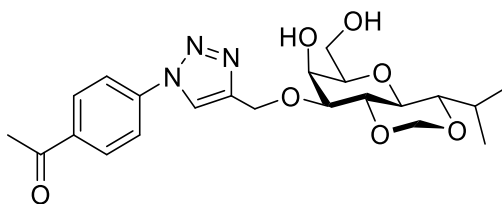
**1-(4-(4-(((2R,3S,4S,5R,6S)-3,5-Dihydroxy-2-(hydroxymethyl)-6-(isopropylthio)tetrahydro-2H-pyran-4-yl)oxy)methyl)-1H-1,2,3-triazol-1-yl)phenyl)ethan-1-one (EH 1284)**

**EH 1275 Ac** (30 mg, 0.07 mmol) was dissolved in a 4:1 mixture of DMF:H<sub>2</sub>O (5 mL). *p*-Azidoacetophenone (18 mg, 0.11 mmol) was added followed by sodium ascorbate (16 mg, 0.08 mmol) and copper sulfate pentahydrate (17 mg, 0.07 mmol) and the reaction mixture was heated to 80°C and stirred for 1 h, after which TLC analysis indicated complete consumption of the starting material. The reaction mixture was then diluted with EtOAc, filtered, washed with water and brine, dried over Na<sub>2</sub>SO<sub>4</sub>, filtered and concentrated. The crude product was dissolved in MeOH, NaOMe (2 mg, 0.04 mmol) was added and the reaction mixture was stirred overnight. The reaction mixture was then neutralized using Dowex (H<sup>+</sup>) resin, filtered and concentrated. Flash chromatography (CH<sub>2</sub>Cl<sub>2</sub>-MeOH 9:1) provided the product (21 mg, 60% over two steps) as a white solid.; <sup>1</sup>H-NMR (500 MHz, CD<sub>3</sub>OD) δ 8.67 (s, 1H), 8.20 (d, *J* = 8.7 Hz, 2H), 8.02 (d, *J* = 8.7 Hz, 2H) (each Ar-H), 4.95 (d, *J* = 12.5 Hz, 1H, *CHH*), 4.89 (overlapping signals, 1H, *CHH*) 4.44 (d, *J* = 9.8 Hz, 1H, H-1), 4.16 (d, *J* = 3.2 Hz, 1H, H-4), 3.75 (dd, *J* = 11.4, 6.7 Hz, 1H, H-6a), 3.71 (dd, *J* = 11.3, 5.7 Hz, 1H, H-6b), 3.68 (t, *J* = 9.4 Hz, 1H, H-2), 3.53 (bt, *J* = 6.1 Hz, 1H, H-5), 3.47 (dd, *J* = 9.1, 3.2 Hz, 1H, H-3), 3.24 (p, *J* = 6.8 Hz, 1H, isopropyl CH), 2.66 (s, 3H, C=OCH<sub>3</sub>), 1.31 (d, *J* = 7.1 Hz, 3H), 1.30 (d, *J* = 7.5 Hz, 3H) (each CH<sub>3</sub>); <sup>13</sup>C-NMR (126 MHz, CD<sub>3</sub>OD) δ 197.63 (C=O), 146.32, 140.09, 136.88, 129.92, 121.78, 119.79 (each Ar-C/ C-H), 85.60 (C-1), 82.82 (C-3), 78.88 (C-5), 69.35 (C-2), 65.89 (C-4), 62.23 (CH<sub>2</sub>), 61.13 (C-6), 34.37 (C-2'), 25.37 (C=OCH<sub>3</sub>), 22.98, 22.90 (each CH<sub>3</sub>).



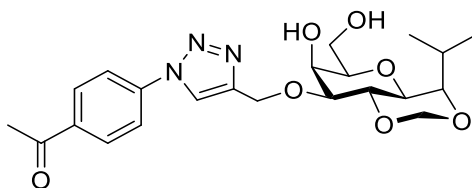
**1-(4-(4-(((2R,3S,4R,5S,6S)-3,5-Dihydroxy-2-(hydroxymethyl)-6-isobutyltetrahydro-2H-pyran-4-yl)oxy)methyl)-1H-1,2,3-triazol-1-yl)phenyl)ethan-1-one (EH 1285)**

**EH 1278 Ac** (30 mg, 0.08 mmol) was dissolved in a 4:1 mixture of DMF:H<sub>2</sub>O (5 mL). *p*-Azidoacetophenone (19 mg, 0.12 mmol) was added followed by sodium ascorbate (17 mg, 0.08 mmol) and copper sulfate pentahydrate (18 mg, 0.07 mmol) and the reaction mixture was heated to 80°C and stirred for 1 h, after which TLC analysis indicated complete consumption of the starting material. The reaction mixture was then diluted with EtOAc, filtered, washed with water and brine, dried over Na<sub>2</sub>SO<sub>4</sub>, filtered and concentrated. The crude product was dissolved in MeOH, NaOMe (2.0 mg, 0.04 mmol) was added and the reaction mixture was stirred overnight. The reaction mixture was then neutralized using Dowex (H<sup>+</sup>) resin, filtered and concentrated. Flash chromatography (CH<sub>2</sub>Cl<sub>2</sub>-MeOH 9:1) provided the product (23 mg, 68% over two steps) as a white solid.; <sup>1</sup>H-NMR (500 MHz, CD<sub>3</sub>OD) δ 8.67 (s, 1H), 8.21 (d, *J* = 8.8 Hz, 2H), 8.03 (d, *J* = 8.8 Hz, 2H) (each Ar-H), 4.94 (d, *J* = 12.6 Hz, 1H, *CHH*), 4.94 (overlapping signals, 1H, *CHH*), 4.16 (dd, *J* = 3.1, 1.1 Hz, 1H, H-4), 3.72 (dd, *J* = 11.2, 6.3 Hz, 1H, H-6a), 3.69 (dd, *J* = 11.9, 6.0 Hz, 1H, H-6b), 3.49 (t, *J* = 9.3 Hz, 1H, H-2), 3.43 (td, *J* = 6.1, 1.1 Hz, 1H, H-5), 3.40 (dd, *J* = 9.3, 3.2 Hz, 1H, H-3), 3.19 (td, *J* = 9.8, 2.1 Hz, 1H, H-1), 2.66 (s, 3H, C=OCH<sub>3</sub>), 1.92 (dddd, *J* = 13.7, 10.9, 6.7, 4.2 Hz, 1H, isopropyl CH), 1.64 (ddd, *J* = 14.1, 9.8, 2.1 Hz, 1H, *CHH*), 1.42 (ddd, *J* = 14.2, 9.9, 4.3 Hz, 1H, *CHH*), 0.94 (d, *J* = 6.7 Hz, 3H), 0.90 (d, *J* = 6.6 Hz, 3H) (each CH<sub>3</sub>); <sup>13</sup>C-NMR (126 MHz, CD<sub>3</sub>OD) δ 197.51 (C=O), 146.41, 136.90, 129.90, 121.70, 119.77 (each Ar-C/ C-H), 83.22 (C-3), 78.46 (C-5), 78.34 (C-1), 70.68 (C-2), 65.84 (C-4), 61.82 (*CHH*), 61.26 (C-6), 40.75 (*CHH*), 25.34 (C=OCH<sub>3</sub>), 24.09 (C-2'), 22.87, 20.66 (each CH<sub>3</sub>); HRMS calcd. for C<sub>21</sub>H<sub>29</sub>N<sub>3</sub>O<sub>6</sub>Na [M+Na]<sup>+</sup> 442.1948 found *m/z* 442.1946.



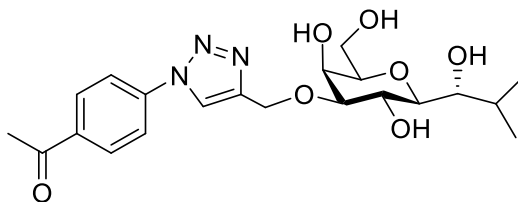
**1-(4-(4-(((4S,4aS,6R,7S,8S,8aR)-7-Hydroxy-6-(hydroxymethyl)-4-isopropylhexahydropyrano[3,2-d][1,3]dioxin-8-yl)oxy)methyl)-1H-1,2,3-triazol-1-yl)phenyl)ethan-1-one (EH 1286)**

**EH 1280 Ac** (25 mg, 0.07 mmol) was dissolved in a 4:1 mixture of DMF:H<sub>2</sub>O (5 mL). *p*-Azidoacetophenone (16 mg, 0.1 mmol) was added followed by sodium ascorbate (15 mg, 0.07 mmol) and copper sulfate pentahydrate (15 mg, 0.06 mmol) and the reaction mixture was heated to 80°C and stirred for 1 h, after which TLC analysis indicated complete consumption of the starting material. The reaction mixture was then diluted with EtOAc, filtered, washed with water and brine, dried over Na<sub>2</sub>SO<sub>4</sub>, filtered and concentrated. The crude product was dissolved in MeOH, NaOMe (2 mg, 0.04 mmol) was added and the reaction mixture was stirred overnight. The reaction mixture was then neutralized using Dowex (H<sup>+</sup>) resin, filtered and concentrated. Flash chromatography (CH<sub>2</sub>Cl<sub>2</sub>-MeOH 9:1) provided the product (10 mg, 34% over two steps) as a white solid.; <sup>1</sup>H-NMR (500 MHz, CD<sub>3</sub>OD) δ 8.64 (s, 1H), 8.18 (d, *J* = 8.8 Hz, 2H), 8.00 (d, *J* = 8.8 Hz, 2H) (each Ar-H), 5.03 (d, *J* = 6.2 Hz, 1H, methylene CHH), 4.91 (s, 2H, CHH & CHH), 4.71 (d, *J* = 6.2 Hz, 1H, methylene CHH), 4.17 (dd, *J* = 3.1, 1.2 Hz, 1H, H-4), 3.79 – 3.72 (overlapping signals, 1H, H-2), 3.55 (td, *J* = 6.7, 5.4, 1.3 Hz, 1H, H-5), 3.39 (dd, *J* = 9.3, 2.8 Hz, 1H, H-1'), 3.14 (t, *J* = 9.1 Hz, 1H, H-1), 2.65 (s, 3H, C=OCH<sub>3</sub>), 2.09 (pd, *J* = 7.0, 2.7 Hz, 1H, isopropyl CH), 1.00 (d, *J* = 7.1 Hz, 3H), 0.92 (d, *J* = 7.0 Hz, 3H) (each CH<sub>3</sub>); <sup>13</sup>C-NMR (126 MHz, CD<sub>3</sub>OD) δ 197.48 (C=O), 140.06, 136.85, 129.89, 121.74, 119.75 (each Ar-C/ C-H), 93.36 (methylene CH<sub>2</sub>), 82.60 (C-1'), 79.58 (C-5), 79.33 (C-3), 77.93 (C-2), 73.57 (C-1), 67.10 (C-4), 62.44 (CHH), 61.18 (C-6), 27.74 (C-2'), 25.36 (C=OCH<sub>3</sub>), 18.21, 14.65 (each CH<sub>3</sub>).



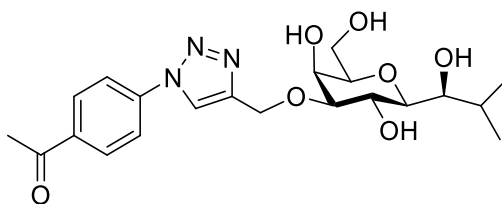
**1-(4-(4-(((4R,4aS,6R,7S,8S,8aR)-7-Hydroxy-6-(hydroxymethyl)-4-isopropylhexahydropyrano[3,2-*d*][1,3]dioxin-8-yl)oxy)methyl)-1H-1,2,3-triazol-1-yl)phenyl)ethan-1-one (EH 1287)**

**EH 1282 Ac** (15 mg, 0.04 mmol) was dissolved in a 4:1 mixture of DMF:H<sub>2</sub>O (3 mL). *p*-Azidoacetophenone (10 mg, 0.06 mmol) was added followed by sodium ascorbate (9 mg, 0.04 mmol) and copper sulfate pentahydrate (9 mg, 0.03 mmol) and the reaction mixture was heated to 80°C and stirred for 1 h, after which TLC analysis indicated complete consumption of the starting material. The reaction mixture was then diluted with EtOAc, filtered, washed with water and brine, dried over Na<sub>2</sub>SO<sub>4</sub>, filtered and concentrated. The crude product was dissolved in MeOH, NaOMe (2.0 mg, 0.04 mmol) was added and the reaction mixture was stirred overnight. The reaction mixture was then neutralized using Dowex (H<sup>+</sup>) resin, filtered and concentrated. Flash chromatography (CH<sub>2</sub>Cl<sub>2</sub>-MeOH 9:1) provided the product (10 mg, 57% over two steps) as a white solid.; <sup>1</sup>H-NMR (500 MHz, CDCl<sub>3</sub>) δ 8.13 (d, *J* = 8.3 Hz, 2H), 7.86 (d, *J* = 8.3 Hz, 2H) (each Ar-H), 5.02 (d, *J* = 12.8 Hz, 1H, *CHH*), 4.90 (d, *J* = 12.8 Hz, 1H, *CHH*), 4.84 (d, *J* = 6.6 Hz, 1H), 4.82 (d, *J* = 6.6 Hz, 1H) (each methylene CH<sub>2</sub>), 4.27 (d, *J* = 3.5 Hz, 1H, H-4), 4.09 (t, *J* = 9.2 Hz, 1H, H-2), 3.93 (dd, *J* = 11.8, 6.0 Hz, 1H, H-6a), 3.82 (dd, *J* = 11.6, 4.3 Hz, 1H, H-6b), 3.76 – 3.69 (overlapping signals, 2H, H-1 & H-1'), 3.68 (dd, *J* = 9.3, 2.7 Hz, 1H, H-3), 3.55 (t, *J* = 5.4 Hz, 1H, H-5), 2.66 (s, 3H, C=OCH<sub>3</sub>), 2.43 (ddd, *J* = 16.4, 13.1, 10.0, 6.4 Hz, 1H, isopropyl CH), 1.07 (d, *J* = 6.4 Hz, 3H), 0.98 (d, *J* = 6.6 Hz, 3H) (each CH<sub>3</sub>); <sup>13</sup>C-NMR (126 MHz, CDCl<sub>3</sub>) δ 196.49 (C=O), 137.03, 130.15, 120.12 (each Ar-C/ C-H), 87.87 (methylene CH<sub>2</sub>), 80.15 (C-3), 78.69 (C-1'), 78.32 (C-5), 77.26, 77.21, 77.00, 76.75 (each CDCl<sub>3</sub>), 75.76 (C-1), 72.28 (C-2), 67.87 (C-4), 63.06 (C-6), 62.77 (*CHH*), 26.68 (C=OCH<sub>3</sub>), 24.90 (C-2'), 20.61, 19.58 (each CH<sub>3</sub>); HRMS calcd. for C<sub>22</sub>H<sub>29</sub>N<sub>3</sub>O<sub>7</sub>Na [M+Na]<sup>+</sup> 470.1898 found *m/z* 470.1899.



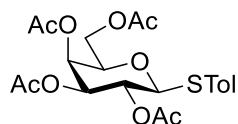
**1-(4-(4-(((2*S*,3*R*,4*S*,5*S*,6*R*)-3,5-Dihydroxy-2-((*S*)-1-hydroxy-2-methylpropyl)-6-(hydroxymethyl)tetrahydro-2*H*-pyran-4-yl)oxy)methyl)-1*H*-1,2,3-triazol-1-yl)phenyl)ethan-1-one (EH 1288)**

**EH 1281 Ac** (30 mg, 0.07 mmol) was dissolved in a 4:1 mixture of DMF:H<sub>2</sub>O (5 mL). *p*-Azidoacetophenone (17 mg, 0.1 mmol) was added followed by sodium ascorbate (15 mg, 0.07 mmol) and copper sulfate pentahydrate (15 mg, 0.06 mmol) and the reaction mixture was heated to 80°C and stirred for 1 h, after which TLC analysis indicated complete consumption of the starting material. The reaction mixture was then diluted with EtOAc, filtered, washed with water and brine, dried over Na<sub>2</sub>SO<sub>4</sub>, filtered and concentrated. The crude product was dissolved in MeOH, NaOMe (2 mg, 0.04 mmol) was added and the reaction mixture was stirred overnight. The reaction mixture was then neutralized using Dowex (H<sup>+</sup>) resin, filtered and concentrated. Flash chromatography (CH<sub>2</sub>Cl<sub>2</sub>-MeOH 9:1) provided the product (18 mg, 57% over two steps) as a white solid.; <sup>1</sup>H-NMR (500 MHz, CD<sub>3</sub>OD) δ 8.68 (s, 1H), 8.20 (d, *J* = 8.7 Hz, 2H), 8.02 (d, *J* = 8.7 Hz, 2H) (each Ar-H), 4.95 (d, *J* = 12.5 Hz, 1H, *CHH*), 4.84 (d, *J* = 12.5 Hz, 1H, *CHH*), 4.14 (dd, *J* = 3.1, 1.1 Hz, 1H, H-4), 3.93 (t, *J* = 9.3 Hz, 1H, H-2), 3.74 (dd, *J* = 11.4, 7.0 Hz, 1H, H-6a), 3.67 (dd, *J* = 11.3, 5.1 Hz, 1H, H-6b), 3.65 – 3.61 (m, 1H, H-1'), 3.51 – 3.42 (overlapping signals, 2H, H-3 & H-5), 3.26 (dd, *J* = 9.4, 6.0 Hz, 1H, H-1), 2.66 (s, 3H, C=OCH<sub>3</sub>), 2.09 (pd, *J* = 6.9, 4.1 Hz, 1H, isopropyl CH), 0.97 (d, *J* = 7.0 Hz, 3H), 0.93 (d, *J* = 6.8 Hz, 3H) (each CH<sub>3</sub>); <sup>13</sup>C-NMR (126 MHz, CD<sub>3</sub>OD) δ 197.48 (C=O), 146.36, 140.09, 136.89, 129.90, 121.73, 119.75 (each Ar-C/ C-H), 83.21 (C-3), 79.16 (C-1), 78.89 (C-5), 77.73 (C-1'), 69.50 (C-2), 65.73 (C-4), 61.88 (*CHH*), 61.55 (C-6), 29.04 (C-2'), 25.34 (C=OCH<sub>3</sub>), 18.89, 15.44 (each CH<sub>3</sub>).



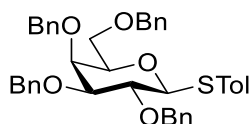
**1-(4-(4-(((2*S*,3*R*,4*S*,5*S*,6*R*)-3,5-Dihydroxy-2-((*R*)-1-hydroxy-2-methylpropyl)-6-(hydroxymethyl)tetrahydro-2*H*-pyran-4-yl)oxy)methyl)-1*H*-1,2,3-triazol-1-yl)phenyl)ethan-1-one (EH 1289)**

**EH 1283 Ac** (31 mg, 0.07 mmol) was dissolved in a 4:1 mixture of DMF:H<sub>2</sub>O (5 mL). *p*-Azidoacetophenone (17 mg, 0.1 mmol) was added followed by sodium ascorbate (15 mg, 0.08 mmol) and copper sulfate pentahydrate (16 mg, 0.06 mmol) and the reaction mixture was heated to 80°C and stirred for 1 h, after which TLC analysis indicated complete consumption of the starting material. The reaction mixture was then diluted with EtOAc, filtered, washed with water and brine, dried over Na<sub>2</sub>SO<sub>4</sub>, filtered and concentrated. The crude product was dissolved in MeOH, NaOMe (2.0 mg, 0.04 mmol) was added and the reaction mixture was stirred overnight. The reaction mixture was then neutralized using Dowex (H<sup>+</sup>) resin, filtered and concentrated. Flash chromatography (CH<sub>2</sub>Cl<sub>2</sub>-MeOH 9:1) provided the product (9 mg, 28% over two steps) as a white solid.; <sup>1</sup>H-NMR (500 MHz, CD<sub>3</sub>OD) δ 8.68 (s, 1H), 8.21 (d, *J* = 8.8 Hz, 2H), 8.03 (d, *J* = 8.8 Hz, 2H) (each Ar-H), 4.96 (d, *J* = 12.5 Hz, 1H, *CHH*), 4.85 (overlapping signal, 1H, *CHH*) 4.16 (dd, *J* = 3.2, 1.1 Hz, 1H, H-4), 3.97 (t, *J* = 9.5 Hz, 1H, H-2), 3.73 (dd, *J* = 11.4, 6.6 Hz, 1H, H-6a), 3.70 (dd, *J* = 11.3, 5.6 Hz, 1H, H-6b), 3.47 (td, *J* = 6.8, 5.7, 1.1 Hz, 1H, H-5), 3.46 (dd, *J* = 9.4, 3.1 Hz, 1H, H-3), 3.40 (dd, *J* = 8.8, 1.5 Hz, 1H, H-1'), 2.66 (s, 3H, C=OCH<sub>3</sub>), 1.95 (doublet of pentets, *J* = 8.8, 6.7 Hz, 1H, isopropyl CH), 1.03 (d, *J* = 6.7 Hz, 3H), 0.90 (d, *J* = 6.7 Hz, 3H) (each CH<sub>3</sub>); <sup>13</sup>C-NMR (126 MHz, CD<sub>3</sub>OD) δ 197.50 (C=O), 146.40, 140.11, 136.90, 129.90, 121.73, 119.77 (each Ar-C/ C-H), 83.55 (C-3), 79.17 (C-1), 78.61 (C-5), 74.14 (C-1'), 66.05 (C-4), 65.99 (C-2), 61.83 (*CHH*), 61.24 (C-6), 30.57 (C-2'), 25.34 (C=OCH<sub>3</sub>), 18.81, 18.12 (each CH<sub>3</sub>).



***para*-Tolyl 2,3,4,6-tetra-*O*-acetyl-1-thio- $\beta$ -D-galactopyranose (EH 161)**

$\text{BF}_3 \cdot \text{OEt}_2$  (4.24 mL, 34.3 mmol) was added to a mixture of **EH 1197** (5.00 g, 12.8 mmol) and *p*-thiocresol (3.18 g, 25.62 mmol) in anhydrous  $\text{CH}_2\text{Cl}_2$  (50 mL) at 0 °C. The mixture was stirred for 2 h at 0 °C before being allowed to warm to room temperature followed by continuous stirring overnight. The reaction mixture was diluted with  $\text{CH}_2\text{Cl}_2$  (100 mL), washed with saturated  $\text{NaHCO}_3$  and then with brine. It was then dried over  $\text{MgSO}_4$ , filtered, and concentrated under reduced pressure. Flash chromatography (cyclohexane-EtOAc 2:1) provided the product (4.03 g, 95%) as a syrup.;  $^1\text{H-NMR}$  (500 MHz,  $\text{CDCl}_3$ )  $\delta$  7.40 (d,  $J = 8.1$  Hz, 2H), 7.11 (d,  $J = 8.0$  Hz, 2H) (each Ar-H), 5.39 (dd,  $J = 3.5, 0.9$  Hz, 1H, H-4), 5.20 (t,  $J = 9.9$  Hz, 1H, H-2), 5.03 (dd,  $J = 10.0, 3.3$  Hz, 1H, H-3), 4.64 (d,  $J = 9.9$  Hz, 1H, H-1), 4.17 (dd,  $J = 11.3, 6.9$  Hz, 1H, H-6a), 4.10 (dd,  $J = 11.3, 6.3$  Hz, 1H, H-6b), 3.90 (t,  $J = 6.6$  Hz, 1H, H-5), 2.33 (s, 3H,  $\text{CH}_3$ ), 2.10 (s, 3H), 2.09 (s, 3H), 2.03 (s, 3H), 1.96 (s, 3H) (each OAc);  $^{13}\text{C-NMR}$  (126 MHz,  $\text{CDCl}_3$ )  $\delta$  170.36, 170.19, 170.06, 169.42 (each C=O), 138.47, 133.15, 129.63, 128.61 (each Ar-C/ C-H), 86.97 (C-1), 77.25, 76.99, 76.74, 74.35 (C-5), 72.03 (C-3), 67.30 (C-2), 67.21 (C-4), 61.57 (C-6), 21.14 ( $\text{CH}_3$ ), 20.85, 20.65, 20.61, 20.57 (each  $\text{OCH}_3$ ).



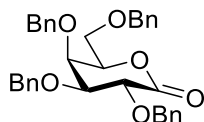
***para*-Tolyl 2,3,4,6-tetra-*O*-benzyl-1-thio- $\beta$ -D-galactopyranose (EH 162)**

**EH 161** (5.00 g, 15.1 mmol) was dissolved in dry MeOH (100 mL). NaOMe was added (580 mg, 10.7 mmol) and the reaction mixture was allowed to stir for 1 h, after which time, TLC analysis indicated disappearance of the starting material. Amberlite ( $\text{H}^+$ ) was added to neutralise the reaction mixture, which was concentrated to give free galactose. The crude galactose (2.00 g, 12.3 mmol) was dissolved in DMF and cooled to 0°C. NaH (2.2 g, 55.2 mmol) was added slowly, causing liberation of  $\text{H}_2$  and fizzing. The reaction was stirred for 10 mins followed by addition of BnBr (6.55 mL, 55.2 mmol). The reaction was allowed to warm to room temperature overnight and was eventually quenched with MeOH following indication



of product formation via TLC. The reaction mixture was extracted with EtOAc and the combined organic layers were washed with water, dried with Na<sub>2</sub>SO<sub>4</sub> and the solvent was removed under reduced pressure. Chromatography (cyclohexane-EtOAc 2:1) afforded the product as a white solid (4.8 g, 61% over two steps). *R*<sub>f</sub> 0.67 (cyclohexane-EtOAc 2:1); <sup>1</sup>H-NMR (500 MHz, CDCl<sub>3</sub>) δ 7.47 (d, *J* = 8.1 Hz, 2H), 7.44 – 7.16 (overlapping signals, 20H), 7.07 (d, *J* = 7.8 Hz, 1H), 6.99 (d, *J* = 7.9 Hz, 2H) (each Ar-H), 4.96 (d, *J* = 11.5 Hz, 1H), 4.80 (d, *J* = 10.3 Hz, 1H), 4.74 (d, *J* = 10.2 Hz, 2H), 4.71 (d, *J* = 11.7 Hz, 1H), 4.60 (d, *J* = 11.6 Hz, 1H) (each Bn-CH<sub>2</sub>), 4.59 (d, *J* = 9.7 Hz, 1H, H-1), 4.47 (d, *J* = 11.7 Hz, 1H, Bn-CH<sub>2</sub>), 4.42 (d, *J* = 11.7 Hz, 1H, Bn-CH<sub>2</sub>), 3.98 (d, *J* = 2.8 Hz, 1H, H-4), 3.90 (t, *J* = 9.4 Hz, 1H, H-2), 3.65 (overlapping signals, 2H, H-6a & H-6b), 3.63 – 3.56 (overlapping signals, 2H, H-3 & H-5), 2.29 (s, 3H, CH<sub>3</sub>); <sup>13</sup>C-NMR (126 MHz, CDCl<sub>3</sub>) δ 138.79, 138.39, 138.28, 137.90, 137.18, 136.57, 132.17, 130.71, 130.21, 129.60, 129.54, 128.82, 128.41, 128.34, 128.32, 128.16, 127.92, 127.84, 127.78, 127.70, 127.66, 127.56, 127.42, 127.06 (each Ar-C/ C-H), 88.05 (C-1), 84.22 (C-3), 77.34 (C-2), 77.27, 77.24 (C-5), 77.01, 76.76, 75.61 (Bn-CH<sub>2</sub>), 74.41 (Bn-CH<sub>2</sub>), 73.57 (C-4), 72.72 (Bn-CH<sub>2</sub>), 68.77 (C-6), 21.09 (CH<sub>3</sub>).

NMR data obtained was in good agreement with the literature.<sup>15</sup>

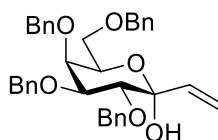


### 2,3,4,6-Tetra-*O*-benzyl-D-galactonolactone (EH 164)

**EH 162** (1.00 g, 1.91 mmol) was dissolved in Acetone:H<sub>2</sub>O (4:1) (50 mL). *N*-bromosuccinimide (374 mg, 2.1 mmol) was added at 0°C and the reaction mixture was allowed to stir at room temperature overnight, after which time TLC analysis indicated complete consumption of the starting material. The reaction mixture was then diluted with EtOAc, washed with H<sub>2</sub>O, aq. Na<sub>2</sub>S<sub>2</sub>O<sub>3</sub>, brine and dried over MgSO<sub>4</sub>. The solvent was then removed under reduced pressure. Flash chromatography (cyclohexane-EtOAc 7:3) gave the hemiacetal intermediate as a white solid (750 mg, 73%). *R*<sub>f</sub> 0.57 (cyclohexane-EtOAc 7:3); The intermediate (230 mg, 0.42 mmol) was dissolved in CH<sub>2</sub>Cl<sub>2</sub> and cooled to 0°C, Dess-Martin Periodinane (406 mg, 0.96 mmol) was added and the reaction mixture was stirred overnight, after which time TLC analysis indicated complete consumption of the starting material. The

reaction mixture was then washed with aq.  $\text{Na}_2\text{S}_2\text{O}_3$ , aq.  $\text{NaHCO}_3$ ,  $\text{H}_2\text{O}$  and brine, dried over  $\text{MgSO}_4$  and the solvent removed under reduced pressure. Flash chromatography (cyclohexane-EtOAc 7:3) provided the lactone product as a white solid (170 mg, 74%);  $R_f$  0.8 (cyclohexane-EtOAc 7:3);  $^1\text{H-NMR}$  (500 MHz,  $\text{CDCl}_3$ )  $\delta$  7.49 – 7.24 (overlapping signals, 18H, each Ar-H), 5.23 (d,  $J = 11.0$  Hz, 1H), 4.98 (d,  $J = 11.3$  Hz, 1H), 4.83 (d,  $J = 11.0$  Hz, 1H), 4.79 (d,  $J = 11.9$  Hz, 1H), 4.73 (d,  $J = 11.9$  Hz, 1H), 4.65 (d,  $J = 11.3$  Hz, 1H) (each Bn- $\text{CH}_2$ ), 4.56 – 4.46 (overlapping signals, 3H, H-2, Bn- $\text{CH}_2$  & Bn- $\text{CH}_2$ ), 4.38 (td,  $J = 7.6, 5.7, 1.6$  Hz, 1H, H-5), 4.20 (t,  $J = 2.0$  Hz, 1H, H-4), 3.93 (dd,  $J = 9.7, 2.2$  Hz, 1H, H-3), 3.75 (dd,  $J = 8.9, 8.1$  Hz, 1H, H-6a), 3.70 (dd,  $J = 9.3, 5.6$  Hz, 1H, H-6b);  $^{13}\text{C-NMR}$  (126 MHz,  $\text{CDCl}_3$ )  $\delta$  170.06 (C=O), 137.85, 137.83, 137.60, 137.46, 128.55, 128.54, 128.51, 128.41, 128.05, 128.01, 127.96, 127.93, 127.87, 127.58 (each Ar-C/ C-H), 80.16 (C-3), 77.37 (C-2), 77.35 (C-5), 75.33, 74.78, 73.69, 72.85 (each Bn- $\text{CH}_2$ ), 72.59 (C-4), 67.59 (C-6); HRMS calcd. for  $\text{C}_{34}\text{H}_{34}\text{O}_6\text{Na}$   $[\text{M}+\text{Na}]^+$  561.2247 found  $m/z$  561.2249.

NMR data obtained was in good agreement with the literature <sup>16</sup>

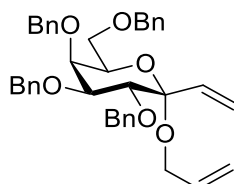


### 2,3,4,6-Tetra-*O*-benzyl-1-*C*-vinyl- $\alpha$ -D-galactopyranose (EH 1229)

**EH 164** (1.0 g, 1.85 mmol) was dissolved in THF and cooled to  $-78^\circ\text{C}$ . Vinyl Magnesium Bromide (0.1 M in THF) (22.3 mL, 2.23 mmol) was added dropwise via cannula. The reaction mixture was stirred for 3 h at  $-78^\circ\text{C}$ , after which time TLC analysis indicated complete consumption of the starting material. The reaction mixture was then quenched using a satd. aq. Solution of  $\text{NH}_4\text{Cl}$ , diluted with EtOAc and the organic layer was separated, dried over  $\text{MgSO}_4$  and the solvent removed under reduced pressure. Column chromatography (cyclohexane-EtOAc 4:1) provided the vinyl product as a syrup (301 mg, 29%);  $R_f$  0.43 (cyclohexane-EtOAc 7:3);  $^1\text{H-NMR}$  (500 MHz,  $\text{CDCl}_3$ )  $\delta$  7.43 – 7.23 (m, 25H, each Ar-H), 6.01 (dd,  $J = 17.2, 10.6$  Hz, 1H,  $\text{CH}=\text{CHH}$ ), 5.59 (dd,  $J = 17.3, 1.4$  Hz, 1H,  $\text{CH}=\text{CHH}$ ), 5.29 (dd,  $J = 10.7, 1.4$  Hz, 1H,  $\text{CH}=\text{CHH}$ ), 4.96 (d,  $J = 11.6$  Hz, 1H), 4.84 (d,  $J = 10.7$  Hz, 1H), 4.75 (d,  $J = 11.7$  Hz, 1H), 4.72 (d,  $J = 11.7$  Hz, 1H), 4.66 (d,  $J = 10.4$  Hz, 1H), 4.64 (d,  $J = 11.7$  Hz, 2H), 4.48 (d,  $J = 11.8$  Hz, 1H), 4.44 (d,  $J = 11.9$  Hz, 1H) (each Bn- $\text{CH}_2$ ), 4.19 (ddd,  $J = 7.2, 5.7, 1.3$  Hz, 1H, H-5), 4.03

(dd,  $J = 2.6, 1.3$  Hz, 1H, H-4), 3.93 (dd,  $J = 9.8, 2.5$  Hz, 1H, H-3), 3.89 (d,  $J = 9.7$  Hz, 1H, H-2), 3.61 (dd,  $J = 9.1, 7.5$  Hz, 1H, H-6a), 3.57 (dd,  $J = 9.1, 5.8$  Hz, 1H, H-6b), 2.84 (s, 1H, OH); HRMS calcd. for  $C_{36}H_{38}O_6Na$   $[M+Na]^+$  589.2560 found  $m/z$  589.2561.

NMR data obtained was in good agreement with the literature <sup>17</sup>

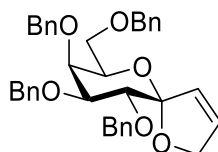


### Allyl 4,5,6,8-tetra-*O*-benzyl-1,2-dideoxy- $\alpha$ -D-galacto-oct-3-ulo-1-enopyranose (EH 1267)

18

To a flask containing Montmorillonite K-10 clay (220 mg) and powdered molecular sieves 4 Å (220 mg) (both flame-dried under vacuum) was added a mixture of **EH 1229** (109 mg, 0.19 mmol) and allyl alcohol (0.08 mL, 1.16 mmol) in anhydrous  $CH_2Cl_2$  (5 mL) under an argon atmosphere. The resulting suspension was stirred vigorously until TLC analysis indicated complete consumption of the starting material. A mixture of methanol–pyridine (5 mL, 1:1) was added and stirring was continued for 10 min. The suspension was filtered through celite and the solvent removed under reduced pressure. Column chromatography (cyclohexane–EtOAc 9:1) provided the glycosylation product as a syrup (61 mg, 52%);  $R_f$  0.61 (cyclohexane–EtOAc 4:1);  $^1H$ -NMR (500 MHz,  $CDCl_3$ )  $\delta$  7.73 – 7.03 (m, 20H) (each Ar-H), 5.99 – 5.88 (overlapping signals, 2H,  $CH=CHH$  &  $CH=CHH$ ), 5.53 (dd,  $J = 17.5, 1.9$  Hz, 1H,  $CH=CHH$ ), 5.28 – 5.21 (m, 2H,  $CH=CHH$  &  $CH=CHH$ ), 5.10 (dq,  $J = 10.4, 1.5$  Hz, 1H,  $CH=CHH$ ), 4.97 (d,  $J = 11.6$  Hz, 1H), 4.89 (d,  $J = 11.2$  Hz, 1H), 4.78 (d,  $J = 11.6$  Hz, 1H), 4.74 (d,  $J = 11.7$  Hz, 1H), 4.65 (d,  $J = 11.3$  Hz, 1H), 4.63 (d,  $J = 11.7$  Hz, 1H), 4.51 (d,  $J = 11.9$  Hz, 1H), 4.47 (d,  $J = 11.9$  Hz, 1H) (each Bn- $CH_2$ ), 4.11 (dd,  $J = 10.0, 2.8$  Hz, 1H, H-3), 4.01 (dd,  $J = 2.9, 1.4$  Hz, 1H, H-4), 3.99 - 3.86 (overlapping signals, 3H, H-5,  $CHH$  &  $CHH$ ), 3.63 (dd,  $J = 9.4, 7.0$  Hz, 1H, H-6a), 3.58 (dd,  $J = 9.4, 6.0$  Hz, 1H, H-6b);  $^{13}C$ -NMR (126 MHz,  $CDCl_3$ )  $\delta$  139.00, 138.77, 138.46, 138.17, 135.26, 135.12, 128.40, 128.38, 128.34, 128.18, 128.14, 128.13, 128.01, 127.69, 127.66, 127.48, 127.47, 127.45, 118.65, 116.30, 100.25, 80.39, 80.37, 77.27, 77.02, 76.77, 75.76, 75.03, 74.51, 73.42, 72.91, 70.45, 69.02, 63.07.

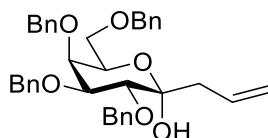
NMR data obtained was in good agreement with the literature <sup>19</sup>



**(5*S*,7*S*,8*R*,9*S*,10*R*)-7,8,9,10-Tetrakis(benzyloxy)-1,6-dioxaspiro[4.5]dec-3-ene (EH 1269)**

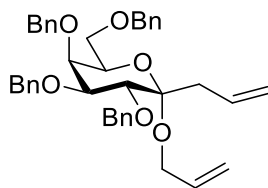
18

A 0.08 M solution of the **EH 1267** (56 mg, 0.09 mmol) in anhydrous toluene (~2 mL) was purged for 15 min with Nitrogen. Grubbs' catalyst (1<sup>st</sup> Generation) (5 mg, 0.005 mmol) was added and the mixture was purged with argon for an additional 15 min, after which the solution was heated to 60 °C. Stirring was continued under an argon atmosphere until TLC analysis indicated complete consumption of the starting material. The mixture was allowed to cool to room temperature and was concentrated. Column chromatography (cyclohexane-EtOAc 4:1) provided the product as a syrup (32 mg, 60%);  $R_f$  0.40 (cyclohexane-EtOAc 4:1); <sup>1</sup>H-NMR (500 MHz, CDCl<sub>3</sub>)  $\delta$  7.71 – 7.02 (overlapping signals, 21H, each Ar-H), 6.23 (dt,  $J$  = 6.0, 1.6 Hz, 1H, CH=CH), 5.64 (dt,  $J$  = 6.0, 2.4 Hz, 1H, CH=CH), 4.96 (d,  $J$  = 11.4 Hz, 1H), 4.79 (d,  $J$  = 11.3 Hz, 1H), 4.74 (d,  $J$  = 11.5 Hz, 1H) (each Bn-CH<sub>2</sub>), 4.73 – 4.70 (overlapping signals, 2H, O-CH<sub>2</sub>), 4.64 (d,  $J$  = 11.4 Hz, 1H), 4.61 (d,  $J$  = 11.3 Hz, 1H), 4.46 (d,  $J$  = 11.9 Hz, 1H), 4.41 (d,  $J$  = 11.8 Hz, 1H) (each Bn-CH<sub>2</sub>), 4.14 (ddd,  $J$  = 8.1, 5.4, 1.3 Hz, 1H, H-5), 4.11 (d,  $J$  = 10.0 Hz, 1H, H-2), 4.07 (dd,  $J$  = 2.9, 1.3 Hz, 1H, H-4), 4.01 (dd,  $J$  = 10.0, 2.8 Hz, 1H, H-3), 3.59 (t,  $J$  = 8.6 Hz, 1H, H-6a), 3.51 (dd,  $J$  = 9.0, 5.4 Hz, 1H, H-6b); <sup>13</sup>C-NMR (126 MHz, CDCl<sub>3</sub>)  $\delta$  142.54, 138.86, 138.77, 138.51, 138.02, 137.81, 132.16, 128.35, 128.33, 128.31, 128.26, 128.24, 128.20, 128.18, 128.14, 128.13, 127.97, 127.91, 127.72, 127.68, 127.67, 127.58, 127.51, 127.47, 127.44, 127.40, 112.77, 110.44, 109.75, 81.68, 81.02, 77.95, 77.25, 77.00, 76.75, 75.54, 75.37, 74.96, 74.75, 74.70, 73.39, 72.98, 72.51, 71.11, 70.88, 70.84, 68.58.



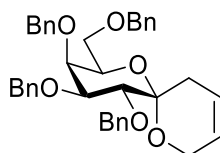
### 2,3,4,6-Tetra-*O*-benzyl-1-*C*-allyl- $\alpha$ -D-galactopyranose (EH 1229 Allyl)

**EH 164** (2.00 g, 3.44 mmol) was dissolved in THF and cooled to  $-78^{\circ}\text{C}$ . Vinyl Magnesium Bromide (0.1 M in THF) (41.3 mL, 4.13 mmol) was added dropwise via cannula. The reaction mixture was stirred for 3 h at  $-78^{\circ}\text{C}$ , after which time TLC analysis indicated complete consumption of the starting material. The reaction mixture was then quenched using a satd. aq. Solution of  $\text{NH}_4\text{Cl}$ , diluted with EtOAc and the organic layer was separated, dried over  $\text{MgSO}_4$  and the solvent removed under reduced pressure. Column chromatography (cyclohexane-EtOAc 4:1) provided the vinyl product as a syrup (701 mg, 34%);  $R_f$  0.43 (cyclohexane-EtOAc 7:3);  $^1\text{H-NMR}$  (500 MHz,  $\text{CDCl}_3$ )  $\delta$  7.91 – 6.61 (overlapping signals, 20H, each Ar-H) 5.90 (ddt,  $J = 16.9, 10.3, 8.0, 6.5$  Hz, 1H,  $\text{CH}=\text{CHH}$ ), 5.19 (dd,  $J = 10.3, 2.2$  Hz, 1H,  $\text{CH}=\text{CHH}$ ), 5.14 (dd,  $J = 17.3, 2.2$  Hz, 1H,  $\text{CH}=\text{CHH}$ ), 4.99 (d,  $J = 10.8$  Hz, 1H), 4.97 (d,  $J = 11.1$  Hz, 1H), 4.77 (d,  $J = 11.7$  Hz, 1H), 4.71 (d,  $J = 10.8$  Hz, 2H), 4.64 (d,  $J = 11.7$  Hz, 1H), 4.49 (d,  $J = 12.0$  Hz, 1H), 4.45 (d,  $J = 11.9$  Hz, 1H) (each Bn- $\text{CH}_2$ ), 4.12 (td,  $J = 7.1, 5.6, 1.3$  Hz, 1H, H-5), 4.04 (t,  $J = 2.8, 1.3$  Hz, 1H, H-4), 3.98 (dd,  $J = 9.8, 2.6$  Hz, 1H, H-3), 3.91 (d,  $J = 9.8$  Hz, 1H, H-2), 3.61 (dd,  $J = 9.2, 7.7$  Hz, 1H, H-6a), 3.54 (dd,  $J = 9.2, 5.6$  Hz, 1H, H-6b), 2.51 (ddt,  $J = 13.8, 8.0, 1.2$  Hz, 1H,  $\text{CHH}$ ), 2.43 (ddt,  $J = 13.8, 6.6, 1.3$  Hz, 1H,  $\text{CHH}$ );  $^{13}\text{C-NMR}$  (126 MHz,  $\text{CDCl}_3$ )  $\delta$  138.96, 138.47, 138.23, 138.10, 132.34, 128.42, 128.39, 128.38, 128.33, 128.19, 127.91, 127.83, 127.75, 127.70, 127.58, 127.51, 127.45 (each Ar-C/ C-H), 119.86 ( $\text{CH}=\text{CHH}$ ), 98.01 (C-1), 81.11 (C-3), 78.23 (C-2), 77.28, 77.03, 76.77, 75.47 (Bn- $\text{CH}_2$ ), 74.41 (C-4), 74.34, 73.42, 72.44 (each Bn- $\text{CH}_2$ ), 70.15 (C-5), 68.78 (C-6), 42.87 ( $\text{CHH}$ ); HRMS calcd. for  $\text{C}_{37}\text{H}_{40}\text{O}_6\text{Na}$   $[\text{M}+\text{Na}]^+$  603.2717 found  $m/z$  603.2714.



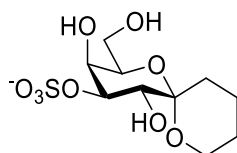
**Allyl 5,6,7,9-Tetra-*O*-benzyl-1,2,3-trideoxy- $\alpha$ -D-galacto-non-4-ulo-1-enopyranose (EH 1270)**

To a flask containing Montmorillonite K-10 clay (220 mg) and powdered molecular sieves 4 Å (220 mg) (both flame-dried under vacuum) was added a mixture of **EH 1229 Allyl** (300 mg, 0.51 mmol) and allyl alcohol (0.18 mL, 3.1 mmol) in anhydrous CH<sub>2</sub>Cl<sub>2</sub> (5 mL) under an argon atmosphere. The resulting suspension was stirred vigorously until TLC analysis indicated complete consumption of the starting material. A mixture of methanol–pyridine (5 mL, 1:1) was added and stirring was continued for 10 min. The suspension was filtered through celite and the solvent removed under reduced pressure. Column chromatography (cyclohexane–EtOAc 9:1) provided the glycosylation product as a syrup (200 mg, 62%); *R*<sub>f</sub> 0.65 (cyclohexane–EtOAc 4:1); <sup>1</sup>H-NMR (500 MHz, CDCl<sub>3</sub>)  $\delta$  7.42 – 7.22 (overlapping signals, 18H, each Ar-H), 5.95 (ddt, *J* = 17.3, 10.6, 5.4 Hz, 1H, CH=CHH), 5.86 (dddd, *J* = 17.2, 10.3, 8.2, 5.7 Hz, 1H, CH=CHH), 5.26 (dq, *J* = 17.1, 1.7 Hz, 1H, CH=CHH), 5.11 (dq, *J* = 10.4, 1.6 Hz, 1H, CH=CHH), 5.05 – 4.95 (overlapping signals, 3H, CH=CHH, CH=CHH & Bn-CH<sub>2</sub>), 4.94 (d, *J* = 11.3 Hz, 1H, ), 4.74 (d, *J* = 11.6 Hz, 1H), 4.73 – 4.67 (overlapping signals, 2H), 4.59 (d, *J* = 11.8 Hz, 1H), 4.50 (d, *J* = 11.9 Hz, 1H), 4.45 (d, *J* = 11.9 Hz, 1H) (each Bn-CH<sub>2</sub>), 4.13 – 4.03 (overlapping signals, 3H, CHH, CHH & H-3), 4.01 (d, *J* = 9.9 Hz, 1H, H-2), 3.99 (t, *J* = 2.8, 1.4 Hz, 1H, H-4), 3.84 (td, *J* = 7.2, 6.0, 1.3 Hz, 1H, H-5), 3.60 (dd, *J* = 9.3, 7.0 Hz, 1H, H-6a), 3.56 (dd, *J* = 9.3, 6.0 Hz, 1H, H-6b), 2.63 (ddt, *J* = 14.8, 8.2, 1.3 Hz, 1H, CHH), 2.58 (ddt, *J* = 14.7, 5.7, 1.8 Hz, 1H, CHH); <sup>13</sup>C-NMR (126 MHz, CDCl<sub>3</sub>)  $\delta$  139.21, 138.93, 138.65, 138.14 (each Ar-C/ C-H), 135.27 (CH=CHH), 133.80 (CH=CHH), 128.38, 128.33, 128.14, 127.99, 127.69, 127.66, 127.51, 127.48, 127.45, 127.32, 127.26 (each Ar-C/ C-H), 117.42 (CH=CHH), 116.04 (CH=CHH), 102.15 (C-1), 80.87 (C-3), 77.89 (C-2), 75.00 (Bn-CH<sub>2</sub>), 74.77 (C-4), 74.21, 73.40, 72.55 (each Bn-CH<sub>2</sub>), 70.44 (C-5), 69.03 (C-6), 61.75 (CHH), 38.68 (CHH).



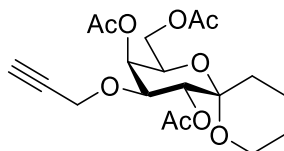
**(6*S*,8*S*,9*R*,10*S*,11*R*)-8,9,10,11-Tetrakis(benzyloxy)-1,7-dioxaspiro[5.5]undec-3-ene (EH 1271)**<sup>18</sup>

A 0.08 M solution of the **EH 1270** (126 mg, 0.2 mmol) in anhydrous toluene (~2.5 mL) was purged for 15 min with Nitrogen. Grubbs' catalyst (1<sup>st</sup> Generation) (10 mg, 0.01 mmol) was added and the mixture was purged with argon for an additional 15 min, after which the solution was heated to 60 °C. Stirring was continued under an argon atmosphere until TLC analysis indicated complete consumption of the starting material. The mixture was allowed to cool to room temperature and was concentrated. Column chromatography (cyclohexane-EtOAc 4:1) provided the product as a syrup (87 mg, 73%);  $R_f$  0.45 (cyclohexane-EtOAc 4:1); <sup>1</sup>H-NMR (500 MHz, CDCl<sub>3</sub>)  $\delta$  7.66 – 6.97 (m, 19H, each Ar-H), 5.70 – 5.61 (overlapping signals, 2H, CH=CH & CH=CH), 5.00 (d,  $J$  = 11.5 Hz, 1H), 4.97 (d,  $J$  = 12.2 Hz, 1H), 4.76 (s, 2H), 4.71 (d,  $J$  = 11.3 Hz, 1H), 4.63 (d,  $J$  = 11.6 Hz, 1H), 4.51 (d,  $J$  = 11.8 Hz, 1H), 4.42 (d,  $J$  = 11.8 Hz, 1H) (each Bn-CH<sub>2</sub>), 4.19 – 4.06 (overlapping signals, 3H, H-3 & O-CH<sub>2</sub>), 4.02 (dd,  $J$  = 2.9, 1.2 Hz, 1H, H-4), 3.91 (td,  $J$  = 6.5, 5.9, 1.3 Hz, 1H, H-5), 3.84 (d,  $J$  = 9.9 Hz, 1H, H-2), 3.61 (dd,  $J$  = 9.4, 7.0 Hz, 1H, H-6a), 3.55 (dd,  $J$  = 9.4, 6.0 Hz, 1H, H-6b), 2.59 (ddd,  $J$  = 17.5, 4.4, 2.4 Hz, 1H), 1.82 (dt,  $J$  = 17.3, 3.7 Hz, 1H) (each CH<sub>2</sub>).; <sup>13</sup>C-NMR (126 MHz, CDCl<sub>3</sub>)  $\delta$  138.84, 138.56, 138.11, 128.77, 128.42, 128.36, 128.28, 128.27, 128.21, 128.08, 127.77, 127.72, 127.67, 127.56, 127.54, 123.79, 121.44 (each Ar-C/ C-H), 97.75 (C-1), 80.66 (C-3), 78.63 (C-2), 75.89 (Bn-CH<sub>2</sub>), 74.79 (C-4), 74.52, 73.52, 72.68 (each Bn-CH<sub>2</sub>), 70.50 (C-5), 69.08 (C-6), 60.38 (O-CH<sub>2</sub>), 30.20 (CH<sub>2</sub>).



**(2*R*,3*S*,4*S*,5*R*,6*S*)-3,5-Dihydroxy-2-(hydroxymethyl)-1,7-dioxaspiro[5.5]undecan-4-yl sulfate (EH 1293)**

**EH 1271** (150 mg, 0.25 mmol) was dissolved in MeOH and Pd/C (10%) was added to a round bottomed flask. The flask was fitted with a H<sub>2</sub> balloon and left to stir overnight. TLC analysis indicated complete consumption of the starting material. The reaction mixture was then filtered through celite and the solvent removed under reduced pressure. Flash chromatography (CH<sub>2</sub>Cl<sub>2</sub>-MeOH 9:1) provided the deprotected intermediate (50 mg, 84%) as a white solid.; R<sub>f</sub> 0.2 (CH<sub>2</sub>Cl<sub>2</sub>-MeOH 9:1). The intermediate (20 mg, 0.08 mmol) was stirred in refluxing MeOH (3 mL), with Bu<sub>2</sub>SnO (32 mg, 0.13 mmol) for 2 h under nitrogen. The solvent was removed under reduced pressure and the dry dibutylstannylene complex was treated with Me<sub>3</sub>N·SO<sub>3</sub> (24 mg, 0.17 mmol) in THF (4 mL) at room temperature for 30 h. The reaction mixture was diluted with MeOH (3 mL), filtered and the solvent removed under reduced pressure. Flash chromatography (CH<sub>2</sub>Cl<sub>2</sub>-MeOH 4:1) provided the product (15 mg, 58%) as a white solid.; <sup>1</sup>H-NMR (500 MHz, CD<sub>3</sub>OD) δ 4.47 (dd, *J* = 10.0, 3.1 Hz, 1H, H-3), 4.30 (d, *J* = 3.2 Hz, 1H, H-4), 3.80 – 3.63 (overlapping signals, 6H, H-5, H-6a, H-6b & CH<sub>2</sub>), 3.60 (d, *J* = 10.0 Hz, 1H, H-2), 2.03 (td, *J* = 13.6, 4.5 Hz, 1H, *CHH*), 1.94 (dtd, *J* = 17.0, 13.1, 4.0 Hz, 1H, *CHH*), 1.67 – 1.56 (m, 2H), 1.54 – 1.45 (m, 2H) (each CH<sub>2</sub>); <sup>13</sup>C-NMR (126 MHz, CD<sub>3</sub>OD) δ 98.22, 78.49, 70.78, 70.42, 68.03, 61.33, 60.58, 48.09, 47.92, 47.75, 47.58, 47.41, 47.24, 47.07, 29.67, 24.42, 17.80.

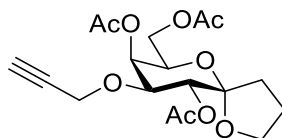


**(2*R*,3*S*,4*S*,5*R*,6*S*)-2-(Acetoxymethyl)-4-(prop-2-yn-1-yloxy)-1,7-dioxaspiro[5.5]undecane-3,5-diyl diacetate (EH 1295 Ac)**

**EH 1271 H<sub>2</sub>** (60 mg, 0.26 mmol) was stirred in refluxing MeOH (10 mL), with Bu<sub>2</sub>SnO (96 mg, 0.38 mmol) for 2 h under nitrogen. The solvent was removed under reduced pressure and



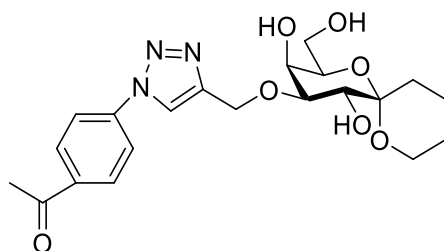
the dry dibutylstannylene complex was treated with tetra butyl ammonium iodide (95 mg, 0.26 mmol) and propargyl bromide (80% wt. in toluene) (0.15 mL, 1.54 mmol) in toluene (4 mL) at 80°C for 30h. The solvent was then removed under reduced pressure. The crude reaction mixture was dissolved in Ac<sub>2</sub>O (5 mL) and pyridine (5 mL) and stirred overnight. The reaction mixture was diluted with EtOAc, washed with 1 M HCl, water and brine, dried over Na<sub>2</sub>SO<sub>4</sub>, filtered and concentrated. Flash chromatography (cyclohexane-EtOAc 3:2) provided the product (70 mg, 68% over two steps) as a white solid.; <sup>1</sup>H-NMR (500 MHz, CDCl<sub>3</sub>) δ 5.46 (dd, *J* = 3.5, 1.4 Hz, 1H, H-4), 5.03 (d, *J* = 10.2 Hz, 1H, H-2), 4.21 – 4.15 (overlapping signals, 3H, H-6a, CHH & CHH), 4.13 (dd, *J* = 11.4, 6.0 Hz, 1H, H-6b), 4.10 (dd, *J* = 10.2, 3.5 Hz, 1H, H-3), 4.05 (ddd, *J* = 7.3, 6.0, 1.5 Hz, 1H, H-5), 3.77 (dd, *J* = 10.6, 4.4 Hz, 1H), 3.62 (td, *J* = 12.0, 10.9, 2.5 Hz, 1H) (each CH<sub>2</sub>), 2.41 (t, *J* = 2.4 Hz, 1H, C≡C-H), 2.17 (s, 3H), 2.14 (s, 3H), 2.07 (s, 3H) (each OAc), 1.89 – 1.76 (m, 1H), 1.69 – 1.48 (m, 5H) (each CH<sub>2</sub>); <sup>13</sup>C-NMR (126 MHz, CDCl<sub>3</sub>) δ 170.55 (C=O), 97.68 (C-1), 79.29 (C≡C-H), 74.82 (C≡C-H), 73.01 (C-3), 71.64 (C-2), 66.96 (C-4), 66.68 (C-5), 62.32 (C-6), 61.50 (CH<sub>2</sub>), 56.62 (CHH), 30.26 (CH<sub>2</sub>), 24.45 (CH<sub>2</sub>), 21.13, 20.83, 20.75 (each OCH<sub>3</sub>), 17.88 (CH<sub>2</sub>).



**(5*S*,7*R*,8*S*,9*S*,10*R*)-7-(Acetoxymethyl)-9-(prop-2-yn-1-yloxy)-1,6-dioxaspiro[4.5]decane-8,10-diyl diacetate (EH 1296 Ac)**

**EH 1269 H<sub>2</sub>** (61 mg, 0.27 mmol) was stirred in refluxing MeOH (10 mL), with Bu<sub>2</sub>SnO (96 mg, 0.38 mmol) for 2 h under nitrogen. The solvent was removed under reduced pressure and the dry dibutylstannylene complex was treated with tetra butyl ammonium iodide (101 mg, 0.27 mmol) and propargyl bromide (80% wt. in toluene) (0.16 mL, 1.6 mmol) in toluene (4 mL) at 80°C for 30h. The solvent was then removed under reduced pressure. The crude reaction mixture was dissolved in Ac<sub>2</sub>O (5 mL) and pyridine (5 mL) and stirred overnight. The reaction mixture was diluted with EtOAc, washed with 1 M HCl, water and brine, dried over Na<sub>2</sub>SO<sub>4</sub>, filtered and concentrated. Flash chromatography (cyclohexane-EtOAc 3:2) provided the product (50 mg, 46% over two steps) as a white solid.; <sup>1</sup>H-NMR (500 MHz, CDCl<sub>3</sub>) δ 5.44 (dd, *J* = 3.5, 1.4 Hz, 1H, H-4), 5.30 (d, *J* = 10.2 Hz, 1H, H-2), 4.19 (td, *J* = 6.8, 1.4 Hz, 1H, H-

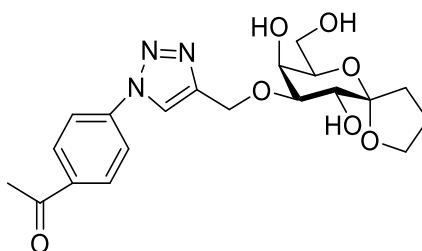
5), 4.17 (t,  $J = 2.4$  Hz, 2H, CHH & CHH), 4.15 – 4.02 (overlapping signals, 3H, H-3, H-6a & H-6b), 4.02 – 3.97 (m, 1H), 3.94 – 3.87 (m, 1H) (each CH<sub>2</sub>), 2.42 (t,  $J = 2.4$  Hz, 1H, C≡C-H), 2.13 (s, 3H), 2.13 (s, 3H), 2.05 (s, 3H) (each OAc), 2.03 – 1.93 (m, 1H), 1.90 – 1.80 (m, 2H) (each CH<sub>2</sub>); <sup>13</sup>C-NMR (126 MHz, CDCl<sub>3</sub>) δ 170.65, 170.55, 170.52 (each C=O), 106.71 (C-1), 79.28 (C≡C-H), 77.26, 77.00, 76.75, 74.79 (C≡C-H), 74.29 (C-3), 69.08 (C-2), 68.46 (CH<sub>2</sub>), 67.47 (C-5), 66.90 (C-4), 62.15 (C-6), 56.67 (CHH), 33.67 (CH<sub>2</sub>), 23.65 (CH<sub>2</sub>), 21.01, 20.82, 20.74 (each OCH<sub>3</sub>).



**1-(4-(4-(((2R,3S,4S,5R,6S)-3,5-Dihydroxy-2-(hydroxymethyl)-1,7-dioxaspiro[5.5]undecan-4-yl)oxy)methyl)-1H-1,2,3-triazol-1-yl)phenyl)ethan-1-one (EH 1305)**

**EH 1295 Ac** (55 mg, 0.14 mmol) was dissolved in a 4:1 mixture of DMF:H<sub>2</sub>O (10 mL). *p*-Azidoacetophenone (33 mg, 0.21 mmol) was added followed by sodium ascorbate (30 mg, 0.15 mmol) and copper sulfate pentahydrate (31 mg, 0.12 mmol) and the reaction mixture was heated to 80°C and stirred for 1 h, after which TLC analysis indicated complete consumption of the starting material. The reaction mixture was then diluted with EtOAc, filtered, washed with water and brine, dried over Na<sub>2</sub>SO<sub>4</sub>, filtered and concentrated. The crude product was dissolved in MeOH, NaOMe (2 mg, 0.04 mmol) was added and the reaction mixture was stirred overnight. The reaction mixture was then neutralized using Dowex (H<sup>+</sup>) resin, filtered and concentrated. Flash chromatography (CH<sub>2</sub>Cl<sub>2</sub>-MeOH 9:1) provided the product (20 mg, 34% over two steps) as a white solid.; <sup>1</sup>H-NMR (500 MHz, CD<sub>3</sub>OD) δ 8.65 (s, 1H), 8.18 (d,  $J = 8.8$  Hz, 2H), 8.00 (d,  $J = 8.8$  Hz, 2H) (each Ar-H), 4.91 (d,  $J = 12.7$  Hz, 1H, CHH), 4.84 (overlapping signals, 1H, CHH), 4.16 (t,  $J = 3.3, 1.2$  Hz, 1H, H-4), 3.80 – 3.70 (overlapping signals, 4H, H-6a, H-6b, & CH<sub>2</sub>), 3.69 (dd,  $J = 9.8, 3.3$  Hz, 1H, H-3), 3.63 (m, 1H, H-5), 3.57 (d,  $J = 9.7$  Hz, 1H, H-2), 2.65 (s, 3H, C=OCH<sub>3</sub>), 2.03 (td,  $J = 13.5, 12.9, 4.3$  Hz, 1H), 1.93 (ddt,  $J = 26.9, 13.3, 3.7, 3.3$  Hz, 1H), 1.67 – 1.54 (m, 2H), 1.54 – 1.44 (m, 2H) (each CH<sub>2</sub>); <sup>13</sup>C-

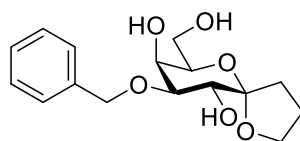
NMR (126 MHz, CD<sub>3</sub>OD)  $\delta$  197.50 (C=O), 146.48, 140.07, 136.83, 129.88, 121.66, 119.72 (each Ar-C/ C-H), 98.03 (C-1), 79.00, 71.60 (C-2), 70.76 (CH<sub>2</sub>), 66.51 (C-4), 62.16 (CH<sub>2</sub>), 61.40 (C<sub>6</sub>), 60.51 (C-5), 29.68 (CH<sub>2</sub>), 25.36 (C=OCH<sub>3</sub>), 24.50, 17.87 (each CH<sub>2</sub>); HRMS calcd. for C<sub>21</sub>H<sub>27</sub>N<sub>3</sub>O<sub>7</sub>Na [M+Na]<sup>+</sup> 456.1741, found m/z 456.1743.



**1-(4-(4-(((5S,7R,8S,9S,10R)-8,10-Dihydroxy-7-(hydroxymethyl)-1,6-dioxaspiro[4.5]decan-9-yl)oxy)methyl)-1H-1,2,3-triazol-1-yl)phenyl)ethan-1-one (EH 1306)**

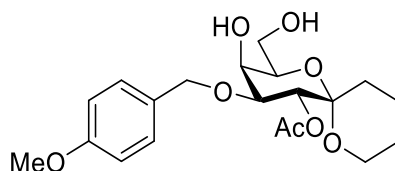
**EH 1296 Ac** (55 mg, 0.14 mmol) was dissolved in a 4:1 mixture of DMF:H<sub>2</sub>O (10 mL). *p*-Azidoacetophenone (35 mg, 0.21 mmol) was added followed by sodium ascorbate (31 mg, 0.16 mmol) and copper sulfate pentahydrate (32 mg, 0.13 mmol) and the reaction mixture was heated to 80 °C and stirred for 1 h, after which TLC analysis indicated complete consumption of the starting material. The reaction mixture was then diluted with EtOAc, filtered, washed with water and brine, dried over Na<sub>2</sub>SO<sub>4</sub>, filtered and concentrated. The crude product was dissolved in MeOH, NaOMe (2 mg, 0.04 mmol) was added and the reaction mixture was stirred overnight. The reaction mixture was then neutralized using Dowex (H<sup>+</sup>) resin, filtered and concentrated. Flash chromatography (CH<sub>2</sub>Cl<sub>2</sub>-MeOH 9:1) provided the product (21 mg, 34% over two steps) as a white solid.; <sup>1</sup>H-NMR (500 MHz, CD<sub>3</sub>OD)  $\delta$  8.67 (s, 1H), 8.21 (d, *J* = 8.8 Hz, 2H), 8.03 (d, *J* = 8.8 Hz, 2H) (each Ar-H), 4.93 (d, *J* = 12.6 Hz, 1H, CHH), 4.87 (d, *J* = 12.8 Hz, 1H, CHH), 4.16 (dd, *J* = 3.2, 1.3 Hz, 1H, H-4), 3.94 (td, *J* = 7.8, 5.7, 1.2 Hz, 2H, each CH<sub>2</sub>), 3.89 (d, *J* = 9.9 Hz, 1H, H-2), 3.83 (td, *J* = 6.8, 5.6, 1.3 Hz, 1H, H-5), 3.73 – 3.64 (overlapping signals, 3H, H-3, H-6a & H-6b), 2.66 (s, 3H, C=OCH<sub>3</sub>), 2.26 – 2.17 (m, 1H), 2.10 – 1.99 (m, 1H), 1.94 – 1.82 (m, 2H) (each CH<sub>2</sub>); <sup>13</sup>C-NMR (126 MHz, CD<sub>3</sub>OD)  $\delta$  197.48 (C=O), 146.44, 129.88, 121.69, 119.76 (each Ar-C/ C-H), 107.99 (C-1), 80.08 (C-3), 71.63 (C-5), 68.88 (C-2), 68.09 (CH<sub>2</sub>), 66.55 (C-4), 62.15 (CH<sub>2</sub>), 61.33 (C-6), 33.20 (CH<sub>2</sub>), 25.34

(C=OCH<sub>3</sub>), 23.46 (CH<sub>2</sub>); HRMS calcd. for C<sub>20</sub>H<sub>26</sub>N<sub>3</sub>O<sub>7</sub> [M+H]<sup>+</sup> 420.1765, found m/z 420.1764.



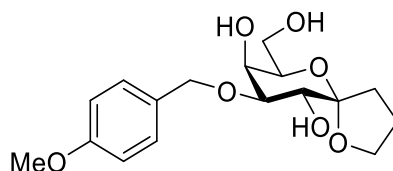
**(5*S*,7*R*,8*S*,9*S*,10*R*)-9-(Benzyloxy)-7-(hydroxymethyl)-1,6-dioxaspiro[4.5]decane-8,10-diol (EH 1307)**

**EH 1269 H<sub>2</sub>** (36 mg, 0.16 mmol) was stirred in refluxing MeOH (10 mL), with Bu<sub>2</sub>SnO (60 mg, 0.24 mmol) for 2 h under nitrogen. The solvent was removed under reduced pressure and the dry dibutylstannylene complex was treated with tetra butyl ammonium iodide (59 mg, 0.16 mmol) and benzyl bromide (0.12 mL, 0.97 mmol) in toluene (8 mL) at 80°C for 30h. The solvent was then removed under reduced pressure. Flash chromatography (CH<sub>2</sub>Cl<sub>2</sub>-MeOH 9:1) provided the product (16 mg, 31%) as a white solid.; R<sub>f</sub> 0.24 (CH<sub>2</sub>Cl<sub>2</sub>-MeOH 9:1); <sup>1</sup>H-NMR (500 MHz, CD<sub>3</sub>OD) δ 7.46 – 7.42 (overlapping signals, 2H), 7.35 – 7.30 (overlapping signals, 2H), 7.28 – 7.23 (m, 1H), 4.75 (d, *J* = 11.8 Hz, 1H, *CHH*), 4.67 (d, *J* = 11.8 Hz, 1H, *CHH*), 4.06 (dd, *J* = 3.2, 1.3 Hz, 1H, H-4), 3.97 – 3.90 (m, 2H, CH<sub>2</sub>), 3.89 (d, *J* = 9.8 Hz, 1H, H-2), 3.76 (td, *J* = 6.7, 5.6, 1.3 Hz, 1H, H-5), 3.67 (dd, *J* = 11.3, 5.5 Hz, 1H, H-6a), 3.64 (dd, *J* = 11.2, 6.7 Hz, 1H, H-6b), 3.59 (dd, *J* = 9.9, 3.2 Hz, 1H, H-3), 2.25 – 2.17 (m, 1H), 2.08 – 1.97 (m, 1H), 1.92 – 1.81 (m, 2H) (each CH<sub>2</sub>); <sup>13</sup>C-NMR (126 MHz, CD<sub>3</sub>OD) δ 208.69 (C=O), 138.65, 127.87, 127.85, 127.66, 127.17 (each Ar-C/ C-H), 108.04 (C-1), 79.47 (C-3), 71.66 (C-5), 71.26 (CH<sub>2</sub>), 69.02 (C-2), 68.05 (CH<sub>2</sub>), 66.84 (C-4), 61.34 (C-6), 33.21 (CH<sub>2</sub>), 29.26 (CH<sub>3</sub>), 23.48 (CH<sub>2</sub>); HRMS calcd. for C<sub>16</sub>H<sub>22</sub>O<sub>6</sub>Na [M+Na]<sup>+</sup> 333.1308, found m/z 333.1308.



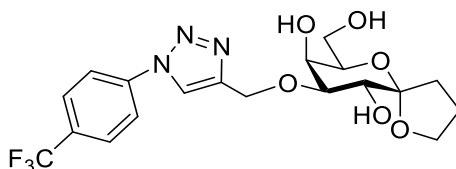
**(2*R*,3*S*,4*S*,5*R*,6*S*)-3-Hydroxy-2-(hydroxymethyl)-4-((4-methoxybenzyl)oxy)-1,7-dioxaspiro[5.5]undecan-5-yl acetate (EH 1308)**

**EH 1301 Ac** (60 mg, 0.15 mmol) was stirred in MeOH (20 mL) with NaOMe (3 mg, 0.05 mmol) for 2 h. The reaction mixture was then neutralized using Dowex (H<sup>+</sup>) resin, filtered and concentrated. The partially deprotected product was refluxed in MeOH with Bu<sub>2</sub>SnO (74 mg, 0.3 mmol) for 2 h under nitrogen. The solvent was removed under reduced pressure and the dry dibutylstannylene complex was treated with tetra butyl ammonium iodide (55 mg, 0.14 mmol) and PMBCl (0.12 mL, 0.89 mmol) in toluene (20 mL) at 80°C for 30h. The solvent was then removed under reduced pressure. Flash chromatography (CH<sub>2</sub>Cl<sub>2</sub>-MeOH 9:1) provided the product (28 mg, 47%) as a white solid; R<sub>f</sub> 0.54 (CH<sub>2</sub>Cl<sub>2</sub>-MeOH 9:1); <sup>1</sup>H-NMR (500 MHz, CD<sub>3</sub>OD) δ 7.24 (d, *J* = 8.7 Hz, 1H), 6.88 (d, *J* = 8.7 Hz, 1H) (each Ar-H), 5.09 (d, *J* = 10.1 Hz, 1H, H-2), 4.60 (d, *J* = 11.8 Hz, 1H, CHH), 4.42 (d, *J* = 11.8 Hz, 1H, CHH), 4.11 (dd, *J* = 3.1, 1.3 Hz, 1H, H-4), 3.78 (s, 3H, OCH<sub>3</sub>), 3.77 – 3.70 (overlapping signals, 3H, H-3, H-6a & H-6b), 3.66 (td, *J* = 6.7, 5.2, 1.3 Hz, 1H, H-5), 3.63 – 3.58 (m, 1H, CH<sub>2</sub>), 2.04 (s, 3H, OAc), 1.92 (ddt, *J* = 25.1, 13.3, 4.7 Hz, 1H), 1.61 – 1.44 (m, 5H) (each CH<sub>2</sub>); <sup>13</sup>C-NMR (126 MHz, CD<sub>3</sub>OD) δ 171.00, 159.42 (each C=O), 130.30, 129.04, 113.32 (each Ar-C/ C-H), 97.17 (C-1), 75.73 (C-3), 72.37 (C-2), 71.01 (C-5), 70.39 (Bn-CH<sub>2</sub>), 66.52 (C-4), 61.28 (C-6), 60.63 (CH<sub>2</sub>), 54.26 (OCH<sub>3</sub>), 30.29 (CH<sub>2</sub>), 24.38 (CH<sub>2</sub>), 19.65 (OCH<sub>3</sub>), 17.61 (CH<sub>2</sub>); HRMS calcd. for C<sub>20</sub>H<sub>28</sub>O<sub>8</sub>Na [M+Na]<sup>+</sup> 419.1676, found *m/z* 419.1673.



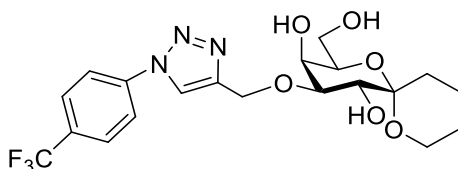
**(5*S*,7*R*,8*S*,9*S*,10*R*)-7-(Hydroxymethyl)-9-((4-methoxybenzyl)oxy)-1,6-dioxaspiro[4.5]decane-8,10-diol (EH 1309)**

**EH 1302 Ac** (29 mg, 0.13 mmol) was stirred in MeOH (20 mL) with NaOMe (3 mg, 0.05 mmol) for 2 h. The reaction mixture was then neutralized using Dowex (H<sup>+</sup>) resin, filtered and concentrated. The deprotected product was stirred in refluxing MeOH (10 mL), with Bu<sub>2</sub>SnO (66 mg, 0.26 mmol) for 2 h under nitrogen. The solvent was removed under reduced pressure and the dry dibutylstannylene complex was treated with tetra butyl ammonium iodide (49 mg, 0.13 mmol) and PMBCl (0.09 mL, 0.8 mmol) in toluene (10 mL) at 80°C for 30 h. The solvent was then removed under reduced pressure. Flash chromatography (CH<sub>2</sub>Cl<sub>2</sub>-MeOH 9:1) provided the product (21 mg, 46%) as a white solid; R<sub>f</sub> 0.63 (CH<sub>2</sub>Cl<sub>2</sub>-MeOH 9:1); <sup>1</sup>H-NMR (500 MHz, CD<sub>3</sub>OD) δ 7.35 (d, *J* = 8.7 Hz, 2H), 6.88 (d, *J* = 8.6 Hz, 2H) (each Ar-H), 4.67 (d, *J* = 11.4 Hz, 1H, *CHH*), 4.60 (d, *J* = 11.4 Hz, 1H, *CHH*), 4.02 (dd, *J* = 3.3, 1.3 Hz, 1H, H-4), 3.94 (dd, *J* = 12.6, 6.3 Hz, 1H), 3.91 (dd, *J* = 11.6, 6.2 Hz, 1H) (each CH<sub>2</sub>), 3.86 (d, *J* = 9.8 Hz, 1H, H-2), 3.78 (s, 3H, OCH<sub>3</sub>), 3.75 (td, *J* = 6.7, 5.6, 1.2 Hz, 1H, H-5), 3.66 (dd, *J* = 11.3, 5.7 Hz, 1H, H-6a), 3.63 (dd, *J* = 11.2, 6.8 Hz, 1H, H-6b), 3.57 (dd, *J* = 9.9, 3.2 Hz, 1H, H-3), 2.24 – 2.16 (m, 1H), 2.08 – 1.96 (m, 1H), 1.91 – 1.81 (m, 2H) (each CH<sub>2</sub>); <sup>13</sup>C-NMR (126 MHz, CD<sub>3</sub>OD) δ 159.37, 130.58, 129.29, 113.25 (each Ar-C/ C-H), 108.03 (C-1), 79.08 (C-3), 71.64 (C-5), 70.93 (Bn-CH<sub>2</sub>), 68.98 (C-2), 68.03 (CH<sub>2</sub>), 66.86 (C-4), 61.33 (C-6), 33.20, 23.46 (each CH<sub>2</sub>); HRMS calcd. for C<sub>17</sub>H<sub>24</sub>O<sub>7</sub>Na [M+Na]<sup>+</sup> 363.1414, found *m/z* 363.1419.



**(5*S*,7*R*,8*S*,9*S*,10*R*)-7-(Hydroxymethyl)-9-((1-(4-(trifluoromethyl)phenyl)-1*H*-1,2,3-triazol-4-yl)methoxy)-1,6-dioxaspiro[4.5]decane-8,10-diol (EH 1310)**

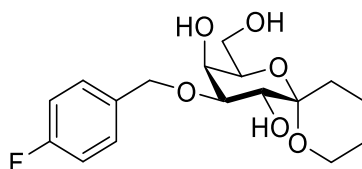
**EH 1296 Ac** (55 mg, 0.14 mmol) was dissolved in a 4:1 mixture of DMF:H<sub>2</sub>O (10 mL). *p*-Azidotrifluoromethylbenzene (0.5 M in tert-butyl methyl ether) (0.4 mL, 0.22 mmol) was added followed by sodium ascorbate (31 mg, 0.16 mmol) and copper sulfate pentahydrate (32 mg, 0.13 mmol) and the reaction mixture was heated to 80°C and stirred for 1 h, after which TLC analysis indicated complete consumption of the starting material. The reaction mixture was then diluted with EtOAc, filtered, washed with water and brine, dried over Na<sub>2</sub>SO<sub>4</sub>, filtered and concentrated. The crude product was dissolved in MeOH, NaOMe (3 mg, 0.05 mmol) was added and the reaction mixture was stirred overnight. The reaction mixture was then neutralized using Dowex (H<sup>+</sup>) resin, filtered and concentrated. Flash chromatography (CH<sub>2</sub>Cl<sub>2</sub>-MeOH 9:1) provided the product (21 mg, 33% over two steps) as a white solid.; <sup>1</sup>H-NMR (500 MHz, CD<sub>3</sub>OD) δ 8.67 (s, 1H), 8.10 (d, *J* = 8.3 Hz, 2H), 7.91 (d, *J* = 8.3 Hz, 2H) (each Ar-H), 4.93 (d, *J* = 12.6 Hz, 1H, *CHH*), 4.87 (d, *J* = 12.6 Hz, 1H, *CHH*), 4.16 (dd, *J* = 3.2, 1.3 Hz, 1H, H-4), 3.94 (td, *J* = 7.3, 6.6, 1.1 Hz, 2H, each CH<sub>2</sub>), 3.89 (d, *J* = 9.8 Hz, 1H, H-2), 3.83 (ddd, *J* = 6.8, 5.6, 1.3 Hz, 1H, H-5), 3.70 (dd, *J* = 11.2, 5.6 Hz, 1H, H-6a), 3.69 – 3.65 (overlapping signals, 2H, H-3 & H-6b), 2.26 – 2.17 (m, 1H), 2.09 – 1.99 (m, 1H), 1.93 – 1.83 (m, 2H) (each CH<sub>2</sub>); <sup>13</sup>C-NMR (126 MHz, CD<sub>3</sub>OD) δ 146.50, 126.84, 126.81, 121.77, 120.37 (each Ar-C/ C-H), 107.99 (C-1), 80.07 (C-3), 71.63 (C-5), 68.88 (C-2), 68.09 (CH<sub>2</sub>), 66.55 (C-4), 62.13 (CH<sub>2</sub>), 61.32 (C-6), 33.19, 23.46 (each CH<sub>2</sub>); HRMS calcd. for C<sub>19</sub>H<sub>22</sub>F<sub>3</sub>N<sub>3</sub>O<sub>6</sub>Na [M+Na]<sup>+</sup> 468.1353, found *m/z* 468.1357.



**(2*R*,3*S*,4*S*,5*R*,6*S*)-2-(Hydroxymethyl)-4-((1-(*para*-(trifluoromethyl)phenyl)-1*H*-1,2,3-triazol-4-yl)methoxy)-1,7-dioxaspiro[5.5]undecane-3,5-diol (EH 1311)**

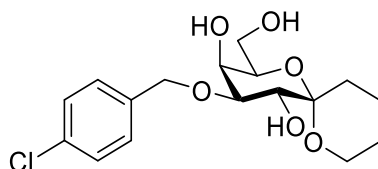
**EH 1304 Ac** (45 mg, 0.1 mmol) was dissolved in a 4:1 mixture of DMF:H<sub>2</sub>O (10 mL). *p*-Azidotrifluoromethylbenzene (0.5 M in tert-butyl methyl ether) (0.3 mL, 0.15 mmol) was added followed by sodium ascorbate (25 mg, 0.12 mmol) and copper sulfate pentahydrate (25 mg, 0.1 mmol) and the reaction mixture was heated to 80°C and stirred for 1 h, after which TLC analysis indicated complete consumption of the starting material. The reaction mixture was then diluted with EtOAc, filtered, washed with water and brine, dried over Na<sub>2</sub>SO<sub>4</sub>, filtered and concentrated. The crude product was dissolved in MeOH, NaOMe (2 mg, 0.35 mmol) was added and the reaction mixture was stirred overnight. The reaction mixture was then neutralized using Dowex (H<sup>+</sup>) resin, filtered and concentrated. Flash chromatography (CH<sub>2</sub>Cl<sub>2</sub>-MeOH 9:1) provided the product (20 mg, 45% over two steps) as a white solid.; R<sub>f</sub> 0.2 (CH<sub>2</sub>Cl<sub>2</sub>-MeOH 9:1); <sup>1</sup>H-NMR (500 MHz, CD<sub>3</sub>OD) δ 8.66 (s, 1H), 8.10 (d, *J* = 8.4 Hz, 2H), 7.91 (d, *J* = 8.5 Hz, 2H) (each Ar-H), 4.92 (d, *J* = 12.7 Hz, 1H, *CHH*), 4.84 (overlapping signal, 1H, *CHH*), 4.15 (dd, *J* = 3.3, 1.2 Hz, 1H, H-4), 3.80 – 3.68 (overlapping signals, 4H, H-5, H-6a, H-6b & CH<sub>2</sub>), 3.68 (dd, *J* = 9.8, 3.2 Hz, 1H, H-3), 3.66 – 3.59 (m, 1H, CH<sub>2</sub>), 3.57 (d, *J* = 9.8 Hz, 1H, H-2), 2.03 (td, *J* = 13.3, 4.3 Hz, 1H), 1.94 (ddt, *J* = 27.1, 13.1, 3.5 Hz, 1H), 1.66 – 1.55 (m, 2H), 1.55 – 1.45 (m, 2H) (each CH<sub>2</sub>); <sup>13</sup>C-NMR (126 MHz, CD<sub>3</sub>OD) δ 146.55, 126.83, 126.80, 121.75, 120.38 (each Ar-C/ C-H), 98.03 (C-1), 78.98 (C-3), 71.59 (C-2), 70.76 (C-5), 66.50 (C-4), 62.15 (CH<sub>2</sub>), 61.39 (C-6), 60.50 (CH<sub>2</sub>), 29.67, 24.50, 17.86 (each CH<sub>2</sub>); HRMS calcd. for C<sub>20</sub>H<sub>24</sub>F<sub>3</sub>N<sub>3</sub>O<sub>6</sub>Na [M+Na]<sup>+</sup> 460.1689, found *m/z* 460.1689.





**(2*R*,3*S*,4*S*,5*R*,6*S*)-4-((*para*-Fluorobenzyl)oxy)-2-(hydroxymethyl)-1,7-dioxaspiro[5.5]undecane-3,5-diol (EH 1313)**

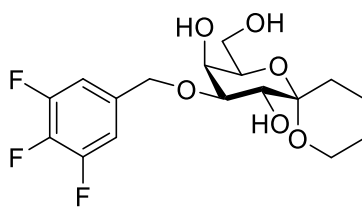
**EH 1271 H<sub>2</sub>** (40 mg, 0.17 mmol) was stirred in refluxing MeOH (10 mL), with Bu<sub>2</sub>SnO (63 mg, 0.251 mmol) for 2 h under nitrogen. The solvent was removed under reduced pressure and the dry dibutylstannylene complex was treated with tetra butyl ammonium iodide (62 mg, 0.17 mmol) and 4-fluorobenzyl bromide (0.11 mL, 0.84 mmol) in toluene (4 mL) at 80°C for 30 h. The solvent was then removed under reduced pressure. Flash chromatography (CH<sub>2</sub>Cl<sub>2</sub>-MeOH 9:1) provided the product (15.2 mg, 26.5%) as a white solid.; <sup>1</sup>H-NMR (500 MHz, CD<sub>3</sub>OD) δ 7.45 (dd, *J* = 8.4, 5.6 Hz, 2H), 7.04 (t, *J* = 8.8 Hz, 2H) (each Ar-H), 4.71 (d, *J* = 11.8 Hz, 1H, CHH), 4.62 (d, *J* = 11.8 Hz, 1H, CHH), 4.05 (dd, *J* = 3.0, 1.3 Hz, 1H, H-4), 3.77 – 3.68 (overlapping signals, 3H, H-6a, H-6b & CH<sub>2</sub>), 3.63 (td, *J* = 6.7, 5.3, 1.3 Hz, 2H, H-5 & CH<sub>2</sub>), 3.59 (dd, *J* = 9.8, 3.0 Hz, 1H, H-3), 3.55 (d, *J* = 9.8 Hz, 1H, H-2), 2.02 (td, *J* = 13.5, 12.9, 4.3 Hz, 1H), 1.93 (ddt, *J* = 27.1, 13.3, 4.0 Hz, 1H), 1.66 – 1.54 (m, 2H), 1.53 – 1.44 (m, 2H) (each CH<sub>2</sub>); <sup>13</sup>C-NMR (126 MHz, CD<sub>3</sub>OD) δ 163.27, 161.32, 134.77, 134.75, 129.56, 129.50, 114.53, 114.35 (each Ar-C/ C-H), 98.05 (C-1), 78.36 (C-3), 71.70 (C-2), 70.77 (C-5), 70.42 (Bn-CH<sub>2</sub>), 66.75 (C-4), 61.38 (C-6), 60.47 (CH<sub>2</sub>), 29.66, 24.50, 17.88 (each CH<sub>2</sub>); HRMS calcd. for C<sub>17</sub>H<sub>23</sub>FO<sub>6</sub>Na [M+Na]<sup>+</sup> 365.1371, found *m/z* 365.1373.



**(2*R*,3*S*,4*S*,5*R*,6*S*)-4-((*para*-Chlorobenzyl)oxy)-2-(hydroxymethyl)-1,7-dioxaspiro[5.5]undecane-3,5-diol (EH 1314)**

**EH 1271 H<sub>2</sub>** (40 mg, 0.17 mmol) was stirred in refluxing MeOH (10 mL), with Bu<sub>2</sub>SnO (86 mg, 0.34 mmol) for 2 h under nitrogen. The solvent was removed under reduced pressure and the dry dibutylstannylene complex was treated with tetra butyl ammonium iodide (64 mg, 0.17

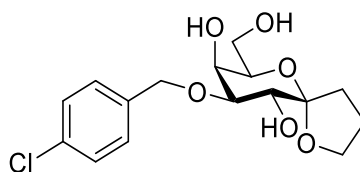
mmol) and 4-chlorobenzyl bromide (177 mg, 0.86 mmol) in toluene (4 mL) at 80°C for 30h. The solvent was then removed under reduced pressure. Flash chromatography (CH<sub>2</sub>Cl<sub>2</sub>-MeOH 9:1) provided the product (14 mg, 22%) as a white solid.; <sup>1</sup>H-NMR (500 MHz, CD<sub>3</sub>OD) δ 7.42 (d, *J* = 8.4 Hz, 2H), 7.31 (d, *J* = 8.4 Hz, 2H) (each Ar-H), 4.72 (d, *J* = 12.2 Hz, 1H, CHH), 4.63 (d, *J* = 12.2 Hz, 1H, CHH), 4.06 (dd, *J* = 2.9, 1.3 Hz, 1H, H-4), 3.77 – 3.67 (overlapping signals, 3H, H-6a, H-6b & CH<sub>2</sub>), 3.63 (td, *J* = 6.8, 5.3, 1.2 Hz, 2H, H-5 & CH<sub>2</sub>), 3.59 (dd, *J* = 9.8, 2.9 Hz, 1H, H-3), 3.56 (d, *J* = 9.8 Hz, 1H, H-2), 2.02 (td, *J* = 13.5, 12.9, 4.3 Hz, 1H), 1.93 (ddt, *J* = 27.2, 13.3, 3.8 Hz, 1H), 1.67 – 1.54 (m, 2H), 1.54 – 1.43 (m, 2H) (each CH<sub>2</sub>); <sup>13</sup>C-NMR (126 MHz, CD<sub>3</sub>OD) δ 137.62, 132.78, 129.07, 127.89 (each Ar-C/ C-H), 98.05 (C-1), 78.50 (C-3), 71.70 (C-2), 70.77 (C-5), 70.30 (Bn-CH<sub>2</sub>), 66.72 (C-4), 61.37, 60.46 (each CH<sub>2</sub>), 29.65, 24.50, 17.87 (each CH<sub>2</sub>); HRMS calcd. for C<sub>17</sub>H<sub>23</sub>ClO<sub>6</sub>Na [M+Na]<sup>+</sup> 381.1075, found *m/z* 381.1077.



**(2*R*,3*S*,4*S*,5*R*,6*S*)-2-(Hydroxymethyl)-4-((3,4,5-trifluorobenzyl)oxy)-1,7-dioxaspiro[5.5]undecane-3,5-diol (EH 1315)**

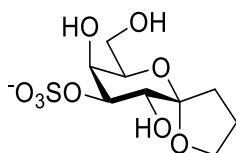
**EH 1271 H<sub>2</sub>** (40 mg, 0.17 mmol) was stirred in refluxing MeOH (10 mL), with Bu<sub>2</sub>SnO (63 mg, 0.25 mmol) for 2 h under nitrogen. The solvent was removed under reduced pressure and the dry dibutylstannylene complex was treated with tetra butyl ammonium iodide (62 mg, 0.17 mmol) and 3,4,5-trifluorobenzyl bromide (0.11 mL, 0.84 mmol) in toluene (4 mL) at 80°C for 30h. The solvent was then removed under reduced pressure. Flash chromatography (CH<sub>2</sub>Cl<sub>2</sub>-MeOH 9:1) provided the product (18 mg, 29%) as a white solid.; <sup>1</sup>H-NMR (500 MHz, CD<sub>3</sub>OD) δ 7.27 – 7.20 (overlapping signals, 2H, each Ar-H), 4.70 (d, *J* = 12.7 Hz, 1H, CHH), 4.60 (d, *J* = 12.8 Hz, 1H, CHH), 4.08 (d, *J* = 1.5 Hz, 1H, H-4), 3.78 – 3.69 (overlapping signals, 3H, H-6a, H-6b & CH<sub>2</sub>), 3.66 – 3.63 (overlapping signals, 2H, H-5 & CH<sub>2</sub>), 3.63 – 3.59 (m, 1H, CH<sub>2</sub>), 3.57 (overlapping signals, 2H, H-2 & H-3), 2.02 (td, *J* = 13.6, 13.2, 4.3 Hz, 1H), 1.93 (ddt, *J* = 27.0, 13.4, 3.9 Hz, 1H), 1.66 – 1.55 (m, 2H), 1.54 – 1.44 (m, 2H) (each CH<sub>2</sub>); <sup>13</sup>C-NMR (126 MHz, CD<sub>3</sub>OD) δ 151.85, 136.27, 111.16, 111.12, 111.03, 110.99 (each Ar-C/ C-H), 98.06 (C-

1), 78.92 (C-3), 71.61 (C-2), 70.74 (C-6), 69.27 (Bn-CH<sub>2</sub>), 66.62 (C-4), 61.34 (C-6), 60.49 (CH<sub>2</sub>), 29.63, 24.48, 17.87 (each CH<sub>2</sub>).



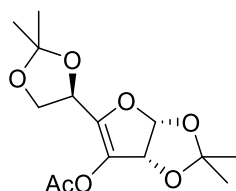
**(5*S*,7*R*,8*S*,9*S*,10*R*)-9-((*para*-Chlorobenzyl)oxy)-7-(hydroxymethyl)-1,6-dioxaspiro[4.5]decane-8,10-diol (EH 1317)**

**EH 1269 H<sub>2</sub>** (49 mg, 0.22 mmol) was stirred in refluxing MeOH (10 mL), with Bu<sub>2</sub>SnO (83 mg, 0.33 mmol) for 2 h under nitrogen. The solvent was removed under reduced pressure and the dry dibutylstannylene complex was treated with tetra butyl ammonium iodide (82 mg, 0.22 mmol) and PMBCl (0.2 mL, 1.1 mmol) in toluene (10 mL) at 80°C for 30h. The solvent was then removed under reduced pressure. Flash chromatography (CH<sub>2</sub>Cl<sub>2</sub>-MeOH 9:1) provided the product (30 mg, 40%) as a white solid; R<sub>f</sub> 0.63 (CH<sub>2</sub>Cl<sub>2</sub>-MeOH 9:1); <sup>1</sup>H-NMR (500 MHz, CD<sub>3</sub>OD) δ 7.43 (d, *J* = 8.3 Hz, 2H), 7.32 (d, *J* = 8.4 Hz, 2H) (each Ar-H), 4.73 (d, *J* = 12.1 Hz, 1H, *CHH*), 4.64 (d, *J* = 12.1 Hz, 1H, *CHH*), 4.07 (d, *J* = 3.2 Hz, 1H, H-4), 3.98 – 3.90 (overlapping signals, 2H, each CH<sub>2</sub>), 3.88 (d, *J* = 9.9 Hz, 1H, H-2), 3.77 (m, 1H, H-5), 3.67 (dd, *J* = 11.2, 5.5 Hz, 1H, H-6a), 3.65 (dd, *J* = 11.3, 6.7 Hz, 1H, H-6b), 3.58 (dd, *J* = 9.8, 3.1 Hz, 1H, H-3), 3.26 – 3.20 (m, 1H, N-CH<sub>2</sub>-CH<sub>2</sub>-CH<sub>2</sub>-CH<sub>3</sub>) 2.25 – 2.17 (m, 1H), 2.08 – 1.97 (m, 1H), 1.93 – 1.82 (m, 2H) (each CH<sub>2</sub>), 1.66 (p, *J* = 7.9 Hz, 1H, N-CH<sub>2</sub>-CH<sub>2</sub>-CH<sub>2</sub>-CH<sub>3</sub>), 1.41 (h, *J* = 7.4 Hz, 1H, N-CH<sub>2</sub>-CH<sub>2</sub>-CH<sub>2</sub>-CH<sub>3</sub>), 1.02 (t, *J* = 7.3 Hz, 1H, N-CH<sub>2</sub>-CH<sub>2</sub>-CH<sub>2</sub>-CH<sub>3</sub>); <sup>13</sup>C-NMR (126 MHz, CD<sub>3</sub>OD) δ 137.57, 132.81, 129.10, 127.91 (each Ar-C/ C-H), 108.04 (C-1), 79.66 (C-3), 71.64 (C-5), 70.30 (Bn-CH<sub>2</sub>), 68.97 (C-2), 68.07 (CH<sub>2</sub>), 66.75 (C-4), 61.31 (C-6), 58.09 (N-CH<sub>2</sub>-CH<sub>2</sub>-CH<sub>2</sub>-CH<sub>3</sub>), 33.21, 23.47 (each CH<sub>2</sub>), 23.36 (N-CH<sub>2</sub>-CH<sub>2</sub>-CH<sub>2</sub>-CH<sub>3</sub>), 19.30 (N-CH<sub>2</sub>-CH<sub>2</sub>-CH<sub>2</sub>-CH<sub>3</sub>), 12.51 (N-CH<sub>2</sub>-CH<sub>2</sub>-CH<sub>2</sub>-CH<sub>3</sub>); HRMS calcd. for C<sub>16</sub>H<sub>21</sub>ClO<sub>6</sub>Na [M+Na]<sup>+</sup> 367.0919, found *m/z* 367.0922.



**(5*S*,7*R*,8*S*,9*S*,10*R*)-8,10-Dihydroxy-7-(hydroxymethyl)-1,6-dioxaspiro[4.5]decan-9-yl sulfate (EH 1319)**

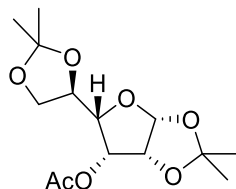
**EH 1269 H<sub>2</sub>** (98 mg, 0.45 mmol) was stirred in refluxing MeOH (30 mL), with Bu<sub>2</sub>SnO (222 mg, 0.89 mmol) for 2 h under nitrogen. The solvent was removed under reduced pressure and the dry dibutylstannylene complex was treated with Me<sub>3</sub>N.SO<sub>3</sub> (123 mg, 0.89 mmol) in THF (30 mL) at room temperature for 30h. The reaction mixture was diluted with MeOH (20 mL), filtered and the solvent removed under reduced pressure. Flash chromatography (CH<sub>2</sub>Cl<sub>2</sub>-MeOH 4:1) provided the product (40 mg, 30%) as a white solid.; <sup>1</sup>H-NMR (500 MHz, CD<sub>3</sub>OD) δ 4.45 (dd, *J* = 10.1, 3.1 Hz, 1H, H-3), 4.31 (d, *J* = 3.2 Hz, 1H, H-4), 4.01 – 3.93 (m, 2H, each CH<sub>2</sub>), 3.92 (d, *J* = 10.0 Hz, 1H, H-2), 3.86 (t, *J* = 6.1 Hz, 1H, H-5), 3.68 (dd, *J* = 11.2, 5.7 Hz, 1H, H-6a), 3.65 (dd, *J* = 11.3, 6.6 Hz, 1H, H-6b), 2.27 – 2.17 (m, 1H), 2.09 – 1.98 (m, 1H), 1.95 – 1.82 (m, 2H) (each CH<sub>2</sub>); <sup>13</sup>C-NMR (126 MHz, CD<sub>3</sub>OD) δ 108.08 (C-1), 79.35 (C-3), 71.49 (C-5), 68.19 (CH<sub>2</sub>), 68.15 (C-4), 67.68 (C-2), 61.25 (C-6), 33.20, 23.39 (each CH<sub>2</sub>).



**3-*O*-Acetyl-1,2:5,6-di-*O*-isopropylidene- $\alpha$ -D-erythrohex-3-enose (EH 150)**

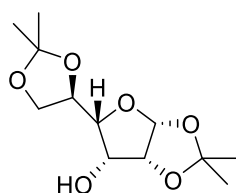
1,2:5,6-di-*O*-isopropylidene- $\alpha$ -D-ribo-hexofuranos-3-ulose (2.29 g, 8.86 mmol) was dissolved in pyridine and heated to 115 °C, to this Ac<sub>2</sub>O was added and the reaction was stirred for 16 h. The reaction mixture was then diluted with Et<sub>2</sub>O, washed with water, 1M HCl, water, brine, dried over MgSO<sub>4</sub> and the solvent was removed under reduced pressure. Chromatography (cyclohexane-EtOAc 7:3) gave the product as a white solid (1.35 g, 51%); *R<sub>f</sub>* 0.68 (Toluene-MeOH 19:1); <sup>1</sup>H-NMR (500 MHz, CDCl<sub>3</sub>) δ 6.03 (d, *J* = 5.5 Hz, 1H, H-1), 5.39 (d, *J* = 5.5 Hz, 1H, H-2), 4.70 (t, *J* = 6.5 Hz, 1H, H-5), 4.16 – 4.01 (2H, overlapping signals, H-6a & H-6b), 2.21 (s, 3H, OAc), 1.53 (s, 3H), 1.47 (s, 3H), 1.45 (s, 3H), 1.38 (s, 3H) (each CH<sub>3</sub>); <sup>13</sup>C-

NMR (126 MHz, CDCl<sub>3</sub>)  $\delta$  168.9 (C=O), 145.3 (C-4), 129.0 (C-3), 113.4 (4° C), 110.4 (4° C), 104.0 (C-1), 80.8 (C-2), 68.6 (C-5), 65.9 (C-6), 27.9, 27.8, 25.8, 25.6 (each CH<sub>3</sub>), 20.5 (OAc).



### 3-*O*-Acetyl-1,2:5,6-di-*O*-isopropylidene- $\alpha$ -D-glucofuranose (EH 154)

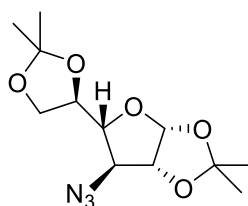
**EH 150** (1.35 g, 4.51 mmol) was dissolved in EtOAc (15 mL). Pd/C 10% (1.35 g, 1.27 mmol) was added and the reaction mixture was purged with H<sub>2</sub>. The mixture was left to stir under a positive pressure of H<sub>2</sub> overnight. After 16 h, TLC analysis indicated complete consumption of the starting material. The reaction mixture was filtered through celite and the solvent was removed under reduced pressure. Chromatography (cyclohexane-EtOAc 7:3) gave the product as a white solid (1.06 g, 78%); R<sub>f</sub> 0.48 (cyclohexane-EtOAc 7:3); <sup>1</sup>H-NMR (500 MHz, CDCl<sub>3</sub>)  $\delta$  5.82 (d, *J* = 4.1 Hz, 1H, H-1), 5.07 (t, *J* = 6.8, 5.7 Hz, 1H, H-3), 4.81 (dd, *J* = 5.7, 4.1 Hz, 1H, H-2), 4.62 (approx. dt, *J* = 9.3, 7.3, 6.5 Hz, 1H, H-5), 4.11 (dd, *J* = 8.4, 6.5 Hz, 1H, H-6a), 4.08 (dd, *J* = 9.2, 6.8 Hz, 1H, H-4), 3.53 (dd, *J* = 8.4, 7.3 Hz, 1H, H-6b), 2.13 (s, 3H, OAc), 1.58 (s, 3H), 1.44 (s, 3H), 1.39 (s, 3H), 1.35 (s, 3H) (each CH<sub>3</sub>); <sup>13</sup>C-NMR (126 MHz, CDCl<sub>3</sub>)  $\delta$  169.6 (C=O) 114.5 (4° C), 109.3 (4° C) 105.0 (C-1), 81.3 (C-4), 78.5 (C-2), 75.2 (C-5), 71.7 (C-3), 66.3 (C-6), 26.7, 26.7, 25.2 (each CH<sub>3</sub>), 20.6 (OAc).



### 1,2:5,6-Di-*O*-isopropylidene- $\alpha$ -D-glucofuranose (EH 155)

**EH 154** (784 mg, 2.59 mmol) was dissolved in MeOH (5 mL). K<sub>2</sub>CO<sub>3</sub> (35 mg, 0.26 mmol) was added and the reaction was left to stir for 2h, after which time TLC analysis indicated complete consumption of the starting material. The solvent was removed under reduced pressure and the product was purified using flash chromatography (cyclohexane-EtOAc 7:3)

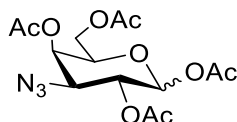
as a white solid (501 mg, 74%);  $R_f$  0.25 (cyclohexane-EtOAc 7:3);  $^1\text{H-NMR}$  (500 MHz,  $\text{CD}_3\text{OD}$ )  $\delta$  5.75 (d,  $J = 3.8$  Hz, 1H, H-1), 4.64 (dt,  $J = 9.7, 6.8$  Hz, 1H, H-5), 4.61 (dd,  $J = 5.4, 3.8$  Hz, 1H, H-2), 4.37 (dd,  $J = 7.2, 5.3$  Hz, 1H, H-3), 4.14 (dd,  $J = 8.8, 6.5$  Hz, 1H, H-6a), 3.96 (dd,  $J = 9.7, 7.2$  Hz, 1H, H-4), 3.63 (dd,  $J = 8.8, 7.2$  Hz, 1H, H-6b), 1.59 (s, 3H), 1.39 (s, 3H), 1.35 (s, 3H), 1.33 (s, 3H) (each  $\text{CH}_3$ );  $^{13}\text{C-NMR}$  (126 MHz,  $\text{CD}_3\text{OD}$ ,)  $\delta$  113.4 ( $4^\circ\text{C}$ ), 108.1 ( $4^\circ\text{C}$ ), 104.7 (C-1), 83.6 (C-4), 80.0 (C-2), 75.6 (C-5), 70.4 (C-3), 66.5 (C-6), 25.7, 25.6, 25.0, 24.1 (each  $\text{CH}_3$ ); HRMS calcd. for  $\text{C}_{12}\text{H}_{20}\text{O}_6\text{Na}$   $[\text{M}+\text{Na}]^+$  283.1152, found  $m/z$  283.1150.



### 3-Azido-3-deoxy-1,2:5,6-di-*O*-isopropylidene- $\alpha$ -D-galactofuranose (EH 156)

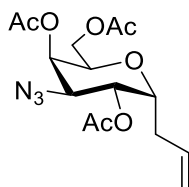
**EH 155** (7.00 g, 26.9 mmol) was dissolved in dry  $\text{CH}_2\text{Cl}_2$  (140 mL) and cooled to  $-10^\circ\text{C}$ . To the cooled reaction mixture trifluoromethanesulfonic acid anhydride (4.2 mL, 40.3 mmol) was added followed by the slowly addition of the dry pyridine (6.5 mL, 80.7 mmol). Additional  $\text{CH}_2\text{Cl}_2$  was added to prevent the mixture from freezing. After 2 h, the reaction mixture was diluted with  $\text{CH}_2\text{Cl}_2$  (140 mL) and washed with ice-cold 1 M HCl and ice-cold  $\text{NaHCO}_3$  solution. The organic solution was dried over  $\text{Na}_2\text{SO}_4$ , filtered and concentrated at low temperature to give an orange oily residue. The residue was dried over high vacuum for 2-3 hours. The residue was dissolved in 50 mL of dry DMF. To the glucose-3-*O*-triflate solution,  $\text{NaN}_3$  (3.5 g, 53.8 mmol) was added and the mixture was stirred at room temperature for 6 h. TLC analysis showed the complete disappearance of the triflate. The reaction mixture was diluted with water (300 mL) and the aqueous layer washed with  $\text{CH}_2\text{Cl}_2$ . The combined organic layer was dried over  $\text{Na}_2\text{SO}_4$  and concentrated. Flash chromatography (cyclohexane-EtOAc 4:1) provided the product as an oily residue (5.8 g, 76%);  $R_f$  0.47 (cyclohexane-EtOAc 7:3);  $^1\text{H-NMR}$  (500 MHz,  $\text{CDCl}_3$ )  $\delta$  5.78 (d,  $J = 3.9$  Hz, 1H, H-1), 4.58 (dd,  $J = 3.8, 1.9$  Hz, 1H, H-2), 4.33 (q,  $J = 6.4$  Hz, 1H, H-5), 4.06 (t,  $J = 8.6, 6.8$  Hz, 1H, H-6a), 3.92 (dd,  $J = 5.7, 1.8$  Hz, 1H, H-3), 3.85 (t,  $J = 8.6, 6.8$  Hz, 1H, H-6b), 3.80 (t,  $J = 5.7$  Hz, 1H, H-4), 1.55 (s, 3H), 1.43 (s, 3H), 1.36 (s, 3H), 1.35 (s, 3H) (each  $\text{CH}_3$ );  $^{13}\text{C-NMR}$  (126 MHz,  $\text{CDCl}_3$ )  $\delta$  114.37, 110.05 (each  $4^\circ\text{C}$ ), 104.82 (C-1), 85.71 (C-2), 83.09 (C-4), 77.29, 77.04, 76.78, 74.53 (C-5), 65.55

(C-6), 65.51 (C-3), 27.47, 26.85, 26.32, 25.16 (each CH<sub>3</sub>); HRMS calcd. for C<sub>12</sub>H<sub>19</sub>N<sub>3</sub>O<sub>5</sub>Na [M+Na]<sup>+</sup> 308.1217, found m/z 308.1214.



### 3-Azido-3-deoxy-1,2,4,6-tetra-*O*-acetyl-( $\alpha/\beta$ )-D-galactopyranose (EH 158)

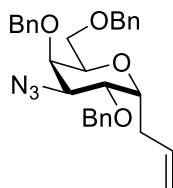
To a suspension of **EH 156** (5.55 g, 19.5 mmol) in water (100 mL), 5.00 g of IR-20 (H<sup>+</sup>) was added. The mixture was heated at 80°C. for 3 h until the sugar became soluble in water. The mixture was then rapidly filtered and the water was evaporated using a vacuum pump to give a white solid. Pyridine (20 mL) and Ac<sub>2</sub>O (20 mL) were added to the residue and the reaction was stirred for 2 h after which the solvent was evaporated and the residue dried by repeated coevaporation with toluene. Column chromatography (cyclohexane-EtOAc 4:1) provided the mixture of anomers as a white solid (5.8 g, 80%); R<sub>f</sub> 0.42 (cyclohexane-EtOAc 7:3); <sup>1</sup>H-NMR (500 MHz, CDCl<sub>3</sub>)  $\delta$  6.35 (d, *J* = 3.6 Hz, 1H, H-1 $\alpha$ ), 5.67 (d, *J* = 8.2 Hz, 1H, H-1 $\beta$ ), 5.49 (dd, *J* = 3.4, 1.5 Hz, 1H, H-4 $\alpha$ ), 5.45 (dd, *J* = 3.4, 1.1 Hz, 1H, H-4 $\beta$ ), 5.30 – 5.22 (overlapping signals, 2H, H-2 $\alpha$  & H-2 $\beta$ ), 4.28 (td, *J* = 6.6, 1.8 Hz, 1H, H-5 $\alpha$ ), 4.18 – 3.96 (overlapping signals, 7H, H-3 $\alpha$ , H-5 $\beta$ , H-6 $\alpha\alpha$ , H-6 $\beta\alpha$ , H-6 $\alpha\beta$  & H-6 $\beta\beta$ ), 3.67 (dd, *J* = 10.6, 3.4 Hz, 1H, H-3 $\beta$ ), 2.21 (s, 3H), 2.17 (s, 3H), 2.16 (s, 6H), 2.11 (s, 3H), 2.11 (s, 3H), 2.08 (s, 3H), 2.04 (s, 6H) (each OAc); <sup>13</sup>C-NMR (126 MHz, CDCl<sub>3</sub>)  $\delta$  170.39, 170.37, 169.85, 169.63, 169.22, 169.03, 168.75, 166.38 (each C=O), 92.19 (C-1 $\beta$ ), 89.22 (C-1 $\alpha$ ), 77.27, 77.02, 76.76, 72.67 (H-5 $\beta$ ), 69.01 (C-5 $\alpha$ ), 68.69 (C-2 $\beta$ ), 68.00 (C-2 $\alpha$ ), 67.60 (C-4 $\alpha$ ), 67.35 (C-4 $\beta$ ), 61.63 (C-3 $\beta$ ), 61.42 (C-6 $\alpha$ ), 61.22 (C-6 $\beta$ ), 57.59 (C-3 $\alpha$ ), 22.15, 20.85, 20.78, 20.63, 20.57, 20.51 (each OCH<sub>3</sub>); HRMS calcd. for C<sub>14</sub>H<sub>19</sub>N<sub>3</sub>O<sub>9</sub>Na [M+Na]<sup>+</sup> 396.1013 found m/z 396.1014.



### 1-*C*-Allyl-1-deoxy-3-azido-3-deoxy-2,4,6-tri-*O*-acetyl- $\alpha$ -D-galactopyranose (EH 1137)

To a stirred suspension of **EH 158** (500 mg, 1.34 mmol) and allyltrimethylsilane (0.64 mL, 4.02 mmol) in Acetonitrile (20 mL) was added BF<sub>3</sub>.Et<sub>2</sub>O (0.83 mL, 6.7 mmol). The reaction

was heated at reflux overnight, diluted with EtOAc and quenched with satd NaHCO<sub>3</sub>. Phases were separated and the aqueous layer was washed with EtOAc. The combined organic phases were washed with H<sub>2</sub>O, brine, dried over MgSO<sub>4</sub>, filtered and the solvents were concentrated under reduced pressure. Column chromatography (cyclohexane-EtOAc 4:1) gave the product (356 mg, 75%) as a viscous oil.; R<sub>f</sub> 0.58 (cyclohexane-EtOAc 7:3); <sup>1</sup>H-NMR (500 MHz, CDCl<sub>3</sub>) δ 5.74 (ddt, *J* = 17.1, 10.2, 6.8 Hz, 1H, CH<sub>2</sub>CH=CHH), 5.41 (t, *J* = 3.4 Hz, 1H, H-4), 5.18 – 5.05 (overlapping signals, 3H, H-2, CH<sub>2</sub>CH=CHH & CH<sub>2</sub>CH=CHH), 4.29 (dd, *J* = 11.6, 7.8 Hz, 1H, H-6a), 4.22 (dt, *J* = 9.7, 4.8 Hz, 1H, H-1), 4.12 (dd, *J* = 11.3, 4.8 Hz, 1H, H-6b), 4.08 (ddd, *J* = 8.9, 4.8, 1.5 Hz, 1H, H-5), 3.89 (dd, *J* = 8.4, 3.5 Hz, 1H, H-3), 2.41 (dddd, *J* = 15.1, 9.8, 7.1, 1.4 Hz, 1H, CHH), 2.32-2.21 (overlapping signals, 3H, CHH), 2.15 (s, 3H), 2.13 (s, 3H), 2.05 (s, 3H) (each OAc); <sup>13</sup>C-NMR (126 MHz, CDCl<sub>3</sub>) δ 170.64, 169.84, 169.78 (each C=O), 133.14 (CH<sub>2</sub>CH=CHH), 117.76 (CH<sub>2</sub>CH=CHH), 77.25, 77.00, 76.75, 70.03 (C-2) 69.81 (C-1), 69.09 (C-5), 68.05 (C-4), 61.20 (C-6), 58.52 (C-3), 31.30 (CHH), 20.79, 20.75, 20.62 (each OCH<sub>3</sub>); HRMS calcd. for C<sub>15</sub>H<sub>21</sub>N<sub>3</sub>O<sub>7</sub>Na [M+Na]<sup>+</sup> 378.1272 found *m/z* 378.1280.

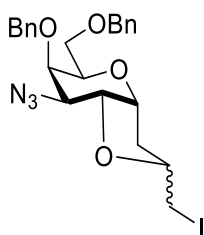


### 1-C-Allyl-1-deoxy-3-azido-3-deoxy-2,4,6-tri-*O*-benzyl- $\alpha$ -D-galactopyranose (EH 1155)

**EH 1137** (350 mg, 0.98 mmol) was dissolved in dry MeOH (100 mL). NaOMe was added (21 mg, 0.39 mmol) and the reaction mixture was allowed to stir for 15 mins, after which time, TLC analysis indicated disappearance of the starting material. Amberlite (H<sup>+</sup>) was added to neutralise the reaction mixture, which was concentrated to give free intermediate. The crude intermediate (120 mg, 0.5 mmol) was dissolved in DMF and cooled to 0°C. NaH (95 mg, 2.3 mmol) was added slowly, causing liberation of H<sub>2</sub> and fizzing. The reaction was stirred for 10 mins followed by addition of BnBr (0.28 mL, 2.3 mmol). The reaction was allowed to warm to room temperature overnight and was eventually quenched with MeOH following indication of product formation via TLC. The reaction mixture was extracted with EtOAc and the combined organic layers were washed with water, dried with Na<sub>2</sub>SO<sub>4</sub> and the solvent was removed under reduced pressure. Column chromatography (cyclohexane-EtOAc 9:1) afforded the product as a white solid (290 mg, 59%); <sup>1</sup>H-NMR (500 MHz, CDCl<sub>3</sub>) δ 7.86 – 6.83 (m,



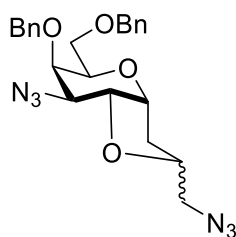
15H, each Ar-H), 5.77 (ddt,  $J = 17.1, 10.2, 6.9$  Hz, 1H,  $\text{CH}_2\text{CH}=\text{CH}_2$ ), 5.14 – 5.03 (overlapping signals, 2H,  $\text{CH}_2\text{CH}=\text{CH}_2$ ), 4.79 (d,  $J = 11.3$  Hz, 1H), 4.65 (d,  $J = 11.3$  Hz, 1H), 4.57 (d,  $J = 11.3$  Hz, 1H), 4.56 (d,  $J = 11.3$  Hz, 1H), 4.50 (d,  $J = 11.8$  Hz, 1H), 4.44 (d,  $J = 11.8$  Hz, 1H) (each Bn- $\text{CH}_2$ ), 4.08 (p,  $J = 5.3, 4.8$  Hz, 1H, H-1), 3.99 (dd,  $J = 9.1, 5.0$  Hz, 1H, H-2), 3.95 (t,  $J = 2.9$  Hz, 1H, H-4), 3.88 (td,  $J = 6.5, 2.2$  Hz, 1H, H-5), 3.66 (dd,  $J = 9.2, 3.1$  Hz, 1H, H-3), 3.61 (dd,  $J = 9.7, 6.1$  Hz, 1H, H-6a), 3.58 (dd,  $J = 9.7, 6.7$  Hz, 1H, H-6b), 2.48 – 2.32 (overlapping signals, 2H, each  $\text{CH}_2\text{CH}=\text{CH}_2$ );  $^{13}\text{C}$ -NMR (126 MHz,  $\text{CDCl}_3$ )  $\delta$  137.99, 137.88, 137.52 (each Ar-C/ C-H), 134.59 ( $\text{CH}_2\text{CH}=\text{CH}_2$ ), 129.02, 128.50, 128.39, 128.34, 128.16, 128.07, 128.03, 127.81, 127.72, 127.70 (each Ar-C/ C-H), 117.10 ( $\text{CH}_2\text{CH}=\text{CH}_2$ ), 77.26, 77.00, 76.75, 75.60 (C-2), 75.35 (C-4), 74.63, 73.36, 72.84 (each Bn- $\text{CH}_2$ ), 70.65 (C-5), 67.84 (C-6), 61.21 (C-3), 30.02 ( $\text{CH}_2\text{CH}=\text{CH}_2$ ); HRMS calcd. for  $\text{C}_{30}\text{H}_{33}\text{N}_3\text{O}_4\text{Na}$   $[\text{M}+\text{Na}]^+$  522.2363 found  $m/z$  522.2341.



**(3aR,5R,6R,7S,7aR)-7-Azido-6-(benzyloxy)-5-((benzyloxy)methyl)-2-(iodomethyl)hexahydro-2H-furo[3,2-b]pyran (EH 1157 US)**

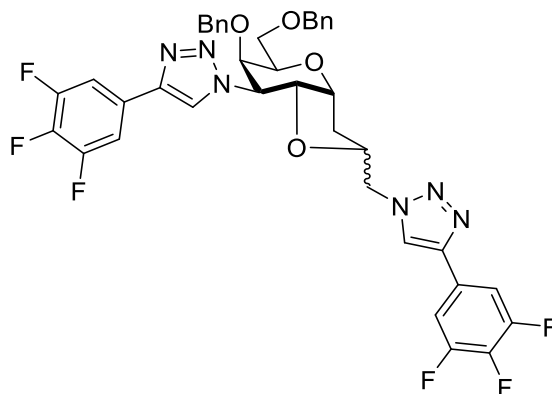
**EH 1155** (140 mg, 0.28 mmol) was taken up in THF (30 mL) and cooled to 0 °C.  $\text{I}_2$  (355 mg, 1.4 mmol) was added and the reaction mixture was allowed to stir for 2 h. The reaction mixture was diluted with EtOAc and 1M  $\text{Na}_2\text{S}_2\text{O}_3$  solution was added and stirring was continued for 10 min. Phases were separated and aqueous layer was extracted into EtOAc. The combined organic layers were washed with brine, dried over  $\text{MgSO}_4$  and concentrated under reduced pressure. Flash chromatography (cyclohexane-EtOAc 9:1) provided the product as a colourless oil (124 mg, 82%);  $R_f$  0.56 (cyclohexane-EtOAc 9:1);  $^1\text{H}$ -NMR (500 MHz,  $\text{CDCl}_3$ )  $\delta$  7.43 – 7.23 (overlapping signals, 10H, each Ar-H), 4.76 (d,  $J = 11.3$  Hz, 1H), 4.59 (d,  $J = 11.2$  Hz, 1H), 4.57 (overlapping signal, 1H), 4.54 (d,  $J = 12.1$  Hz, 1H) (each Bn- $\text{CH}_2$ ), 4.40 (p,  $J = 3.5$  Hz, 1H, H-1), 4.19 – 4.11 (overlapping signals, 2H,  $\text{CH}$  & H-5), 4.05 (dd,  $J = 5.7, 4.1$  Hz, 1H, H-2), 4.01 (dd,  $J = 4.7, 2.6$  Hz, 1H, H-4), 3.84 – 3.77 (overlapping signals, 2H, H-3 & H-6a), 3.64 (dd,  $J = 10.3, 5.2$  Hz, 1H, H-6b), 3.36 (dd,  $J = 9.7, 5.5$  Hz, 1H,  $\text{CHH}$ -1), 3.30 (dd,  $J = 9.8,$

7.4 Hz, 1H, CHH-I), 2.26 (dt,  $J = 13.8, 7.8, 6.2$  Hz, 1H, CHH), 2.00 (ddd,  $J = 13.8, 5.2, 3.1$  Hz, 1H, CHH);  $^{13}$  C-NMR (126 MHz, CDCl<sub>3</sub>)  $\delta$  137.95, 137.65, 134.59, 129.02, 128.78, 128.72, 128.50, 128.42, 128.39, 128.34, 128.16, 128.07, 128.02, 127.90, 127.83, 127.82, 127.78, 127.75, 127.70 (each Ar-C/ C-H), 81.11 (C-2), 78.60, 77.26, 77.01, 76.75, 74.67, 74.24 (C-4), 73.86, 73.39 (each Bn-CH<sub>2</sub>), 72.18 (C-1), 66.37 (C-6), 62.08 (C-3), 37.20 (CHH), 9.75 (CHH-I); HRMS calcd. for C<sub>23</sub>H<sub>26</sub>IN<sub>3</sub>O<sub>4</sub>Na [M+Na]<sup>+</sup> 558.0860 found m/z 558.0828.



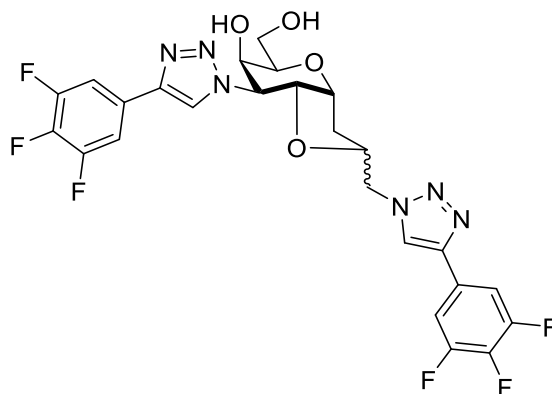
**(3aR,5R,6R,7S,7aR)-7-Azido-2-(azidomethyl)-6-(benzyloxy)-5-(benzyloxy)methylhexahydro-2H-furo[3,2-b]pyran (EH 1158 US)**

**EH 1157 US** (446 mg, 0.83 mmol) was dissolved in dry DMF (30 mL). NaN<sub>3</sub> (216 mg, 3.33 mmol) was added under N<sub>2</sub> atmosphere at room temperature and the reaction mixture was heated to 80°C and stirred overnight, after which time TLC analysis indicated complete consumption of the starting material. The reaction mixture was diluted with water (50 mL) and the aqueous layer washed with EtOAc. The combined organic layers were dried over Na<sub>2</sub>SO<sub>4</sub> and concentrated. Flash chromatography (cyclohexane-EtOAc 4:1) provided the product as an oily residue (250 mg, 67%); R<sub>f</sub> 0.57 (cyclohexane-EtOAc 4:1);  $^1$ H-NMR (500 MHz, CDCl<sub>3</sub>)  $\delta$  7.42 – 7.24 (overlapping signals, 10H, each Ar-H), 4.74 (d,  $J = 11.3$  Hz, 1H), 4.57 (d,  $J = 11.3$  Hz, 1H), 4.56 (d,  $J = 12.1$  Hz, 1H), 4.52 (d,  $J = 12.2$  Hz, 1H) (each Bn-CH<sub>2</sub>), 4.35 (p,  $J = 3.4$  Hz, 1H, H-1), 4.20 – 4.09 (overlapping signals, 2H, CH & H-5), 4.01 (dd,  $J = 4.8, 2.8$  Hz, 1H, H-4), 3.97 (dd,  $J = 5.5, 3.9$  Hz, 1H, H-2), 3.83 – 3.77 (overlapping signals, 2H, H-3 & H-6a), 3.62 (dd,  $J = 10.4, 5.1$  Hz, 1H, H-6b), 3.40 (dd,  $J = 12.8, 6.5$  Hz, 1H, CHH-N<sub>3</sub>), 3.34 (dd,  $J = 12.8, 4.1$  Hz, 1H, CHH-N<sub>3</sub>), 2.20 (ddd,  $J = 14.0, 8.2, 6.3$  Hz, 1H, CHH), 1.88 (ddd,  $J = 13.7, 5.9, 3.0$  Hz, 1H, CHH);  $^{13}$  C-NMR (126 MHz, CDCl<sub>3</sub>)  $\delta$  137.99, 137.67, 128.41, 127.89, 127.82, 127.79, 127.74 (each Ar-C/ C-H), 80.70 (C-2), 77.40 (C-2'), 77.27, 77.02, 76.76, 74.78 (C-5), 74.25 (C-4), 73.88, 73.36 (each Bn-CH<sub>2</sub>), 71.98 (C-1), 66.35 (C-6), 61.70 (C-3), 54.63 (CHH-N<sub>3</sub>), 34.57 (CHH); HRMS calcd. for C<sub>23</sub>H<sub>26</sub>N<sub>6</sub>O<sub>4</sub>Na [M+Na]<sup>+</sup> 473.1908 found m/z 473.1880.



**1-((3aR,5R,6R,7S,7aR)-6-(Benzyloxy)-5-((benzyloxy)methyl)-2-((4-(3,4,5-trifluorophenyl)-1H-1,2,3-triazol-1-yl)methyl)hexahydro-2H-furo[3,2-b]pyran-7-yl)-4-(3,4,5-trifluorophenyl)-1H-1,2,3-triazole (EH 1159 US)**

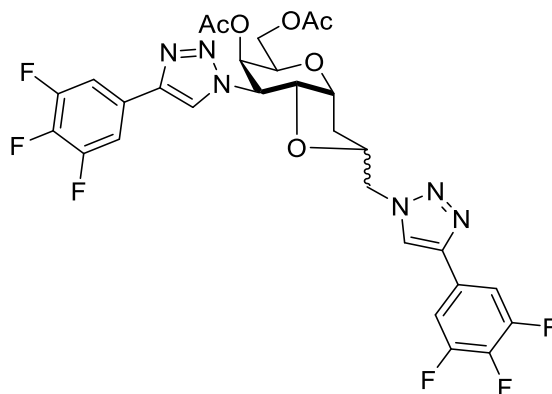
**EH 1158 US** (30 mg, 0.07 mmol) was dissolved in a 4:1 mixture of DMF:H<sub>2</sub>O (20 mL). 3,4,5-trifluorophenylacetylene (0.03 mL, 0.2 mmol) was added followed by sodium ascorbate (33 mg, 0.16 mmol) and copper sulfate pentahydrate (42 mg, 0.16 mmol) and the reaction mixture was heated to 80°C and stirred for 1 h, after which TLC analysis indicated complete consumption of the starting material. The reaction mixture was then diluted with EtOAc, filtered, washed with water and brine, dried over Na<sub>2</sub>SO<sub>4</sub>, filtered and concentrated. Flash chromatography (cyclohexane-EtOAc 3:2) provided the product (40 mg, 78%) as a white solid.; <sup>1</sup>H-NMR (500 MHz, CDCl<sub>3</sub>) δ 7.88 (s, 1H), 7.81 (s, 1H), 7.52 – 7.44 (overlapping signals, 2H), 7.37 – 7.22 (overlapping signals, 9H), 7.14 – 7.06 (overlapping signals, 2H) (each Ar-H), 4.75 (q, *J* = 6.9, 5.2 Hz, 1H, H-1), 4.66 – 4.47 (overlapping signals, 7H, H-2, H-3, 3x Bn-CH<sub>2</sub>, CHH-N & CHH-N), 4.39 (qd, *J* = 7.1, 3.5 Hz, 1H, CH), 4.34 (dd, *J* = 3.5, 2.4 Hz, 1H, H-4), 4.21 (td, *J* = 7.7, 6.2, 3.5 Hz, 1H, H-5), 4.17 (d, *J* = 11.1 Hz, 1H, Bn-CH<sub>2</sub>), 3.73 (dd, *J* = 9.6, 7.6 Hz, 1H, H-6a), 3.67 (dd, *J* = 9.6, 6.1 Hz, 1H, H-6b), 2.41 (p, *J* = 7.1 Hz, 1H, CHH), 1.99 (dt, *J* = 13.8, 7.2, 5.1 Hz, 1H, CHH); <sup>13</sup>C-NMR (126 MHz, CDCl<sub>3</sub>) δ 152.63, 152.54, 150.61, 145.44, 145.22, 137.30, 137.02, 136.98, 128.65, 128.59, 128.54, 128.52, 128.34, 128.29, 128.05, 127.99, 127.91, 127.85, 126.64, 121.78, 121.41, 119.64, 109.91, 109.86, 109.77, 109.71, 109.65, 109.56, 109.52 (each Ar-C/ C-H), 78.75 (C-2), 77.28, 77.02, 76.96 (CH), 76.77, 76.15 (C-4), 75.65 (Bn-CH<sub>2</sub>), 74.59 (C-1), 74.52 (C-5), 73.66 (Bn-CH<sub>2</sub>), 66.99 (C-6), 64.16 (C-3), 54.04 (CHH-N), 33.31 (CHH); HRMS calcd. for C<sub>39</sub>H<sub>33</sub>F<sub>6</sub>N<sub>6</sub>O<sub>4</sub> [M+H]<sup>+</sup> 763.2461 found *m/z* 763.2468.



**(3aR,5R,6R,7S,7aR)-5-(hydroxymethyl)-7-(4-(3,4,5-trifluorophenyl)-1H-1,2,3-triazol-1-yl)-2-((4-(3,4,5-trifluorophenyl)-1H-1,2,3-triazol-1-yl)methyl)hexahydro-2H-furo[3,2-b]pyran-6-ol (EH 1163 US)**

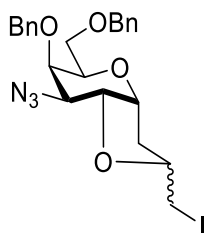
**EH 1159 US** (30 mg, 0.04 mmol) was dissolved in EtOAc:MeOH (1:1) (30 mL) and Pd/C (10%) was added to the reaction mixture. The flask was fitted with a H<sub>2</sub> balloon and left to stir overnight. TLC analysis indicated complete consumption of the starting material. The reaction mixture was then filtered through celite and the solvent removed under reduced pressure. Flash chromatography (CH<sub>2</sub>Cl<sub>2</sub>-MeOH 9:1) provided the product (16 mg, 69%) as a white solid.; R<sub>f</sub> 0.1 (CH<sub>2</sub>Cl<sub>2</sub>-MeOH 9:1); <sup>1</sup>H-NMR (500 MHz, Acetone-*d*<sub>6</sub>) δ 8.69 (s, 1H), 8.47 (s, 1H), 7.78 – 7.70 (overlapping signals, 2H), 7.70 – 7.62 (overlapping signals, 2H), 4.91 – 4.83 (overlapping signals, 2H), 4.80 – 4.70 (overlapping signals, 3H), 4.61 (dd, *J* = 8.5, 5.7 Hz, 1H), 4.49 (dt, *J* = 5.1, 2.5 Hz, 1H), 4.45 (tt, *J* = 7.1, 3.6 Hz, 1H), 4.09 (td, *J* = 6.1, 3.0 Hz, 1H), 3.94 (dd, *J* = 6.4, 5.1 Hz, 1H), 3.81 (overlapping signals, 2H), 3.31 (d, *J* = 5.4 Hz, 2H, CH<sub>3</sub>OH), 3.11 (q, *J* = 5.4 Hz, 1H, CH<sub>3</sub>OH), 2.85 (s, 2H, H<sub>2</sub>O), 2.46 (dt, *J* = 13.7, 7.0 Hz, 1H), 2.16 (dt, *J* = 13.4, 7.1 Hz, 1H); <sup>13</sup>C-NMR (126 MHz, Acetone-*d*<sub>6</sub>) δ 123.14, 121.32, 109.52, 109.48, 109.38, 109.33, 77.88, 76.66, 75.43, 74.52, 67.91, 65.17, 60.34, 54.07, 32.51, 29.38, 29.32, 29.23, 29.17, 29.08, 29.02, 28.92, 28.77, 28.61, 28.46.

Due to the high degree of signal overlap in the deprotected compound, signals are assigned after acetylation.



**((3aR,5R,6R,7R,7aR)-6-acetoxy-7-(4-(3,4,5-trifluorophenyl)-1H-1,2,3-triazol-1-yl)-2-((4-(3,4,5-trifluorophenyl)-1H-1,2,3-triazol-1-yl)methyl)hexahydro-2H-furo[3,2-b]pyran-5-yl)methyl acetate (EH 1163 US Ac)**

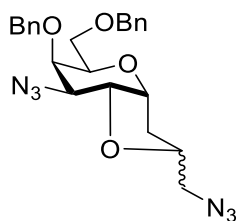
**EH 1163 US** (16 mg, 0.03 mmol) was dissolved in Ac<sub>2</sub>O (3 mL) and pyridine (3 mL) and stirred overnight at 0 °C. The reaction mixture was diluted with EtOAc, washed with 1 M HCl, water and brine, dried over Na<sub>2</sub>SO<sub>4</sub>, filtered and concentrated. Flash chromatography (cyclohexane-EtOAc 1:4) provided the product (17 mg, 93%) as a white solid.; R<sub>f</sub> 0.4 (cyclohexane-EtOAc 1:4); <sup>1</sup>H-NMR (500 MHz, CDCl<sub>3</sub>) δ 7.84 (s, 1H), 7.80 (s, 1H), 7.46 – 7.41 (overlapping signals, 2H), 7.41 – 7.36 (overlapping signals, 2H) (each Ar-H), 5.79 (dd, *J* = 4.5, 2.2 Hz, 1H, H-4), 4.83–4.76 (overlapping signals, 2H, H-1 & H-2), 4.72 (dd, *J* = 14.4, 7.5 Hz, 1H, CHH-N), 4.65 (dd, *J* = 7.4, 2.2 Hz, 1H, H-3), 4.57 (dd, *J* = 14.4, 3.8 Hz, 1H, CHH-N), 4.50 – 4.44 (m, 1H, CH), 4.40 (dt, *J* = 7.7, 5.2 Hz, 1H, H-5), 4.31 (dd, *J* = 11.6, 7.7 Hz, 1H, H-6a), 4.03 (dd, *J* = 11.6, 5.6 Hz, 1H, H-6b), 2.53 (dt, *J* = 14.0, 7.0 Hz, 1H, CHH), 2.11 (ddd, *J* = 14.1, 5.9, 3.4 Hz, 1H, CHH), 2.08 (s, 3H), 2.05 (s, 3H) (each OAc).; <sup>13</sup>C-NMR (126 MHz, CDCl<sub>3</sub>) δ 170.58, 169.27 (each C=O), 150.62, 145.44, 145.22, 140.62, 138.61, 126.31, 121.06, 120.71, 109.83, 109.81, 109.79, 109.76, 109.69, 109.65, 109.63, (each Ar-C/ C-H) 78.91 (C-2), 77.03 (CH), 74.31 (C-1), 72.89 (C-5), 67.72 (C-4), 62.55 (C-3), 59.96 (C-6), 53.88 (CHH-N), 34.36 (CHH), 20.69, 20.59 (each OCH<sub>3</sub>).



**(3aR,5R,6R,7S,7aR)-7-Azido-6-(benzyloxy)-5-((benzyloxy)methyl)-2-(iodomethyl)hexahydro-2H-furo[3,2-*b*]pyran (EH 1157 LS)**

See EH 1157 US for procedure.

(82%) <sup>1</sup>H-NMR (500 MHz, CDCl<sub>3</sub>) δ 7.98 – 6.27 (overlapping signals, 10H, each Ar-H), 4.72 (d, *J* = 11.4 Hz, 1H, Bn-CH<sub>2</sub>), 4.58 - 4.48 (overlapping signals, 3H, each Bn-CH<sub>2</sub>), 4.41 – 4.37 (m, 1H, H-1), 4.24 – 4.18 (overlapping signals, 2H, H-2 & CH), 4.15 (dt, *J* = 8.1, 4.9 Hz, 1H, H-5), 3.99 (dd, *J* = 5.1, 2.7 Hz, 1H, H-4), 3.82 (dd, *J* = 10.5, 8.0 Hz, 1H, H-6a), 3.78 (dd, *J* = 5.4, 2.7 Hz, 1H, H-3), 3.63 (dd, *J* = 10.5, 4.6 Hz, 1H, H-6b), 3.30 (dd, *J* = 10.1, 4.4 Hz, 1H, CHH-I), 3.27 (dd, *J* = 10.1, 6.2 Hz, 1H, CHH-I), 2.23 (ddd, *J* = 13.5, 5.8, 1.5 Hz, 1H, CHH), 1.78 (ddd, *J* = 13.4, 9.2, 5.2 Hz, 1H, CHH).; <sup>13</sup>C-NMR (126 MHz, CDCl<sub>3</sub>) δ 138.01, 137.65, 128.43, 128.41, 128.34, 128.22, 127.89, 127.79, 127.73, 127.66, 127.60, 127.48 (each Ar-C/C-H), 81.30 (C-2), 77.36 (CH), 74.80 (C-5), 74.36 (C-4), 73.62, 73.34, 72.84 (each Bn-CH<sub>2</sub>), 72.42 (C-1), 66.25 (C-6), 61.17 (C-3), 39.25 (CHH), 10.17 (CHH-I).

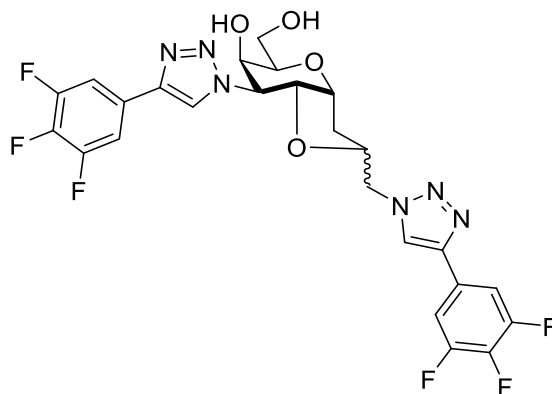


**(3aR,5R,6R,7S,7aR)-7-Azido-2-(azidomethyl)-6-(benzyloxy)-5-((benzyloxy)methyl)hexahydro-2H-furo[3,2-*b*]pyran (EH 1158 LS)**

See EH 1158 US for procedure.

(67%) <sup>1</sup>H-NMR (500 MHz, CDCl<sub>3</sub>) δ 7.42 – 7.22 (m, 9H, each Ar-H), 4.73 (d, *J* = 11.4 Hz, 1H, Bn-CH<sub>2</sub>), 4.57 (d, *J* = 11.7 Hz, 2H), 4.54 (d, *J* = 12.2 Hz, 1H) (each Bn-CH<sub>2</sub>), 4.46 – 4.38 (m, 2H, H-1 & CH), 4.15 (overlapping signals, 2H, H-2 & H-5), 4.00 (dd, *J* = 5.1, 2.7 Hz, 1H, H-4), 3.83 (dd, *J* = 10.5, 8.0 Hz, 1H, H-6a), 3.79 (dd, *J* = 5.4, 2.7 Hz, 1H, H-3), 3.63 (dd, *J* = 10.5, 4.6 Hz, 1H, H-6b), 3.49 (dd, *J* = 13.0, 3.6 Hz, 1H, CHH-N<sub>3</sub>), 3.22 (dd, *J* = 13.0, 4.9 Hz,

1H, CHH-N<sub>3</sub>), 2.06 (ddd,  $J = 13.3, 5.9, 1.5$  Hz, 1H, CHH), 1.88 (ddd,  $J = 13.4, 9.4, 5.2$  Hz, 1H, CHH).; <sup>13</sup>C-NMR (126 MHz, CDCl<sub>3</sub>)  $\delta$  138.02, 137.67, 128.42, 128.41, 127.88, 127.80, 127.73, 127.67 (each Ar-C/ C-H), 80.86 (C-2), 77.38 (CH), 74.82 (C-5), 74.39 (C-4), 73.67, 73.34 (each Bn-CH<sub>2</sub>), 72.33 (C-1), 66.30 (C-6), 61.15 (C-3), 53.98 (CHH-N<sub>3</sub>), 35.33 (CHH).

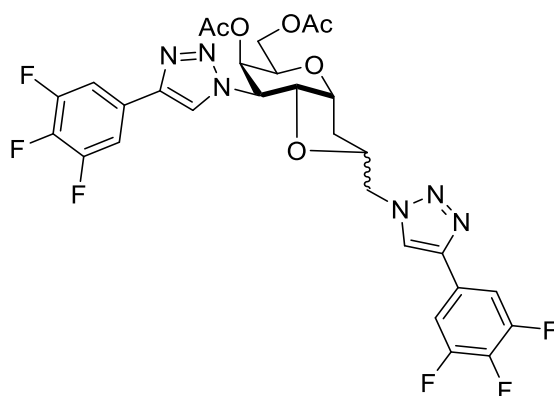


**(3aR,5R,6R,7S,7aR)-5-(hydroxymethyl)-7-(4-(3,4,5-trifluorophenyl)-1H-1,2,3-triazol-1-yl)-2-((4-(3,4,5-trifluorophenyl)-1H-1,2,3-triazol-1-yl)methyl)hexahydro-2H-furo[3,2-b]pyran-6-ol (EH 1163 LS)**

**EH 1158 LS** (26 mg, 0.06 mmol) was dissolved in a 4:1 mixture of DMF:H<sub>2</sub>O (20 mL). 3,4,5-trifluorophenylacetylene (0.02 mL, 0.17 mmol) was added followed by sodium ascorbate (28 mg, 0.14 mmol) and copper sulfate pentahydrate (36 mg, 0.14 mmol) and the reaction mixture was heated to 80°C and stirred for 1 h, after which TLC analysis indicated complete consumption of the starting material. The reaction mixture was then diluted with EtOAc, filtered, washed with water and brine, dried over Na<sub>2</sub>SO<sub>4</sub>, filtered and concentrated. The crude product was dissolved in EtOAc:MeOH (1:1) (20 mL) and Pd/C (10%) was added to the reaction mixture. The flask was fitted with a H<sub>2</sub> balloon and left to stir overnight. TLC analysis indicated complete consumption of the starting material. The reaction mixture was then filtered through celite and the solvent removed under reduced pressure. Flash chromatography (CH<sub>2</sub>Cl<sub>2</sub>-MeOH 9:1) provided the product (18 mg, 53% over two steps) as a white solid.; R<sub>f</sub> 0.1 (CH<sub>2</sub>Cl<sub>2</sub>-MeOH 9:1); <sup>1</sup>H-NMR (500 MHz, Acetone-*d*<sub>6</sub>)  $\delta$  8.65 (s, 1H), 8.45 (s, 1H), 7.73 (overlapping signals, 2H), 7.67 (overlapping signals, 2H), 4.85 (dd,  $J = 8.2, 2.1$  Hz, 1H, ), 4.79 – 4.71 (overlapping signals, 2H), 4.68 (dd,  $J = 14.4, 3.8$  Hz, 1H), 4.65 – 4.59 (overlapping signals, 2H), 4.52 (m, 1H), 4.12 (td,  $J = 6.2, 3.5$  Hz, 1H), 3.84 – 3.76 (overlapping signals, 2H), 2.37 (ddd,  $J = 13.5, 6.8, 3.9$  Hz, 1H), 2.04 – 2.00 (overlapping signals, 1H).; <sup>13</sup>C-NMR (126

MHz, Acetone- $d_6$ )  $\delta$  122.79, 121.32, 109.54, 109.49, 109.45, 109.40, 109.35, 109.31, 78.55, 76.17, 75.76, 74.13, 68.14, 63.57, 60.10, 53.12, 33.37.

Due to the high degree of signal overlap in the deprotected compound, signals are assigned after acetylation.



**((3aR,5R,6R,7R,7aR)-6-acetoxy-7-(4-(3,4,5-trifluorophenyl)-1H-1,2,3-triazol-1-yl)-2-((4-(3,4,5-trifluorophenyl)-1H-1,2,3-triazol-1-yl)methyl)hexahydro-2H-furo[3,2-b]pyran-5-yl)methyl acetate (EH 1163 LS Ac)**

See **EH 1163 LS** for procedure.

(53%)  $^1\text{H-NMR}$  (500 MHz,  $\text{CDCl}_3$ )  $\delta$  7.83 (s, 1H), 7.80 (s, 1H), 7.49 – 7.37 (overlapping signals, 4H), 5.82 (dd,  $J = 5.1, 2.0$  Hz, 1H, H-4), 4.98 (dd,  $J = 7.3, 4.2$  Hz, 1H, H-2), 4.66-4.60 (overlapping signals, 2H, H-3 & CHH-N), 4.52 (dd,  $J = 14.5, 5.5$  Hz, 1H, CHH-N), 4.45 (dt,  $J = 7.8, 5.4$  Hz, 1H, H-5), 4.33 (dd,  $J = 11.7, 7.8$  Hz, 1H, H-6a), 4.04 (dd,  $J = 11.6, 5.7$  Hz, 1H, H-6b), 2.29 (ddd,  $J = 13.9, 5.4, 1.4$  Hz, 1H, CHH), 2.05 (s, 6H, each  $\text{OCH}_3$ ), 1.91 (ddd,  $J = 13.7, 9.5, 5.8$  Hz, 1H, CHH);  $^{13}\text{C-NMR}$  (126 MHz,  $\text{CDCl}_3$ )  $\delta$  170.57, 169.22 (each  $\text{C=O}$ ), 152.67, 121.50, 120.46, 109.93, 109.88, 109.87, 109.82, 109.79, 109.75, 109.69 (each Ar-C/C-H), 79.07 (C-2), 76.91 (CH), 74.37 (C-1), 73.00 (C-5), 68.11 (C-4), 61.91 (C-3), 59.71 (C-6), 52.68 (CHH-N), 35.29 (CHH), 20.69, 20.55 (each  $\text{OCH}_3$ ).



## References

- (1) Collins, P. M.; Öberg, C. T.; Leffler, H.; Nilsson, U. J.; Blanchard, H. Taloside Inhibitors of Galectin-1 and Galectin-3. *Chem. Biol. Drug Des.* **2012**, *79*, 339–346.
- (2) Yoshida, H.; Yamashita, S.; Teraoka, M.; Itoh, A.; Nakakita, S.; Nishi, N.; Kamitori, S. X-Ray Structure of a Protease-Resistant Mutant Form of Human Galectin-8 with Two Carbohydrate Recognition Domains. *FEBS J.* **2012**, *279*, 3937–3951.
- (3) Hassan, M.; Baussière, F.; Guzelj, S.; Sundin, A. P.; Håkansson, M.; Kovačič, R.; Leffler, H.; Tomašič, T.; Anderluh, M.; Jakopin, Ž.; Nilsson, U. J. Structure-Guided Design of d-Galactal Derivatives with High Affinity and Selectivity for the Galectin-8 N-Terminal Domain. *ACS Med. Chem. Lett.* **2021**, *12*, 1745–1752.
- (4) Yoshida, H.; Teraoka, M.; Nishi, N.; Nakakita, S.; Nakamura, T.; Hirashima, M.; Kamitori, S. X-Ray Structures of Human Galectin-9 C-Terminal Domain in Complexes with a Biantennary Oligosaccharide and Sialyllactose\*. *J. Biol. Chem.* **2010**, *285*, 36969–36976.
- (5) Nagae, M.; Nishi, N.; Nakamura-Tsuruta, S.; Hirabayashi, J.; Wakatsuki, S.; Kato, R. Structural Analysis of the Human Galectin-9 N-Terminal Carbohydrate Recognition Domain Reveals Unexpected Properties That Differ from the Mouse Orthologue. *J. Mol. Biol.* **2008**, *375*, 119–135.
- (6) Bum-Erdene, K.; Leffler, H.; Nilsson, U. J.; Blanchard, H. Structural Characterization of Human Galectin-4 C-Terminal Domain: Elucidating the Molecular Basis for Recognition of Glycosphingolipids, Sulfated Saccharides and Blood Group Antigens. *FEBS J.* **2015**, *282*, 3348–3367.
- (7) Bum-Erdene, K.; Leffler, H.; Nilsson, U. J.; Blanchard, H. Structural Characterisation of Human Galectin-4 N-Terminal Carbohydrate Recognition Domain in Complex with Glycerol, Lactose, 3'-Sulfo-Lactose and 2'-Fucosyllactose. *Sci. Rep.* **2016**, *6*, 20289.
- (8) van Hattum, H.; Branderhorst, H. M.; Moret, E. E.; Nilsson, U. J.; Leffler, H.; Pieters, R. J. Tuning the Preference of Thiodigalactoside-and Lactosamine-Based Ligands to Galectin-3 over Galectin-1. *J. Med. Chem.* **2013**, *56*, 1350–1354.
- (9) Bum-Erdene, K.; Collins, P. M.; Hugo, M. W.; Tarighat, S. S.; Fei, F.; Kishor, C.; Leffler, H.; Nilsson, U. J.; Groffen, J.; Grice, I. D.; Heisterkamp, N.; Blanchard, H. Novel Selective Galectin-3 Antagonists Are Cytotoxic to Acute Lymphoblastic Leukemia. *J. Med. Chem.* **2022**, *65*, 5975–5989.
- (10) Mohy El Dine, T.; Jimmidi, R.; Diaconu, A.; Fransolet, M.; Michiels, C.; De Winter, J.; Gillon, E.; Imberty, A.; Coenye, T.; Vincent, S. P. Pillar[5]Arene-Based Polycationic Glyco[2]Rotaxanes Designed as Pseudomonas Aeruginosa Antibiofilm Agents. *J. Med. Chem.* **2021**, *64*, 14728–14744.
- (11) Doyle, L. M.; O'Sullivan, S.; Di Salvo, C.; McKinney, M.; McArdle, P.; Murphy, P. V. Stereoselective Epimerizations of Glycosyl Thiols. *Org. Lett.* **2017**, *19*, 5802–5805.
- (12) Zhang, J.; Zhang, B.; Zhou, J.; Li, J.; Shi, C.; Huang, T.; Wang, Z.; Tang, J. H<sub>2</sub>SO<sub>4</sub>-SiO<sub>2</sub>: Highly Efficient and Reusable Catalyst for per-O-Acetylation of Carbohydrates Under Solvent-Free Conditions. *J. Carbohydr. Chem.* **2011**, *30*, 165–177.

- (13) Wang, B.; Xiong, D.-C.; Ye, X.-S. Direct C–H Trifluoromethylation of Glycals by Photoredox Catalysis. *Org. Lett.* **2015**, *17*, 5698–5701.
- (14) Ko, K.-S.; Kruse, J.; Pohl, N. L. Synthesis of Isobutyl-C-Galactoside (IBCG) as an Isopropylthiogalactoside (IPTG) Substitute for Increased Induction of Protein Expression. *Org. Lett.* **2003**, *5*, 1781–1783.
- (15) Hsieh, S.-Y.; Jan, M.-D.; Patkar, L. N.; Chen, C.-T.; Lin, C.-C. Synthesis of a Carboxyl Linker Containing Pk Trisaccharide. *Carbohydr. Res.* **2005**, *340*, 49–57.
- (16) Frédéric, C. J.-M.; Cornil, J.; Vandamme, M.; Dumitrescu, L.; Tikad, A.; Robiette, R.; Vincent, S. P. Highly (Z)-Diastereoselective Synthesis of Trifluoromethylated Exo-Glycals via Photoredox and Copper Catalysis. *Org. Lett.* **2018**, *20*, 6769–6773.
- (17) Li, X.; Ohtake, H.; Takahashi, H.; Ikegami, S. A Facile Synthesis of 1'-C-Alkyl- $\alpha$ -Disaccharides from 1-C-Alkyl-Hexopyranoses and Methyl 1-C-Methyl-Hexopyranosides. *Tetrahedron* **2001**, *57*, 4297–4309.
- (18) van Hooft, P. A. V; El Oualid, F.; Overkleeft, H. S.; van der Marel, G. A.; van Boom, J. H.; Leeuwenburgh, M. A. Synthesis and Elaboration of Functionalised Carbohydrate-Derived Spiroketal. *Org. Biomol. Chem.* **2004**, *2*, 1395–1403.
- (19) Chen, Y.-B.; Wang, S.-I.; Lin, Z.-P.; Lin, C.-H.; Hsieh, M.-T.; Lin, H.-C. Stereoselective Glycosylation of D-Galactals by Diethyl Phosphorochloridite- and AlCl<sub>3</sub>-Assisted Ferrier Rearrangement. *Tetrahedron* **2015**, *71*, 350–358.